Chemical and structural variations of bivalve shells at the micrometer scale – taking sclerochronology to the next level

Dissertation zur Erlangung des Grades “Doktor der Naturwissenschaften” im Promotionsfach Geowissenschaften/Paläontologie

Am Fachbereich 09 für Chemie, Pharmazie und Geowissenschaften der Johannes Gutenberg-Universität Mainz

Cornélia BROSSET

geb. 14.05.1998 in Vendôme, France

Mainz, 2025

1. Berichterstatter: Removed for reasons of data protection
2. Berichterstatter: Removed for reasons of data protection

Tag der mündlichen Prüfung: Removed for reasons of data protection

Hiermit erkläre ich, dass ich die vorliegende Arbeit selbstständig verfasst und keine anderen als die angegebenen Quellen und Hilfsmittel benutzt habe.

Cornélia BROSSET

Abstract

Shells of marine bivalves are exceptional high-resolution archives of climate variability. Their chemical and structural properties reflect the environmental conditions prevailing at the time of shell formation. These records can be placed in a temporal context by the analysis of growth patterns. Yet, reliable temperature estimates from bivalve shells remain scarce. Stable oxygen isotope values ($\delta^{18}O_{shell}$) are widely used in sclerochronology but often rely on poorly documented $\delta^{18}O_{water}$ values. Carbonate clumped isotope (Δ_{47}) analyses overcome this limitation but are analytically demanding and rarely applicable at high-resolution. Trace and minor element-to-calcium ratios (Ele/Ca), specifically strontium-to-Ca (Sr/Ca), can be obtained using high-resolution and minimally destructive analytical techniques. In many taxa, these data serve as a proxy for temperature but yielded inconsistent and often contradictory results in bivalves. These discrepancies were attributed to physiological controls over trace and minor element incorporation into shell material. However, most attempts to calibrate the Sr/Ca-thermometer overlooked the internal complexity of the shells, treating them as structurally uniform materials. Yet, they are composed of distinct layers and periodic growth features, each defined by specific ultrastructures. Ultrastructural variations of bivalve shells reflect changes in organic composition and crystal growth dynamics, directly influencing Sr incorporation. Although shell Sr/Ca may capture ambient temperature variability, the signal is likely distorted by vital effects that are sometimes expressed in the form of ultrastructural heterogeneity. To reliably reconstruct past temperatures from shell Sr/Ca, identifying and accounting for these potential biases is essential.

This thesis evaluated whether variability in shell ultrastructural properties systematically biases the relationship between seawater temperature and Sr/Ca ratios in aragonitic shells of marine bivalves. Specifically, it was tested whether factors controlling shell architecture (i.e., shell layers and growth patterns), growth rate and biomineral unit (BMU) morphology affect Sr incorporation into the shells and thus compromise the link between ambient temperature and shell Sr/Ca ratios. To assess the accuracy of Sr/Ca-based temperature estimates once these potential biases were resolved, high-resolution ultrastructural and geochemical analyses were performed on two long-lived bivalve species widely employed in paleoclimate studies. This project included the publication of three scientific manuscripts in international peer-reviewed journals that document the main findings.

Manuscript 1 reported on the relationship between seasonal temperature variations and shell Sr/Ca ratios in *Arctica islandica*, a long-lived marine bivalve broadly distributed in the North Atlantic and exhibiting annual shell growth patterns. Consistent with thermodynamic predictions, shell Sr/Ca was positively linked to seasonal temperature. However, the correlation was weak (Pearson $r = 0.15$) and only improved moderately after mathematical adjustment for

ultrastructural and growth rate-related biases (maximum Pearson $r = 0.51$). These results show that ultrastructure and growth rate influences bias Sr/Ca-based temperature reconstructions and suggest additional environmental factors strongly affect the shell Sr/Ca-temperature relationship in wild *A. islandica*. This currently limits the use of shell Sr/Ca as a reliable paleothermometer.

Manuscript 2 addressed the confounding environmental drivers of shell Sr/Ca. Juvenile *A. islandica* specimens were cultured at various stable temperatures in the laboratory to isolate the Sr/Ca-temperature relationship from other external factors. Shell Sr/Ca ratios increased with temperature (R^2 up to 0.38), and this correlation improved substantially after correcting the Sr/Ca profiles for ultrastructural and growth rate-related influences (R^2 up to 0.75). These results further indicate that the temperature signal recorded in shell Sr/Ca profiles of field-grown specimens is superimposed by other environmental variables. Such factors influence Sr incorporation either directly or indirectly by increasing ultrastructural variability and associated bias. Consequently, transfer functions for the Sr/Ca-thermometer derived from ultrastructurally more uniform shells of laboratory-grown specimens (uncertainty of ± 1.0 °C) cannot be directly applied to wild specimens due to unresolved environmental forcings ($R^2 = 0.26$, uncertainty of ± 2.1 °C).

Manuscript 3 examined whether temperature variations could be reliably inferred from Sr/Ca profiles measured in the daily shell growth increments and lines of the tropical photosymbiotic giant clam *Tridacna squamosa*. Combining sub-daily resolved Sr/Ca data with detailed ultrastructure-specific analyses revealed that Sr/Ca ratios were correlated with seawater temperature ($R^2 = 0.36$). This relationship was previously masked by lack of consideration for shell structural heterogeneity. However, the uncertainty of the temperature estimates (± 1.5 to 2.8 °C) remained close to the natural range of variability in tropical settings. Additionally, shell Sr/Ca showed consistent daily cycles with local maxima at growth lines, even when the ultrastructure morphology varied or deviated from its typical configuration during extreme environmental disturbances. This suggests common control factors on both ultrastructure and Sr incorporation rather than a direct causal relationship. The findings of this study highlight both the potential and complexity of using shell Sr/Ca as a sub-daily resolved temperature proxy in fast-growing tropical bivalves and the necessity of ultrastructure-specific analyses in calibration studies.

In summary, this thesis demonstrated that ultrastructural variability in marine bivalve shells significantly affects the reliability of Sr/Ca as a (paleo)temperature proxy. High-resolution ultrastructure-specific analyses are essential to isolate shell Sr/Ca variations reflecting ambient temperature. The Sr/Ca-temperature relationship was stronger under controlled conditions in the laboratory and after correction for ultrastructural and growth rate-related influences. Other natural environmental and physiological drivers still limit the accuracy of the shell Sr/Ca-thermometer. The approaches developed in this study provide a reproducible framework for refining the calibration of Ele/Ca-based proxies in sclerochronological research.

Zusammenfassung

Die Schalen mariner Muscheln sind hervorragende, hochauflösende Archive klimatischer Variabilität. Ihre chemischen und strukturellen Eigenschaften zeichnen die zum Zeitpunkt der Schalenbildung vorherrschenden Umweltbedingungen auf. Diese Aufzeichnungen können durch die Analyse von Wachstumsmustern zeitlich kontextualisiert werden. Dennoch sind zuverlässige Temperaturrekonstruktionen aus Muschelschalen nach wie vor selten. Die stabilen Isotope des Sauerstoffs ($\delta^{18}O_{shell}$) sind in der Sklerochronologie weit verbreitet, setzen jedoch oft schlecht dokumentierten Werte des $\delta^{18}O_{water}$ voraus. Clumped isotope (Δ_{47}) Analysen an Karbonaten sind von dieser Begrenzung nicht betroffen, jedoch analytisch anspruchsvoll und selten mit hoher Auflösung anwendbar. Spuren- und Nebenelemente im Verhältnis zu Kalzium (Ele/Ca), insbesondere Strontium-Ca-Verhältnisse (Sr/Ca), können mit hochauflösenden und minimal invasiven Analysetechniken ermittelt werden. Bei vielen Taxa dienen diese Daten als Temperaturproxy, ergaben bei Muschelschalen jedoch uneinheitliche und oft widersprüchliche Ergebnisse. Solche Diskrepanzen wurden auf physiologische Kontrollen beim Einbau von Spuren- und Nebenelementen in das Schalenmaterial zurückgeführt. Jedoch wurde bei den meisten Ansätzen, das Sr/Ca-Thermometer zu kalibrieren, die innere Komplexität der Schalen außer Acht gelassen und diese als strukturell einheitliches Material behandelt. Diese besteht jedoch aus verschiedenen Schichten und periodischen Wachstumsmerkmalen, welche jeweils über spezifische Ultrastrukturen definiert sind. Diese ultrastrukturellen Variationen spiegeln Veränderungen in der organischen Zusammensetzung und der Kristallwachstumsdynamik wider, - Prozesse, die sich direkt auf den Sr-Einbau auswirken. Obwohl Sr/Ca der Schale die Variabilität der Umgebungstemperatur erfassen kann, wird das Signal wahrscheinlich durch vitale Effekte verzerrt, die sich ebenfalls in Form von ultrastruktureller Heterogenität äußern. Um vergangene Temperaturen zuverlässig aus dem Sr/Ca-Wert der Schale zu rekonstruieren, ist es daher wichtig, diese potenziellen Verzerrungen zu erkennen und zu berücksichtigen.

In der vorliegenden Arbeit wurde untersucht, ob die Variabilität der ultrastrukturellen Eigenschaften von Muschelschalen die Beziehung zwischen der Meerwassertemperatur und dem Sr/Ca-Verhältnis in aragonitischen Muschelschalen systematisch verzerrt. Insbesondere wurde getestet, ob Faktoren, welche die Schalenarchitektur (d.h. Schalenschichten und Wachstumsmuster), die Wachstumsrate und die Morphologie der Biomineral Einheiten (BMU) kontrollieren, den Einbau von Sr in die Schalen beeinflussen und somit die Verbindung zwischen Umgebungstemperatur und dem Sr/Ca-Verhältnis der Schalen beeinträchtigen. Um die Genauigkeit von Sr/Ca-basierten Temperaturschätzungen zu bewerten, sobald diese potenziellen Verzerrungen beseitigt sind, wurden hochauflösende ultrastrukturelle und geochemische Analysen an zwei langlebigen Muschelarten durchgeführt, die häufig in

Paläoklima-Studien verwendet werden. Im Rahmen dieses Projekts wurden drei wissenschaftliche Manuskripte in internationalen, peer-reviewten Fachzeitschriften veröffentlicht, welche die wichtigsten Ergebnisse dokumentieren.

Manuskript 1 berichtete über die Beziehung zwischen saisonalen Temperaturschwankungen und dem Sr/Ca-Verhältnis der Schale von *Arctica islandica*, einer langlebigen Meeresmuschel, die im Nordatlantik weit verbreitet ist und jährliche Schalenwachstumsmuster aufweist. In Übereinstimmung mit thermodynamischen Vorhersagen stand das Sr/Ca-Verhältnis der Schale positiv mit der saisonalen Temperatur im Zusammenhang. Die Korrelation war jedoch schwach (Pearson $r = 0.15$) und verbesserte sich nur mäßig nach mathematischer Anpassung für ultrastrukturelle und wachstumsratenbezogene Einflüsse (maximales Pearson $r = 0.51$). Diese Ergebnisse zeigen, dass Ultrastruktur und Wachstumsrate Sr/Ca-basierte Temperaturrekonstruktionen verzerren und legen nahe, dass zusätzliche Umweltfaktoren die Sr/Ca-Temperaturbeziehung in Schalen wildlebender *A. islandica* deutlich beeinflussen. Dies schränkt derzeit die Verwendung von Sr/Ca in der Schale als zuverlässiges Paläothermometer ein.

Manuskript 2 befasste sich mit den umweltbedingten Einflüssen auf Sr/Ca in der Schale. Juvenile *A. islandica*-Exemplare wurden bei verschiedenen stabilen Temperaturen im Labor kultiviert, um die Sr/Ca-Temperatur-Beziehung von anderen externen Faktoren zu isolieren. Das Sr/Ca-Verhältnis der Schale nahm mit der Temperatur zu (R^2 bis zu 0.38), und diese Korrelation verbesserte sich erheblich, nachdem die Sr/Ca-Profile um ultrastrukturelle und wachstumsbedingte Einflüsse korrigiert worden waren (R^2 bis zu 0.75). Diese Resultate deuten zudem darauf hin, dass das Temperatursignal in den Sr/Ca-Profilen der im natürlichen Lebensraum aufgewachsenen Individuen von anderen Umweltvariablen überlagert wird. Solche Faktoren beeinflussen den Sr-Einbau entweder direkt oder indirekt, indem sie die ultrastrukturelle Variabilität und die damit verbundene Verzerrung erhöhen. Folglich können Transferfunktionen für das Sr/Ca-Thermometer, die von ultrastrukturell einheitlicheren Schalen im Labor gehaltener Exemplare abgeleitet wurden (Unsicherheit von ± 1.0 °C), aufgrund ungeklärter Umwelteinflüsse nicht direkt auf in der Natur aufgewachsene Individuen übertragen werden ($R^2 = 0.26$, Unsicherheit von ± 2.1 °C).

Manuskript 3 untersuchte, ob aus Sr/Ca-Profilen, die in den täglichen Wachstumsinkrementen und -linien der tropischen photosymbiotischen Riesenmuschel *Tridacna squamosa* gemessen wurden, zuverlässig auf Temperaturschwankungen geschlossen werden kann. Die Kombination von sub-täglich aufgelösten Sr/Ca-Werten mit detaillierten ultrastrukturspezifischen Analysen ergab, dass das Sr/Ca-Verhältnis mit der Meerwassertemperatur korreliert ($R^2 = 0.36$). Diese Beziehung wurde zuvor durch die fehlende Berücksichtigung der strukturellen Heterogenität der Schale nicht erkannt. Die Unsicherheit der

Temperaturschätzungen (± 1.5 bis 2.8 °C) lag jedoch nahe an der saisonalen Schwankungsbreite in tropischen Gebieten. Darüber hinaus zeigte das Sr/Ca der Schalen konsistente tägliche Zyklen mit lokalen Maxima an den Wachstumslinien, selbst wenn die Ultrastrukturmorphologie während extremer Umweltstörungen variierte oder von ihrer typischen Konfiguration abwich. Dies deutet eher auf gemeinsame Kontrollfaktoren für die Ultrastruktur und den Sr-Einbau hin als auf eine direkte kausale Beziehung. Die Ergebnisse dieser Arbeit verdeutlichen sowohl das Potenzial als auch die Komplexität der Verwendung des Sr/Ca-Verhältnisses der Schale als subtäglich aufgelöster Temperaturproxy bei schnell wachsenden tropischen Muscheln und die Notwendigkeit ultrastrukturspezifischer Analysen in Kalibrierungsstudien.

Zusammenfassend konnte in dieser Arbeit gezeigt werden, dass die ultrastrukturelle Variabilität in marinen Muschelschalen die Zuverlässigkeit von Sr/Ca als (Paläo-)Temperaturproxy erheblich beeinflusst. Hochauflösende ultrastrukturspezifische Analysen sind unerlässlich, um temperaturabhängige Sr/Ca-Schalenvariationen zu isolieren. Die Sr/Ca-Temperatur-Beziehung war unter kontrollierten Bedingungen im Labor und nach Korrektur der ultrastrukturellen und wachstumsratenbezogenen Einflüsse stärker. Andere natürliche Umwelteinflüsse und physiologische Faktoren schränken die Genauigkeit des Schalen basierten Sr/Ca-Thermometers weiterhin ein. Die in dieser Studie entwickelten Ansätze bieten einen reproduzierbaren Rahmen für die Verfeinerung der Kalibrierung von Ele/Ca-basierten Proxies in der sklerochronologischen Forschung.

Contents

Acknowledgements

Removed for reasons of data protection

List of abbreviations

$\delta^{18}O$	Stable oxygen isotope value
Δ_{47}	Carbonate clumped isotope value
LA-ICP-MS	Laser ablation – inductively coupled plasma – mass spectrometry
SIMS	Secondary ion mass spectrometry
NanoSIMS	Nanoscale secondary ion mass spectrometry (nanometer-scale)
Ele/Ca	Trace and minor element-to-calcium ratio
EPS	Extrapallial space
BMU	Biomineral unit
OSL	Outer shell layer
ISL	Inner shell layer
oOSL	Outer portion of the OSL
iOSL	Inner portion of the OSL
ISP	Irregular simple prismatic ultrastructure
CCL	Complex crossed-lamellar ultrastructure
CA	Crossed-acicular ultrastructure
HOM	Homogeneous ultrastructure
SEM	Scanning electron microscopy
SST	Sea surface temperature

List of Figures

List of Tables

1 Introduction

1.1 Climate reconstruction: marine bivalve shells as proxy archives

Climate change poses a threat to all ecosystems across the biosphere (Markham, 1996; McCarty, 2001; Scholze et al., 2006; Mooney et al., 2009; Scholes, 2016; Malhi et al., 2020; Wernberg et al., 2024). Shifts in environmental forcings operating both globally (e.g., solar radiation, ocean currents, volcanic eruptions; Budyko, 1969; Manabe, 1969; Robock, 2000) and regionally (e.g., El Niño-Southern Oscillation, North Atlantic Oscillation; Schlesinger and Ramankutty, 1994; Stenseth et al., 2003) are driving climate dynamics beyond their historical range of natural variability (Diaz et al., 2001; Gillett et al., 2003; Trenberth and Fasullo, 2009). While abiotic parameters (e.g., temperature, precipitation) inherently fluctuate, anthropogenic pressures have caused increasingly irreversible alterations of climate systems (Karl and Trenberth, 2003; Salinger, 2005; Solomon et al., 2009; IPCC, 2023). Industrial fisheries (Pauly et al., 2005), land-use changes (Foley et al., 2005) and fossil fuel exploitation (Lincoln, 2005) have impaired ecological processes essential to the maintenance of critical carbon sinks (e.g., oceans, forests and permafrost), leading to an increase in atmospheric greenhouse gas concentrations and heat retention (Schuur et al., 2015; Gruber et al., 2023; Pan et al., 2024). As a result, 2024 marked the warmest year on record and average global temperatures reached + 1.5 °C above pre-industrial levels (C3S, 2025). At this threshold, for example, 3 to 14 % of terrestrial species face a very high risk of extinction while 90 % of coral reefs are projected to undergo severe degradation during the 21st century (IPCC, 2023). The development of effective mitigation strategies is urgently needed and requires accurate predictive climate models (Weaver et al., 2013), informed by distinctions between anthropogenic drivers and natural variability (Hegerl et al., 1996; Phipps et al., 2013) as well as comparisons with paleoclimates (Jones et al., 2001; Kageyama et al., 2024). However, the limited spatiotemporal coverage of instrumental records (i.e., widespread only since the mid-19th century and moderately reliable in the earlier decades, e.g., Hulme and Jones, 1994; Jones et al., 1999; Houghton et al., 2001) constrains the accuracy of numerical climate models. Modelled

environmental data therefore need to be refined beyond the instrumental era (Kaufman and Broadman, 2023).

Climate studies increasingly rely on proxy data – i.e., chemical and structural properties reflecting environmental variables – derived from natural archives (i.e., abiogenic and biogenic materials that record the local conditions which occurred during their formation). Once calibrated, these proxies can provide valuable insights into ecosystems from the recent past and up to millions of years ago (Clemens, 2006; Li et al., 2010; Tierney et al., 2020). For example, dendrochronology uses tree ring properties to reconstruct terrestrial hydrology and temperature changes (e.g., Fritts, 1971; Briffa, 2000; Gholami et al., 2015), reaching back more than 14,000 years at some sites (Bard et al., 2023), while speleothems formed in caves can yield multi-millennia scale records (e.g., Fairchild et al., 2006; Scholz et al., 2012; Columbu et al., 2020). Likewise, ice cores from polar regions can provide climate records extending back over a million years (e.g., Bond et al., 1993; Dansgaard et al., 1993; Higgins et al., 2015). As oceans cover most of the Earth and play a fundamental role in climate regulation (Bigg et al., 2003; Schmitt, 2018), obtaining high-resolution data from specific past marine conditions is as essential as paleoclimate proxy data provided by terrestrial archives. For instance, marine sedimentary deposits record long-term environmental changes (e.g., Martinson et al., 1987; Arz et al., 1999), although chronologies obtained from sediments can be affected by post-depositional processes (e.g., bioturbation, remobilization; Smith, 2001; Anderson, 2001; Martinez-Ruiz et al., 2015).

In contrast, sclerochronology (i.e., the study of sequentially deposited biogenic hard tissues in invertebrates, fish and coralline algae) provides temporally well-constrained and high-resolution proxy data for a broad range of marine environments (Butler and Schöne, 2017; Gillikin et al., 2019), but limitations in this field often arise from the nature of the studied archives themselves. Namely, while fish preserve environmental signals in their otoliths (Mulcahy et al., 1979; Rowell et al., 2010), making such structures valuable proxy archives, their mobility compromises the reliability of local reconstructions. Conversely, biomineralized tissues of shallow-water corals merely provide environmental records from tropical regions (Weber and Woodhead, 1970; Cobb et al., 2003; Erler et al., 2016).

Among sclerochronological archives, marine bivalves provide an exceptional alternative, effectively addressing both mobility and geographic constraints. Bivalve mollusks remain predominantly sessile after a brief planktonic larval stage (Gosling, 2003), ensuring that their shell records ambient conditions from a fixed locality. Their broad biogeographical distribution, from intertidal zones to the deep sea in a wide range of latitudes (Jablonski et al., 2013), provides paleoenvironmental insights from a broad variety of different ecosystems. Finally, with over 500 million years of evolutionary history (Sepkoski, 1981; Fraiser and Bottjer, 2007) and a great

diversity of extant and extinct species (Flessa and Jablonksi, 1995; Crame, 2000; Roy et al., 2000; Jablonski et al., 2003), marine bivalves offer an extensive framework for paleoclimate research.

Bivalve shells grow sequentially, with shell material deposited as distinct growth increments and lines formed through alternating periods of rapid and slow growth (Clark, 1968, 1974; Lutz and Rhoads, 1980; Thompson et al., 1980). These growth patterns provide the temporal framework for precisely dated environmental reconstructions. In many species, these periodic features develop annually (Jones, 1980, 1983; Ropes et al., 1984; Trutschler and Samtleben, 1988) and, if the time of death of the specimen is known, can be assigned a precise calendar year. Shell growth patterns of higher frequency, such as those formed at fortnightly, circadian or tidal periodicity, also occur in many bivalves and provide sub-annual chronological frameworks (Clark, 1968; Evans, 1972; Kennish and Olsson, 1975; Ohno, 1989; Chauvaud et al., 1998; Schöne et al., 2005b; Hallman et al., 2009). Growth records are limited by the lifespan of mollusk specimens, which can range from merely a year to several centuries depending on the species (Turekian et al., 1975; Zolotarev, 1980; Rhoads et al., 1981; Jones, 1983; Ropes and Murawski, 1983; Schöne et al., 2005a; Abele et al., 2009; Moss et al., 2016). Cross-referencing bivalves with chronologically overlapping lifetimes, as well as multiple coeval specimens, provides longer and more robust frameworks for the temporal alignment of *in-situ* measurements (i.e., assigning proxy data to specific temporal reference points based on growth analyses; Black et al., 2019). In turn, these extended chronologies support potential reconstructions far beyond individual lifetimes (e.g., Scourse et al., 2006; Butler et al., 2013; Reynolds et al., 2017; Edge et al., 2021). However, while several environmental proxies retrieved from bivalve shells have been successfully calibrated, many require further investigation before they can support reliable paleoclimate reconstructions.

1.2 Geochemical composition of bivalve shells as an environmental proxy

One way to reconstruct environmental conditions using bivalve shells is through the analysis of their geochemistry. Among the geochemical proxies available within these archives, their isotopic composition remains the most extensively used one, particularly for paleothermometry owing to the central role of temperature in climate dynamics (Manabe and Wetherald, 1967; Hansen et al., 1984; Manabe and Stouffer, 1993; Wanner et al., 2001; Van Der Wiel and Bintanja, 2021; Forster et al., 2023; IPCC, 2023). As most bivalve shells precipitate near oxygen isotopic equilibrium with ambient seawater (Epstein et al., 1953; Mook and Vogel, 1968; Jones et al., 1983), temperature variations which occurred during shell formation can be precisely reconstructed from $\delta^{18}O_{shell}$ (Epstein et al., 1953; Grossman and Ku, 1986; Schöne et al., 2004), provided that

$\delta^{18}O_{water}$ is known. Alternatively, $\delta^{18}O_{water}$ can be inferred from ambient salinity data using the local seawater-freshwater mixing line (e.g., Weiss et al., 1979; Strain and Tan, 1993; Rohling and Bigg, 1998; Gillikin et al., 2005a). The equation (Eq. 1.1) proposed by Grossman and Ku (1986) with the VPDB-VSMOW scale correction of -0.27 ‰ (Gonfiantini et al., 1995; Dettman et al., 1999) is commonly used in paleoclimate studies to reconstruct temperature (T) based on $\delta^{18}O_{shell}$:

$$T = 20.6 - 4.34 \times (\delta^{18}O_{shell} - (\delta^{18}O_{water} - 0.27) \quad (1.1)$$

Carbonate clumped isotope (Δ_{47}) analysis, in comparison, directly quantifies the temperature-dependent tendency of heavy isotopes (^{13}C and ^{18}O) to bond with each other relative to bonds with light isotopes (Eiler, 2007, 2011). This approach therefore provides temperature estimates independent of $\delta^{18}O_{water}$ (e.g., De Winter et al., 2021, 2024). However, Δ_{47}-based temperature reconstructions are often hindered by time-consuming and labor-intensive analyses (Huntington et al., 2009; Fiebig et al., 2016; Fernandez et al., 2017). Due to substantial shell material requirements (Eiler, 2011; Meckler et al., 2014; Fernandez et al., 2017; Müller et al., 2017) and sensitivity of samples to diagenetic alteration (Affek, 2012; Winkelstern and Lohmann, 2016), the temporal coverage and resolution of Δ_{47}-based temperature estimates are also often limited.

To overcome challenges associated with the traditional $\delta^{18}O_{shell}$-based and Δ_{47}-based temperature reconstructions, efforts have been undertaken to use trace and minor element-to-calcium (Ele/Ca) ratios as paleothermometers instead (Gillikin et al., 2019; Peharda et al., 2021). Analytical protocols for measuring shell Ele/Ca ratios are relatively fast, cost-effective and minimally destructive (Marali et al., 2017). Techniques such as laser ablation – inductively coupled plasma – mass spectrometry (LA-ICP-MS; e.g., Marali et al., 2017) and secondary ion mass spectrometry (SIMS; e.g., Freitas et al., 2009) enable *in-situ* measurements of shell element chemistry at a micrometer-scale resolution, with even finer scales achievable using NanoSIMS (e.g., Shirai et al., 2008). Notably, strontium- and magnesium-to-Ca (Sr/Ca and Mg/Ca) ratios from the biogenic carbonates of many non-molluscan taxa (e.g., corals, foraminifera, brachiopods) have been used as proxies for paleotemperature reconstructions (Lowenstam, 1961; Beck et al., 1992; Nürnberg et al., 1996; Tripati et al., 2003; Goodkin et al., 2007; Cléroux et al., 2008; Powell et al., 2009; DeLong et al., 2013; Clark et al., 2016; Evans et al., 2016; Zinke et al., 2019). However, extracting reliable temperature information from Sr/Ca and Mg/Ca ratios in bivalve shells remains challenging and both proxies are often confounded by species-specific shell properties and physiological processes (Vihtakari et al., 2017).

Namely, Mg/Ca ratios in aragonitic bivalve shells vary substantially across species, shell portions and ontogenetic stages (e.g., Elliot et al., 2009; Schöne et al., 2011; Markulin et al., 2019; Piwoni-Piórewicz et al., 2021) and are typically low (i.e., barely reaching 1 mmol/mol; e.g. Schöne et al., 2010; Marali et al., 2017; Chamberlayne et al., 2020). This is partly explained by the poorer compatibility of magnesium ions (Mg^{2+}) with aragonite than with the rhombohedral calcite

lattice (Dodd, 1967; Shannon, 1976; Soldati et al., 2016), in which shell Mg/Ca tends to correlate more strongly with temperature (e.g., Wanamaker et al., 2008a; Tynan et al., 2017). In contrast, strontium ions (Sr^{2+}) fit better in the orthorhombic lattice of aragonite (Speer, 1983), resulting in higher Sr/Ca levels in aragonitic shells (i.e., typically between 1 and 3 mmol/mol; e.g., Schöne et al., 2010; Marali et al., 2017; Chamberlayne et al., 2020). During shell formation, Sr ions can substitute for Ca ions (Ca^{2+}) in the aragonite lattice (Gaetani and Cohen, 2006) due to their identical charge and similar ionic radii (Ca^{2+} = 1.18 Å, Sr^{2+} = 1.31 Å in a 9-fold coordination; Shannon, 1976). This process is inherently endothermic (Gaetani and Cohen, 2006) and, because thermodynamic principles promote equilibrium in a warming system, Sr^{2+} incorporation is favored when higher temperatures enhance aragonite lattice distortions and ion mobility at the calcification site (Gaetani and Cohen, 2006; Menadakis et al., 2008). Additionally, while $Sr/Ca_{seawater}$ remains relatively stable above a salinity threshold of ca. 10 (Dodd and Crisp, 1982), variations occurring in coastal and estuarine environments (Lebrato et al., 2020, 2021; Khare et al., 2023) need to be considered, particularly when the temperature sensitivity of shell Sr/Ca is low. Considering all these aspects, Sr/Ca in aragonitic bivalve shells formed in fully marine settings can, in principle, yield reliable paleotemperature reconstructions.

However, while thermodynamic models provide a compelling rationale for using Sr/Ca ratios of aragonite as a seawater temperature proxy, empirical data often deviate from predictions (Gaetani and Cohen, 2006). Such discrepancies are associated with complex interactions between kinetic processes and physiological influences affecting strontium incorporation (Gaetani and Cohen, 2006). For example, precipitation experiments conducted on abiogenic aragonite have revealed unexpectedly high Sr/Ca values (Mucci et al., 1989; Zhong and Mucci, 1989; Gaetani and Cohen, 2006). This enrichment was attributed to the surface entrapment of Sr^{2+} when crystal growth outpaces ion diffusion away from the growth front (Watson, 1996, 2004; Gaetani and Cohen, 2006). As the competition between precipitation and diffusion rates decreases under warmer conditions, this kinetic effect becomes less prominent, resulting in the apparent negative correlation between temperature and Sr/Ca (Gaetani and Cohen, 2006). Comparable patterns have been documented in scleractinian corals (e.g., Beck et al., 1992; Corrège, 2006; Gaetani and Cohen, 2006), for which Sr/Ca signatures are likely further overprinted by physiological factors such as calcifying fluid dynamics, skeletal precipitation efficiency and photosymbiotic activity (Allison et al., 2010; Gagnon et al., 2012; D'Olivo and McCulloch, 2017). In bivalve shells, the relationship between Sr/Ca and seawater temperature remains particularly ambiguous (e.g., Schöne et al., 2013; Yan et al., 2013). Inconsistencies are commonly attributed to "vital effects" (i.e., the physiologically mediated processes that modulate shell formation; Urey et al., 1951), with studies across various aragonitic taxa reporting positive, negative or no correlations at all between Sr/Ca and ambient temperature (e.g., Dodd, 1965;

Surge and Walker, 2006; Foster et al., 2009; Schöne et al., 2011; Sano et al., 2012; Arias-Ruiz et al., 2017; Liu et al., 2021).

In addition to temperature, other physicochemical parameters have been investigated using shell Ele/Ca ratios as proxies. For instance, shell manganese-to-Ca (Mn/Ca) ratios provide insight into local oxygen availability (Schöne et al., 2021, 2022; Huang et al., 2023), as portions deposited under low-oxygen conditions often exhibit elevated Mn/Ca values. This is because suboxic conditions promote the reduction of particulate Mn oxides into dissolved Mn ions (Mn^{2+}; Middelburg et al., 1987), effectively mobilizing manganese into a highly bioavailable form (Langlet et al., 2006). In hypoxic environments, Mn^{2+} accumulates in sediment pore waters and subsequently diffuses into the water column (Tebo, 1991; Pakhomova et al., 2007), where it is incorporated into the bivalve shell during biomineralization (Schöne et al., 2022). Shell Mn/Ca ratios therefore reflect the redox conditions prevailing at the time of shell formation. So far, however, this proxy remains largely qualitative and requires further calibration (Huang et al., 2023). Additionally, variability in shell sodium-, boron- and uranium-to-Ca (Na/Ca, B/Ca and U/Ca) profiles may reflect seawater salinity (e.g., Ishikawa and Ichikuni, 1984; Roopnarine et al., 1998) and pH dynamics (e.g., Frieder et al., 2014; Zhao et al., 2017), while lead-, copper-, cadmium- and zinc-to-Ca (Pb/Ca, Cu/Ca, Cd/Ca and Zn/Ca) ratios have been examined as potential proxies for anthropogenic impacts and trace metal contamination (e.g., Liehr et al., 2005; Pearce and Mann, 2006; Dunca et al., 2009; Holland et al., 2014; O'Neil and Gillikin, 2014), although all remain rarely applied.

Several Ele/Ca ratios have also been investigated in bivalve shells for the reconstruction of parameters related to ecological productivity. Namely, shell barium-to-Ca (Ba/Ca) profiles typically exhibit baseline values reflecting $Ba/Ca_{seawater}$ (Gillikin et al., 2006; Barats et al., 2009; Poulain et al., 2015), interspersed with sharp peaks linked to primary production events (Fröhlich et al., 2022a). A detailed analysis of Ba/Ca peak morphology in bivalve shells can, for example, reveal the specific composition of a phytoplankton bloom when local microalgae communities are well-characterized. This has been done by using Ba/Ca profiles from *Pecten maximus* shells collected in the highly monitored Bay of Brest (Fröhlich et al., 2022a, 2022b, 2023). Likewise, shell lithium- and molybdenum-to-Ca (Li/Ca and Mo/Ca) data show empirical relationships with phytoplankton dynamics and nutrient cycles (Thébault et al., 2009; Fröhlich et al., 2022b, 2023), although underlying processes remain only partially understood.

Understanding shell Ele/Ca variability requires consideration of the processes regulating aragonite biomineralization. In bivalves, shell formation occurs within an enclosed compartment between the shell inner surface and the outer mantle epithelium (e.g., Nakahara and Bevelander, 1971; Crenshaw, 1972; Wilbur, 1972; Wheeler, 1992; Checa et al., 2014), i.e., the extrapallial space (EPS), where the chemical properties are actively regulated by the organism to

promote calcium carbonate precipitation (Stemmer et al., 2019; Schwaner et al., 2022a, 2022b). To supply the biomineralization front, $CaCO_3$ precursor ions (i.e., Ca^{2+}, HCO_3^- or CO_3^{2-}) derived from seawater filtration and metabolic processes (Carré et al., 2006; Marin et al., 2012) enter the hemolymph of the mollusk. These ions are transported across the mantle epithelial membrane into the EPS through passive diffusion, passive transmembrane transport via Ca^{2+} channels or active transport through Ca^{2+}-ATPase pumps (Wheeler, 1992; Carré et al., 2006; Marin et al., 2012; Clark et al., 2020). Bivalve shells also contain organic components which are synthesized from dietary intakes (Marin et al., 2012) and form a structural scaffolding that defines the boundaries of the calcification compartments (Bevelander and Nakahara, 1980; Levi-Kalisman et al., 2001; Suzuki et al., 2017), regulates ion fluxes (Le Roy et al., 2014; Clark et al., 2020) and promotes the nucleation of carbonate crystals (Clark, 1980; Song et al., 2019). Shell formation therefore results from complex interactions between mineral and organic phases, both of which modulate shell trace and minor element content (Takesue et al., 2008; Schöne et al., 2010; Shirai et al., 2014). Moreover, the contents of the EPS and the organization of the shell organic matrix are further influenced by external physicochemical factors (e.g., temperature, ionic availability, redox state; Cameron et al., 2019, 2022), likely introducing more variability in shell chemical properties. Shell Ele/Ca ratios thus reflect additional sources of variability beyond the environmental and ecological signals that they are thought to reflect. Therefore, many Ele/Ca-based proxies remain poorly calibrated in bivalve shells due to limited investigation, analytical constraints or unresolved environmental drivers.

1.3 Shell architecture and ultrastructure: implications for Sr/Ca-thermometry

The general architecture of bivalve shells is preserved across most taxa (Fig. 1.1A; Bøggild, 1930). The outer shell layer (OSL) located near the periostracum (Bøggild, 1930) is separated by the myostracum (i.e., organic-rich layer secreted by the mantle at its attachment point along the growth front; Carter et al., 2012) from the inner shell layer (ISL; Fig. 1.1A; Bøggild, 1930). The OSL and ISL form in separated EPSs (i.e., the outer and inner EPS, respectively; Wilbur and Saleunddin, 1983; Schöne and Surge, 2012; Curley et al., 2023). As the OSL grows faster than the ISL, it was often the preferred target material of element chemical analyses (e.g., Gillikin et al., 2005a; Lazareth et al., 2013; Schöne et al., 2013; Füllenbach et al., 2017). Based on ultrastructural differences, the OSL can be subdivided into an outer and inner portion (oOSL and iOSL, respectively; Fig. 1.1A) in many bivalve taxa (e.g., Schöne et al., 2013; Otter et al., 2019; Höche et al., 2020). This complex architecture is often reflected by differences in shell element chemistry

(e.g., Shirai et al., 2008; Foster et al., 2009; Lazareth et al., 2013; Füllenbach et al., 2017; Marali et al., 2017; Roger et al., 2017) and needs to be considered when developing Ele/Ca-based proxies.

The architecture of bivalve shells is further characterized by growth patterns (i.e., internal growth bands; Fig. 1.1A), which not only provide a blueprint for temporal alignment of the proxy record but also capture the circumstances under which they were formed. Each growth band consists of a growth increment, deposited when shell accretion is the most active (Lutz and Rhoads, 1977; Louis et al., 2022), typically when local conditions promote shell growth (e.g., species-specific optimal temperature, adequate food availability; Ballesta-Artero et al., 2018; Killam and Clapham, 2018); followed by a growth line (Clark, 1968, 1974), marking reduced growth (Lutz and Rhoads, 1977) and typically corresponding to recurring events (e.g., winter, nightfall, tidal emersion; Hallman et al., 2009; Sano et al., 2012) that can temporarily sharply reduce biomineralization rate. Shell growth patterns can, for instance, serve as indicators of acute stress events (e.g., disturbance lines caused by heatwaves, cold spells and hypoxia; Clark, 1974; Kennish and Olsson, 1975; Höche et al., 2023) and records of the animal ontogenetic history (e.g., progressively narrower increments in mature specimens as energy is reallocated toward maintenance and gamete production instead of shell growth; Jones, 1980; Thompson et al., 1980; Schöne, 2008). The width, shape and ultrastructural properties of growth lines and increments can be measured in bivalve shells and further inform the interpretation of proxy records preserved in these archives.

The ultrastructure of bivalve shells refers to their spatial organization at the sub-micrometer scale, based on the arrangement of individual biomineral units (BMUs), i.e., the carbonate aggregates arranged within an organic matrix which forms the shell ultrastructure in bivalves (Bevelander and Nakahara, 1980; Jones, 1983; Levi-Kalisman et al., 2001; Höche et al., 2020). The morphology of these BMUs (e.g., size, elongation, shape, orientation) varies considerably within different portions of the shell (Höche et al., 2020, 2022) and influences the shell mechanical properties (e.g., hardness, fracture toughness, compressive strength; Li et al., 2017). Ultrastructural organization patterns recur across individuals and species of bivalve mollusks (Clark et al., 2020), allowing the characterization of distinct ultrastructure types. While many different types occur depending on the bivalve taxon and its phylogenetic history (Carter and Clark, 1985; Clark et al., 2020), only the four types of aragonitic ultrastructures investigated for the purpose of this thesis are described hereafter.

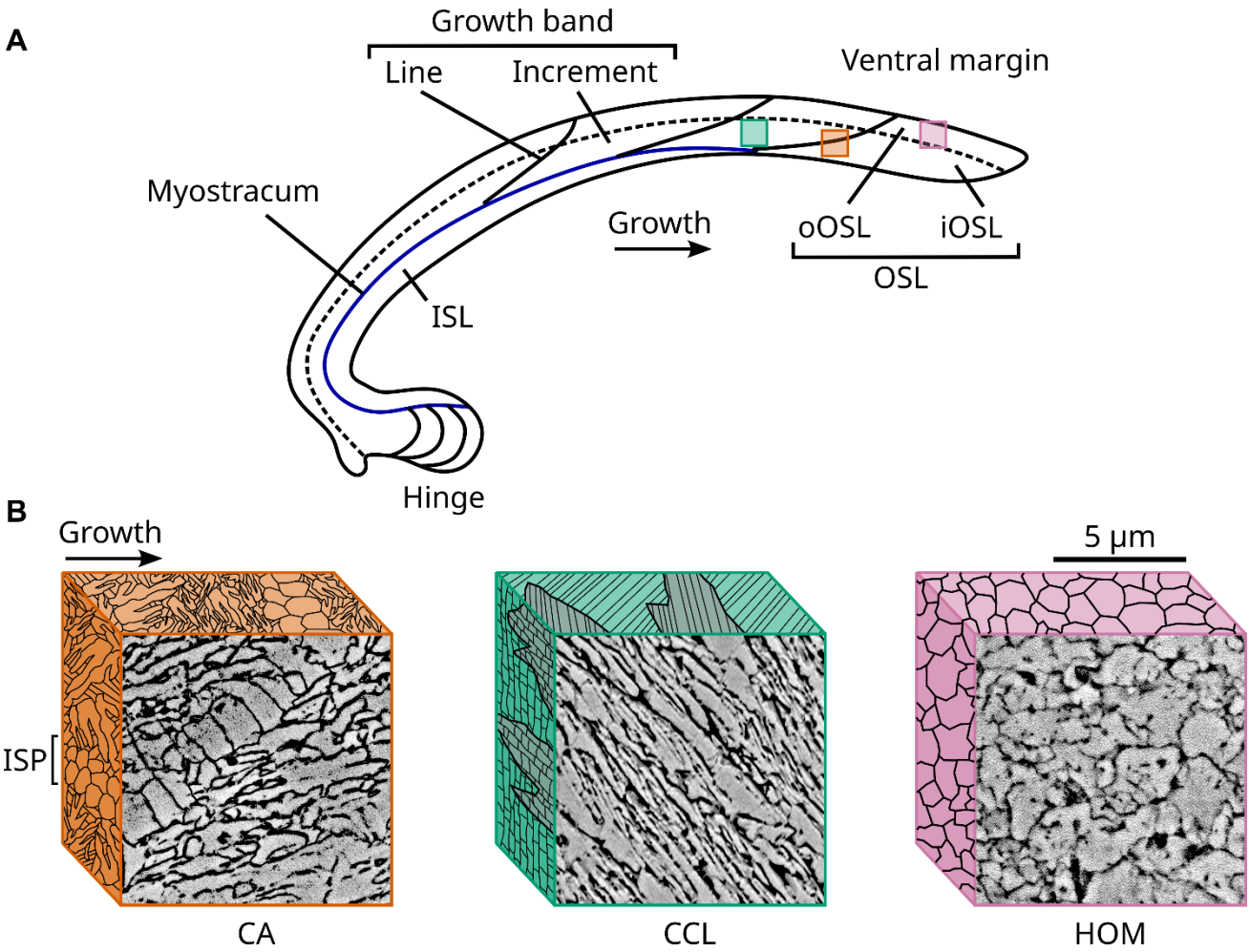

Figure 1.1 Sketches of internal bivalve shell architecture and ultrastructure types. (A) Schematic cross-section of a bivalve shell illustrating its internal architecture. The shell is composed of an outer shell layer (OSL) and an inner shell layer (ISL), separated by the myostracum (blue). The OSL is often subdivided into ultrastructurally distinct outer and inner portions (oOSL and iOSL, respectively). Each growth band consists of a growth line and an increment. The relative position of each structure shown in (B) is indicated within the shell in (A) using the corresponding color. (B) SEM images and schematic three-dimensional representations of the aragonitic shell ultrastructure types studied in this thesis. The irregular simple prismatic ultrastructure (ISP; orange block) consists of elongated prisms with uniform orientation and typically forms the myostracum and periodic growth lines. The complex crossed-lamellar ultrastructure (CCL; green block) presents a hierarchical arrangement of aragonitic lamellae on three levels and forms the primary structure in many taxa. The crossed-acicular ultrastructure (CA; orange block), found in the iOSL of many bivalves, is composed of needle-shaped biomineral units (BMUs) intersecting at steep angles. The homogeneous ultrastructure (HOM; pink block) consists of tightly packed and round granular units without higher-order organization, typically observed in the oOSL alongside the CA-dominated iOSL. Scale and growth direction apply to all SEM images.

The irregular simple prismatic ultrastructure (ISP; Fig. 1.1B) belongs to the broader category of prismatic structures and consists of elongated BMUs typically aligned perpendicularly or obliquely to the shell surface, embedded within organic matrices (Bøggild, 1930; Nakahara and Bevelander, 1971; Checa et al., 2014). These BMUs are often visualized within

the shell as relatively large prisms measuring tens of micrometers in diameter (Checa, 2018) that can extend continuously for several hundreds of micrometers in length (Cuif et al., 2020). Each prism generally exhibits a uniform internal orientation and lacks further hierarchical organization. In nearly all bivalve species, the periodic growth lines and the myostracum consist of ISP (Jones, 1980; Thompson et al., 1980; Ropes et al., 1984). In contrast, shell growth increments are largely composed of more complex arrangements. Namely, crossed-lamellar ultrastructures, present in over 90 % of bivalve taxa (Almagro et al., 2016), compose the primary shell structure in many aragonitic species. The complex crossed-lamellar ultrastructure (CCL; Fig. 1.1B) is an intricate variant of this category which consists of a complex hierarchical arrangement of aragonitic lamellae at three levels (Kobayashi and Akai, 1994; Almagro et al., 2016; Agbaje et al., 2017; Li et al., 2017). The BMUs of CCL consist of elongated, rod-shaped crystallites (third-order lamellae) grouped into thin, parallel sheets (second-order lamellae), which are stacked to form broader bands (first-order lamellae; Agbaje et al., 2017). These bands are oriented in at least three distinct directions that vary throughout shell growth (Almagro et al., 2016; Agbaje et al., 2017), producing irregular block-shaped structures visible in scanning electron microscopy (SEM). The hierarchical organization of CCL contributes to the shell mechanical properties by dispersing stress into various directions (Agbaje et al., 2017). In comparison, the crossed-acicular ultrastructure (CA; Fig. 1.1B), which also occurs in many bivalve species where it typically forms the iOSL, lacks such high-order organization. CA consists of elongated, needle-shaped BMUs arranged in two directions that intersect at steep angles within the growth plane of the shell (Carter, 1980; Carter and Clark, 1985). Each BMU in CA is composed of co-oriented crystallites (Carter and Clark, 1985; Karney et al., 2012), with their long morphological axis – corresponding to their crystallographic *c*-axis in this context – typically oriented perpendicularly to the shell surface and aligned with the growth plane (Carter et al., 2012). Frequently observed alongside CA, the homogeneous ultrastructure (HOM; Fig. 1.1B) often composes the outermost portion of the shell (oOSL; e.g., Harper et al., 2009; Sato and Sasaki, 2015; Höche et al., 2022, 2023). HOM consists of densely arranged aragonitic granular structures visible in SEM (Fig. 1.1B), but lacks discernible organization in optical microcopy (i.e., appears structurally homogeneous; Carter et al., 2012). The BMUs of HOM are typically uniform and round, each built from small, needle-shaped crystallites with a consistent orientation (Bøggild, 1930; Dunca et al., 2009; Carter et al., 2012), but without any higher order arrangement. HOM is observed in several aragonitic bivalve species and forms a rigid shell framework (Mu et al., 2018).

The heterogeneous distributions of Sr/Ca within aragonitic bivalve shells, i.e., through lifetime and across ultrastructurally distinct layers, unlikely result from external forcing alone. Some studies have reported consistent differences in shell Sr/Ca averages not only between the inner and outer portions of the shell (i.e., oOSL and iOSL; Foster et al., 2009; Lazareth et al., 2013),

but also between adjacent growth lines and increments (Schöne et al., 2010; Füllenbach et al., 2017), as well as within portions dominated by a single ultrastructure type (Schöne et al., 2011; Marali et al., 2017). Sr/Ca variability therefore appears to be reflected within the shell architecture and ultrastructure. This suggests that Sr^{2+} incorporation is strongly influenced by the carbonate material structure or is affected by underlying processes similar to those controlling ultrastructural development, rather than solely reflecting ambient temperatures through thermodynamic partitioning. Several ultrastructure-dependent parameters may explain the Sr/Ca patterns often reported in bivalve shells, with higher ratios in growth lines, intermediate values in the oOSL and lower levels in the iOSL (Schöne et al., 2010, 2011; Lazareth et al., 2013; Marali et al., 2017; Chamberlayne et al., 2020). Specifically, the efficiency of Sr^{2+} substitution into the aragonite lattice is controlled by kinetic factors related to the crystal growth rate and orientation (Watson, 1996, 2004; Gaetani and Cohen, 2006), the effective surface area available for ion exchange (Menadakis et al., 2008; Kawano et al., 2015) and the composition of organic material within and between individual BMUs (Schöne et al., 2013; Shirai et al., 2014; Roger et al., 2017), all of which differ substantially between ultrastructure types. For example, localized strontium incorporation may be facilitated at growth lines by the well-developed crystal faces and uniform orientation of ISP (Fig. 1.1B; Menadakis et al., 2008; Kawano et al., 2015). In contrast, less exposed crystal faces in the compact granular BMUs of HOM and the densely interwoven lamellae of CA (Fig. 1.1B) likely limit Sr incorporation (Menadakis et al., 2008; Kawano et al., 2015). Since BMU morphology varies both between and within ultrastructure types and is thought to respond to environmental fluctuations (Höche et al., 2020, 2022, 2023), the shell Sr/Ca signature likely reflects factors intrinsic to the shell ultrastructure. Consequently, Sr/Ca profiles preserved in aragonitic bivalve shells may partly reflect architectural and ultrastructural influences, and partly the thermodynamic response of strontium partitioning to variations in ambient seawater temperature.

1.4 Motivation and aim of the research

This thesis investigates whether the trace and minor elemental composition of marine bivalve shells enables reliable environmental reconstructions when shell structural variability is accounted for. The relationship between Sr/Ca and ambient temperature in bivalve shells, so far, remains ambiguous and is often confounded by kinetics and physiological mechanisms (e.g., Dodd, 1965; Gillikin et al., 2005b; Carré et al., 2006; Freitas et al., 2009; Poulain et al., 2015). Hence, the precision of the Sr/Ca-thermometer might be significantly improved by considering the ultrastructural organization of the shells. Previous studies have reported substantial heterogeneity in Sr/Ca values across shells (Schöne et al., 2011; Marali et al., 2017), as well as

between shell layers (Foster et al., 2009; Lazareth et al., 2013) and periodic growth features (Schöne et al., 2010; Füllenbach et al., 2017). Similarly, the ultrastructural properties of these shells vary during the life of the mollusk (Füllenbach et al., 2017; Höche et al., 2020, 2022) and typically align with the architecture of the shell (i.e., shells layers and growth patterns). However, the extent to which ultrastructural variability influences Sr^{2+} incorporation in marine bivalve shells remains unclear. Previous studies either disregarded shell architecture altogether or focused on Sr/Ca from individual shell layers while overlooking their internal BMU morphology or that of periodic growth features (i.e., growth increments and lines). Considering these aspects is essential to determine whether Sr/Ca is influenced by the shell structural properties, and whether such bias can be disentangled from the environmental signal that shell Sr/Ca profiles are thought to contain.

For this purpose, shell Sr/Ca ratios, growth patterns and structural properties (architecture and ultrastructure) were examined in specimens of two long-lived aragonitic bivalve species, i.e., the boreal *Arctica islandica* and the tropical *Tridacna squamosa*. Both species were selected for their complementary relevance to this study, as they present various ultrastructure types (ISP, CCL, CA and HOM; Fig. 1.1B) and are frequently investigated in sclerochronology, with *A. islandica* providing extended annual records (e.g., Schöne et al., 2004; Wanamaker et al., 2008b; Butler et al., 2013; Reynolds et al., 2017) and *T. squamosa* enabling high-resolution analyses (e.g., Yan et al., 2013; Hori et al., 2015; Arias-Ruiz et al., 2017; Komagoe et al., 2018). Element chemical data were acquired using LA-ICP-MS and NanoSIMS while high-resolution SEM images were used for identification of the shell structural framework and BMU morphometry. The results of this thesis were published in three peer-reviewed international journals, each manuscript addressing a distinct aspect of ultrastructural bias on Sr/Ca-thermometry in bivalve shells.

Manuscript 1 presents a detailed examination of the link between Sr/Ca ratios from field-grown bivalve shells and seasonal variations of temperature while accounting for shell ultrastructural and growth-rate related influences. This study focuses on *A. islandica*, a species extensively employed in sclerochronology due to its exceptionally long lifespan (Schöne et al., 2005a; Wanamaker et al., 2008b; Butler et al., 2013), broad distribution across the North Atlantic (Nicol, 1951) and clearly defined annual growth bands (Thompson et al., 1980; Ropes et al., 1984). The aragonitic shell of *A. islandica* is particularly well-suited for investigating ultrastructure-related Sr/Ca variability, as substantial differences in Sr/Ca levels between OSL sub-layers have been reported (Schöne et al., 2013). In this species, the oOSL is dominated by HOM while the iOSL is primarily composed of CA (Fig. 1.1; Höche et al., 2022), providing an ideal framework for evaluating the structural contribution relative to the observed geochemical patterns. Juvenile specimens were selected for analysis due to elevated growth rates in early ontogeny (Jones, 1980;

Thompson et al., 1980; Schöne, 2008), resulting in relatively wide increments suitable for high-resolution sampling. Shell Sr/Ca molar ratios were acquired using LA-ICP-MS, and corresponding ultrastructural properties were quantified from high-resolution SEM images. Ultrastructure and growth-rate related influences were isolated from the shell Sr/Ca profiles, and the residual signal was then compared to seasonal variation in local seawater temperature. This study revealed a weak correlation between shell Sr/Ca and seasonal temperature, which only slightly strengthened after the hypothesized biases were confirmed and accounted for, likely due to additional external drivers.

Manuscript 2 builds on these findings and investigates the shell Sr/Ca-temperature relationship in juvenile *A. islandica* specimens grown under controlled laboratory conditions. Specimens were cultured in aquaria maintained at fixed temperature regimes (1, 3, 6, 9, 10.3, 12 and 15 °C), minimizing environmental forcings other than temperature. The central hypothesis was that, under more equable conditions, shell Sr/Ca values would more reliably capture the ambient temperature, particularly when the signal is adjusted for potential growth rate and ultrastructural biases. Since BMU morphology is influenced by environmental conditions (Höche et al., 2022, 2023), lab-grown shells were expected to exhibit more uniform HOM and CA than their field-grown counterparts. Reduced ultrastructural variability would likely limit its influence on strontium incorporation and potentially facilitate the assessment of the Sr/Ca-temperature relationship. Shell element chemistry, growth rate and ultrastructural composition were analyzed according to the protocols of the previous study. Ultimately, transfer functions for temperature inference from shell Sr/Ca were calibrated for these lab-grown specimens and compared to those derived from field-grown shells.

Manuscript 3 further investigates the relationship between shell Sr/Ca and temperature at a much higher resolution than the previous manuscripts (i.e., sub-daily vs seasonal timescales). *T. squamosa* found in tropical reefs was selected as a representative of tridacnid bivalves, a taxon of long-lived species that has demonstrated significant sclerochronological value over decades of research. Owing to their large size (Rosewater, 1965), rapid growth in early ontogeny (Lucas et al., 1989; Van Wynsberge et al., 2017) and ultrastructurally distinct features (Agbaje et al., 2017), tridacnids are particularly well-suited for high-resolution analyses and ideal for the aims of this study. Specifically, the driver of Sr/Ca variability in tridacnid shells at sub-daily resolution remains a matter of debate. Previous studies have reported diurnal Sr/Ca cycles (Sano et al., 2012; Warter et al., 2018) and attributed shell Sr/Ca control to either temperature fluctuation (Elliot et al., 2009; Yan et al., 2013; Liu et al., 2021), light availability (Sano et al., 2012) or endogenous biological rhythms (Warter et al., 2018). To address this ambiguity, analyses were conducted within the iOSL of *T. squamosa* by comparing sub-daily data measured in daily growth lines and increments, each dominated by CCL and ISP, respectively (Fig. 1.1; Agbaje et al., 2017).

Shell Sr/Ca ratios were acquired using NanoSIMS while ultrastructural properties were quantified from SEM images using an adapted procedure developed for shells exhibiting CCL (*Glycymeris bimaculata*; Höche et al., 2020). For sub-daily non-linear temporal alignment of the data, a new semi-automated protocol was developed based on empirical activity patterns of *T. squamosa* (Killam et al., 2023) and its photosymbionts (Bonham, 1965; Rosewater, 1965; Griffiths and Klumpp, 1996), addressing potential bias from earlier studies that assumed linear growth (e.g., Yan et al., 2013). Sr/Ca-to-temperature transfer functions were then computed from shell Sr/Ca data at various resolutions after accounting for architectural and ultrastructural influences. Finally, the reconstructed temperature profiles were compared with local instrumental sea surface temperature (SST) records and the shell Sr/Ca-thermometer was evaluated in this context.

References

Abele, D., Brey, T., Philipp, E., 2009. Bivalve models of aging and the determination of molluscan lifespans. Exp. Gerontol. 44, 307–315.

Affek, H. P., 2012. Clumped isotope paleothermometry: Principles, applications, and challenges. Paleontol. Soc. Pap. 18, 101–114.

Agbaje, O. B. A., Wirth, R., Morales, L. F. G., Shirai, K., Kosnik, M., Watanabe, T., Jacob, D. E., 2017. Architecture of crossed-lamellar bivalve shells: The southern giant clam (*Tridacna derasa*, Röding, 1798). R. Soc. Open Sci. 4, 170622.

Allison, N., Finch, A. A., EIMF, 2010. δ^{11}B, Sr, Mg and B in a modern Porites coral: The relationship between calcification site pH and skeletal chemistry. Geochim. Cosmochim. Acta 74, 1790–1800.

Almagro, I., Drzymała, P., Berent, K., Sainz-Díaz, C. I., Willinger, M. G., Bonarski, J., Checa, A. G., 2016. New crystallographic relationships in biogenic aragonite: The crossed-lamellar microstructures of mollusks. Cryst. Growth Des. 16, 2083–2093.

Anderson, D. M., 2001. Attenuation of millennial-scale events by bioturbation in marine sediments. Paleoceanography 16, 352–357.

Arias-Ruiz, C., Elliot, M., Bézos, A., Pedoja, K., Husson, L., Cahyarini, S. Y., Cariou, E., Michel, E., La, C., Manssouri, F., 2017. Geochemical fingerprints of climate variation and the extreme La Niña 2010–11 as recorded in a *Tridacna squamosa* shell from Sulawesi, Indonesia. Palaeogeogr. Palaeoclimatol. Palaeoecol. 487, 216–228.

Arz, H. W., Pätzold, J., Wefer, G., 1999. Climatic changes during the last deglaciation recorded in sediment cores from the northeastern Brazilian Continental Margin. Geo-Mar. Lett. 19, 209–218.

Ballesta-Artero, I., Janssen, R., Van Der Meer, J., Witbaard, R., 2018. Interactive effects of temperature and food availability on the growth of *Arctica islandica* (Bivalvia) juveniles. Mar. Environ. Res. 133, 67–77.

Barats, A., Amouroux, D., Chauvaud, L., Pécheyran, C., Lorrain, A., Thébault, J., Church, T. M., Donard, O. F. X., 2009. High frequency barium profiles in shells of the great scallop *Pecten maximus*: A methodical long-term and multi-site survey in Western Europe. Biogeosciences 6, 157–170.

Bard, E., Miramont, C., Capano, M., Guibal, F., Marschal, C., Rostek, F., Tuna, T., Fagault, Y., Heaton, T. J., 2023. A radiocarbon spike at 14,300 cal yr BP in subfossil trees provides the impulse response function of the global carbon cycle during the Late Glacial. Philos. T. R. Soc. A. 381, 20220206.

Beck, J. W., Edwards, R. L., Ito, E., Taylor, F. W., Recy, J., Rougerie, F., Joannot, P., Henin, C., 1992. Sea-surface temperature from coral skeletal strontium/calcium ratios. Science 257, 644–647.

Bevelander, G., Nakahara, H., 1980. Compartment and envelope formation in the process of biological mineralization. In: The Mechanisms of Biomineralization in Animals and Plants. Eds. by M. Ōmori and N. Watabe Tokyo: Tokai University Press, 19–27.

Bigg, G. R., Jickells, T. D., Liss, P. S., Osborn, T. J., 2003. The role of the oceans in climate. Int. J. Climatol. 23, 1127–1159.

Black, B. A., Andersson, C., Butler, P. G., Carroll, M. L., DeLong, K. L., Reynolds, D. J., Schöne, B. R., Scourse, J., Van Der Sleen, P., Wanamaker, A. D., Witbaard, R., 2019. The revolution of crossdating in marine palaeoecology and palaeoclimatology. Biol. Lett. 15, 20180665.

Bøggild, O. B., 1930. The Shell Structure of the Molluscs. Vol. 9.2, 231. Copenhagen, Denmark: Det Kongelige Danske Videnskabernes Selskabs Skrifter. Naturvidenskabelig og Mathematisk Afdeling.

Bond, G., Broecker, W., Johnsen, S., McManus, J., Labeyrie, L., Jouzel, J., Bonani, G., 1993. Correlations between climate records from North Atlantic sediments and Greenland ice. Nature 365, 143–147.

Bonham, K., 1965. Growth rate of giant clam *Tridacna gigas* at Bikini Atoll as revealed by radioautography. Science 149, 300–302.

Briffa, K. R., 2000. Annual climate variability in the Holocene: Interpreting the message of ancient trees. Quat. Sci. Rev. 19, 87–105.

Budyko, M. I., 1969. The effect of solar radiation variations on the climate of the Earth. Tellus A Dyn. Meteorol. Oceanogr. 21, 611.

Butler, P. G., Wanamaker, A. D., Scourse, J. D., Richardson, C. A., Reynolds, D. J., 2013. Variability of marine climate on the North Icelandic Shelf in a 1357-year proxy archive based on growth increments in the bivalve *Arctica islandica*. Palaeogeogr. Palaeoclimatol. Palaeoecol. 373, 141–151.

Butler, P. G., Schöne, B. R., 2017. New research in the methods and applications of sclerochronology. Palaeogeogr. Palaeoclimatol. Palaeoecol. 465, 295–299.

C3S, 2025. ERA5 hourly data on single levels from 1940 to present. Copernicus Climate Change Service (C3S), Climate Data Store (CDS).

Cameron, L. P., Reymond, C. E., Müller-Lundin, F., Westfield, I., Grabowski, J. H., Westphal, H., Ries, J. B., 2019. Effects of temperature and ocean acidification on the extrapallial fluid pH, calcification rate, and condition factor of the king scallop *Pecten maximus*. J. Shellfish Res. 38, 763–777.

Cameron, L. P., Grabowski, J. H., Ries, J. B., 2022. Effects of elevated pCO_2 and temperature on the calcification rate, survival, extrapallial fluid chemistry, and respiration of the Atlantic Sea scallop *Placopecten magellanicus*. Limnol. Oceanogr 67, 1670–1686.

Carré, M., Bentaleb, I., Bruguier, O., Ordinola, E., Barrett, N. T., Fontugne, M., 2006. Calcification rate influence on trace element concentrations in aragonitic bivalve shells: Evidences and mechanisms. Geochim. Cosmochim. Acta 70, 4906–4920.

Carter, J. G., 1980. Selected mineralogical data for the Bivalvia. In: Skeletal Growth of Aquatic Organisms: Biological Records of Environmental Change. Eds. by D. C. Rhoads and R. A. Lutz New York: Plenum Press, 627–631.

Carter, J. G., Harries, P. J., Malchus, N., Sartori, A. F., Anderson, L. C., Bieler, R., Bogan, A. E., Coan, E. V., Cope, J. C. W., Cragg, S. M., García-March, J. R., Hylleberg, J., Kelley, P., Kleemann, K., Kříž, J., McRoberts, C. A., Mikkelsen, P. M., Pojeta Jr., J., Tëmkin, I., Yancey, T., Zieritz, A., 2012. Part N, revised, volume 1, chapter 31: Illustrated glossary of the Bivalvia. Treatise Online 48, 1–209.

Carter, J. G., Clark, G. R., 1985. Classification and phylogenetic significance of molluscan shell microstructure. Stud. Geol. (Knoxville) 13, 50–71.

Chamberlayne, B. K., Tyler, J. J., Gillanders, B. M., 2020. Environmental controls on the geochemistry of a short-lived bivalve in southeastern australian estuaries. Estuar. Coasts 43, 86–101.

Chauvaud, L., Thouzeau, G., Paulet, Y.-M., 1998. Effects of environmental factors on the daily growth rate of *Pecten maximus* juveniles in the Bay of Brest (France). J. Exp. Mar. Biol. Ecol. 227, 83–111.

Checa, A. G., Salas, C., Harper, E. M., Bueno-Pérez, J. de D., 2014. Early stage biomineralization in the periostracum of the 'living fossil' bivalve *Neotrigonia*. PLoS One 9, 1–17.

Checa, A. G., 2018. Physical and biological determinants of the fabrication of molluscan shell microstructures. Front. Mar. Sci. 5, 353.

Clark, G. R., 1974. Growth lines in invertebrate skeletons. Annu. Rev. Earth Planet. Sci. 2, 77–99.

Clark, G. R., 1980. Study of molluscan shell structure and growth lines using thin sections. In: Skeletal Growth of Aquatic Organisms: Biological Records of Environmental Change. Eds. by R. A. Lutz and D. C. Rhoads New York: Plenum Press, 603–606.

Clark, G. R., 1968. Mollusk shell: Daily growth lines. Science 161, 800–802.

Clark, J. V., Pérez-Huerta, A., Gillikin, D. P., Aldridge, A. E., Reolid, M., Endo, K., 2016. Determination of paleoseasonality of fossil brachiopods using shell spiral deviations and chemical proxies. Palaeoworld 25, 662–674.

Clark, M. S., Peck, L. S., Arivalagan, J., Backeljau, T., Berland, S., Cardoso, J. C. R., Caurcel, C., Chapelle, G., De Noia, M., Dupont, S., Gharbi, K., Hoffman, J. I., Last, K. S., Marie, A., Melzner, F., Michalek, K., Morris, J., Power, D. M., Ramesh, K., Sanders, T., Sillanpää, K., Sleight, V. A., Stewart-Sinclair, P. J., Sundell, K., Telesca, L., Vendrami, D. L. J., Ventura, A., Wilding, T. A., Yarra, T., Harper, E. M., 2020. Deciphering mollusc shell production: The roles of genetic mechanisms through to ecology, aquaculture and biomimetics. Biol. Rev. 95, 1812–1837.

Clemens, S., 2006. Extending the historical record by proxy. In: The Asian Monsoon. Springer Berlin Heidelberg, 615–630.

Cléroux, C., Cortijo, E., Anand, P., Labeyrie, L., Bassinot, F., Caillon, N., Duplessy, J., 2008. Mg/Ca and Sr/Ca ratios in planktonic foraminifera: Proxies for upper water column temperature reconstruction. Paleoceanography 23, 2007PA001505.

Cobb, K. M., Charles, C. D., Cheng, H., Edwards, R. L., 2003. El Niño/Southern Oscillation and tropical Pacific climate during the last millennium. Nature 424, 271–276.

Columbu, A., Chiarini, V., Spötl, C., Benazzi, S., Hellstrom, J., Cheng, H., De Waele, J., 2020. Speleothem record attests to stable environmental conditions during Neanderthal–modern human turnover in southern Italy. Nat. Ecol. Evol. 4, 1188–1195.

Corrège, T., 2006. Sea surface temperature and salinity reconstruction from coral geochemical tracers. Palaeogeogr. Palaeoclimatol. Palaeoecol. 232, 408–428.

Crame, J. A., 2000. Evolution of taxonomic diversity gradients in the marine realm: Evidence from the composition of recent bivalve faunas. Paleobiology 26, 188–214.

Crenshaw, M. A., 1972. The inorganic composition of molluscan extrapallial fluid. Biol. Bull. 143, 506–512.

Cuif, J.-P., Belhadj, O., Borensztajn, S., Gèze, M., Trigos-Santos, S., Prado, P., Dauphin, Y., 2020. Prism substructures in the shell of *Pinna nobilis* (Linnaeus, 1758), Mollusca – Evidence for a three-dimensional pulsed-growth model. Heliyon 6, e04513.

Curley, A. N., Petersen, S. V., Edie, S. M., Guo, W., 2023. Biologically driven isotopic fractionations in bivalves: From palaeoenvironmental problem to palaeophysiological proxy. Biological Reviews 98, 1016–1032.

Dansgaard, W., Johnsen, S. J., Clausen, H. B., Dahl-Jensen, D., Gundestrup, N. S., Hammer, C. U., Hvidberg, C. S., Steffensen, J. P., Sveinbjörnsdottir, A. E., Jouzel, J., Bond, G., 1993. Evidence for general instability of past climate from a 250-kyr ice-core record. Nature 364, 218–220.

De Winter, N. J., Müller, I. A., Kocken, I. J., Thibault, N., Ullmann, C. V., Farnsworth, A., Lunt, D. J., Claeys, P., Ziegler, M., 2021. Absolute seasonal temperature estimates from clumped isotopes in bivalve shells suggest warm and variable greenhouse climate. Commun. Earth Environ. 2, 121.

De Winter, N. J., Tindall, J., Johnson, A. L. A., Goudsmit-Harzevoort, B., Wichern, N., Kaskes, P., Claeys, P., Huygen, F., Van Leeuwen, S., Metcalfe, B., Bakker, P., Goolaerts, S., Wesselingh, F., Ziegler, M., 2024. Amplified seasonality in western Europe in a warmer world. Sci. Adv. 10, eadl6717.

DeLong, K. L., Quinn, T. M., Taylor, F. W., Shen, C.-C., Lin, K., 2013. Improving coral-base paleoclimate reconstructions by replicating 350 years of coral Sr/Ca variations. Palaeogeogr. Palaeoclimatol. Palaeoecol. 373, 6–24.

Dettman, D. L., Reische, A. K., Lohmann, K. C., 1999. Controls on the stable isotope composition of seasonal growth bands in aragonitic fresh-water bivalves (unionidae). Geochim. Cosmochim. Acta 63, 1049–1057.

Diaz, H. F., Hoerling, M. P., Eischeid, J. K., 2001. ENSO variability, teleconnections and climate change. Int. J. Climatol. 21, 1845–1862.

Dodd, J. R., 1967. Magnesium and strontium in calcareous skeletons: A review. J. Paleontol. 41, 1313–1329.

Dodd, J. R., Crisp, E. L., 1982. Non-linear variation with salinity of Sr/Ca and Mg/Ca ratios in water and aragonitic bivalve shells and implications for paleosalinity studies. Palaeogeogr. Palaeoclimatol. Palaeoecol. 38, 45–56.

Dodd, J. R., 1965. Environmental control of strontium and magnesium in *Mytilus*. Geochim. Cosmochim. Acta 29, 385–398.

D'Olivo, J. P., McCulloch, M. T., 2017. Response of coral calcification and calcifying fluid composition to thermally induced bleaching stress. Sci. Rep. 7, 2207.

Dunca, E., Mutvei, H., Göransson, P., Mörth, C.-M., Schöne, B. R., Whitehouse, M. J., Elfman, M., Baden, S. P., 2009. Using ocean quahog (*Arctica islandica*) shells to reconstruct palaeoenvironment in Öresund, Kattegat and Skagerrak, Sweden. Int. J. Earth Sci. 98, 3–17.

Edge, D. C., Reynolds, D. J., Wanamaker, A. D., Griffin, D., Bureau, D., Outridge, C., Stevick, B. C., Weng, R., Black, B. A., 2021. A multicentennial proxy record of Northeast Pacific sea surface semperatures from the annual growth increments of *Panopea generosa*. Paleoceanogr. Paleoclimatol. 36, e2021PA004291.

Eiler, J. M., 2007. "Clumped-isotope" geochemistry – The study of naturally-occurring, multiply-substituted isotopologues. Earth Planet. Sci. Lett. 262, 309–327.

Eiler, J. M., 2011. Paleoclimate reconstruction using carbonate clumped isotope thermometry. Quat. Sci. Rev. 30, 3575–3588.

Elliot, M., Welsh, K., Chilcott, C., McCulloch, M., Chappell, J., Ayling, B., 2009. Profiles of trace elements and stable isotopes derived from giant long-lived *Tridacna gigas* bivalves: Potential applications in paleoclimate studies. Palaeogeogr. Palaeoclimatol. Palaeoecol. 280, 132–142.

Epstein, S., Buchsbaum, R., Lowenstam, H. A., Urey, H. C., 1953. Revised carbonate-water isotopic temperature scale. Geol. Soc. America Bull. 64, 1315.

Erler, D. V., Wang, X. T., Sigman, D. M., Scheffers, S. R., Martínez-García, A., Haug, G. H., 2016. Nitrogen isotopic composition of organic matter from a 168 year-old coral skeleton: Implications for coastal nutrient cycling in the Great Barrier Reef Lagoon. Earth Planet. Sci. Lett. 434, 161–170.

Evans, D., Brierley, C., Raymo, M. E., Erez, J., Müller, W., 2016. Planktic foraminifera shell chemistry response to seawater chemistry: Pliocene–Pleistocene seawater Mg/Ca, temperature and sea level change. Earth Planet. Sci. Lett. 438, 139–148.

Evans, J. W., 1972. Tidal Growth Increments in the Cockle *Clinocardium nuttalli*. Science 176, 416–417.

Fairchild, I. J., Smith, C. L., Baker, A., Fuller, L., Spötl, C., Mattey, D., McDermott, F., E.I.M.F., 2006. Modification and preservation of environmental signals in speleothems. Earth-Sci. Rev. 75, 105–153.

Fernandez, A., Müller, I. A., Rodríguez-Sanz, L., Van Dijk, J., Looser, N., Bernasconi, S. M., 2017. A reassessment of the precision of carbonate clumped isotope measurements: Implications

for calibrations and paleoclimate reconstructions. Geochem. Geophys. Geosyst. 18, 4375–4386.

Fiebig, J., Hofmann, S., Löffler, N., Lüdecke, T., Methner, K., Wacker, U., 2016. Slight pressure imbalances can affect accuracy and precision of dual inlet-based clumped isotope analysis. Isot. Environ. Healt. S. 52, 12–28.

Flessa, K. W., Jablonski, D., 1995. Biogeography of recent marine bivalve molluscs and its implications for paleobiogeography and the geography of extinction: A progress report. Hist. Biol. 10, 25–47.

Foley, J. A., DeFries, R., Asner, G. P., Barford, C., Bonan, G., Carpenter, S. R., Chapin, F. S., Coe, M. T., Daily, G. C., Gibbs, H. K., Helkowski, J. H., Holloway, T., Howard, E. A., Kucharik, C. J., Monfreda, C., Patz, J. A., Prentice, I. C., Ramankutty, N., Snyder, P. K., 2005. Global consequences of land use. Science 309, 570–574.

Forster, P. M., Smith, C. J., Walsh, T., Lamb, W. F., Lamboll, R., Hauser, M., Ribes, A., Rosen, D., Gillett, N., Palmer, M. D., Rogelj, J., Von Schuckmann, K., Seneviratne, S. I., Trewin, B., Zhang, X., Allen, M., Andrew, R., Birt, A., Borger, A., Boyer, T., Broersma, J. A., Cheng, L., Dentener, F., Friedlingstein, P., Gutiérrez, J. M., Gütschow, J., Hall, B., Ishii, M., Jenkins, S., Lan, X., Lee, J.-Y., Morice, C., Kadow, C., Kennedy, J., Killick, R., Minx, J. C., Naik, V., Peters, G. P., Pirani, A., Pongratz, J., Schleussner, C.-F., Szopa, S., Thorne, P., Rohde, R., Rojas Corradi, M., Schumacher, D., Vose, R., Zickfeld, K., Masson-Delmotte, V., Zhai, P., 2023. Indicators of Global Climate Change 2022: Annual update of large-scale indicators of the state of the climate system and human influence. Earth Syst. Sci. Data 15, 2295–2327.

Foster, L. C., Allison, N., Finch, A. A., Andersson, C., 2009. Strontium distribution in the shell of the aragonite bivalve *Arctica islandica*. Geochem. Geophys. Geosyst. 10, 1–14.

Fraiser, M. L., Bottjer, D. J., 2007. When bivalves took over the world. Paleobiology 33, 397–413.

Freitas, P. S., Clarke, L. J., Kennedy, H., Richardson, C. A., 2009. Ion microprobe assessment of the heterogeneity of Mg/Ca, Sr/Ca and Mn/Ca ratios in *Pecten maximus* and *Mytilus edulis* (Bivalvia) shell calcite precipitated at constant temperature. Biogeosciences 6, 1209–1227.

Frieder, C. A., Gonzalez, J. P., Levin, L. A., 2014. Uranium in larval shells as a barometer of molluscan ocean acidification exposure. Environ. Sci. Technol. 48, 6401–6408.

Fritts, H. C., 1971. Dendroclimatology and dendroecology. Quat. Res. 1, 419–449.

Fröhlich, L., Siebert, V., Walliser, E. O., Thébault, J., Jochum, K. P., Chauvaud, L., Schöne, B. R., 2022a. Ba/Ca profiles in shells of *Pecten maximus* – A proxy for specific primary producers rather than bulk phytoplankton. Chem. Geol. 593, 120743.

Fröhlich, L., Siebert, V., Huang, Q., Thébault, J., Jochum, K. P., Schöne, B. R., 2022b. Deciphering the potential of Ba/Ca, Mo/Ca and Li/Ca profiles in the bivalve shell *Pecten maximus* as proxies for the reconstruction of phytoplankton dynamics. Ecol. Indic. 141, 109121.

Fröhlich, L., Siebert, V., Huang, Q., Thébault, J., Moriceau, B., Jochum, K. P., Schöne, B. R., 2023. Uptake of barium, molybdenum, and lithium and incorporation into scallop shells: Refining proxies for primary production dynamics. Limnol. Oceanogr. 68, 2544–2561.

Füllenbach, C. S., Schöne, B. R., Shirai, K., Takahata, N., Ishida, A., Sano, Y., 2017. Minute co-variations of Sr/Ca ratios and microstructures in the aragonitic shell of *Cerastoderma edule* (Bivalvia) – Are geochemical variations at the ultra-scale masking potential environmental signals? Geochim. Cosmochim. Acta 205, 256–271.

Gaetani, G. A., Cohen, A. L., 2006. Element partitioning during precipitation of aragonite from seawater: A framework for understanding paleoproxies. Geochim. Cosmochim. Acta 70, 4617–4634.

Gagnon, A. C., Adkins, J. F., Erez, J., 2012. Seawater transport during coral biomineralization. Earth Planet. Sci. Lett. 329–330, 150–161.

Gholami, V., Chau, K. W., Fadaee, F., Torkaman, J., Ghaffari, A., 2015. Modeling of groundwater level fluctuations using dendrochronology in alluvial aquifers. J. Hydrol. 529, 1060–1069.

Gillett, N. P., Graf, H. F., Osborn, T. J., 2003. Climate change and the North Atlantic Oscillation. In: Geophysical Monograph Series. Eds. by J. W. Hurrell, Y. Kushnir, G. Ottersen, and M. Visbeck Washington, D. C.: American Geophysical Union, 193–209.

Gillikin, D. P., Dehairs, F., Lorrain, A., Steenmans, D., Baeyens, W., André, L., 2006. Barium uptake into the shells of the common mussel (*Mytilus edulis*) and the potential for estuarine paleo-chemistry reconstruction. Geochim. Cosmochim. Acta 70, 395–407.

Gillikin, D. P., Wanamaker, A. D., Andrus, C. F. T., 2019. Chemical sclerochronology. Chem. Geol. 526, 1–6.

Gillikin, D. P., De Ridder, F., Ulens, H., Elskens, M., Keppens, E., Baeyens, W., Dehairs, F., 2005a. Assessing the reproducibility and reliability of estuarine bivalve shells (*Saxidomus giganteus*) for sea surface temperature reconstruction: Implications for paleoclimate studies. Palaeogeogr. Palaeoclimatol. Palaeoecol. 228, 70–85.

Gillikin, D. P., Lorrain, A., Navez, J., Taylor, J. W., André, L., Keppens, E., Baeyens, W., Dehairs, F., 2005b. Strong biological controls on Sr/Ca ratios in aragonitic marine bivalve shells. Geochem. Geophys. Geosyst. 6, Q05009.

Gonfiantini, R., Stichler, W., Rozanski, K., 1995. Standards and intercomparison materials distributed by the International Atomic Energy Agency for stable isotope measurements. International Atomic Energy Agency (IAEA).

Goodkin, N. F., Hughen, K. A., Cohen, A. L., 2007. A multicoral calibration method to approximate a universal equation relating Sr/Ca and growth rate to sea surface temperature. Paleoceanography 22, PA1214.

Gosling, E., 2003. Reproduction, settlement and recruitment. In: Bivalve Molluscs. Wiley, 131–168.

Griffiths, C., Klumpp, D., 1996. Relationships between size, mantle area and zooxanthellae numbers in five species of giant clam (Tridacnidae). Mar. Ecol. Prog. Ser. 137, 139–147.

Grossman, E. L., Ku, T.-L., 1986. Oxygen and carbon isotope fractionation in biogenic aragonite: Temperature effects. Chem. Geol. 59, 59–74.

Gruber, N., Bakker, D. C. E., DeVries, T., Gregor, L., Hauck, J., Landschützer, P., McKinley, G. A., Müller, J. D., 2023. Trends and variability in the ocean carbon sink. Nat. Rev. Earth Environ. 4, 119–134.

Hallmann, N., Burchell, M., Schöne, B. R., Irvine, G. V., Maxwell, D., 2009. High-resolution sclerochronological analysis of the bivalve mollusk *Saxidomus gigantea* from Alaska and British Columbia: Techniques for revealing environmental archives and archaeological seasonality. J. Archaeol. Sci. 36, 2353–2364.

Hansen, J., Lacis, A., Rind, D., Russell, G., Stone, P., Fung, I., Ruedy, R., Lerner, J., 1984. Climate sensitivity: Analysis of feedback mechanisms. In: Geophysical Monograph Series. Eds. by J. E. Hansen and T. Takahashi Washington, D. C.: American Geophysical Union, 130–163.

Harper, E. M., Checa, A. G., Rodríguez-Navarro, A. B., 2009. Organization and mode of secretion of the granular prismatic microstructure of *Entodesma navicula* (Bivalvia: Mollusca). Acta Zool. 90, 132–141.

Hegerl, G. C., Von Storch, H., Hasselmann, K., Santer, B. D., Cubasch, U., Jones, P. D., 1996. Detecting greenhouse-gas-induced climate change with an optimal fingerprint method. J. Clim. 9, 2281–2306.

Higgins, J. A., Kurbatov, A. V., Spaulding, N. E., Brook, E., Introne, D. S., Chimiak, L. M., Yan, Y., Mayewski, P. A., Bender, M. L., 2015. Atmospheric composition 1 million years ago from blue ice in the Allan Hills, Antarctica. Proc. Natl. Acad. Sci. U.S.A. 112, 6887–6891.

Höche, N., Peharda, M., Walliser, E. O., Schöne, B. R., 2020. Morphological variations of crossed-lamellar ultrastructures of *Glycymeris bimaculata* (Bivalvia) serve as a marine temperature proxy. Estuar. Coast. Shelf Sci. 237, 106658.

Höche, N., Walliser, E. O., Schöne, B. R., 2022. Microstructural mapping of *Arctica islandica* shells reveals environmental and physiological controls on biomineral size. Front. Earth Sci. 9, 781305.

Höche, N., Zettler, M. L., Huang, X., Schöne, B. R., 2023. Shell microstructures (disturbance lines) of *Arctica islandica* (Bivalvia): A potential proxy for severe oxygen depletion. Front. Mar. Sci. 10, 1219716.

Holland, H. A., Schöne, B. R., Marali, S., Jochum, K. P., 2014. History of bioavailable lead and iron in the Greater North Sea and Iceland during the last millennium – A bivalve sclerochronological reconstruction. Mar. Pollut. Bull. 87, 104–116.

Hori, M., Sano, Y., Ishida, A., Takahata, N., Shirai, K., Watanabe, T., 2015. Middle Holocene daily light cycle reconstructed from the strontium/calcium ratios of a fossil giant clam shell. Sci. Rep. 5, 8734.

Houghton, J. T., Ding, Y., Griggs, D. J., Noguer, M., van der Linden, P. J., Dai, X., Maskell, K., Johnson, C. A., 2001. Climate Change 2001: The Scientific Basis. Contribution of Working Group I to the Third Assessment Report of the Intergovernmental Panel on Climate Change. 1038. Cambridge, UK: Cambridge University Press.

Huang, X., Zhao, L., Zettler, M. L., Mertz-Kraus, R., Jochum, K. P., Schöne, B. R., 2023. High-resolution history of oxygen depletion in the SW Baltic Sea since the mid-19th century as revealed by bivalve shells. Sci. Total Environ. 888, 164011.

Hulme, M., Jones, P. D., 1994. Global climate change in the instrumental period. Environ. Pollut. 83, 23–36.

Huntington, K. W., Eiler, J. M., Affek, H. P., Guo, W., Bonifacie, M., Yeung, L. Y., Thiagarajan, N., Passey, B., Tripati, A., Daëron, M., Came, R., 2009. Methods and limitations of 'clumped' CO_2 isotope (Δ_{47}) analysis by gas-source isotope ratio mass spectrometry. J. Mass Spectrom. 44, 1318–1329.

IPCC, 2023. Climate change 2023: Synthesis report. Contribution of working groups I, II and III to the sixth assessment report of the Intergovernmental Panel on Climate Change [Core Writing Team, H. Lee and J. Romero (eds.)]. Intergovernmental Panel on Climate Change (IPCC) Geneva, Switzerland, 35–115.

Ishikawa, M., Ichikuni, M., 1984. Uptake of sodium and potassium by calcite. Chem. Geol. 42, 137–146.

Jablonski, D., Roy, K., Valentine, J. W., Price, R. M., Anderson, P. S., 2003. The impact of the Pull of the Recent on the history of marine diversity. Science 300, 1133–1135.

Jablonski, D., Belanger, C. L., Berke, S. K., Huang, S., Krug, A. Z., Roy, K., Tomasovych, A., Valentine, J. W., 2013. Out of the tropics, but how? Fossils, bridge species, and thermal ranges in the dynamics of the marine latitudinal diversity gradient. Proc. Natl. Acad. Sci. USA 110, 10487–10494.

Jones, D. S., 1980. Annual cycle of shell growth increment formation in two continental shelf bivalves and its paleoecologic significance. Paleobiology 6, 331–340.

Jones, D. S., Williams, D. F., Arthur, M. A., 1983. Growth history and ecology of the Atlantic surf clam, *Spisula solidissima* (Dillwyn), as revealed by stable isotopes and annual shell increments. J. Exp. Mar. Biol. Ecol. 73, 225–242.

Jones, D. S., 1983. Sclerochronology: Reading the record of the molluscan shell – Annual growth increments in the shells of bivalve molluscs record marine climatic changes and reveal surprising longevity. Am. Sci. 71, 384–391.

Jones, P. D., New, M., Parker, D. E., Martin, S., Rigor, I. G., 1999. Surface air temperature and its changes over the past 150 years. Rev. Geophys. 37, 173–199.

Jones, P. D., Osborn, T. J., Briffa, K. R., 2001. The evolution of climate over the last millennium. Science 292, 662–667.

Kageyama, M., Braconnot, P., Chiessi, C. M., Rehfeld, K., Ait Brahim, Y., Dütsch, M., Gwinneth, B., Hou, A., Loutre, M.-F., Hendrizan, M., Meissner, K., Mongwe, P., Otto-Bliesner, B., Pezzi, L. P., Rovere, A., Seltzer, A., Sime, L., Zhu, J., 2024. Lessons from paleoclimates for recent and future climate change: Opportunities and insights. Front. Clim. 6, 1511997.

Karl, T. R., Trenberth, K. E., 2003. Modern global climate change. Science 302, 1719–1723.

Karney, G. B., Butler, P. G., Speller, S., Scourse, J. D., Richardson, C. A., Schröder, M., Hughes, G. M., Czernuszka, J. T., Grovenor, C. R. M., 2012. Characterizing the microstructure of *Arctica islandica* shells using NanoSIMS and EBSD. Geochem. Geophys. Geosyst. 13, Q04002.

Kaufman, D. S., Broadman, E., 2023. Revisiting the Holocene global temperature conundrum. Nature 614, 425–435.

Kawano, J., Sakuma, H., Nagai, T., 2015. Incorporation of Mg^{2+} in surface Ca^{2+} sites of aragonite: An *ab initio* study. Prog. in Earth and Planet. Sci. 2, 7.

Kennish, M. J., Olsson, R. K., 1975. Effects of thermal discharges on the microstructural growth of *Mercenaria mercenaria*. Environ. Geol. 1, 41–64.

Khare, A., Hughes, H. P., Schijf, J., Kilbourne, K. H., 2023. Apparently seasonal variations of the seawater Sr/Ca ratio across the Florida Keys Reef Tract. Geochem. Geophys. Geosyst. 24, e2022GC010728.

Killam, D., Thompson, D., Morgan, K., Russell, M., 2023. Giant clams as open-source, scalable reef environmental biomonitors. PLoS ONE 18, e0278752.

Killam, D. E., Clapham, M. E., 2018. Identifying the ticks of bivalve shell clocks: Seasonal growth in relation to temperature and food supply. Palaios 33, 228–236.

Kobayashi, I., Akai, J., 1994. Twinned aragonite crystals found in the bivalvian crossed lamellar shell structure. Jour. Geol. Soc. Japan 100, 177–180.

Komagoe, T., Watanabe, T., Shirai, K., Yamazaki, A., Uematu, M., 2018. Geochemical and microstructural signals in giant clam *Tridacna maxima* recorded typhoon events at Okinotori Island, Japan. J. Geophys. Res. Biogeo. 123, 1460–1474.

Langlet, D., Alunno-Bruscia, M., Rafélis, M., Renard, M., Roux, M., Schein, E., Buestel, D., 2006. Experimental and natural cathodoluminescence in the shell of *Crassostrea gigas* from Thau lagoon (France): Ecological and environmental implications. Mar. Ecol. Prog. Ser. 317, 143–156.

Lazareth, C. E., Cornec, F. L., Candaudap, F., Freydier, R., 2013. Trace element heterogeneity along isochronous growth layers in bivalve shell: Consequences for environmental reconstruction. Palaeogeogr. Palaeoclimatol. Palaeoecol. 373, 39–49.

Le Roy, N., Jackson, D. J., Marie, B., Ramos-Silva, P., Marin, F., 2014. The evolution of metazoan α-carbonic anhydrases and their roles in calcium carbonate biomineralization. Front. Zool. 11, 75.

Lebrato, M., Garbe-Schönberg, D., Müller, M. N., Blanco-Ameijeiras, S., Feely, R. A., Lorenzoni, L., Molinero, J.-C., Bremer, K., Jones, D. O. B., Iglesias-Rodriguez, D., Greeley, D., Lamare, M. D., Paulmier, A., Graco, M., Cartes, J., Barcelos E Ramos, J., De Lara, A., Sanchez-Leal, R., Jimenez, P., Paparazzo, F. E., Hartman, S. E., Westernströer, U., Küter, M., Benavides, R., Da Silva, A. F., Bell, S., Payne, C., Olafsdottir, S., Robinson, K., Jantunen, L. M., Korablev, A., Webster, R. J., Jones, E. M., Gilg, O., Bailly Du Bois, P., Beldowski, J., Ashjian, C., Yahia, N. D., Twining, B., Chen, X.-G., Tseng, L.-C., Hwang, J.-S., Dahms, H.-U., Oschlies, A., 2020. Global variability in seawater Mg:Ca and Sr:Ca ratios in the modern ocean. Proc. Natl. Acad. Sci. U.S.A. 117, 22281–22292.

Lebrato, M., Garbe-Schönberg, D., Müller, M. N., Blanco-Ameijeiras, S., Feely, R. A., Lorenzoni, L., Molinero, J.-C., Bremer, K., Jones, D. O. B., Iglesias-Rodriguez, D., Greeley, D., Lamare, M. D., Paulmier, A., Graco, M., Cartes, J., Barcelos E Ramos, J., De Lara, A., Sanchez-Leal, R., Jimenez, P., Paparazzo, F. E., Hartman, S. E., Westernströer, U., Küter, M., Benavides, R., Da Silva, A. F., Bell, S., Payne, C., Olafsdottir, S., Robinson, K., Jantunen, L. M., Korablev, A., Webster, R. J., Jones, E. M., Gilg, O., Bailly Du Bois, P., Beldowski, J., Ashjian, C., Yahia, N. D., Twining, B., Chen, X.-G., Tseng, L.-C., Hwang, J.-S., Dahms, H.-U., Oschlies, A., 2021. Correction for Lebrato et al., Global variability in seawater Mg:Ca and Sr:Ca ratios in the modern ocean. Proc. Natl. Acad. Sci. U.S.A. 118, e2119099118.

Levi-Kalisman, Y., Falini, G., Addadi, L., Weiner, S., 2001. Structure of the nacreous organic matrix of a bivalve mollusk shell examined in the hydrated state using Cryo-TEM. J. Struct. Biol. 135, 8–17.

Li, B., Nychka, D. W., Ammann, C. M., 2010. The value of multiproxy reconstruction of past climate. J. Am. Stat. Assoc. 105, 883–895.

Li, X. W., Ji, H. M., Yang, W., Zhang, G. P., Chen, D. L., 2017. Mechanical properties of crossed-lamellar structures in biological shells: A review. J. Mech. Behav. Biomed. Mater. 74, 54–71.

Liehr, G. A., Zettler, M. L., Leipe, T., Witt, G., 2005. The ocean quahog *Arctica islandica* L.: A bioindicator for contaminated sediments. Mar. Biol. 147, 671–679.

Lincoln, S. F., 2005. Fossil fuels in the 21st century. Ambio 34, 621–627.

Liu, C., Yan, H., Wang, G., Zhao, L., Hu, Y., Zhou, P., Luo, F., Yang, H., Dodson, J., 2021. Species specific Sr/Ca-δ^{18}O relationships for three Tridacnidae species from the northern South China Sea. Chem. Geol. 584, 120519.

Louis, V., Besseau, L., Lartaud, F., 2022. *Step in Time*: Biomineralisation of bivalve's shell. Front. Mar. Sci. 9, 906085.

Lowenstam, H. A., 1961. Mineralogy, O^{18} /O^{16} ratios, and strontium and magnesium contents of recent and fossil brachiopods and their bearing on the history of the oceans. J. Geol. 69, 241–260.

Lucas, J. S., Nash, W. J., Crawford, C. M., Braley, R. D., 1989. Environmental influences on growth and survival during the ocean-nursery rearing of giant clams, *Tridacna gigas* (L.). Aquaculture 80, 45–61.

Lutz, R. A., Rhoads, D. C., 1977. Anaerobiosis and a theory of growth Line formation: Micro- and ultrastructural growth patterns within the molluscan shell reflect periodic respiratory changes. Science 198, 1222–1227.

Lutz, R. A., Rhoads, D. C., 1980. Growth patterns within the molluscan shell - An overview. In: Skeletal Growth of Aquatic Organisms: Biological Records of Environmental Change. Eds. by D. C. Rhoads and R. A. Lutz New York: Plenum Press, 203–254.

Malhi, Y., Franklin, J., Seddon, N., Solan, M., Turner, M. G., Field, C. B., Knowlton, N., 2020. Climate change and ecosystems: Threats, opportunities and solutions. Phil. Trans. R. Soc. B 375, 20190104.

Manabe, S., Wetherald, R. T., 1967. Thermal equilibrium of the atmosphere with a given distribution of relative humidity. J. Atmos. Sci. 24, 241–259.

Manabe, S., 1969. Climate and the ocean circulation: I. The atmospheric circulation and the hydrology of the Earth's surface. Mon. Wea. Rev. 97, 739–774.

Manabe, S., Stouffer, R. J., 1993. Century-scale effects of increased atmospheric CO_2 on the ocean-atmosphere system. Nature 364, 215–218.

Marali, S., Schöne, B. R., Mertz-Kraus, R., Griffin, S. M., Wanamaker, A. D., Butler, P. G., Holland, H. A., Jochum, K. P., 2017. Reproducibility of trace element time-series (Na/Ca, Mg/Ca, Mn/Ca, Sr/Ca, and Ba/Ca) within and between specimens of the bivalve *Arctica islandica* – A LA-ICP-MS line scan study. Palaeogeogr. Palaeoclimatol. Palaeoecol. 484, 109–128.

Marin, F., Roy, N. L., Marie, B., 2012. The formation and mineralization of mollusk shell. Front. Biosci. (Schol. Ed.) 4, 1099–1125.

Markham, A., 1996. Potential impacts of climate change on ecosystems: A review of implications for policymakers and conservation biologists. Clim. Res. 6, 179–191.

Markulin, K., Peharda, M., Mertz-Kraus, R., Schöne, B. R., Uvanović, H., Kovač, Ž., Janeković, I., 2019. Trace and minor element records in aragonitic bivalve shells as environmental proxies. Chem. Geol. 507, 120–133.

Martinez-Ruiz, F., Kastner, M., Gallego-Torres, D., Rodrigo-Gámiz, M., Nieto-Moreno, V., Ortega-Huertas, M., 2015. Paleoclimate and paleoceanography over the past 20,000 yr in the Mediterranean Sea Basins as indicated by sediment elemental proxies. Quaternary Sci. Rev. 107, 25–46.

Martinson, D. G., Pisias, N. G., Hays, J. D., Imbrie, J., Moore, T. C., Shackleton, N. J., 1987. Age dating and the orbital theory of the Ice Ages: Development of a high-resolution 0 to 300,000-year chronostratigraphy. Quat. Res. 27, 1–29.

McCarty, J. P., 2001. Ecological consequences of recent climate change. Conserv. Biol. 15, 320–331.

Meckler, A. N., Ziegler, M., Millán, M. I., Breitenbach, S. F. M., Bernasconi, S. M., 2014. Long-term performance of the Kiel carbonate device with a new correction scheme for clumped isotope measurements. Rapid Commun. Mass Sp. 28, 1705–1715.

Menadakis, M., Maroulis, G., Koutsoukos, P. G., 2008. Incorporation of Mg^{2+}, Sr^{2+}, Ba^{2+} and Zn^{2+} into aragonite and comparison with calcite. J. Math. Chem. 46, 484–491.

Middelburg, J. J., De Lange, G. J., Van Der Weijden, C. H., 1987. Manganese solubility control in marine pore waters. Geochim. Cosmochim. Acta 51, 759–763.

Mook, W. G., Vogel, J. C., 1968. Isotopic equilibrium between shells and their environment. Science 159, 874–875.

Mooney, H., Larigauderie, A., Cesario, M., Elmquist, T., Hoegh-Guldberg, O., Lavorel, S., Mace, G. M., Palmer, M., Scholes, R., Yahara, T., 2009. Biodiversity, climate change, and ecosystem services. Curr. Opin. Environ. Sustain. 1, 46–54.

Moss, D. K., Ivany, L. C., Judd, E. J., Cummings, P. W., Bearden, C. E., Kim, W.-J., Artruc, E. G., Driscoll, J. R., 2016. Lifespan, growth rate, and body size across latitude in marine Bivalvia, with implications for Phanerozoic evolution. Proc. R. Soc. B Biol. Sci. 283, 20161364.

Mu, G., Duan, F., Zhang, G., Li, X., Ding, X., Zhang, L., 2018. Microstructure and mechanical property of *Ruditapes philippinarum* shell. J. Mech. Behav. Biomed. Mater. 85, 209–217.

Mucci, A., Canuel, R., Zhong, S., 1989. The solubility of calcite and aragonite in sulfate-free seawater and the seeded growth kinetics and composition of the precipitates at 25°C. Chem. Geol. 74, 309–320.

Mulcahy, S. A., Killingley, J. S., Phleger, C. F., Berger, W. H., 1979. Isotopic composition of otoliths from a benthopelagic fish, *Coryphaenoides acrolepis*, Macrouridae: Gadiformes. Oceanol. Acta 2, 423–427.

Müller, I. A., Violay, M. E. S., Storck, J.-C., Fernandez, A., Van Dijk, J., Madonna, C., Bernasconi, S. M., 2017. Clumped isotope fractionation during phosphoric acid digestion of carbonates at 70 °C. Chem. Geol. 449, 1–14.

Nakahara, H., Bevelander, G., 1971. The formation and growth of the prismatic layer of *Pinctada radiata*. Calc. Tis. Res. 7, 31–45.

Nicol, D., 1951. Recent species of the veneroid pelecypod *Arctica*. J. Wash. Acad. Sci. 41, 102–106.

Nürnberg, D., Bijma, J., Hemleben, C., 1996. Assessing the reliability of magnesium in foraminiferal calcite as a proxy for water mass temperatures. Geochim. Cosmochim. Acta 60, 803–814.

Ohno, T., 1989. Palaeotidal characteristics determined by micro-growth patterns in bivalves. Palaeontology 32, 237–263.

O'Neil, D. D., Gillikin, D. P., 2014. Do freshwater mussel shells record road-salt pollution? Sci. Rep. 4, 7168.

Otter, L. M., Agbaje, O. B. A., Kilburn, M. R., Lenz, C., Henry, H., Trimby, P., Hoppe, P., Jacob, D. E., 2019. Insights into architecture, growth dynamics, and biomineralization from pulsed Sr-labelled *Katelysia rhytiphora* shells (Mollusca, Bivalvia). Biogeosciences 16, 3439–3455.

Pakhomova, S. V., Hall, P. O. J., Kononets, M. Yu., Rozanov, A. G., Tengberg, A., Vershinin, A. V., 2007. Fluxes of iron and manganese across the sediment–water interface under various redox conditions. Mar. Chem. 107, 319–331.

Pan, Y., Birdsey, R. A., Phillips, O. L., Houghton, R. A., Fang, J., Kauppi, P. E., Keith, H., Kurz, W. A., Ito, A., Lewis, S. L., Nabuurs, G.-J., Shvidenko, A., Hashimoto, S., Lerink, B., Schepaschenko, D., Castanho, A., Murdiyarso, D., 2024. The enduring world forest carbon sink. Nature 631, 563–569.

Pauly, D., Watson, R., Alder, J., 2005. Global trends in world fisheries: Impacts on marine ecosystems and food security. Phil. Trans. R. Soc. B 360, 5–12.

Pearce, N. J. G., Mann, V. L., 2006. Trace metal variations in the shells of Ensis siliqua record pollution and environmental conditions in the sea to the west of mainland Britain. Mar. Pollut. Bull. 52, 739–755.

Peharda, M., Schöne, B. R., Black, B. A., Corrège, T., 2021. Advances of sclerochronology research in the last decade. Palaeogeogr. Palaeoclimatol. Palaeoecol. 570, 110371.

Phipps, S. J., McGregor, H. V., Gergis, J., Gallant, A. J. E., Neukom, R., Stevenson, S., Ackerley, D., Brown, J. R., Fischer, M. J., Van Ommen, T. D., 2013. Paleoclimate data–model comparison and the role of climate forcings over the past 1500 years. J. Clim. 26, 6915–6936.

Piwoni-Piórewicz, A., Strekopytov, S., Humphreys-Williams, E., Kukliński, P., 2021. The patterns of elemental concentration (Ca, Na, Sr, Mg, Mn, Ba, Cu, Pb, V, Y, U and Cd) in shells of invertebrates representing different $CaCO_3$ polymorphs: A case study from the brackish Gulf of Gdańsk (the Baltic Sea). Biogeosciences 18, 707–728.

Poulain, C., Gillikin, D. P., Thébault, J., Munaron, J. M., Bohn, M., Robert, R., Paulet, Y.-M., Lorrain, A., 2015. An evaluation of Mg/Ca, Sr/Ca, and Ba/Ca ratios as environmental proxies in aragonite bivalve shells. Chem. Geol. 396, 42–50.

Powell, M. G., Schöne, B. R., Jacob, D. E., 2009. Tropical marine climate during the late Paleozoic ice age using trace element analyses of brachiopods. Palaeogeogr. Palaeoclimatol. Palaeoecol. 280, 143–149.

Reynolds, D. J., Hall, I. R., Scourse, J. D., Richardson, C. A., Wanamaker, A. D., Butler, P. G., 2017. Biological and climate controls on north Atlantic marine carbon dynamics over the last millennium: Insights from an absolutely dated shell-based record from the North Icelandic Shelf. Glob. Biogeochem. Cycles 31, 1718–1735.

Rhoads, D. C., Lutz, R. A., Revelas, E. C., Cerrato, R. M., 1981. Growth of bivalves at deep-sea hydrothermal vents along the Galápagos Rift. Science 214, 911–913.

Robock, A., 2000. Volcanic eruptions and climate. Rev. Geophys. 38, 191–219.

Roger, L. M., George, A. D., Shaw, J., Hart, R. D., Roberts, M., Becker, T., McDonald, B. J., Evans, N. J., 2017. Geochemical and microstructural characterisation of two species of cool-water bivalves (*Fulvia tenuicostata* and *Soletellina biradiata*) from Western Australia. Biogeosciences 14, 1721–1737.

Rohling, E. J., Bigg, G. R., 1998. Paleosalinity and δ^{18} O: A critical assessment. J. Geophys. Res. 103, 1307–1318.

Roopnarine, P. D., Fitzgerald, P., Byars, G., Kilb, K., 1998. Coincident boron profiles of bivalves from the Gulf of California: Implications for the calculation of paleosalinities. Palaios 13, 395.

Ropes, J. W., Jones, D., Murawski, S., Serchuk, F., Jearld, A., 1984. Documentation of annual growth lines in ocean quahogs, *Arctica islandica* Linné. Fish. Bull. 82, 1–19.

Ropes, J. W., Murawski, S. A., 1983. Maximum shell length and longevity in ocean quahogs, *Arctica islandica* Linne. ICES CM/K 32, 1–8.

Rosewater, J., 1965. The family Tridacnidae in the Indo-Pacific. Indo-Pac. Moll 1, 347–396.

Rowell, K., Dettman, D. L., Dietz, R., 2010. Nitrogen isotopes in otoliths reconstruct ancient trophic position. Environ. Biol. Fishes 89, 415–425.

Roy, K., Jablonski, D., Valentine, J. W., 2000. Dissecting latitudinal diversity gradients: Functional groups and clades of marine bivalves. Proc. R. Soc. Lond. B 267, 293–299.

Salinger, M. J., 2005. Climate variability and change: past, present and future – An overview. Clim. Change 70, 9–29.

Sano, Y., Kobayashi, S., Shirai, K., Takahata, N., Matsumoto, K., Watanabe, T., Sowa, K., Iwai, K., 2012. Past daily light cycle recorded in the strontium/calcium ratios of giant clam shells. Nat. Commun. 3, 761.

Sato, K., Sasaki, T., 2015. Shell microstructure of protobranchia (Mollusca: Bivalvia): Diversity, new microstructures and systematic implications. Malacologia 59, 45–103.

Schlesinger, M. E., Ramankutty, N., 1994. An oscillation in the global climate system of period 65–70 years. Nature 367, 723–726.

Schmitt, R. W., 2018. The ocean's role in climate. Oceanography 31, 32–40.

Scholes, R. J., 2016. Climate change and ecosystem services. WIREs Clim. Change 7, 537–550.

Scholz, D., Frisia, S., Borsato, A., Spötl, C., Fohlmeister, J., Mudelsee, M., Miorandi, R., Mangini, A., 2012. Holocene climate variability in north-eastern Italy: Potential influence of the NAO and solar activity recorded by speleothem data. Clim. Past 8, 1367–1383.

Scholze, M., Knorr, W., Arnell, N. W., Prentice, I. C., 2006. A climate-change risk analysis for world ecosystems. Proc. Natl. Acad. Sci. USA 103, 13116–13120.

Schöne, B. R., Freyre Castro, A. D., Fiebig, J., Houk, S. D., Oschmann, W., Kröncke, I., 2004. Sea surface water temperatures over the period 1884–1983 reconstructed from oxygen isotope ratios of a bivalve mollusk shell (*Arctica islandica*, southern North Sea). Palaeogeogr. Palaeoclimatol. Palaeoecol. 212, 215–232.

Schöne, B. R., Fiebig, J., Pfeiffer, M., Gleβ, R., Hickson, J., Johnson, A. L. A., Dreyer, W., Oschmann, W., 2005a. Climate records from a bivalved Methuselah (*Arctica islandica*, Mollusca; Iceland). Palaeogeogr. Palaeoclimatol. Palaeoecol. 228, 130–148.

Schöne, B. R., Dunca, E., Fiebig, J., Pfeiffer, M., 2005b. Mutvei's solution: An ideal agent for resolving microgrowth structures of biogenic carbonates. Palaeogeogr. Palaeoclimatol. Palaeoecol. 228, 149–166.

Schöne, B. R., 2008. The curse of physiology – Challenges and opportunities in the interpretation of geochemical data from mollusk shells. Geo-Mar. Lett. 28, 269–285.

Schöne, B. R., Zhang, Z., Radermacher, P., Thébault, J., Jacob, D. E., Nunn, E. V., Maurer, A.-F., 2011. Sr/Ca and Mg/Ca ratios of ontogenetically old, long-lived bivalve shells (*Arctica islandica*) and their function as paleotemperature proxies. Palaeogeogr. Palaeoclimatol. Palaeoecol. 302, 52–64.

Schöne, B. R., Surge, D. M., 2012. Part N, revised, volume 1, chapter 14: Bivalve sclerochronology and geochemistry. Treatise Online 46, 1–24.

Schöne, B. R., Radermacher, P., Zhang, Z., Jacob, D. E., 2013. Crystal fabrics and element impurities (Sr/Ca, Mg/Ca, and Ba/Ca) in shells of *Arctica islandica* – Implications for paleoclimate reconstructions. Palaeogeogr. Palaeoclimatol. Palaeoecol. 373, 50–59.

Schöne, B. R., Huang, X., Zettler, M. L., Zhao, L., Mertz-Kraus, R., Jochum, K. P., Walliser, E. O., 2021. Mn/Ca in shells of *Arctica islandica* (Baltic Sea) – A potential proxy for ocean hypoxia? Estuar. Coast. Shelf Sci. 251, 107257.

Schöne, B. R., Huang, X., Jantschke, A., Mertz-Kraus, R., Zettler, M. L., 2022. High-resolution reconstruction of dissolved oxygen levels in the Baltic Sea with bivalves – A multi-species comparison (*Arctica islandica*, *Astarte borealis*, *Astarte elliptica*). Front. Mar. Sci. 9, 820731.

Schöne, B. R., Zhang, Z., Jacob, D., Gillikin, D. P., Tütken, T., Garbe-Schönberg, D., McConnaughey, T., Soldati, A., 2010. Effect of organic matrices on the determination of the trace element chemistry (Mg, Sr, Mg/Ca, Sr/Ca) of aragonitic bivalve shells (*Arctica islandica*) – Comparison of ICP-OES and LA-ICP-MS data. Geochem. J. 44, 23–37.

Schuur, E. A. G., McGuire, A. D., Schädel, C., Grosse, G., Harden, J. W., Hayes, D. J., Hugelius, G., Koven, C. D., Kuhry, P., Lawrence, D. M., Natali, S. M., Olefeldt, D., Romanovsky, V. E., Schaefer, K., Turetsky, M. R., Treat, C. C., Vonk, J. E., 2015. Climate change and the permafrost carbon feedback. Nature 520, 171–179.

Schwaner, C., Farhat, S., Haley, J., Pales Espinosa, E., Allam, B., 2022a. Proteomic and transcriptomic responses enable clams to correct the pH of calcifying fluids and sustain biomineralization in acidified environments. Int. J. Mol. Sci. 23.

Schwaner, C., Farhat, S., Haley, J., Pales Espinosa, E., Allam, B., 2022b. Transcriptomic, proteomic, and functional assays underline the dual role of extrapallial hemocytes in immunity and biomineralization in the hard clam *Mercenaria mercenaria*. Front. Immunol. 13, 838530.

Scourse, J., Richardson, C., Forsythe, G., Harris, I., Heinemeier, J., Fraser, N., Briffa, K., Jones, P., 2006. First cross-matched floating chronology from the marine fossil record: Data from growth lines of the long-lived bivalve mollusc *Arctica islandica*. Holocene 16, 967–974.

Sepkoski, J. J., 1981. A factor analytic description of the Phanerozoic marine fossil record. Paleobiology 7, 36–53.

Shannon, R. D., 1976. Revised effective ionic radii and systematic studies of interatomic distances in halides and chalcogenides. Acta Crystallogr. A 32, 751–767.

Shirai, K., Takahata, N., Yamamoto, H., Omata, T., Sasaki, T., Sano, Y., 2008. Novel analytical approach to bivalve shell biogeochemistry: A case study of hydrothermal mussel shell. Geochem. J. 42, 413–420.

Shirai, K., Schöne, B. R., Miyaji, T., Radarmacher, P., Krause, R. A., Tanabe, K., 2014. Assessment of the mechanism of elemental incorporation into bivalve shells (*Arctica islandica*) based on elemental distribution at the microstructural scale. Geochim. Cosmochim. Acta 126, 307–320.

Smith, J. N., 2001. Why should we believe 210Pb sediment geochronologies? J. Environ. Radioact. 55, 121–123.

Soldati, A. L., Jacob, D. E., Glatzel, P., Swarbrick, J. C., Geck, J., 2016. Element substitution by living organisms: The case of manganese in mollusc shell aragonite. Sci. Rep. 6, 22514.

Solomon, S., Plattner, G.-K., Knutti, R., Friedlingstein, P., 2009. Irreversible climate change due to carbon dioxide emissions. Proc. Natl. Acad. Sci. USA 106, 1704–1709.

Song, X., Liu, Z., Wang, L., Song, L., 2019. Recent advances of shell matrix proteins and cellular orchestration in marine molluscan shell biomineralization. Front. Mar. Sci. 6, 41.

Speer, J. A., 1983. Chapter 5. Crystal chemistry and phase relations of orthorhombic carbonates. In: Mineralogy and Chemistry. Ed. by R. J. Reeder Berlin, Boston: De Gruyter, 145–190.

Stemmer, K., Brey, T., Gutbrod, M. S., Beutler, M., Schalkhausser, B., Beer, D. de, 2019. In situ Measurements of pH, Ca^{2+}, and Dic dynamics within the extrapallial fluid of the ocean quahog *Arctica islandica*. J. Shellfish Res. 38, 71–78.

Stenseth, N. Chr., Ottersen, G., Hurrell, J. W., Mysterud, A., Lima, M., Chan, K., Yoccoz, N. G., Ådlandsvik, B., 2003. Studying climate effects on ecology through the use of climate indices: The North Atlantic Oscillation, El Niño Southern Oscillation and beyond. Proc. R. Soc. Lond. B 270, 2087–2096.

Strain, P. M., Tan, F. C., 1993. Seasonal evolution of oxygen isotope-salinity relationships in high-latitude surface waters. J. Geophys. Res. 98, 14589–14598.

Surge, D., Walker, K. J., 2006. Geochemical variation in microstructural shell layers of the southern quahog (*Mercenaria campechiensis*): Implications for reconstructing seasonality. Palaeogeogr. Palaeoclimatol. Palaeoecol. 237, 182–190.

Suzuki, M., Kogure, T., Nagasawa, H., 2017. Studies on the chemical structures of organic matrices and their functions in the biomineralization processes of molluscan shells. AGri-Biosci. Monogr. (AGBM) 7, 25–39.

Takesue, R. K., Bacon, C. R., Thompson, J. K., 2008. Influences of organic matter and calcification rate on trace elements in aragonitic estuarine bivalve shells. Geochim. Cosmochim. Acta 72, 5431–5445.

Tebo, B. M., 1991. Manganese(II) oxidation in the suboxic zone of the Black Sea. Deep Sea Res. Part A Oceanogr. Res. Pap. 38, S883–S905.

Thébault, J., Chauvaud, L., L'Helguen, S., Clavier, J., Barats, A., Jacquet, Sé., PÉcheyran, C., Amouroux, D., 2009. Barium and molybdenum records in bivalve shells: Geochemical proxies for phytoplankton dynamics in coastal environments? Limnol. Oceanogr. 54, 1002–1014.

Thompson, I., Jones, D. S., Dreibelbis, D., 1980. Annual internal growth banding and life history of the ocean quahog *Arctica islandica* (Mollusca: Bivalvia). Mar. Biol. 57, 25–34.

Tierney, J. E., Poulsen, C. J., Montañez, I. P., Bhattacharya, T., Feng, R., Ford, H. L., Hönisch, B., Inglis, G. N., Petersen, S. V., Sagoo, N., Tabor, C. R., Thirumalai, K., Zhu, J., Burls, N. J., Foster, G. L., Goddéris, Y., Huber, B. T., Ivany, L. C., Kirtland Turner, S., Lunt, D. J., McElwain, J. C., Mills, B. J. W., Otto-Bliesner, B. L., Ridgwell, A., Zhang, Y. G., 2020. Past climates inform our future. Science 370, eaay3701.

Trenberth, K. E., Fasullo, J. T., 2009. Global warming due to increasing absorbed solar radiation. Geophys. Res. Lett. 36, L07706.

Tripati, A. K., Delaney, M. L., Zachos, J. C., Anderson, L. D., Kelly, D. C., Elderfield, H., 2003. Tropical sea-surface temperature reconstruction for the early Paleogene using Mg/Ca ratios of planktonic foraminifera. Paleoceanography 18, 1101.

Trutschler, K., Samtleben, C., 1988. Shell growth of *Astarte elliptica* (Bivalvia) from Kiel Bay (Western Baltic Sea). Mar. Ecol. Prog. Ser. 42, 155–162.

Turekian, K. K., Cochran, J. K., Kharkar, D. P., Cerrato, R. M., Vaisnys, J. R., Sanders, H. L., Grassle, J. F., Allen, J. A., 1975. Slow growth rate of a deep-sea clam determined by 228Ra chronology. Proc. Natl. Acad. Sci. U.S.A. 72, 2829–2832.

Tynan, S., Opdyke, B. N., Walczak, M., Eggins, S., Dutton, A., 2017. Assessment of Mg/Ca in *Saccostrea glomerata* (the Sydney rock oyster) shell as a potential temperature record. Palaeogeogr. Palaeoclimatol. Palaeoecol. 484, 79–88.

Urey, H. C., Lowenstam, H. A., Epstein, S., McKinney, C. R., 1951. Measurement of paleotemperatures and temperatures of the Upper Cretaceous of England, Denmark, and the Southeastern United States. Geol. Soc. Am. Bull. 62, 399.

Van Der Wiel, K., Bintanja, R., 2021. Contribution of climatic changes in mean and variability to monthly temperature and precipitation extremes. Commun Earth Environ 2, 1.

Van Wynsberge, S., Andréfouët, S., Gaertner-Mazouni, N., Wabnitz, C. C. C., Menoud, M., Le Moullac, G., Levy, P., Gilbert, A., Remoissenet, G., 2017. Growth, survival and reproduction of the giant clam *Tridacna maxima* (Röding 1798, Bivalvia) in two contrasting lagoons in French Polynesia. PLoS ONE 12, e0170565.

Vihtakari, M., Ambrose, W. G., Renaud, P. E., Locke, W. L., Carroll, M. L., Berge, J., Clarke, L. J., Cottier, F., Hop, H., 2017. A key to the past? Element ratios as environmental proxies in two Arctic bivalves. Palaeogeogr. Palaeoclimatol. Palaeoecol. 465, 316–332.

Wanamaker, A. D., Kreutz, K. J., Wilson, T., Borns Jr, H. W., Introne, D. S., Feindel, S., 2008a. Experimentally determined Mg/Ca and Sr/Ca ratios in juvenile bivalve calcite for *Mytilus edulis*: Implications for paleotemperature reconstructions. Geo-Mar. Lett. 28, 359–368.

Wanamaker, A. D., Heinemeier, J., Scourse, J. D., Richardson, C. A., Butler, P. G., Eiríksson, J., Knudsen, K. L., 2008b. Very long-lived mollusks confirm 17th century AD tephra-based radiocarbon reservoir ages for north Icelandic shelf waters. Radiocarbon 50, 399–412.

Wanner, H., Brönnimann, S., Casty, C., Gyalistras, D., Luterbacher, J., Schmutz, C., Stephenson, D. B., Xoplaki, E., 2001. North Atlantic Oscillation – Concepts and studies. Surv. Geophys. 22, 321–381.

Warter, V., Erez, J., Müller, W., 2018. Environmental and physiological controls on daily trace element incorporation in *Tridacna crocea* from combined laboratory culturing and ultra-high resolution LA-ICP-MS analysis. Palaeogeogr. Palaeoclimatol. Palaeoecol. 496, 32–47.

Watson, E. B., 1996. Surface enrichment and trace-element uptake during crystal growth. Geochim. Cosmochim. Acta 60, 5013–5020.

Watson, E. B., 2004. A conceptual model for near-surface kinetic controls on the trace-element and stable isotope composition of abiogenic calcite crystals. Geochim. Cosmochim. Acta 68, 1473–1488.

Weaver, C. P., Lempert, R. J., Brown, C., Hall, J. A., Revell, D., Sarewitz, D., 2013. Improving the contribution of climate model information to decision making: The value and demands of robust decision frameworks. WIREs Clim. Change 4, 39–60.

Weber, J. N., Woodhead, P. M. J., 1970. Carbon and oxygen isotope fractionation in the skeletal carbonate of reef-building corals. Chem. Geol. 6, 93–117.

Weiss, R. F., Östlund, H. G., Craig, H., 1979. Geochemical studies of the Weddell sea. Deep-Sea Res. A: Oceanogr. Res. Pap. 26, 1093–1120.

Wernberg, T., Thomsen, M. S., Baum, J. K., Bishop, M. J., Bruno, J. F., Coleman, M. A., Filbee-Dexter, K., Gagnon, K., He, Q., Murdiyarso, D., Rogers, K., Silliman, B. R., Smale, D. A., Starko, S., Vanderklift, M. A., 2024. Impacts of climate change on marine foundation species. Annu. Rev. Mar. Sci. 16, 247–282.

Wheeler, A., 1992. Mechanisms of molluscan shell formation. In: Calcification in Biological Systems. Boca Raton: CRC Press, 179–216.

Wilbur, K. M., Saleuddin, A. S. M., 1983. 6 - Shell Formation. In: The Mollusca. Eds. by A. S. M. Saleuddin and K. M. Wilbur Academic Press, 235–287.

Wilbur, K., 1972. Shell formation in mollusks. Chem. Zool. 7, 103–145.

Winkelstern, I. Z., Lohmann, K. C., 2016. Shallow burial alteration of dolomite and limestone clumped isotope geochemistry. Geology 44, 467–470.

Yan, H., Shao, D., Wang, Y., Sun, L., 2013. Sr/Ca profile of long-lived *Tridacna gigas* bivalves from South China Sea: A new high-resolution SST proxy. Geochim. Cosmochim. Acta 112, 52–65.

Zhao, L., Schöne, B. R., Mertz-Kraus, R., Yang, F., 2017. Insights from sodium into the impacts of elevated pCO<sun>2</sub> and temperature on bivalve shell formation. J. Exp. Mar. Biol. Ecol. 486, 148–154.

Zhong, S., Mucci, A., 1989. Calcite and aragonite precipitation from seawater solutions of various salinities: Precipitation rates and overgrowth compositions. Chem. Geol. 78, 283–299.

Zinke, J., D'Olivo, J. P., Gey, C. J., McCulloch, M. T., Bruggemann, J. H., Lough, J. M., Guillaume, M. M. M., 2019. Multi-trace-element sea surface temperature coral reconstruction for the southern Mozambique Channel reveals teleconnections with the tropical Atlantic. Biogeosciences 16, 695–712.

Zolotarev, V. N., 1980. The duration of life in bivalves from Sea of Japan and Sea of Okhotsk. Sov. J. Mar. Biol. 6, 301–308.

2 Strong coupling between biomineral morphology and Sr/Ca of *Arctica islandica* (Bivalvia) – Implications for shell Sr/Ca-based temperature estimates

Cornélia Brosset[1], Nils Höche[1], Kotaro Shirai[2], Kozue Nishida[3], Regina Mertz-Kraus[1], Bernd R. Schöne[1]

[1]*Institute of Geosciences, University of Mainz, Mainz, Germany*

[2]*Atmosphere and Ocean Research Institute, The University of Tokyo, Chiba, Japan*

[3]*Graduate School of Life and Environmental Sciences, University of Tsukuba, Tsukuba, Japan*

Brosset, C., Höche, N., Shirai, K., Nishida, K., Mertz-Kraus, R., Schöne, B. R., 2022. Strong coupling between biomineral morphology and Sr/Ca of *Arctica islandica* (Bivalvia) – Implications for shell Sr/Ca-based temperature estimates. *Minerals* 12, 500.

In this chapter, the relationship between shell Sr/Ca and seasonal temperature was investigated in *Arctica islandica* specimens grown in nature. Despite correcting for ultrastructure and growth rate, Sr/Ca showed a weak and inconsistent correlation with seawater temperature and was affected by unidentified environmental forcings, highlighting the complexity of interpreting shell Sr/Ca in such settings. This manuscript was published in the journal "*Minerals*". I contributed to the conceptualization, methodology, validation, formal analysis, investigation, data curation, visualization, writing – original draft and writing – review and editing of the manuscript. This work was supported by the German Research Foundation (DFG) grant [SCHO793/23] to BRS and the Japan Society for Promotion of Science (JSPS) grant [20181607] to KS under the Joint Research Projects-LEAD with DFG (JRPs-LEAD with DFG).

Note: In this manuscript, the term "microstructure" refers to what is consistently described as "ultrastructure" elsewhere in this thesis. The two terms are used interchangeably in this context.

Author contributions:

CB	Conceptualization, Methodology, Validation, Formal analysis, Investigation, Data curation, Visualization, Writing – original draft, Writing – review and editing.
NH	Conceptualization, Methodology, Formal analysis, Writing – original draft, Writing – review and editing.
KS	Writing – review and editing.
KN	Writing – review and editing.
RMK	Validation, Resources, Writing – review and editing.
BRS	Conceptualization, Validation, Investigation, Data curation, Writing – original draft, Writing – review and editing, Visualization, Supervision, Project administration, Funding acquisition.

2.1 Abstract

Bivalve shells serve as powerful high-resolution paleoclimate archives. However, the number of reliable temperature proxies is limited. It has remained particularly difficult to extract temperature signals from shell Sr/Ca, although Sr is routinely employed in other biogenic aragonites. In bivalves, Sr/Ca is linked to the prevailing microstructure and is sometimes affected by kinetics. Here, the hypothesis is tested that temperature can be reconstructed from shell Sr/Ca once microstructure and/or growth-rate-related bias has been mathematically eliminated. Therefore, the relationship between Sr/Ca and increment width, as well as biomineral unit size, has been studied in three different shell portions of field-grown *Arctica islandica* specimens. Subsequently, microstructure and/or growth-rate-related variation was removed from Sr/Ca data and residuals compared to temperature. As demonstrated, the hypothesis could not be verified. Even after detrending, Sr/Ca remained positively correlated to water temperature, which contradicts thermodynamic expectations and findings from inorganic aragonite. Any temperature signal potentially recorded by shell Sr/Ca is overprinted by other environmental forcings. Unless these variables are identified, it will remain impossible to infer temperature from Sr/Ca. Given the coupling with the biomineral unit size, a detailed characterization of the microstructure should remain an integral part of subsequent attempts to reconstruct temperature from Sr/Ca.

2.2 Introduction

Bivalve mollusks offer outstanding potential for paleoclimate research (Ivany et al., 2011; Wanamaker et al., 2012; Butler et al., 2013; Lohmann and Schöne, 2013; Black et al., 2015, 2016; Walliser et al., 2018). They are biogeographically widely distributed, occur abundantly and are sometimes excellently preserved in the fossil record. Based on shell growth pattern analysis, each sample taken from the shells can be accurately dated to the nearest calendar year (Jones, 1980; Trutschler and Samtleben, 1988), day (Fritz and Haven, 1983; Chauvaud et al., 1998; Clark, 2005) or tidal cycle (Evans, 1972; Ohno, 1989; Hallmann et al., 2009), provided that the time of death or birth is known. While some species only live for several months or years, offering valuable insights into sub-seasonal environmental variability (Thébault et al., 2009; Hatch et al., 2013; Yamanashi et al., 2016; Kodama et al., 2021), others attain a lifespan of several hundred years (Shaul and Goodwin, 1982; Buick and Ivany, 2004; Schöne et al., 2005; Wisshak et al., 2009; Selin and Dulenina, 2012; Wanamaker et al., 2012; Butler et al., 2013; Moss et al., 2017). The latter can be used to reconstruct decadal and century-scale climate dynamics (Schöne et al., 2003; Strom et al., 2005; Scourse et al., 2006; Black et al., 2009; Butler et al., 2010; Lohmann and Schöne, 2013; Reynolds et al., 2016; Mette et al., 2021), specifically if the growth increment series of many specimens with overlapping lifespans are crossdated to form stacked chronologies that cover centuries to millennia, and can provide well replicated climate data (Butler et al., 2013; Holland et al., 2014; Reynolds et al., 2016; Black et al., 2019).

Despite major advances in bivalve sclerochronology during the last decade (Peharda et al., 2021), the quantitative reconstruction of environmental variables from shells, specifically ocean temperature, remains a challenging task owing to the very limited number of well-accepted proxies and the dual nature of many of those. For example, the stable oxygen isotope value, by far the most frequently used surrogate for temperature in bivalves and other biogenic archives, simultaneously records changes in temperature and the $\delta^{18}O$ signature of the ambient water (Grossman and Ku, 1986; Wefer and Berger, 1991). Given that most bivalve species form their shells near oxygen isotopic equilibrium with the water (Epstein et al., 1953; Mook and Vogel, 1968; Killingley and Berger, 1979), temperatures can be reliably estimated from $\delta^{18}O_{shell}$ as long as the $\delta^{18}O_{water}$ value is known or can be otherwise inferred, e.g., from salinity (Witbaard et al., 1994), which is strongly correlated to $\delta^{18}O_{water}$. The shell growth rate, another potential temperature proxy in shells, is likewise controlled by several environmental variables, i.e., temperature, food supply and food quality (e.g., Ansell, 1968; Kennish and Olsson, 1975; Goodwin et al., 2001; Witbaard et al., 2001). Unless the influence of food conditions on the shell growth rate has been quantified, changes in increment width cannot provide precise temperature data. Amongst others, carbonate clumped isotopes overcome the duality dilemma of the aforementioned proxies (Eagle et al., 2013; Henkes et al., 2013; Wacker et al., 2014; Fiebig et al.,

2019) and can potentially occupy a prominent place in future bivalve sclerochronological studies. However, analytical refinement is still needed, namely a reduction in error, sample size, sample throughput, etc.

In many other biogenic carbonates, strontium (in aragonite) and magnesium (in calcite) can provide reliable temperature proxy data (e.g., Nürnberg et al., 1996; Corrège, 2006). However, in bivalves, the interpretation of these elements has remained notoriously difficult. In particular, the use of Sr in aragonitic shells as a proxy for temperature has been hotly debated, and many controversial findings have been reported on the relationship with temperature, ranging from negative to positive correlations to none at all (e.g., Dodd, 1965; Lorrain et al., 2005; Surge and Walker, 2006; Foster et al., 2009; Schöne et al., 2011; Sano et al., 2012; Vihtakari et al., 2016; Wanamaker and Gillikin, 2019). Some studies even reported a link between Sr and the shell growth rate (Izumida et al., 2011), rather than temperature. There is a broad consensus, however, that the incorporation of Sr into shell aragonite is controlled by vital and kinetic effects. This is firstly indicated by much smaller distribution coefficients than in abiogenically precipitated aragonite (Gaetani and Cohen, 2006). Secondly, in most studies in which the expected negative correlation between Sr/Ca and temperature was found, the temperature sensitivity of shell Sr/Ca differed from thermodynamic expectations (Yan et al., 2011, 2013, 2014; Füllenbach et al., 2015; Zhao et al., 2017). Another important, common observation is that the shell Sr content is tightly linked to the prevailing shell microstructure (Shirai et al., 2008; Foster et al., 2009; Füllenbach et al., 2017; Roger et al., 2017), with strong enrichment at the growth lines (reflecting periods of slow growth) and much lower values in the portions between adjacent growth lines (= growth increments, periods of fast growth). For example, in *Arctica islandica*, shell Sr/Ca values of more than 3 mmol/mol were measured in annual growth lines (consisting of irregular simple/spherulitic prismatic [ISP] microstructure; for an overview on abbreviations used in this paper, see Appendix 2.A, Table 2.A1), whereas those in the annual growth increments (homogenous [HOM] microstructure in the outer portion of the outer shell layer [oOSL]; crossed-acicular microstructure [CA] in the inner portion of the outer shell layer [iOSL]) fluctuated between 0.7 and 1.3 mmol/mol (Schöne et al., 2011, 2013). Values in contemporaneous shell portions of the oOSL were higher than those in the iOSL (Schöne et al., 2013; Shirai et al., 2014). Similar differences were observed at a higher resolution within the annual increment of *Cerastoderma edule*. While 3.5 mmol/mol Sr/Ca was measured in circatidal growth lines (formed during low tide; ISP in iOSL), the circatidal increments (reflecting growth during high tide; nondenticular composite prismatic in iOSL) contained only 2.5 mmol/mol (Füllenbach et al., 2017). It is worth noting that, in artificially cultivated bivalves, the shell microstructure is often much more uniform than in field-grown specimens (Höche et al., 2021a), and, in such bivalves, a

statistically significant negative correlation between shell Sr/Ca and temperature has occasionally been reported (Zhao et al., 2017).

Based on these findings, it is hypothesized here that temperature can be reconstructed from shell Sr/Ca data once the microstructure and/or growth-rate-related bias has been mathematically eliminated. To test this hypothesis, we have investigated the relationship between molar shell Sr/Ca values and morphological parameters (area, elongation) of the individual building blocks of the shell microstructure, i.e., individual biomineral units (BMUs), in three different shell portions of field-grown *A. islandica* with a specific microstructure (oOSL: HOM, iOSL and hinge: CA). Furthermore, the coupling between Sr/Ca and the growth rate was studied. In a subsequent step, we have mathematically removed the microstructure and/or growth-rate-related variation from the shell Sr/Ca data and compared the residuals to seasonal water temperature changes. The focus was placed on BMU variations occurring during the main growing season, i.e., within annual increments and, thus, the same microstructure category. If it were possible to unlock the temperature information encoded in shell Sr/Ca, bivalve sclerochronology would make a major leap forward and boost paleoclimate research.

2.3 Materials and methods

2.3.1 Sample material and preparation

To assess the link between Sr/Ca values, growth rate and microstructural properties (BUM area and elongation) of the shells at high resolution (weekly/monthly), three live-collected, juvenile specimens of *A. islandica* were studied (Table 2.1). The bivalves were obtained by dredging from 7 m water depth at Þistilfjördur, NE Iceland (66°11′N, 015°21′W), on 17 August 2006. After return to the coast, the bivalves were shucked, and the shells were rinsed with tap water. In the laboratory, the left valve of each specimen was mounted on an acrylic glass cube using WIKO Multi Power 3 plastic welder. Along the prospective cutting axis, the outer and inner shell surfaces were covered with a protective layer of WIKO 05 metal epoxy resin. Once the plastic welder and epoxy resin had cured, two approx. 2.5 mm-thick sections were cut from each valve along the axis of maximum growth (Fig. 2.1A) using a Buehler IsoMet 1000 low-speed saw (operated at 200 rpm) equipped with a 0.4 mm diamond wafering blade (Buehler 15LC 11-4255). Subsequently, both sections were ground on glass plates using F800 and F1200 SiC suspensions and polished with 1 µm Al_2O_3 suspension on a Buehler MasterTex polishing cloth. After each preparation step, the shell sections were ultrasonically cleaned in tap water. One section of each specimen was then glued to a glass slide and used for *in-situ* chemical analysis via laser ablation inductively coupled plasma mass spectrometry (LA-ICP-MS), whereas the mirroring section was attached to a one-

inch sample holder with a carbon sticker for microstructure analysis via scanning electron microscopy (SEM).

Table 2.1 Overview of specimens of *Arctica islandica* used in present study along with number of chemical analyses and areas in which microstructural analyses were conducted. Bivalves were collected alive at Þistilfjördur, NE Iceland (66°10′N, 015°21′W) on 17 August 2006. SEM = scanning electron microscopy; LA = laser ablation.

Specimen ID	Ontogenic age (yr)	# SEM images		# LA spots	
		Ventral margin	Hinge	Ventral margin	Hinge
ICE06-6.2-A201L	7	318	44	315	31
ICE06-6.2-A202L	6	353	21	351	21
ICE06-6.2-A203L	4	259	15	298	21

2.3.2 *In-situ* chemical analysis (LA-ICP-MS)

The LA-ICP-MS system at the Institute of Geosciences, University of Mainz consisted of a 193 nm ArF Eximer laser (ESI NWR 193) coupled to an Agilent 7500ce quadrupole ICP-MS. The laser repetition rate was set to 10 Hz at an approximate energy density of 3 J/cm^2. For each sample, 15 s of background measurement time were followed by 30 s of ablation and 20 s of wash-out time. Measurements were performed in single spot mode (n = 1037) using a beam diameter of 60 µm. The distance between the spot centers was ca. 90 µm. Laser tracks were positioned parallel to the main growth axis. To assess the relationship between shell Sr/Ca data and the BMU morphology of different microstructure categories (HOM, CA) that were deposited simultaneously in different shell portions, analyses were completed in the hinge and both sublayers of the outer shell layer (oOSL, iOSL; Fig. 2.1B-E; see Table A2.1 for overview on abbreviations used in this paper). This way, three contemporaneous shell Sr/Ca chronologies were measured in each specimen.

Accuracy and precision of the analyses were monitored with USGS MACS-3, BCR-2G, JCp-1 and JCt-1 (for respective quality control data, see Table S2.1). NIST SRM 610 was used to calibrate the element concentrations of shells and the quality control materials using preferred values reported in the GeoReM database (available at http://georem. mpch-mainz.gwdg.de, ver. 30, last access: 1 March 2022; Jochum et al., 2005, 2011). For data reduction, the time-resolved signals were processed using the software Glitter 4.4.1 (Griffin, 2008). Concentrations of strontium were determined from measured intensities of ^{88}Sr. Element-specific RSD% values, and average detection limit (computed as $3\sigma_{\text{background}}$ according to Jochum et al., 2012) is listed in the Table S2.1. ^{43}Ca served as the internal standard for reference materials and shells. To convert the shell Sr concentration data to molar shell Sr/Ca ratios (mmol/mol), a constant ^{43}Ca concentration of 380,000 µg/g was assumed (Marali et al., 2017).

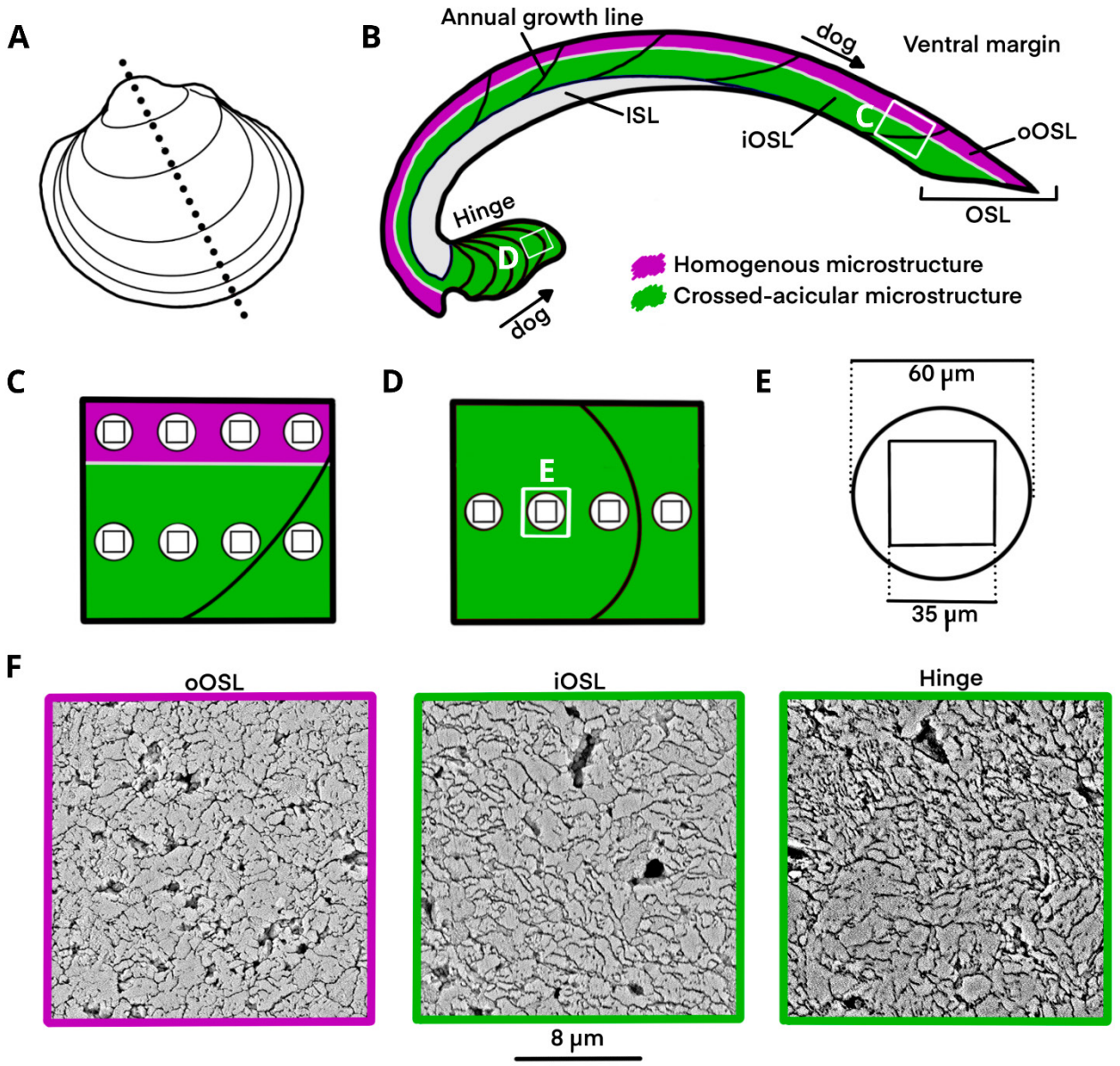

Figure 2.1 Overview of positions where element chemical and microstructural analyses were performed in shells of *Arctica islandica*. (A) Schematic representation of the left valve showing the cutting axis along (black dotted line). (B) Cross-sectioned shell slab showing different shell layers and dominant microstructures. The outer and inner shell layers (OSL, ISL) are separated by the myostracum. The OSL is further subdivided into an outer and inner portion (oOSL, iOSL). Homogenous microstructure (magenta) dominates the oOSL and crossed-acicular microstructure (green) prevails in the iOSL and hinge. The direction of growth (dog) of each shell portion is indicated by arrows. (C) An enlargement of panel (B) showing the sampling positions for microstructural and *in-situ* chemical analyses in the ventral margin. (D) An enlargement of panel (B) showing the sampling positions for microstructural and *in-situ* element chemical analyses in the hinge. (E) Schematic representation of a laser spot (diameter = 60 µm) for *in-situ* chemical analysis and a SEM image (square of 35 µm). (F) Microstructure examples: HOM and CA in the ventral margin, and CA in the hinge. The scale underneath applies to all SEM images.

2.3.3 Microstructure morphometry

The remaining section of each specimen was prepared for microstructure analysis via SEM according to the method reported by Höche et al. (2022). To identify individual BMUs under the SEM, ultrafine chemo-mechanical polishing was performed. For this purpose, the sections were polished for 10 min on a Buehler MetaServ 2000 rotational lap at 50 rpm with a Buehler MasterTex polishing cloth and Buehler MasterMet polishing suspension. This suspension has a grain size of 60 nm and an alkaline pH of ca. 10.1, allowing for removal of the inter-crystalline organics while minimizing crystalline abrasion of the section surface (Höche et al., 2022). In order to directly compare microstructural properties with shell Sr/Ca values, SEM images (35 µm × 35 µm) used for the analysis of BMU area and elongation were taken along contemporaneous transects as the laser ablation spots (Fig. 2.1B-E). The SEM images were taken with a Phenom Pro Desktop SEM (3rd generation) equipped with a CeB_6 electron source and backscatter electron detector at 7700× magnification and 10 keV. To prepare the images for morphometric studies, it was necessary to detect the individual BMUs in the SEM images. This process is called 'image segmentation' and was performed using the machine-learning-based image processing program Ilastik (Berg et al., 2019). After some training, and aside from manual quality screening of the resulting image segmentations, the software program was able to discern individual BMUs without further user interaction. Unsatisfactory results were excluded from further analysis and measurements were repeated. BMU recognition was exclusively performed within annual increments to ensure that data only came from one microstructure category. Therefore, images crossing annual growth lines were discarded. In *A. islandica*, annual growth lines are composed of irregular simple/spherulitic prismatic (ISP) microstructure. It should be added that annual growth lines were also too narrow (barely more than ca. 10 µm in width) to obtain a sufficient number of BMU data required for a statistically sound analysis. In each remaining SEM image (n = 1010), the BMU area and elongation (estimated by an ellipse-fit; measured as the ratio between the longest and shortest BMU axes) were automatically measured using the image processing library scikit-image (van der Walt et al., 2014) and the python script from Höche et al. (2021b). As indicated by previous studies, most morphological variation occurs among the largest BMUs, and, in this size group, the relationship between the microstructural properties and temperature is largest (Höche et al., 2021a). Therefore, only the 15 % largest BMUs of each SEM image were used in subsequent analyses.

2.3.4 Temporal alignment and re-sampling of the shell Sr/Ca and BMU data

In order to compare the datasets with each other, it was firstly required to convert the distance axis (= sample track) to a time axis, i.e., to temporally align the chemical and microstructural data of the shells, considering variable seasonal shell growth rates. For this purpose, the shells were photographed (Canon EOS 600D DSLR) under a reflected light microscope (Leica Stemi 508) and the images were stitched together with the Microsoft Image Composite Editor. Then, the position (= center) of each sample relative to the last annual growth line was determined using the image processing software ImageJ. In conjunction with the cumulative version of the seasonal shell growth model of *A. islandica* for shallow surface waters (recently refined by Höche et al., 2022; Fig. 2.1B), it was then possible to assign a calendar date to the center of each LA spot and each SEM image.

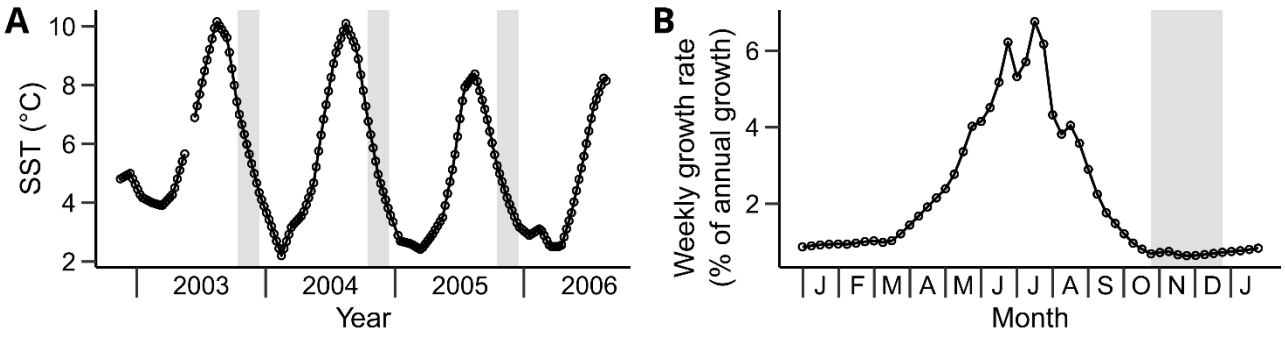

Figure 2.2 Water temperature and typical seasonal shell growth of *Arctica islandica*. (A) Weekly sea surface temperature data at Grímsey station (Hanna et al., 2006) between December 2003 and August 2006. (B) Seasonal shell growth model (weekly resolution) of *A. islandica* in shallow waters based on Höche et al. (2022). Vertical gray bars denote annual growth lines.

Once the sample positions were temporally contextualized, it was necessary to compute a new set of chronologies that can directly be compared with both each other and instrumental sea surface temperature (SST). This mathematical conversion was needed because each of the original samples represented different amounts of time and the time intervals between the centers of the samples varied. To compute chronologies of consistent temporal resolution, the portions between the sample centers were linearly interpolated (i.e., temporally aligned data were connected with lines), and the generated curves were resampled at equidistant time intervals to obtain monthly and weekly resolved chronologies. Due to differences in absolute growth rate, the annual increment width was considerably smaller in the hinge than in contemporaneous portions of the ventral margin. Based on the lowest temporal resolution of the

original data, a monthly resampling was chosen for the data obtained from the hinge, and a weekly resampling for those obtained from the ventral margin.

2.3.5 Regression analysis and detrending of shell Sr/Ca data

To assess the relationship between chemical properties and growth rate, Sr/Ca values were layer-specifically (oOSL, iOSL) plotted against weekly increment width (absolute values deducted from the annual growth model for each annual increment). Linear regression curves were then computed for Sr/Ca_{oOSL} versus weekly increment width and Sr/Ca_{iOSL} versus weekly increment width (Table 2.2). To evaluate the relationship between chemical and microstructural properties of the shells, eight regression curves were computed for the following pairs: (1) Sr/Ca_{vm} vs. BMU area, (2) Sr/Ca_{vm} vs. BMU elongation, (3) Sr/Ca_{oOSL} vs. BMU area, (4) Sr/Ca_{oOSL} vs. BMU elongation, (5) Sr/Ca_{iOSL} vs. BMU area, (6) Sr/Ca_{iOSL} vs. BMU elongation, (7) Sr/Ca_{hinge} vs. BMU area, (8) Sr/Ca_{hinge} vs. BMU elongation.

Table 2.2 Overview of the relationships (Pearson correlation; r = correlation coefficient; R^2 = coefficient of determination; p = probability) between the shell Sr/Ca data of *Artica islandica* and sea surface temperature (SST), biomineral unit (BMU) area and elongation and shell growth rate (weekly increment width). The relationships were examined for undetrended Sr/Ca data of the outer and inner portions of the outer shell layer (oOSL and iOSL, respectively), as well as both sublayers combined (referred to as vm = ventral margin). Regression models were computed for Sr/Ca values detrended (d) for growth rate (d_{GR}) and BMU size (d_{MS})-related effects for the iOSL, oOSL and vm. Magenta vm = homogenous microstructure; green vm = crossed-acicular microstructure. d_{GRMS} stands for double detrending.

Variables		SST (°C)	BMU area (µm²)	Weekly increment width (µm)	BMU elongation
Sr/Ca	vm	$r = 0.15$ $p < 0.001$	$r = -0.56$ $R^2 = 0.31$ $p < 0.001$	$r = 0.13$ $R^2 = 0.02$ $p < 0.001$	$r = -0.03$ $p = 0.465$
	oOSL	$r = 0.10$ $R^2 = 0.01$ $p = 0.069$	$r = -0.39$ $R^2 = 0.15$ $p < 0.001$	$R^2 = 0.02$ $p < 0.001$	$r = 0.02$ $R^2 = 0$ $p = 0.735$
	iOSL	$r = 0.45$ $R^2 = 0.20$ $p < 0.001$	$r = -0.68$ $R^2 = 0.46$ $p < 0.001$	$R^2 = 0.26$ $p < 0.001$	$r = -0.44$ $R^2 = 0.19$ $p < 0.001$
	hinge	$r = -0.04$ $R^2 = 0.01$ $p = 0.823$	$r = -0.12$ $R^2 = 0.01$ $p = 0.560$		$r = 0.01$ $R^2 < 0.01$ $p = 0.980$
$d_{GR}Sr/Ca$	vm	$r = 0.01$ $R^2 < 0.01$ $p = 0.908$			
	vm	$r = 0.40$ $R^2 = 0.16$ $p < 0.001$			
	oOSL	$r = 0.18$ $R^2 = 0.03$ $p < 0.001$	$r = -0.43$ $R^2 = 0.19$ $p < 0.001$		
	iOSL	$r = 0.27$ $R^2 = 0.07$ $p < 0.001$	$r = -0.58$ $R^2 = 0.33$ $p < 0.001$		
$d_{MS}Sr/Ca$	vm	$r = 0.22$ $R^2 = 0.05$ $p < 0.001$			
	vm	$r = 0.49$ $R^2 = 0.24$ $p < 0.001$			
	oOSL	$r = 0.20$ $R^2 = 0.04$ $p < 0.001$			
	iOSL	$r = 0.51$ $R^2 = 0.26$ $p < 0.001$			
$d_{GRMS}Sr/Ca$	iOSL	$r = 0.32$ $R^2 = 0.10$ $p < 0.001$			
	oOSL	$r = 0.29$ $R^2 = 0.08$ $p < 0.001$			

In a subsequent step, the possible influence of BMU area and/or shell growth rate was removed from shell Sr/Ca data measured in the ventral margin (note that the number of hinge data was insufficient for a respective mathematical conversion and that BMU elongation did not show consistent relationships with Sr/Ca). In practice, the correlation between Sr/Ca and BMU area, as well as between Sr/Ca and shell growth, was mathematically eliminated, and shell Sr/Ca thus detrended. This was accomplished in a similar way, as ontogenetic age trends are removed from annual increment widths of bivalves (Schöne, 2013). Detrended Sr/Ca data were computed by subtracting measured by predicted Sr/Ca values, where the predicted values are obtained from the regression curves (Sr/Ca vs. growth rate or BMU area, respectively). The resulting data provide a measure of how shell Sr/Ca values deviate from the regression curve. The following detrended shell Sr/Ca chronologies were computed: (1) $d_{GR}Sr/Ca_{oOSL}$, (2) $d_{GR}Sr/Ca_{iOSL}$, (3) $d_{GR}Sr/Ca_{vm}$, (4) $d_{MS}Sr/Ca_{oOSL}$, (5) $d_{MS}Sr/Ca_{iOSL}$, (6) $d_{MS}Sr/Ca_{vm}$, (7) $d_{GRMS}Sr/Ca_{oOSL}$, (8) $d_{GRMS}Sr/Ca_{iOSL}$ and (9) $d_{GRMS}Sr/Ca_{vm}$, where the prefix 'd' stands for 'detrended' and the following subscript denotes how the Sr/Ca data (of the respective shell portions: oOSL, iOSL and vm) were detrended, i.e., by growth rate (GR), microstructure (MS) or a combination of both (GRMS). Detrended and non-detrended Sr/Ca data, as well as BMU morphology data of the two transects of the ventral margin, oOSL and iOSL, were then compared to each other using non-parametric Mann-Whitney *U* two-sample rank-sum tests. To assess possible links between SST and shell Sr/Ca data before and after detrending, Pearson correlations and corresponding levels of significance were calculated. SST data were obtained from Grímsey station (Fig. 2.2A; Hanna et al., 2006).

2.4 Results

2.4.1 Shell strontium-to-calcium ratios and BMU morphology

Temporally aligned, weekly resolved shell Sr/Ca chronologies were, at large, highly synchronous among the three studied specimens (Fig. 2.3A). In both shell layers of the ventral margin, Sr/Ca_{vm} values gradually increased during the year, reached a maximum in summer (August) and declined toward the following annual growth line. Differences between the Sr/Ca curves of the two sublayers of the outer shell layer were observed during the beginning of the growing season. In the iOSL, the seasonal Sr/Ca minimum was typically attained shortly after the annual growth line (= November), i.e., during the beginning of the growing season (0.70 mmol/mol). However, in the oOSL, Sr/Ca values first increased stronger than in the iOSL, reached a local maximum in February and then declined again to attain the seasonal Sr/Ca minimum ca. half-way between adjacent annual growth lines in the oOSL (1.08 mmol/mol, ca. June/July; Fig. 2.3A). Sr/Ca_{vm} ratios

were generally higher in the oOSL (1.55 ± 0.14 mmol/mol; average ± 1 standard deviation) than in the iOSL (1.11 ± 0.18 mmol/mol). In the iOSL, Sr/Ca attained highest values of 1.59 mmol/mol, whereas those of the oOSL reached 2.14 mmol/mol. Note that samples covering the annual growth lines exceeded the aforementioned values, on average, by 0.25 mmol/mol (Table S2.2). As explained in the preceding section, data from annual growth lines were excluded from the analysis.

As shown in Figure 2.3B, the average Sr/Ca_{vm} data differed significantly between the two sublayers of the outer shell layer (Mann-Whitney *U*, $p < 0.001$). Note that the two sublayers also differed by their shell microstructure. The oOSL consisted of HOM and the iOSL of CA microstructures. In contrast, contemporaneous shell portions of the hinge and ventral margin belonging to the same microstructure category (i.e., CA) contained statistically indistinguishable (Mann-Whitney *U*, $p = 0.299$) concentrations of Sr (Fig. 2.3B). On average, the Sr/Ca values of the hinge (1.25 mmol/mol) were only 0.14 mmol/mol higher than those of the iOSL. However, Sr/Ca data of the hinge were statistically significantly (on average, 0.30 mmol/mol) lower than those of the oOSL (Mann-Whitney *U*, $p < 0.001$).

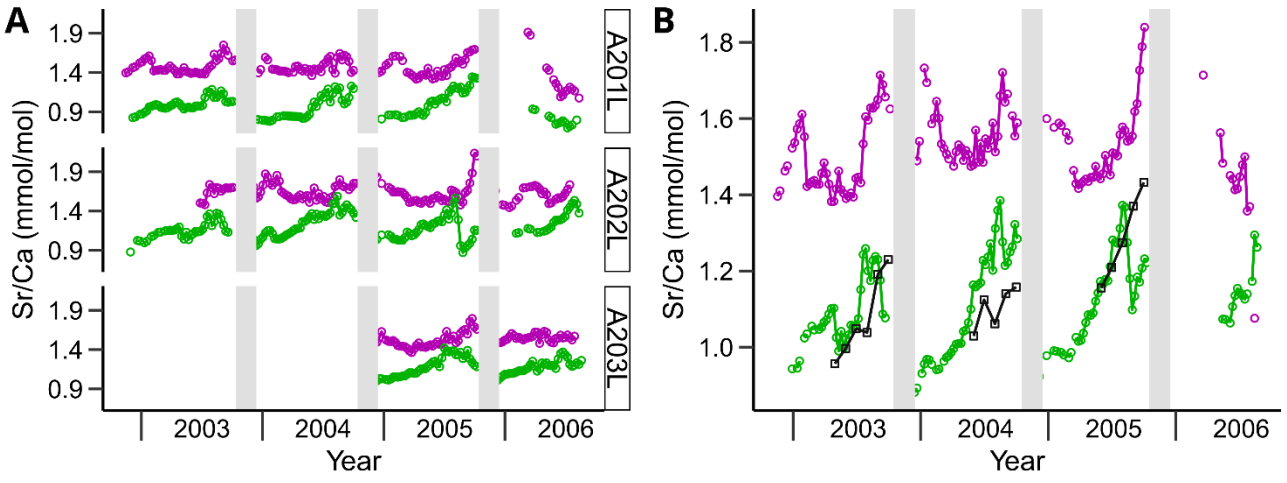

Figure 2.3 Shell Sr/Ca chronologies of the three studied specimens (A201L, A202L and A203L) of *Arctica islandica*. Magenta open circles = data from the outer portion of the outer shell layer (oOSL; homogeneous microstructure, HOM) of the ventral margin; green open circles = data from the inner portion of the outer shell layer (iOSL; crossed-acicular microstructure, CA) of the ventral margin; black open squares = data from the hinge (CA). Vertical gray bars denote annual growth lines. (A) Sr/Ca chronologies of each specimen and sublayer of the outer shell layer (oOSL, iOSL). (B) Average Sr/Ca chronologies computed from curves depicted in (A). Data from the ventral margin are weekly resolved. Monthly Sr/Ca data of the hinge (data from all studied specimens combined) are shown for comparison.

Aside from differences in their element chemistry and overall microstructure, the two sublayers of the outer shell layer revealed a statistically significant difference (Mann-Whitney *U*,

$p < 0.001$) in the size of the biomineral units (BMUs) composing the CA and the HOM microstructures (Fig. 2.4). The BMUs of the iOSL (CA) were generally larger than those of the oOSL (HOM), with average areas of 0.98 ± 0.19 µm² and 0.85 ± 0.17 µm², respectively. While the Sr/Ca_{vm} values were similar for all CA microstructures, irrespective of the shell portion (Sr/Ca_{hinge} and Sr/Ca_{iOSL}), the CA BMUs were significantly larger (range between 0.94 µm² and 1.48 µm²) in the hinger than in the ventral margin (ca. 0.85 µm²; Mann-Whitney *U*, $p < 0.001$; Fig. 2.4).

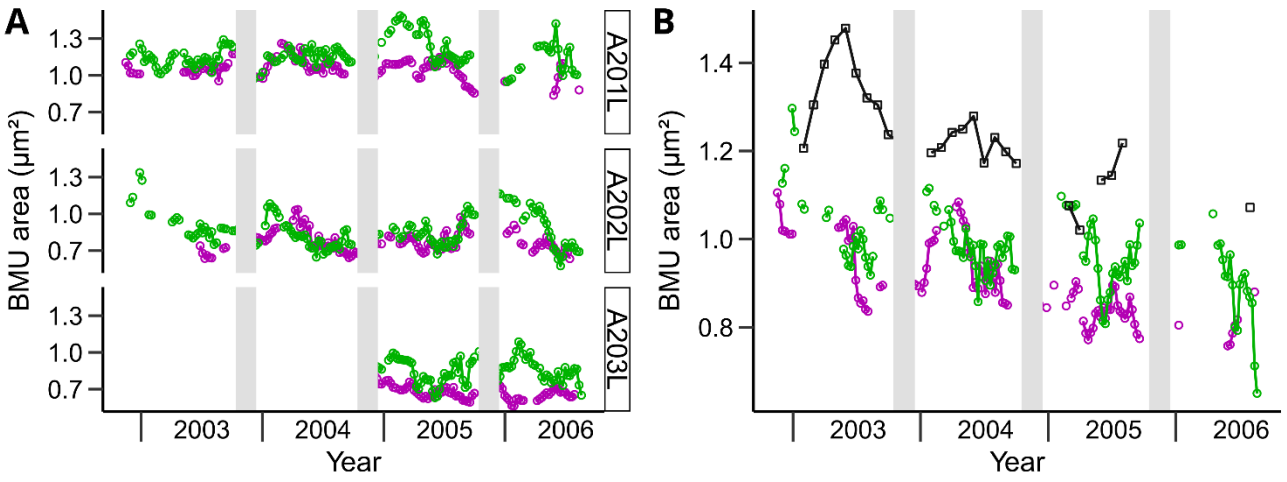

Figure 2.4 Average biomineral unit (BMU) area chronologies of the three studied shells (A201L, A202L and A203L) of *Arctica islandica*. Acronyms and color coding as in caption of Figure 2.3. Note, magenta = homogenous microstructure (oOSL); green = crossed-acicular microstructure (iOSL). Vertical gray bars denote annual growth lines. (A) BMU area chronologies of each specimen and sublayer of the outer shell layer (oOSL, iOSL). (B) Average BMU area chronologies computed from the curves depicted in (A). Data from the ventral margin are weekly resolved. Monthly Sr/Ca data of the hinge (data from all studied specimens combined) are shown for comparison.

The elongation of BMUs, in contrast, did not strongly differ between the specimens or shell portions (Fig. 2.5). On average, the elongation of the CA BMUs of the iOSL was only 0.02 lower than the elongation of the HOM BMUs of the oOSL (average = 1.77 ± 0.05 and 1.79 ± 0.06, respectively). Moreover, the CA BMUs of the hinge were, on average, more elongated than those of the ventral margin. With an average of 1.99 ± 0.06, the elongation of the BMUs in the hinge differed significantly from those of the ventral margin (Mann-Whitney *U*, $p < 0.001$).

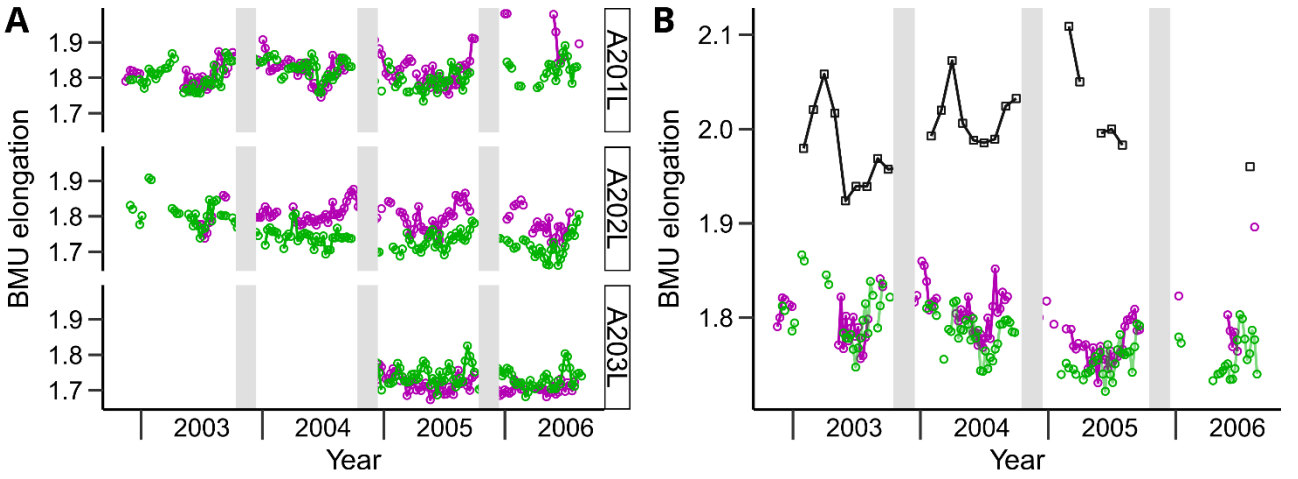

Figure 2.5 Average biomineral unit (BMU) elongation chronologies of the three studied shells (A201L, A202L and A203L) of *Arctica islandica*. Acronyms and color coding as in caption of Figure 2.3. Note, magenta = homogenous microstructure (oOSL); green = crossed-acicular microstructure (iOSL). Vertical gray bars = annual growth lines. (A) BMU elongation chronologies of each specimen and sublayer of the outer shell layer (oOSL, iOSL). (B) Average BMU elongation chronologies computed from the curves depicted in (A). Data from the ventral margin are weekly resolved. Monthly Sr/Ca data of the hinge (data from all studied specimens combined) are shown for comparison.

2.4.2 Relationships between shell Sr/Ca, growth rate and BMU morphology

Regression models for shell Sr/Ca and the growth rate, BMU area and BMU elongation are depicted in Figure 2.6. The mathematical relationship between shell Sr/Ca data and the growth rate was best described with non-linear regression models (Fig. 2.6A and Table 2.2). In the iOSL, Sr/Ca values (Sr/Ca_{iOSL}) increased with the growth rate, but the opposite occurred in the oOSL. The strongest changes in Sr/Ca_{oOSL} and Sr/Ca_{iOSL} were observed during slow growth. If Sr/Ca data from both shell layers were combined (Sr/Ca_{vm}) in a single linear regression model, a weak positive linear correlation was found ($r = 0.13$, $p < 0.001$; Fig. 2.6A and Table 2.2).

Sr/Ca values were negatively coupled with the BMU area (Fig. 2.6B). If data pairs from the ventral margin (oOSL, iOSL) were combined in a regression model, the Pearson r equaled -0.56 ($R^2 = 0.32$, $p < 0.001$; Table 2.2). However, the strength and significance of this correlation varied within the different shell portions. The strongest relationship occurred in the iOSL ($r = -0.68$, $p < 0.001$), and the weakest in the hinge ($r = -0.12$, $p = 0.47$; Table 2.2). A moderately strong, though significant link between Sr/Ca and BMU area was observed in the oOSL ($r = -0.39$, $p < 0.001$; Fig. 2.6B and Table 2.2). Shell portions consisting of the CA microstructure showed a larger variation in BMU area and contained less Sr than shell portions made of HOM. Much less covariation was observed between Sr/Ca and BMU elongation, and only in the iOSL were both parameters

significantly coupled with each other, though not particularly strongly (r = -0.44, p < 0.001; Fig. 2.6C and Table 2.2).

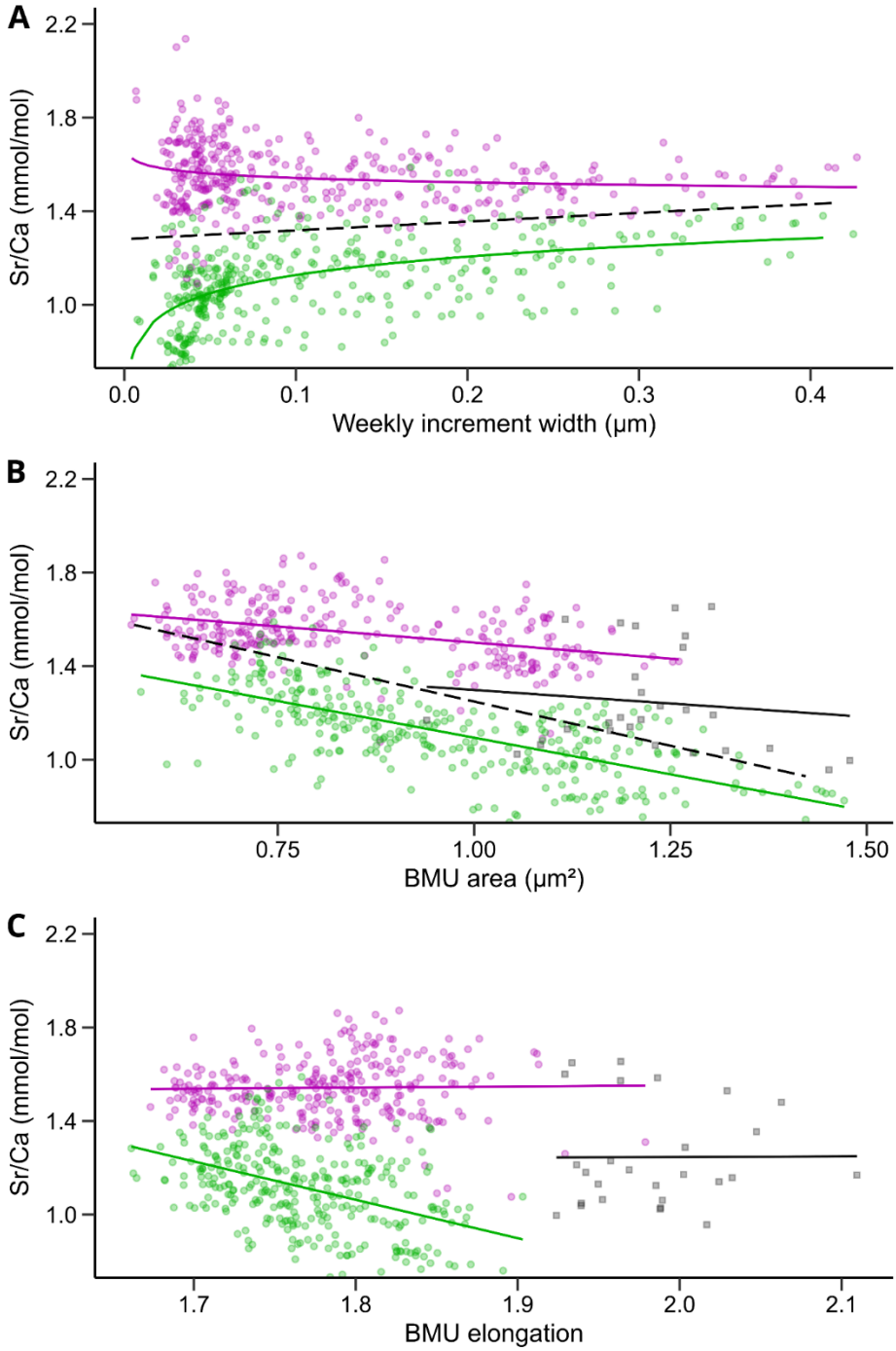

Figure 2.6 Relationships between Sr/Ca data and microstructural properties of *Arctica islandica* shells. Acronyms and color coding as in caption of Figure 2.3. BMU = biomineral unit. Note, magenta = homogenous microstructure (oOSL); green = crossed-acicular microstructure (iOSL); black = hinge. Green and purple data are weekly resolved, black data monthly. Regression curves are depicted in the same color as data of respective shell portion. Black dashed lines represent linear regression model of entire outer shell layer (oOSL + iOSL) dataset. (A) In the inner portion of the outer shell layer (iOSL, magenta), shell

Sr/Ca is weakly negatively linked to increment width, whereas a stronger and positive correlation exists in the outer sublayer of outer shell layer (oOSL, green). Note that non-linear models provided a better fit than linear models. When data from both OSL sublayers (oOSL, iOSL) are combined, a weak positive correlation is found with shell growth rate. (B) Shell Sr/Ca is negatively correlated to BMU area. (C) In the oOSL and hinge, shell Sr/Ca is weekly positively coupled to BMU elongation, but a stronger and negative correlation exists in the iOSL.

2.4.3 Growth rate and BMU area-detrended shell Sr/Ca ratios

Based on the regression models depicted in Figure 2.6, the correlation with growth rate and/or BMU area was mathematically removed from the shell Sr/Ca data (Table 2.2). The resulting chronologies are depicted in Figure 2.7A-D. If the correlation with growth rate was shell-layer-specifically eliminated from the Sr/Ca data using the non-linear models for the iOSL and oOSL (Fig. 2.6A), the resulting $d_{GR}Sr/Ca_{iOSL}$ and $d_{GR}Sr/Ca_{oOSL}$ chronologies (Fig. 2.7A) were plotted much closer together than the non-detrended series depicted in Figure 2.3 and were statistically indistinguishable (Mann-Whitney *U*, $p = 0.808$). The new time-series also conserved most of the seasonal range of the original Sr/Ca_{oOSL} and Sr/Ca_{iOSL} data (Fig. 2.3). However, if detrending was accomplished based on the regression model that combined Sr/Ca and growth rate data from both sublayers (Fig. 2.6A), the new $d_{GR}Sr/Ca_{vm}$ time-series differed significantly from each other (Mann-Whitney *U*, $p < 0.001$; Fig. 2.7B) and were nearly identical to the non-detrended Sr/Ca_{vm} chronologies (Fig. 2.3).

The layer-specific detrending by the microstructure (here: BMU area) based on the regression models shown in Figure 2.6B also produced Sr/Ca chronologies ($d_{MS}Sr/Ca_{iOSL}$ and $d_{MS}Sr/Ca_{oOSL}$) that showed a stronger synchronicity with each other than the original curves (Fig. 2.3), and their distributions were statistically indistinguishable (Mann-Whitney *U*, $p = 0.741$). However, the amplitudes were attenuated compared to the growth rate-detrended (Fig. 2.7A) and non-detrended Sr/Ca chronologies (Fig. 2.3). As in the case of the growth-rate detrending, the Sr/Ca chronologies of the oOSL and iOSL were still strongly offset from each other if detrending was carried out based on the regression model that combined Sr/Ca and BMU size data from both sublayers of the OSL (Fig. 2.7D). The $d_{MS}Sr/Ca_{vm}$ time-series were statistically different from each other (Mann-Whitney *U*, $p < 0.001$; Fig. 2.7D) and revealed similar seasonal ranges to the Sr/Ca_{vm} series (Fig. 2.3).

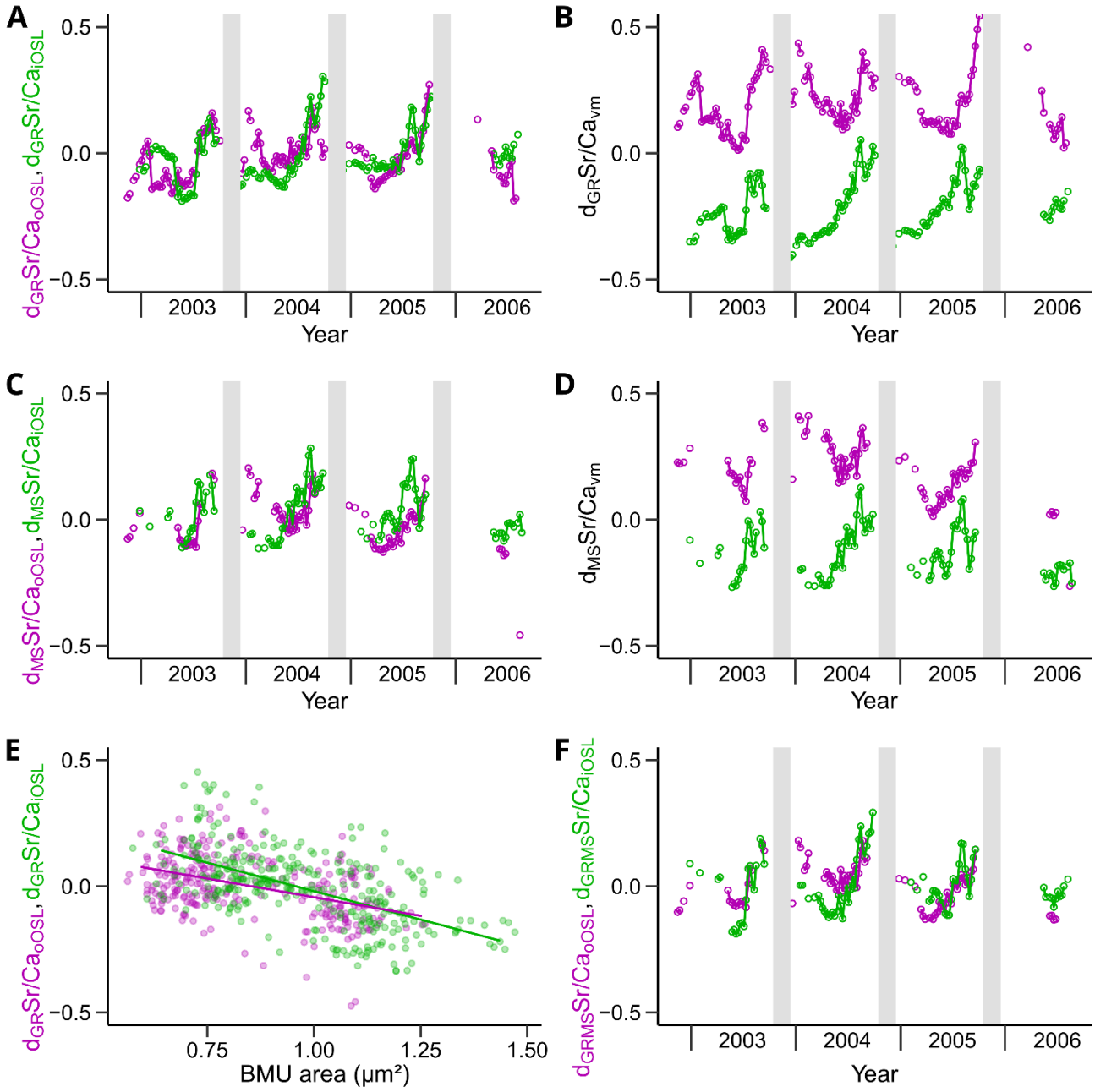

Figure 2.7 Detrended shell Sr/Ca chronologies of the outer and inner sublayers of the outer shell layer (oOSL, iOSL, respectively) of the ventral margin (vm) of *Arctica islandica*. Data represent averages of three specimens. Acronyms and color coding as in caption of Figure 2.3. (A, B) Growth rate (GR)-detrended Sr/Ca data. (A) Shell-sublayer-specific detrending based on non-linear models for oOSL and iOSL depicted in Figure 2.6A (magenta = $d_{GR}Sr/Ca_{oOSL}$; green = $d_{GR}Sr/Ca_{iOSL}$). (B) Detrending based on a regression model in which data from oOSL and iOSL (= 'vm') were combined (Fig. 2.6A) (magenta = $d_{GR}Sr/Ca_{vm}$ of oOSL; green = $d_{GR}Sr/Ca_{vm}$ of iOSL). (C, D) BMU area (MS)-detrended Sr/Ca data. (C) Shell-sublayer-specific detrending based on linear models for oOSL and iOSL depicted in Figure 2.6B (magenta = $d_{MS}Sr/Ca_{oOSL}$; green = $d_{MS}Sr/Ca_{iOSL}$). (D) Detrending based on a regression model in which data from oOSL and iOSL (= 'vm') were combined (Fig. 2.6A) (magenta = $d_{MS}Sr/Ca_{vm}$ of oOSL; green = $d_{MS}Sr/Ca_{vm}$ of iOSL). (E) Crossplot of growth-rate-detrended Sr/Ca (sublayer-specific detrending as in (A)) versus BMU area. (F) Double detrended Sr/Ca chronologies based on linear models depicted in (E) (magenta = $d_{GRMS}Sr/Ca_{oOSL}$; green = $d_{GRMS}Sr/Ca_{iOSL}$).

A double detrending likewise resulted in strongly coherent Sr/Ca chronologies of the oOSL and iOSL (Fig. 2.7F). For this purpose, the layer-specific growth-rate-detrended Sr/Ca data ($d_{GR}Sr/Ca_{iOSL}$ and $d_{GR}Sr/Ca_{oOSL}$) were plotted against the BMU area (Fig. 2.7E). The linear regression curves were then used to further detrend the data, resulting in double-detrended Sr/Ca values. The $d_{GRMS}Sr/Ca_{iOSL}$ and $d_{GRMS}Sr/Ca_{oOSL}$ chronologies showed no statistical difference (Mann-Whitney U, $p = 0.847$), and, when plotted against time (Fig. 2.7F), the seasonal variations had lower amplitudes than the undetrended Sr/Ca series (Fig. 2.3).

2.4.4 Relationships between Sr/Ca ratios and water temperature

Sr/Ca data of the ventral margin were weakly positively correlated to SST ($r = 0.15$, $p < 0.001$; Table 2.2). A slightly stronger link existed when layer-specific regression analyses were conducted (Fig. 2.8A). In fact, Sr/Ca_{iOSL} was the only profile that was significantly coupled to SST ($r = 0.45$, $p < 0.001$), whereas Sr/Ca_{oOSL} was not ($r = 0.10$, $p = 0.07$; Table 2.2). Sr/Ca values of the hinge revealed no correlation with SST ($r = -0.04$, $p = 0.823$; Table 2.2).

While the growth-rate-detrended Sr/Ca data showed only extremely weak though statistically significant positive correlations with SST ($r = 0.18$ to 0.27, $p < 0.001$; Fig. 2.8A, B and Table 2.2), the BMU-area-detrended Sr/Ca data of the iOSL data were more strongly tied to SST ($r = 0.51$, $p < 0.001$; Table 2.2). However, BMU-area-detrended Sr/Ca values of oOSL were only very weakly correlated to SST ($r = 0.20$, $p < 0.001$; Table 2.2). Double detrending resulted in weak correlations between Sr/Ca and SST in both OSL sublayers ($r = 0.30$, $p < 0.001$; Table 2.2).

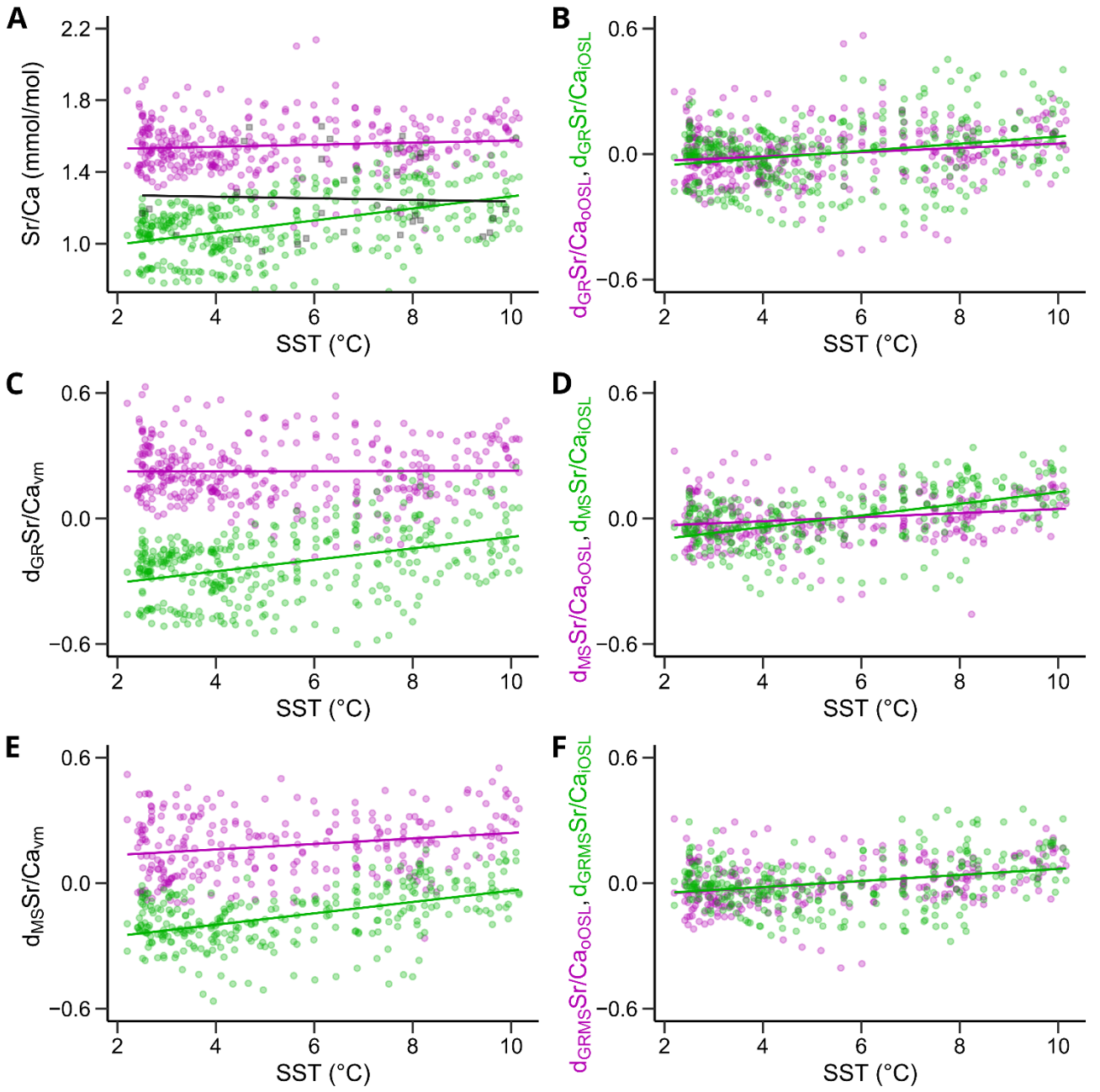

Figure 2.8 Relationships between shell Sr/Ca data of *Arctica islandica* and SST. Acronyms and color coding as in caption of Figure 3. (A) Undetrended Sr/Ca data; (B-F) detrended Sr/Ca data. (A) Shell Sr/Ca of the oOSL and iOSL are weakly positively correlated to sea surface temperature, and those from the hinge are not. (B, C) Growth rate (GR)-detrended Sr/Ca data. (B) Sublayer-specific detrending, (C) detrending based on all ventral margin data. (D, E) BMU area (MS)-detrended Sr/Ca data. (D) Sublayer-specific detrending, (E) detrending based on all ventral margin data. (F) Double-detrended Sr/Ca chronologies (growth rate + BMU area detrending, layer-specific as in (B, D)).

2.5 Discussion

Based on the findings presented here, the hypothesis examined in this study needs to be rejected. It does not seem to be possible to reconstruct water temperature from intra-annual shell Sr/Ca values of *A. islandica*, even if the growth rate and/or microstructure-related bias was mathematically removed from the data. Shell Sr/Ca values were weakly and non-linearly linked to the shell growth rate and more strongly, linearly and likewise statistically significantly coupled with both the biomineral unit size and water temperature (Fig. 2.6 and 2.8A). However, contrary to thermodynamic expectations for aragonite and results from inorganically precipitated aragonite (Kinsman and Holland, 1969; Gaetani and Cohen, 2006), the seasonal shell Sr/Ca values were positively correlated to temperature (r = 0.15; Fig. 2.8A), and remained so even after detrending by the growth rate and/or BMU area (r = 0.01 to 0.49; Fig. 2.8B, D, F). Furthermore, the strong synchronicity among Sr/Ca chronologies of contemporaneous specimens suggests that other, unknown, environmental parameters exerted a strong control over the incorporation of strontium relative to calcium into the shell. Such a covariation would not be expected if the shell Sr content was largely governed by (individual) physiological processes.

2.5.1 Temperature control of shell Sr/Ca?

The development of environmental proxies in bivalve shells and other biogenic hard parts is typically based on empirical observations and supported by thermodynamic considerations or results from synthetically precipitated minerals. A strong running similarity of chemical or structural time-series among different contemporaneous specimens suggests a common response to an extrinsic forcing and represents a major prerequisite to establish an environmental proxy. For example, if shell growth rates change coherently among several contemporaneous specimens from the same habitat, it is highly likely that growth was controlled by environmental factors; in the case of bivalves, by a combination of temperature, food supply and food quality (Ansell, 1968; Kennish and Olsson, 1975; Goodwin et al., 2001; Witbaard et al., 2001). Likewise, a running similarity of element chemical profiles in shells of several coeval specimens – as observed in the present study for Sr/Ca – is typically considered as an indicator of environmental controls (Marali et al., 2017). However, the specific environmental variables causing such common signals often remain enigmatic (e.g., Ba/Ca: Gillikin et al., 2008; various element/Ca ratios: Marali et al., 2017).

It can be tempting to infer causality from synchronicity and a statistically significant correlation between a given environmental variable, e.g., water temperature, and a chemical property, e.g., shell Sr/Ca, specifically if a relationship between these variables has previously been identified in synthetic $CaCO_3$ (Kinsman and Holland, 1969; Gaetani and Cohen, 2006).

However, to substantiate a causal relationship between shell Sr/Ca and temperature, at least the sign of the regression curve needs to be identical to that observed in abiogenic precipitates, and, ideally, the intercept and the steepness of the regression slope should be similar as well. Since the Sr content of synthetic aragonite decreases with rising temperature (Dietzel et al., 2004; Gaetani and Cohen, 2006), the observed positive correlation between the seasonal shell Sr/Ca of *A. islandica* and water temperature most likely does not reflect a causal relationship. The same applies to similar observations made in ocean quahogs in previous studies (Hart and Blusztajn, 1998; Toland et al., 2000), as well as other species with aragonitic skeletons (e.g., Stecher et al., 1996). In most studies in which the thermodynamically expected negative correlation between the two variables could be verified (Füllenbach et al., 2017; Zhao et al., 2017), the temperature sensitivity of -0.02 mmol/mol/°C remained well below that observed in synthetic aragonite (-0.04 mmol/mol/°C, Gaetani and Cohen, 2006; see Yan et al., 2011, 2013, 2014), suggesting that strong vital effects were at work. This view is further supported by consistently low concentrations of Sr in bivalve shells (Gillikin et al., 2005; Sano et al., 2012; Vihtakari et al., 2016; Schleinkofer et al., 2021). For example, in the studied specimens, shell Sr/Ca ratios remained, on average, almost eight to nine times below values expected for equilibrium fractionation at the same temperature range (2 to 10 °C: 1.34 ± 0.11 mmol/mol as opposed to ca. 11 to 12 mmol/mol using Equation (8) of Gaetani and Cohen, 2006; see further details in next section).

Theoretically, it appears possible that seawater Sr/Ca values varied on seasonal timescales – e.g., due to riverine influx (Shen et al., 2005) – and overprinted temperature signals potentially encoded in shell Sr/Ca. In that case, the studied shells would have predominantly recorded changes in seawater Sr/Ca. However, the study region was not affected by major rivers, and highly resolved Sr/Ca_{water} time-series are currently not available to evaluate the temporal variability of the water chemistry where the shells grew. Our own unpublished data indicate that Sr/Ca_{water} near the sample locality can spatially vary between 8.09 and 8.17 mmol/mol in surface water (66°11′58.68′′N, 015°23′32.76′′W and 66°11′23.46′′N, 015°20′34.02′′W, respectively, 21 August 2012), and 8.12 and 8.13 mmol/mol in bottom water (ca. 10 to 20 m water depth; localities and date as before). If these changes remained unconsidered, temperature estimates would be off by 5 to 40 °C considering the weak temperature sensitivity of -0.02 mmol/mol/°C. Near Reykjavík (64°07′52.32′′N, 021°57′38.35′′W), the surface water Sr/Ca varied between 9.49 mmol/mol on 19 April 2012 and 8.02 mmol/mol on 21 May 2012. Certainly, more data are required to test the hypothesis of shells predominantly recording changes in water chemistry rather than temperature.

It remains unclear why annually averaged Sr/Ca values of old-grown *A. islandica* specimens from Iceland were moderately strongly and significantly negatively linked to water temperature (Schöne et al., 2011), whereas intra-annual Sr/Ca values of conspecific specimens

from the same locality (present study), other sites (Hart and Blusztajn, 1998; Toland et al., 2000) or those grown in the laboratory (Wanamaker and Gillikin, 2019), were not. Were Schöne et al. (2011) deceived by a spurious correlation, or were the shell Sr/Ca values of their study less strongly biased by other, unknown extrinsic factors than in the shells studied here, so that the actual negative relationship emerged? Or is the main reason for the significant negative correlation that Sr/Ca data from the annual growth lines were included in their analysis? As the calculations demonstrated in Schöne et al. (2011), annual growth lines may have formed near or even in chemical equilibrium with the ambient water. A possible reason for that is that, during growth line formation, the food supply was strongly reduced and thus so was the production of energy. Energy would be needed to biologically control the incorporation of Sr and other trace impurities into the shell (e.g., by actively pumping Sr^{2+} ions away from the site of biomineralization or producing organic macromolecules that can scavenge Sr^{2+} so that it cannot be incorporated into the shell). The remaining energy sufficed to form biominerals (ISP), but not to precipitate chemically 'pure' shell material. Elevated Sr/Ca values of the growth lines may have strongly contributed to the annual Sr/Ca average, resulting in an inverse relationship between annual Sr/Ca with SST. With an increasing ontogenetic age, annual growth lines become gradually broader and represent an increasingly larger proportion of annual increments. Hence, the contribution of growth line Sr/Ca values to the annual average gradually increases through its lifetime (Schöne et al., 2011). Accordingly, annual Sr/Ca values of ontogenetically older shell portions should be increasingly strongly negatively correlated to SST. These hypotheses should be tested in subsequent studies.

2.5.2 Relationship between Sr/Ca and shell microstructure

In the studied shells of *A. islandica*, the Sr concentration was distinctly inversely correlated to the BMU size, i.e., Sr/Ca values gradually decreased with an increasing BMU area. However, the regression slopes and, more importantly, the intercepts of the regression lines with the y-axis differed between the studied shell portions (Fig. 2.6B). For that reason, it was not possible to effectively reduce the statistical difference between Sr/Ca_{oOSL} and Sr/Ca_{iOSL} chronologies based on a regression model in which data from both OSL sublayers were combined (Fig. 2.6B and 2.7D). The differences in the regression lines suggest that Sr/Ca is not directly coupled to BMU size, but to other properties that covary with BMU area and/or Sr/Ca. This assumption is supported by the following observations: (i) the oOSL contained more Sr than the iOSL (which agrees with previous observations: Schöne et al., 2010, 2013; Shirai et al., 2014) although the BMU size ranges were nearly the same in both OSL sublayers; (ii) based on the negative correlation between Sr/Ca and the BMU size, the lowest Sr concentration should be measured in the annual

growth lines (which were not further analyzed in this study) because they contain the largest BMUs (ISP) of the entire shell (Ropes, 1984; Dunca et al., 2009; Karney et al., 2011, 2012). However, the opposite is the case in *A. islandica* and other hitherto studied bivalves. The highest Sr concentrations are typically found in annual growth lines (Table S2.2; Schöne et al., 2013; Shirai et al., 2014; Füllenbach et al., 2017; Markulin et al., 2019); (iii) Sr/Ca values of the hinge show a different linear relationship with the BMU size than the Sr/Ca of the iOSL, despite consisting of the same microstructure type, i.e., CA (Fig. 2.1B-F and 2.6B).

To identify variables that could have caused the apparent relationship between the BMU size and Sr/Ca values, the mechanism of Sr incorporation into the shells needs to be considered. Due to similar ionic radii and charge, Sr^{2+} (132 pm) can substitute for Ca^{2+} (114 pm) in the crystal lattice of aragonite (Goldschmidt, 1926; Amiel et al., 1973; Speer, 1983). As experimentally demonstrated in inorganically precipitated aragonite, the Sr concentration decreases with an increasing temperature (Kinsman and Holland, 1969). Inorganic aragonite precipitated at 15 °C contained 1.25 times as much Sr as present in the calcifying fluid, whereas, at 25 °C, this value – also known as the Doerner-Hoskins exchange coefficient – decreased to 1.16 (Gaetani and Cohen, 2006). Using the exchange equation provided by Gaetani and Cohen (2006; Equation (8)), and taking Sr/Ca values of the habitat of the studied *A. islandica* specimens into account (i.e., 8.5 to 8.8 mmol/mol, cf. Lebrato et al., 2020), the shell Sr/Ca should vary between 11.05 and 12.24 mmol/mol for the observed temperature range of 2 to 10 °C (Fig. 2.2A), provided the shells formed in chemical equilibrium with the ambient water (or biomineralization fluid). However, the measured shell Sr/Ca values (Fig. 2.3) remained far below that figure, which agrees with many previous findings (Gillikin et al., 2005; Sano et al., 2012; Vihtakari et al., 2016; Schleinkofer et al., 2021), suggesting that the incorporation of Sr into the shell is under strong biological control. This ensures, for example, that the optimal mechanical properties of the shell are maintained, which secures the survival of the bivalve (predator resistance). Increased amounts of trace impurities can increase the hardness of the $CaCO_3$ (Boon et al., 2019) at the expense of elasticity, i.e., a harder shell is more vulnerable to fractures. Given the inverse relationship between the shell Sr content and temperature, it may be possible for Sr to be more effectively removed from the biomineralization site when more energy is available. For the same reason, the bivalve can likely also better control microstructural properties. In contrast, during the formation of the annual growth lines, metabolic rates are strongly reduced, and the energy is thus limited. Instead of highly complex microstructures (HOM, CA), the bivalve then forms Sr-rich irregular simple/spherulitic prisms that are similar in habit though smaller than the spherulitic grains observed in inorganic aragonite (Gaetani and Cohen, 2006). If that interpretation is correct, the shell Sr/Ca and BMU size would be merely indirectly correlated with each other.

The incorporation of trace metals into $CaCO_3$ also depends on the crystal habit and varies among the different crystal faces, amongst others, due to crystal lattice defects. For example, in the case of calcite, Sr^{2+} incorporation is facilitated by increased amounts of crystal lattice defects (Plummer and Busenberg, 1987; Paquette and Reeder, 1995). The same applies to the incorporation of Mg^{2+} into aragonite (Mavromatis et al., 2022). Due to a different mode of growth (Paquette and Reeder, 1995), some crystal faces (e.g., the dominant {1014} face in calcite) develop more lattice defects than others, which significantly lowers the energetic cost of Mg^{2+} and Sr^{2+} incorporation. Furthermore, the substitution of Ca^{2+} by Mg^{2+}, and especially by Sr^{2+}, is energetically less costly on the surface of aragonite than deeper inside the crystal (Menadakis et al., 2008; Kawano et al., 2015). Therefore, large, exposed crystal faces should promote the incorporation of trace impurities. If different crystal faces provide variable opportunities for trace metal incorporation (Reeder and Grams, 1987; Paquette and Reeder, 1995), and larger amounts of trace impurities can be accommodated on large, exposed crystal surfaces (Menadakis et al., 2008; Kawano et al., 2015), the Sr content of the shell may thus be intimately linked to the BMU habit (Foster et al., 2009). Idiomorphic BMUs with well-developed primary crystal faces may thus accommodate a larger number of strontium ions than xenomorphic BMUs, which lack a characteristic habit due to competition with neighboring BMUs during growth. This interpretation would fit well with the observed Sr/Ca differences among the different microstructures. Blocky, idiomorphic BMUs present at annual growth lines possess well-developed crystal faces and, accordingly, show the largest Sr/Ca values (Table S2.2; Schöne et al., 2013; Shirai et al., 2014; Roger et al., 2017). Biomineral units of the oOSL (HOM), in contrast, are not idiomorphic in habit and consist of several co-aligned or twinned crystals (i.e., irregularly shaped crystallites). This suggests that the development of ideal crystal growth faces is inhibited during the formation of BMUs of the homogenous microstructure, which is likely the reason why they contain less Sr^{2+} than the irregular simple/spherulitic prisms found at the annual growth lines. The CA-BMUs of the iOSL are highly ramified, convoluted and interfingered, and hence probably possess the least developed primary crystal faces. Accordingly, the iOSL contains less Sr than the oOSL.

Following the hypothesis that Sr^{2+} incorporation into the shell aragonite depends on the degree of idiomorphism of the BMUs, (microstructure-specific) correlations between Sr/Ca and the BMU size should occur (Fig. 2.6A). Sr/Ca values of both sublayers of the outer shell layer of *A. islandica* decreased with an increasing BMU size, which is expected, given that an increasing size also leads to increased twinning (HOM) and ramification of the BMU outline (CA). In contrast, the large idiomorphic BMUs of the annual growth lines have larger, well-developed crystal faces and, thus, contain more Sr.

If Sr/Ca is indeed coupled to the shell microstructure via preferential incorporation along specific crystal faces, then this coupling could be better described and predicted by the surface area-to-volume (SA/Vol) ratio of the BMUs rather than by the BMU area. Large SA/Vol ratios indicate highly convoluted BMU contours, and, hence, less Sr^{2+} accommodating crystal surfaces. Unfortunately, it is not yet possible to image individual sub-µm-sized BMUs in three dimensions, so the SA/Vol ratios of the BMUs cannot currently be directly measured. However, SA/Vol ratios increase in smaller and less rounded objects. Accordingly, the small, equidimensional HOM-BMUs (Fig. 2.1F) likely come with a lower SA/Vol ratio than the slightly larger, more acute and ramified CA-BMUs (Fig. 2.1F). If this hypothetical correlation between SA/Vol ratios and BMU size actually exists, the microstructure-dependent seasonal variation in Sr/Ca could be related to changing SA/Vol ratios. Element incorporation into shells may generally be affected by changing BMU SA/Vol ratios because they regulate the exchange rates of ions, heat, energy and many other physical properties (Glazier, 2010; Okie, 2013). Thus, SA/Vol ratios could be used as a proxy to explain the preferential incorporation of Sr into the HOM microstructure of the oOSL. If three-dimensional SA/Vol data were available, a more robust relationship could likely be identified between the shell Sr/Ca and microstructure.

Organic components likely also play a major role during microstructure formation and Sr^{2+} incorporation. Organic matrices promote crystal nucleation and spatially confine the BMUs during formation (Gotliv et al., 2003; Cusack and Freer, 2008; Ren et al., 2011), which ultimately not only determines the overall microstructure type but also the mechanical properties of the bioceramic (cf. Boon et al., 2019). Organic matrices can likely also promote or inhibit the incorporation of trace impurities into the crystal lattice by controlling the development of cation-affine crystal surfaces or by causing lattice defects. For example, in abiogenic precipitation experiments, the addition of shell-associated organic components promoted the incorporation of Mg^{2+} into the calcite crystal lattice (Wang et al., 2009; Shirai et al., 2014). A similar mechanism may explain the incorporation of Sr^{2+} into aragonite, because higher Sr/Ca values are typically found in organic-rich shell portions (Lorens and Bender, 1980; Schöne et al., 2010; Karney et al., 2011, 2012), and specifically those dominated by sulfur (Tanabe, 1988; Yoshimura et al., 2013; Shirai et al., 2014). Accordingly, the S/Ca and Sr/Ca of bivalve shells typically co-vary with each other (Shirai et al., 2014; Füllenbach et al., 2017).

However, strontium and sulfur (and thus organics) are not only much higher within, but also somewhat elevated near (= at both side of) the annual growth lines (Shirai et al., 2014; Füllenbach et al., 2017), i.e., in shell portions dominated by the largest and smallest BMUs, respectively. Whereas higher levels of Sr in the ISP-BMUs can be explained by strongly reduced vital effects during formation of the growth lines, the elevated Sr concentration in shell portions with smaller BMUs may be explained by organic-bound Sr. In fact, instead of substituting for

calcium in the crystal lattice, strontium can also be covalently bound to sulfur-rich organic macromolecules (Yoshimura et al., 2013; Shirai et al., 2014). The higher organic content of the portions in the immediate adjacency of the annual growth lines may result from a large SA/Vol ratio of the small HOM and CA-BMUs.

The link between shell organics and strontium content – whether Sr^{2+} is accommodated in the crystal lattice and/or bound to organics – can also help in the understanding of why the amount of this metal is overall higher in the oOSL than in the iOSL. The former contains more organic components than the latter, which is indicated, for example, by higher pigment concentrations in the oOSL (Stemmer and Nehrke, 2014), as well as higher S/Ca values (Shirai et al., 2014). Similar findings have been reported from other bivalve species, e.g., in *Ruditapes philippinarum*, the oOSL is enriched in sulfur and Mg (Poulain et al., 2015). If the BMU size (within the same microstructure type) is negatively correlated to the shell organic content (larger SA/Vol ratio = more organics in smaller BMUs), the BMU area can serve as a surrogate to assess microstructure or organic compound-dependent variations in shell Sr/Ca until high-resolution analyses of shell organics are available.

In conclusion, the data of this study revealed a link between the BMU size and shell Sr/Ca values. This correlation partly explained the Sr partitioning between the biomineralization fluid (extrapallial fluid) and the two sublayers of the outer shell layer (oOSL, iOSL) of *A. islandica*, as well as the intra-annual Sr/Ca variability. However, other properties may be more suitable for explaining the coupling between the shell microstructure and Sr/Ca, because a microstructure-specific Sr enrichment would not be expected if a direct link existed between the BMU size and Sr/Ca. As Sr^{2+} may be preferentially incorporated into aragonite along specific crystal faces, and organics not only control the microstructure formation but can also bind strontium, both the BMU SA/Vol ratios as well as the amount and composition of organic components likely affect shell Sr/Ca values. Until three-dimensional analyses of BMUs are possible and a detailed, high-resolution mapping of shell organics is available, the BMU size serves as a mean to assess microstructure-dependent variations in shell Sr/Ca, even if the two parameters are not directly linked to each other.

2.5.3 The influence of shell growth rate on Sr/Ca

Sr/Ca ratios of both sublayers of the outer shell layer were weakly and non-linearly linked to the shell growth rate (Fig. 2.6A). However, the signs of the regression slopes differed between the iOSL and oOSL. Sr/Ca_{oOSL} correlated negatively with the shell growth rate, whereas the opposite was observed in the iOSL. Furthermore, Sr/Ca_{hinge} values compared well with Sr/Ca_{iOSL} data, irrespective of the drastically different growth rates of the two shell portions (Fig. 2.1B). These

findings may suggest that no direct relationship exists between Sr/Ca_{shell} and the shell growth rate, or that other factors had a larger impact.

Inconsistent results on the relationship between the growth rate and Sr/Ca in shell aragonite have also been reported from many other bivalve species. While some authors noticed positive correlations (*Spisula solidissima*: Stecher et al., 1996; *Leukoma staminea*: Takesue and van Green, 2004; *Saxidomus gigantea*: Gillikin et al., 2005), others observed inverse relationships between Sr/Ca and the growth rate (inner shell layer of *Mytilus edulis*: Dodd, 1965). Opposing findings also came from the same species. For example, in *Mercenaria mercenaria*, Stecher et al. (1996) identified a positive correlation, but according to Gillikin et al. (2005), no relationship exists at all between Sr/Ca and the shell growth rate in this species. In *A. islandica*, similar discrepant findings were made. Whereas Foster et al. (2009) and Wanamaker and Gilliking (2019) did not find any significant correlation between Sr/Ca and the shell growth rate in juvenile, lab-grown and some decades-old field-grown *A. islandica* specimens, respectively, Schöne et al. (2011) identified a negative correlation in the hinge of old-grown (several centuries-old) ocean quahogs collected in the field. These results either suggest that no clear relationship exists between the shell growth rate and Sr/Ca, that the relationship is species-specific or that Sr/Ca is actually coupled to bivalve physiology or metabolism and only correlates mathematically but not causally with the growth rate. In cases where opposite findings were made in the same species, Gillikin et al. (2005) discussed the possibility of habitat-specific differences; specifically, the substrate type.

It is worth noting that controversial findings regarding precipitation rate (= kinetic) effects on the partitioning of Sr between the calcifying fluid and the mineral also came from inorganically precipitated aragonite and theoretical considerations for biomineralized tissues. For example, while Sr/Ca ratios increased non-linearly with the precipitation rate in experiments conducted by Gaetani and Cohen (2006), Zhong and Mucci (1989) found no effect of the precipitation rate on Sr/Ca in inorganic aragonite. Perhaps other experimental parameters had a stronger impact on Sr partitioning than kinetic effects. For coral aragonite, Sinclair et al. (2005) expected a negative correlation because a higher precipitation rate is coupled with an increase in active transmembrane Ca^{2+} transport, which would dilute the Sr^{2+} content in the calcifying fluid. In contrast, Carré et al. (2006) argued that, during faster growth, an increased ATP-mediated transmembrane Ca^{2+} transport across specialized channels would also result in larger amounts of strontium in the extrapallial fluid of bivalves. This is because strontium can diffuse more easily through these calcium channels if the calcium gradient between both sites of the membrane is higher.

While differing environmental regimes could explain differences between species or conspecific specimens from different habitats, it remains difficult to understand why growth-

rate-related kinetics should differently affect the Sr^{2+} incorporation into shell portions with a different microstructure that formed from the exact same calcifying fluid, namely the oOSL and iOSL (Fig. 2.1B). Is the answer again linked to differences in the BMU habit and the preferential substitution of Ca^{2+} along certain crystal faces – cf. Foster et al. (2009)? Is it possible that the incorporation of strontium occurs at a different pace along the different crystal faces that are exposed in the respective microstructures of the oOSL and iOSL? More research is certainly needed to shed light on these aspects.

In summary, both Sr/Ca_{oOSL} and Sr/Ca_{iOSL} were weakly correlated to the shell growth rate, albeit the former negatively and the latter positively. The mechanisms causing these different relationships remain currently unclear and require a better understanding of biomineralization processes.

2.6 Conclusions

According to the findings of the present study, shell Sr/Ca values of *A. islandica* measured between annual growth lines cannot currently be used to reconstruct water temperature. Shell Sr/Ca data were positively correlated to seawater temperature, even when the apparent correlations with the microstructural properties (BMU area) and growth rate (increment width) were mathematically eliminated. This contradicts thermodynamic predictions and results from inorganic aragonite. It cannot be precluded that temperature is still recorded by shell Sr/Ca, but, if so, the signal is superimposed beyond recognition by other, hitherto unknown environmental forcings. Unless these environmental variables are identified, it will remain impossible to infer seasonal temperature changes from shell Sr/Ca values of the studied species. The general agreement between the seasonal shell Sr/Ca chronologies of contemporaneous specimens indicates that a common environment forcing is at work, which should be understood as encouragement toward the identification of this environmental variable in future studies. Given the strong coupling between Sr/Ca and the biomineral unit size, a detailed characterization of the shell microstructure will most likely remain an integral part of subsequent attempts to reconstruct temperature from shell Sr/Ca. Aside from the BMU area, it may be useful to quantify other BMU parameters, such as the shape and habit in two and three dimensions, and to assess relationships with shell Sr/Ca. In addition, an ultra-high-resolution characterization and mapping of shell organics may help to better understand the Sr distribution patterns in the shells.

2.7 Supplementary material

Table S2.1 Quality control data for ^{88}Sr LA-ICP-MS measurements conducted on shells of *Arctica islandica*. NIST SRM 610 was used to calibrate the ^{88}Sr concentrations of the shells. For each quality control material (QCM), the strontium-specific relative standard deviation (RSD%) from their respective preferred literature value (Jochum et al., 2005, 2011) was calculated. conc. = concentration.

Average calibrated ^{88}Sr conc. (µg/g)	Average detection limit ^{88}Sr (µg/g)	QCM	Average ^{88}Sr conc. (µg/g)	Literature ^{88}Sr conc. (µg/g)	RSD%
515.60 ± 0.06	0.01 ± 0.01	NIST SRM 612	79.33 ± 0.21	78.4 ± 0.2	3.45
		BCR-2G	339.51 ± 0.93	342 ± 4	3.40
		MACS-3	7035.68 ± 111.72	6640 ± 170	3.61
		JCp-1	7221.04 ± 90.42	6890 ± 330	3.56
		JCt-1	1428.09 ± 28.08	1410 ± 50	3.47

Table S2.2 Sr/Ca ratios (mmol/mol) of laser spots covering annual growth lines from the three specimens of *Arctica islandica* examined in this study. HOM = homogeneous microstructure, CA = crossed-acicular microstructure.

Specimen	Transect	Calendar year of growth line formation	Sr/Ca from annual growth lines (mmol/mol)
A201L	HOM	2003	1.98
		2004	2.34
		2005	1.99
	CA	2003	1.39
		2004	1.11
		2005	1.22
A202L	HOM	2003	2.21
		2004	1.84
		2005	1.76
	CA	2003	1.17
		2004	1.33
		2005	1.13
A203L	HOM	2004	1.75
		2005	1.81
	CA	2004	1.15
		2005	1.23

Appendix 2.A

Table 2.A1 Overview of the abbreviations used in the paper.

Sclerochronology	
vm	Ventral margin of the shell
OSL	Outer shell layer of the ventral margin of the shell
oOSL	Outer part of the OSL
iOSL	Inner part of the OSL
HOM	Homogenous microstructure, dominating the oOSL
CA	Crossed-acicular microstructure, dominating the iOSL and the hinge
ISP	Irregular simple prismatic microstructure, found at the annual growth lines
BMU	Biomineral unit; microstructures are composed of BMUs and organics
Sr/Ca data	
Sr/Ca_{vm}	Sr/Ca in all of the ventral margin (oOSL and iOSL combined) of the shell
Sr/Ca_{oOSL}	Sr/Ca specifically in the oOSL of the ventral margin of the shell
Sr/Ca_{iOSL}	Sr/Ca specifically in the iOSL of the ventral margin of the shell
Sr/Ca_{hinge}	Sr/Ca in the hinge of the shell
$d_{GR}Sr/Ca_{vm}$	Sr/Ca detrended by a growth rate (GR)-based method for all data from the ventral margin of the shell (colored in magenta or green if the data are for HOM or CA, respectively)
$d_{GR}Sr/Ca_{oOSL}$	Sr/Ca detrended by a growth rate (GR)-based method specifically for oOSL data
$d_{GR}Sr/Ca_{iOSL}$	Sr/Ca detrended by a growth rate (GR)-based method specifically for iOSL data
$d_{MS}Sr/Ca_{vm}$	Sr/Ca detrended by a BMU size (MS)-based method for all data from the ventral margin of the shell (colored in magenta or green if the data are for HOM or CA, respectively)
$d_{MS}Sr/Ca_{oOSL}$	Sr/Ca detrended by a BMU size (MS)-based method specifically for oOSL data
$d_{MS}Sr/Ca_{iOSL}$	Sr/Ca detrended by a BMU size (MS)-based method specifically for iOSL data
$d_{GRMS}Sr/Ca_{vm}$	Sr/Ca detrended by growth rate (GR) and BMU size (MS)-based methods for all data from the ventral margin of the shell (colored in magenta or green if the data are for HOM or CA, respectively)
$d_{GRMS}Sr/Ca_{oOSL}$	Sr/Ca detrended by growth rate (GR) and BMU size (MS)-based methods specifically for oOSL data
$d_{GRMS}Sr/Ca_{iOSL}$	Sr/Ca detrended by growth rate (GR) and BMU size (MS)-based methods specifically for iOSL data
Environmental data set	
SST	Sea surface temperature (°C)

References

Amiel, A. J., Friedman, G. M., Miller, D. S., 1973. Distribution and nature of incorporation of trace elements in modern aragonitic corals. Sedimentology 20, 47–64.

Ansell, A. D., 1968. The rate of growth of the hard clam *Mercenaria mercenaria*(L) throughout the geographical range. ICES J. Mar. Sci. 31, 364–409.

Berg, S., Kutra, D., Kroeger, T., Straehle, C. N., Kausler, B. X., Haubold, C., Schiegg, M., Ales, J., Beier, T., Rudy, M., Eren, K., Cervantes, J. I., Xu, B., Beuttenmueller, F., Wolny, A., Zhang, C., Koethe, U., Hamprecht, F. A., Kreshuk, A., 2019. ilastik: Interactive machine learning for (bio)image analysis. Nat. Methods 16, 1226–1232.

Black, B. A., Copenheaver, C. A., Frank, D. C., Stuckey, M. J., Kormanyos, R. E., 2009. Multi-proxy reconstructions of northeastern Pacific sea surface temperature data from trees and Pacific geoduck. Palaeogeogr. Palaeoclimatol. Palaeoecol. 278, 40–47.

Black, B. A., Dunham, J. B., Blundon, B. W., Brim-Box, J., Tepley, A. J., 2015. Long-term growth-increment chronologies reveal diverse influences of climate forcing on freshwater and forest biota in the Pacific Northwest. Glob. Change. Biol. 21, 594–604.

Black, B. A., Griffin, D., van der Sleen, P., Wanamaker, A. D., Speer, J. H., Frank, D. C., Stahle, D. W., Pederson, N., Copenheaver, C. A., Trouet, V., Griffin, S., Gillanders, B. M., 2016. The value of crossdating to retain high-frequency variability, climate signals, and extreme events in environmental proxies. Glob. Change Biol. 22, 2582–2595.

Black, B. A., Andersson, C., Butler, P. G., Carroll, M. L., DeLong, K. L., Reynolds, D. J., Schöne, B. R., Scourse, J., Van Der Sleen, P., Wanamaker, A. D., Witbaard, R., 2019. The revolution of crossdating in marine palaeoecology and palaeoclimatology. Biol. Lett. 15, 20180665.

Boon, P. J., Cooksley, S. L., Geist, J., Killeen, I. J., Moorkens, E. A., Sime, I., 2019. Developing a standard approach for monitoring freshwater pearl mussel (*Margaritifera margaritifera*) populations in European rivers. Aquatic Conserv: Mar Freshw Ecosyst 29, 1365–1379.

Buick, D. P., Ivany, L. C., 2004. 100 years in the dark: Extreme longevity of Eocene bivalves from Antarctica. Geology 32, 921.

Butler, P. G., Richardson, C. A., Scourse, J. D., Wanamaker, A. D., Shammon, T. M., Bennell, J. D., 2010. Marine climate in the Irish Sea: Analysis of a 489-year marine master chronology derived from growth increments in the shell of the clam *Arctica islandica*. Quat. Sci. Rev. 29, 1614–1632.

Butler, P. G., Wanamaker, A. D., Scourse, J. D., Richardson, C. A., Reynolds, D. J., 2013. Variability of marine climate on the North Icelandic Shelf in a 1357-year proxy archive based on growth increments in the bivalve *Arctica islandica*. Palaeogeogr. Palaeoclimatol. Palaeoecol. 373, 141–151.

Carré, M., Bentaleb, I., Bruguier, O., Ordinola, E., Barrett, N. T., Fontugne, M., 2006. Calcification rate influence on trace element concentrations in aragonitic bivalve shells: Evidences and mechanisms. Geochim. Cosmochim. Acta 70, 4906–4920.

Chauvaud, L., Thouzeau, G., Paulet, Y.-M., 1998. Effects of environmental factors on the daily growth rate of *Pecten maximus* juveniles in the Bay of Brest (France). J. Exp. Mar. Biol. Ecol. 227, 83–111.

Clark, G. R., 2005. Daily growth lines in some living Pectens (Mollusca: Bivalvia), and some applications in a fossil relative: Time and tide will tell. Palaeogeogr. Palaeoclimatol. Palaeoecol. 228, 26–42.

Corrège, T., 2006. Sea surface temperature and salinity reconstruction from coral geochemical tracers. Palaeogeogr. Palaeoclimatol. Palaeoecol. 232, 408–428.

Cusack, M., Freer, A., 2008. Biomineralization: Elemental and organic influence in carbonate systems. Chem. Rev. 108, 4433–4454.

Dietzel, M., Gussone, N., Eisenhauer, A., 2004. Co-precipitation of Sr^{2+} and Ba^{2+} with aragonite by membrane diffusion of CO_2 between 10 and 50 °C. Chem. Geol. 203, 139–151.

Dodd, J. R., 1965. Environmental control of strontium and magnesium in *Mytilus*. Geochim. Cosmochim. Acta 29, 385–398.

Dunca, E., Mutvei, H., Göransson, P., Mörth, C.-M., Schöne, B. R., Whitehouse, M. J., Elfman, M., Baden, S. P., 2009. Using ocean quahog (*Arctica islandica*) shells to reconstruct palaeoenvironment in Öresund, Kattegat and Skagerrak, Sweden. Int. J. Earth Sci. 98, 3–17.

Eagle, R. A., Eiler, J. M., Tripati, A. K., Ries, J. B., Freitas, P. S., Hiebenthal, C., Wanamaker, A. D., Taviani, M., Elliot, M., Marenssi, S., Nakamura, K., Ramirez, P., Roy, K., 2013. The influence of temperature and seawater carbonate saturation state on ^{13}C–^{18}O bond ordering in bivalve mollusks. Biogeosciences 10, 4591–4606.

Epstein, S., Buchsbaum, R., Lowenstam, H. A., Urey, H. C., 1953. Revised carbonate-water isotopic temperature scale. Geol. Soc. America Bull. 64, 1315.

Evans, J. W., 1972. Tidal growth increments in the cockle *Clinocardium nuttalli*. Science 176, 416–417.

Fiebig, J., Bajnai, D., Löffler, N., Methner, K., Krsnik, E., Mulch, A., Hofmann, S., 2019. Combined high-precision Δ_{48} and Δ_{47} analysis of carbonates. Chem. Geol. 522, 186–191.

Foster, L. C., Allison, N., Finch, A. A., Andersson, C., 2009. Strontium distribution in the shell of the aragonite bivalve *Arctica islandica*. Geochem. Geophys. Geosyst. 10, 1–14.

Fritz, L. W., Haven, D. S., 1983. Hard clam, *Mercenaria mercenaria*: Shell growth patterns in Chesapeake Bay. Fish. Bull. 81, 697–708.

Füllenbach, C. S., Schöne, B. R., Mertz-Kraus, R., 2015. Strontium/lithium ratio in aragonitic shells of *Cerastoderma edule* (Bivalvia) – A new potential temperature proxy for brackish environments. Chem. Geol. 417, 341–355.

Füllenbach, C. S., Schöne, B. R., Shirai, K., Takahata, N., Ishida, A., Sano, Y., 2017. Minute co-variations of Sr/Ca ratios and microstructures in the aragonitic shell of *Cerastoderma edule* (Bivalvia) – Are geochemical variations at the ultra-scale masking potential environmental signals? Geochim. Cosmochim. Acta 205, 256–271.

Gaetani, G. A., Cohen, A. L., 2006. Element partitioning during precipitation of aragonite from seawater: A framework for understanding paleoproxies. Geochim. Cosmochim. Acta 70, 4617–4634.

Gillikin, D. P., Lorrain, A., Navez, J., Taylor, J. W., André, L., Keppens, E., Baeyens, W., Dehairs, F., 2005. Strong biological controls on Sr/Ca ratios in aragonitic marine bivalve shells: Controls on Sr/Ca ratios. Geochem. Geophys. Geosyst. 6, 1–16.

Gillikin, D. P., Lorrain, A., Paulet, Y.-M., André, L., Dehairs, F., 2008. Synchronous barium peaks in high-resolution profiles of calcite and aragonite marine bivalve shells. Geo-Mar. Lett. 28, 351–358.

Glazier, D. S., 2010. A unifying explanation for diverse metabolic scaling in animals and plants. Biol. Rev. 85, 111–138.

Goldschmidt, V. M., 1926. Die Gesetze der Krystallochemie. Naturwissenschaften 14, 477–485.

Goodwin, D. H., Flessa, K. W., Schone, B. R., Dettman, D. L., 2001. Cross-calibration of daily growth increments, stable isotope variation, and temperature in the Gulf of California bivalve mollusk *Chione cortezi*: Implications for paleoenvironmental analysis. Palaios 16, 387–398.

Gotliv, B.-A., Addadi, L., Weiner, S., 2003. Mollusk shell acidic proteins: in search of individual functions. ChemBioChem 4, 522–529.

Griffin, W. L., 2008. GLITTER: Data reduction software for laser ablation ICP-MS. Laser Ablation ICP-MS in the Earth Sciences: Current practices and outstanding issues, 308–311.

Grossman, E. L., Ku, T.-L., 1986. Oxygen and carbon isotope fractionation in biogenic aragonite: Temperature effects. Chem. Geol. 59, 59–74.

Hallmann, N., Burchell, M., Schöne, B. R., Irvine, G. V., Maxwell, D., 2009. High-resolution sclerochronological analysis of the bivalve mollusk *Saxidomus gigantea* from Alaska and British Columbia: Techniques for revealing environmental archives and archaeological seasonality. J. Archaeol. Sci. 36, 2353–2364.

Hanna, E., Jónsson, T., Ólafsson, J., Valdimarsson, H., 2006. Icelandic coastal sea surface temperature records constructed: putting the pulse on air–sea–climate interactions in the Northern North Atlantic. Part I: Comparison with HadISST1 open-ocean surface temperatures and preliminary analysis of long-term patterns and anomalies of SSTs around Iceland. J. Clim. 19, 5652–5666.

Hart, S. R., Blusztajn, J., 1998. Clams as recorders of ocean ridge volcanism and hydrothermal vent field activity. Science 280, 883–886.

Hatch, M. B. A., Schellenberg, S. A., Carter, M. L., 2013. Ba/Ca variations in the modern intertidal bean clam *Donax gouldii*: An upwelling proxy? Palaeogeogr. Palaeoclimatol. Palaeoecol. 373, 98–107.

Henkes, G. A., Passey, B. H., Wanamaker, A. D., Grossman, E. L., Ambrose, W. G., Carroll, M. L., 2013. Carbonate clumped isotope compositions of modern marine mollusk and brachiopod shells. Geochim. Cosmochim. Acta 106, 307–325.

Höche, N., Walliser, E. O., Schöne, B. R., 2021a. Data for "Microstructural mapping of *A. islandica* shells reveals environmental and physiological controls on biomineral size."

Höche, N., Walliser, E. O., de Winter, N. J., Witbaard, R., Schöne, B. R., 2021b. Temperature-induced microstructural changes in shells of laboratory-grown *Arctica islandica* (Bivalvia). PLoS ONE 16, e0247968.

Höche, N., Walliser, E. O., Schöne, B. R., 2022. Microstructural mapping of *Arctica islandica* shells reveals environmental and physiological controls on biomineral size. Front. Earth Sci. 9, 781305.

Holland, H. A., Schöne, B. R., Marali, S., Jochum, K. P., 2014. History of bioavailable lead and iron in the Greater North Sea and Iceland during the last millennium – A bivalve sclerochronological reconstruction. Mar. Pollut. Bull. 87, 104–116.

Ivany, L. C., Brey, T., Huber, M., Buick, D. P., Schöne, B. R., 2011. El Niño in the Eocene greenhouse recorded by fossil bivalves and wood from Antarctica. Geophys. Res. Lett. 38, L16709.

Izumida, H., Yoshimura, T., Suzuki, A., Nakashima, R., Ishimura, T., Yasuhara, M., Inamura, A., Shikazono, N., Kawahata, H., 2011. Biological and water chemistry controls on Sr/Ca, Ba/Ca, Mg/Ca and $\delta^{18}O$ profiles in freshwater pearl mussel *Hyriopsis sp.* Palaeogeogr. Palaeoclimatol. Palaeoecol. 309, 298–308.

Jochum, K. P., Nohl, U., Herwig, K., Lammel, E., Stoll, B., Hofmann, A. W., 2005. GeoReM: A new geochemical database for reference materials and isotopic standards. Geostand. Geoanalyt. Res. 29, 333–338.

Jochum, K. P., Weis, U., Stoll, B., Kuzmin, D., Yang, Q., Raczek, I., Jacob, D. E., Stracke, A., Birbaum, K., Frick, D. A., Günther, D., Enzweiler, J., 2011. Determination of Reference Values for NIST SRM 610-617 Glasses Following ISO Guidelines. Geostand. Geoanal. Res. 35, 397–429.

Jochum, K. P., Scholz, D., Stoll, B., Weis, U., Wilson, S. A., Yang, Q., Schwalb, A., Börner, N., Jacob, D. E., Andreae, M. O., 2012. Accurate trace element analysis of speleothems and biogenic calcium carbonates by LA-ICP-MS. Chem. Geol. 318–319, 31–44.

Jones, D. S., 1980. Annual cycle of shell growth increment formation in two continental shelf bivalves and its paleoecologic significance. Paleobiology 6, 331–340.

Karney, G. B., Butler, P. G., Scourse, J. D., Richardson, C. A., Lau, K. H., Czernuszka, J. T., Grovenor, C. R. M., 2011. Identification of growth increments in the shell of the bivalve mollusc *Arctica islandica* using backscattered electron imaging: Identification of growth increments in the shell of the bivalve mollusc. J. Microsc. 241, 29–36.

Karney, G. B., Butler, P. G., Speller, S., Scourse, J. D., Richardson, C. A., Schröder, M., Hughes, G. M., Czernuszka, J. T., Grovenor, C. R. M., 2012. Characterizing the microstructure of *Arctica islandica* shells using NanoSIMS and EBSD. Geochem. Geophys. Geosyst. 13, Q04002.

Kawano, J., Sakuma, H., Nagai, T., 2015. Incorporation of Mg^{2+} in surface Ca^{2+} sites of aragonite: An *ab initio* study. Prog. in Earth and Planet. Sci. 2, 7.

Kennish, M. J., Olsson, R. K., 1975. Effects of thermal discharges on the microstructural growth of *Mercenaria mercenaria*. Environ. Geol. 1, 41–64.

Killingley, J. S., Berger, W. H., 1979. Stable isotopes in a mollusk shell: Detection of upwelling events. Science 205, 186–188.

Kinsman, D. J. J., Holland, H. D., 1969. The co-precipitation of cations with $CaCO_3$—IV. The co-precipitation of Sr^{2+} with aragonite between 16° and 96°C. Geochim. Cosmochim. Acta 33, 1–17.

Kodama, S., Takayanagi, H., Yoshii, K., Nhu Ha, T. T., Asami, R., Abe, O., Iryu, Y., 2021. Carbon and oxygen isotope records of *Tridacna squamosa* shells from two different latitudes in the Ryukyu Islands. Paleontol. Res. 25.

Lebrato, M., Garbe-Schönberg, D., Müller, M. N., Blanco-Ameijeiras, S., Feely, R. A., Lorenzoni, L., Molinero, J.-C., Bremer, K., Jones, D. O. B., Iglesias-Rodriguez, D., Greeley, D., Lamare, M. D., Paulmier, A., Graco, M., Cartes, J., Barcelos e Ramos, J., de Lara, A., Sanchez-Leal, R., Jimenez, P., Paparazzo, F. E., Hartman, S. E., Westernströer, U., Küter, M., Benavides, R., da Silva, A. F., Bell, S., Payne, C., Olafsdottir, S., Robinson, K., Jantunen, L. M., Korablev, A., Webster, R. J., Jones, E. M., Gilg, O., Bailly du Bois, P., Beldowski, J., Ashjian, C., Yahia, N. D., Twining, B., Chen, X.-G., Tseng, L.-C., Hwang, J.-S., Dahms, H.-U., Oschlies, A., 2020. Global variability in seawater Mg:Ca and Sr:Ca ratios in the modern ocean. Proc. Natl. Acad. Sci. U.S.A. 117, 22281–22292.

Lohmann, G., Schöne, B. R., 2013. Climate signatures on decadal to interdecadal time scales as obtained from mollusk shells (*Arctica islandica*) from Iceland. Palaeogeogr. Palaeoclimatol. Palaeoecol. 373, 152–162.

Lorens, R. B., Bender, M. L., 1980. The impact of solution chemistry on *Mytilus edulis* calcite and aragonite. Geochim. Cosmochim. Acta 44, 1265–1278.

Lorrain, A., Gillikin, D. P., Paulet, Y.-M., Chauvaud, L., Mercier, A. L., Navez, J., André, L., 2005. Strong kinetic effects on Sr/Ca ratios in the calcitic bivalve *Pecten maximus*. Geology 33, 965–968.

Marali, S., Schöne, B. R., Mertz-Kraus, R., Griffin, S. M., Wanamaker, A. D., Butler, P. G., Holland, H. A., Jochum, K. P., 2017. Reproducibility of trace element time-series (Na/Ca, Mg/Ca, Mn/Ca, Sr/Ca, and Ba/Ca) within and between specimens of the bivalve *Arctica islandica* – A LA-ICP-MS line scan study. Palaeogeogr. Palaeoclimatol. Palaeoecol. 484, 109–128.

Markulin, K., Peharda, M., Mertz-Kraus, R., Schöne, B. R., Uvanović, H., Kovač, Ž., Janeković, I., 2019. Trace and minor element records in aragonitic bivalve shells as environmental proxies. Chem. Geol. 507, 120–133.

Mavromatis, V., Brazier, J.-M., Goetschl, K. E., 2022. Controls of temperature and mineral growth rate on Mg incorporation in aragonite. Geochim. Cosmochim. Acta 317, 53–64.

Menadakis, M., Maroulis, G., Koutsoukos, P. G., 2008. Incorporation of Mg^{2+}, Sr^{2+}, Ba^{2+} and Zn^{2+} into aragonite and comparison with calcite. J. Math. Chem. 46, 484–491.

Mette, M. J., Wanamaker, A. D., Retelle, M. J., Carroll, M. L., Andersson, C., Ambrose, W. G., 2021. Persistent multidecadal variability since the 15th century in the Southern Barents Sea

derived from annually resolved shell-based records. J. Geophys. Res. Oceans 126, e2020JC017074.

Mook, W. G., Vogel, J. C., 1968. Isotopic equilibrium between shells and their environment. Science 159, 874–875.

Moss, D. K., Ivany, L. C., Silver, R. B., Schue, J., Artruc, E. G., 2017. High-latitude settings promote extreme longevity in fossil marine bivalves. Paleobiology 43, 365–382.

Nürnberg, D., Bijma, J., Hemleben, C., 1996. Assessing the reliability of magnesium in foraminiferal calcite as a proxy for water mass temperatures. Geochim. Cosmochim. Acta 60, 803–814.

Ohno, T., 1989. Palaeotidal characteristics determined by micro-growth patterns in bivalves. Palaeontology 32, 237–263.

Okie, J. G., 2013. General models for the spectra of surface area scaling strategies of cells and organisms: Fractality, geometric dissimilitude, and internalization. Am. Nat. 181, 421–439.

Paquette, J., Reeder, R. J., 1995. Relationship between surface structure, growth mechanism, and trace element incorporation in calcite. Geochim. Cosmochim. Acta 59, 735–749.

Peharda, M., Schöne, B. R., Black, B. A., Corrège, T., 2021. Advances of sclerochronology research in the last decade. Palaeogeogr. Palaeoclimatol. Palaeoecol. 570, 110371.

Plummer, L. N., Busenberg, E., 1987. Thermodynamics of aragonite-strontianite solid solutions: Results from stoichiometric solubility at 25 and 76°C. Geochim. Cosmochim. Acta 51, 1393–1411.

Poulain, C., Gillikin, D. P., Thébault, J., Munaron, J. M., Bohn, M., Robert, R., Paulet, Y.-M., Lorrain, A., 2015. An evaluation of Mg/Ca, Sr/Ca, and Ba/Ca ratios as environmental proxies in aragonite bivalve shells. Chem. Geol. 396, 42–50.

Reeder, R. J., Grams, J. C., 1987. Sector zoning in calcite cement crystals: Implications for trace element distributions in carbonates. Geochim. Cosmochim. Acta 51, 187–194.

Ren, D., Feng, Q., Bourrat, X., 2011. Effects of additives and templates on calcium carbonate mineralization *in vitro*. Micron 42, 228–245.

Reynolds, D. J., Scourse, J. D., Halloran, P. R., Nederbragt, A. J., Wanamaker, A. D., Butler, P. G., Richardson, C. A., Heinemeier, J., Eiríksson, J., Knudsen, K. L., Hall, I. R., 2016. Annually resolved North Atlantic marine climate over the last millennium. Nat. Commun. 7, 13502.

Roger, L. M., George, A. D., Shaw, J., Hart, R. D., Roberts, M., Becker, T., McDonald, B. J., Evans, N. J., 2017. Geochemical and microstructural characterisation of two species of cool-water bivalves (*Fulvia tenuicostata* and *Soletellina biradiata*) from Western Australia. Biogeosciences 14, 1721–1737.

Ropes, J. H., 1984. Procedures for preparing acetate peels and evidence validating the annual periodicity of growth lines formed in the shells of ocean quahogs, *Arctica islandica*. Mar. Fish. Rev. 46, 27–35.

Sano, Y., Kobayashi, S., Shirai, K., Takahata, N., Matsumoto, K., Watanabe, T., Sowa, K., Iwai, K., 2012. Past daily light cycle recorded in the strontium/calcium ratios of giant clam shells. Nat. Commun. 3, 761.

Schleinkofer, N., Raddatz, J., Evans, D., Gerdes, A., Flögel, S., Voigt, S., Büscher, J. V., Wisshak, M., 2021. Compositional variability of Mg/Ca, Sr/Ca, and Na/Ca in the deep-sea bivalve *Acesta excavata* (Fabricius, 1779). PLoS ONE 16, e0245605.

Schöne, B. R., Fiebig, J., Pfeiffer, M., Gleβ, R., Hickson, J., Johnson, A. L. A., Dreyer, W., Oschmann, W., 2005. Climate records from a bivalved Methuselah (*Arctica islandica*, Mollusca; Iceland). Palaeogeogr. Palaeoclimatol. Palaeoecol. 228, 130–148.

Schöne, B. R., Zhang, Z., Radermacher, P., Thébault, J., Jacob, D. E., Nunn, E. V., Maurer, A.-F., 2011. Sr/Ca and Mg/Ca ratios of ontogenetically old, long-lived bivalve shells (*Arctica islandica*) and their function as paleotemperature proxies. Palaeogeogr. Palaeoclimatol. Palaeoecol. 302, 52–64.

Schöne, B. R., 2013. *Arctica islandica* (Bivalvia): A unique paleoenvironmental archive of the northern North Atlantic Ocean. Glob. Planet. Change 111, 199–225.

Schöne, B. R., Radermacher, P., Zhang, Z., Jacob, D. E., 2013. Crystal fabrics and element impurities (Sr/Ca, Mg/Ca, and Ba/Ca) in shells of *Arctica islandica* – Implications for paleoclimate reconstructions. Palaeogeogr. Palaeoclimatol. Palaeoecol. 373, 50–59.

Schöne, B. R., Flessa, K. W., Dettman, D. L., Goodwin, D. H., 2003. Upstream dams and downstream clams: growth rates of bivalve mollusks unveil impact of river management on estuarine ecosystems (Colorado River Delta, Mexico). Estuar. Coast. Shelf Sci. 58, 715–726.

Schöne, B. R., Zhang, Z., Jacob, D., Gillikin, D. P., Tütken, T., Garbe-Schönberg, D., McConnaughey, T., Soldati, A., 2010. Effect of organic matrices on the determination of the trace element chemistry (Mg, Sr, Mg/Ca, Sr/Ca) of aragonitic bivalve shells (*Arctica islandica*) – Comparison of ICP-OES and LA-ICP-MS data. Geochem. J. 44, 23–37.

Scourse, J., Richardson, C., Forsythe, G., Harris, I., Heinemeier, J., Fraser, N., Briffa, K., Jones, P., 2006. First cross-matched floating chronology from the marine fossil record: Data from growth lines of the long-lived bivalve mollusc *Arctica islandica*. Holocene 16, 967–974.

Selin, N. I., Dulenina, P. A., 2012. The growth and lifespan of the mussel *Crenomytilus grayanus* (Bivalvia: Mytilidae) in the Tatar Strait (Sea of Japan) in connection with the conditions of life at the northern border of the species range. Russ. J. Mar. Biol. 38, 318–324.

Shaul, W., Goodwin, L., 1982. Geodock (*Panope generosa*: Bivalvia) age as determined by internal growth lines in the shell. Can. J. Fish. Aquat. Sci. 39, 632–636.

Shen, C.-C., Liu, K.-K., Lee, M.-Y., Lee, T., Wang, C.-H., Lee, H.-J., 2005. A novel method for tracing coastal water masses using Sr/Ca ratios and salinity in Nanwan Bay, southern Taiwan. Estuar. Coast. Shelf Sci. 65, 135–142.

Shirai, K., Takahata, N., Yamamoto, H., Omata, T., Sasaki, T., Sano, Y., 2008. Novel analytical approach to bivalve shell biogeochemistry: A case study of hydrothermal mussel shell. Geochem. J. 42, 413–420.

Shirai, K., Schöne, B. R., Miyaji, T., Radarmacher, P., Krause, R. A., Tanabe, K., 2014. Assessment of the mechanism of elemental incorporation into bivalve shells (*Arctica islandica*) based on elemental distribution at the microstructural scale. Geochim. Cosmochim. Acta 126, 307–320.

Sinclair, D. J., Sherwood, O. A., Risk, M. J., Hillaire-Marcel, C., Tubrett, M., Sylvester, P., McCulloch, M., Kinsley, L., 2005. Testing the reproducibility of Mg/Ca profiles in the deep-water coral *Primnoa resedaeformis*: Putting the proxy through its paces. In: Cold-Water Corals and Ecosystems. Eds. by A. Freiwald and J. M. Roberts Berlin/Heidelberg: Springer-Verlag, 1039–1060.

Speer, J. A., 1983. Chapter 5. Crystal chemistry and phase relations of orthorhombic carbonates. In: Carbonates. Ed. by R. J. Reeder De Gruyter, 145–190.

Stecher, H. A., Krantz, D. E., Lord, C. J., Luther, G. W., Bock, K. W., 1996. Profiles of strontium and barium in *Mercenaria mercenaria* and *Spisula solidissima* shells. Geochim. Cosmochim. Acta 60, 3445–3456.

Stemmer, K., Nehrke, G., 2014. The distribution of polyenes in the shell of *Arctica islandica* from North Atlantic localities: A confocal Raman microscopy study. J. Molluscan Stud. 80, 365–370.

Strom, A., Francis, R. C., Mantua, N. J., Miles, E. L., Peterson, D. L., 2005. Preserving low-frequency climate signals in growth records of geoduck clams (*Panopea abrupta*). Palaeogeogr. Palaeoclimatol. Palaeoecol. 228, 167–178.

Surge, D., Walker, K. J., 2006. Geochemical variation in microstructural shell layers of the southern quahog (*Mercenaria campechiensis*): Implications for reconstructing seasonality. Palaeogeogr. Palaeoclimatol. Palaeoecol. 237, 182–190.

Takesue, R. K., van Geen, A., 2004. Mg/Ca, Sr/Ca, and stable isotopes in modern and Holocene *Protothaca staminea* shells from a northern California coastal upwelling region. Geochim. Cosmochim. Acta 68, 3845–3861.

Tanabe, K., 1988. Age and growth rate determinations of an intertidal bivalve, *Phacosoma japonicum*, using internal shell increments. Lethaia 21, 231–241.

Thébault, J., Chauvaud, L., L'Helguen, S., Clavier, J., Barats, A., Jacquet, Sé., PÉcheyran, C., Amouroux, D., 2009. Barium and molybdenum records in bivalve shells: Geochemical proxies for phytoplankton dynamics in coastal environments? Limnol. Oceanogr. 54, 1002–1014.

Toland, H., Perkins, B., Pearce, N., Keenan, F., Leng, M. J., 2000. A study of sclerochronology by laser ablation ICP-MS. J. Anal. At. Spectrom. 15, 1143–1148.

Trutschler, K., Samtleben, C., 1988. Shell growth of *Astarte elliptica* (Bivalvia) from Kiel Bay (Western Baltic Sea). Mar. Ecol. Prog. Ser. 42, 155–162.

van der Walt, S., Schönberger, J. L., Nunez-Iglesias, J., Boulogne, F., Warner, J. D., Yager, N., Gouillart, E., Yu, T., 2014. scikit-image: Image processing in Python. PeerJ 2, e453.

Vihtakari, M., Ambrose, W. G., Renaud, P. E., Locke, W. L., Carroll, M. L., Berge, J., Clarke, L. J., Cottier, F., Hop, H., 2016. A key to the past? Element ratios as environmental proxies in two Arctic bivalves. Palaeogeogr. Palaeoclimatol. Palaeoecol. 465, 316–332.

Wacker, U., Fiebig, J., Tödter, J., Schöne, B. R., Bahr, A., Friedrich, O., Tütken, T., Gischler, E., Joachimski, M. M., 2014. Empirical calibration of the clumped isotope paleothermometer using calcites of various origins. Geochim. Cosmochim. Acta 141, 127–144.

Walliser, E. O., Mertz-Kraus, R., Schöne, B. R., 2018. The giant inoceramid *Platyceramus platinus* as a high-resolution paleoclimate archive for the Late Cretaceous of the Western Interior Seaway. Cretac. Res. 86, 73–90.

Wanamaker, A. D., Butler, P. G., Scourse, J. D., Heinemeier, J., Eiríksson, J., Knudsen, K. L., Richardson, C. A., 2012. Surface changes in the North Atlantic meridional overturning circulation during the last millennium. Nat. Commun. 3, 1–7.

Wanamaker, A. D., Gillikin, D. P., 2019. Strontium, magnesium, and barium incorporation in aragonitic shells of juvenile *Arctica islandica*: Insights from temperature controlled experiments. Chem. Geol. 526, 117–129.

Wang, D., Wallace, A. F., De Yoreo, J. J., Dove, P. M., 2009. Carboxylated molecules regulate magnesium content of amorphous calcium carbonates during calcification. Proc. Natl. Acad. Sci. U.S.A. 106, 21511–21516.

Wefer, G., Berger, W. H., 1991. Isotope paleontology: Growth and composition of extant calcareous species. Marine Geology 100, 207–248.

Wisshak, M., López Correa, M., Gofas, S., Salas, C., Taviani, M., Jakobsen, J., Freiwald, A., 2009. Shell architecture, element composition, and stable isotope signature of the giant deep-sea oyster *Neopycnodonte zibrowii* sp. n. from the NE Atlantic. Deep Sea Res. Part I Oceanogr. Res. Pap. 56, 374–407.

Witbaard, R., Jenness, M. I., Van Der Borg, K., Ganssen, G., 1994. Verification of annual growth increments in *Arctica islandica* L. from the North Sea by means of oxygen and carbon isotopes. J. Sea Res. 33, 91–101.

Witbaard, R., Duineveld, G. C. A., Bergman, M., 2001. The effect of tidal resuspension on benthic food quality in the southern North Sea. Senckenb. Marit. 31, 225–234.

Yamanashi, J., Takayanagi, H., Isaji, A., Asami, R., Iryu, Y., 2016. Carbon and oxygen isotope records from *Tridacna derasa* shells: Toward establishing a reliable proxy for sea surface environments. PLoS ONE 11, e0157659.

Yan, H., Shao, D., Wang, Yuhong, Sun, L., 2011. High resolution Sr/Ca profile of *Tridacna gigas* from Xisha Islands of South China Sea and its potential application on sea surface temperature reconstruction. J. Earth Environ. 2, 381–386.

Yan, H., Shao, D., Wang, Y., Sun, L., 2013. Sr/Ca profile of long-lived *Tridacna gigas* bivalves from South China Sea: A new high-resolution SST proxy. Geochim. Cosmochim. Acta 112, 52–65.

Yan, H., Shao, D., Wang, Y., Sun, L., 2014. Sr/Ca differences within and among three *Tridacnidae* species from the South China Sea: Implication for paleoclimate reconstruction. Chem. Geol. 390, 22–31.

Yoshimura, T., Tamenori, Y., Suzuki, A., Nakashima, R., Iwasaki, N., Hasegawa, H., Kawahata, H., 2013. Element profile and chemical environment of sulfur in a giant clam shell: Insights from μ-XRF and X-ray absorption near-edge structure. Chem. Geol. 352, 170–175.

Zhao, L., Schöne, B. R., Mertz-Kraus, R., 2017. Controls on strontium and barium incorporation into freshwater bivalve shells (*Corbicula fluminea*). Palaeogeogr. Palaeoclimatol. Palaeoecol. 465, 386–394.

Zhong, S., Mucci, A., 1989. Calcite and aragonite precipitation from seawater solutions of various salinities: Precipitation rates and overgrowth compositions. Chem. Geol. 78, 283–299.

Corrigendum:

Thermodynamic predictions correspond to a positive correlation between shell Sr/Ca and seawater temperature (obtained in this study), inverse to results from inorganically precipitated aragonite (see Abstract and sections 2.1, 2.4, and 2.5). Caption and formatting errors in Table 2.2 and Fig. 2.7–2.8 have been corrected from the published version.

3 Sr/Ca in shells of laboratory-grown bivalves (*Arctica islandica*) serves as a proxy for water temperature – Implications for (paleo)environmental research?

Cornélia BROSSET[1], Nils HÖCHE[1], Rob WITBAARD[2], Kozue NISHIDA[3], Kotaro SHIRAI[4], Regina MERTZ-KRAUS[1], Bernd R. SCHÖNE[1]

[1]*Institute of Geosciences, University of Mainz, Mainz, Germany*

[2]*Department of Estuarine and Delta Systems, Royal Netherlands Institute for Sea Research, Yerseke, The Netherlands*

[3]*Graduate School of Life and Environmental Sciences, University of Tsukuba, Tsukuba, Japan*

[4]*Atmosphere and Ocean Research Institute, The University of Tokyo, Chiba, Japan*

Brosset, C., Höche, N., Witbaard, R., Nishida, K., Shirai, K., Mertz-Kraus, R., Schöne, B. R., 2023. Sr/Ca in shells of laboratory-grown bivalves (*Arctica islandica*) serves as a proxy for water temperature – Implications for (paleo)environmental research? *Front. Mar. Sci.* 10, 1279164.

In this chapter, the Sr/Ca-temperature relationship was examined in juvenile *Arctica islandica* specimens grown under stable laboratory conditions. Shell Sr/Ca increased with water temperature and the correlation strengthened after accounting for growth rate and ultrastructural influences, leading to more robust temperature transfer functions than those obtained under natural conditions. This manuscript was published in the journal "*Frontiers in Marine Science*". I contributed to the data curation, formal analysis, investigation, methodology, validation, visualization, writing – original draft and writing – review and editing of the manuscript. This work was supported by the German Research Foundation (DFG) grant [SCHO793/23] to BRS and the Japan Society for Promotion of Science (JSPS) grant [20181607] to KS under the Joint Research Projects-LEAD with DFG (JRPs-LEAD with DFG).

Author contributions:

CB	Data curation, Formal Analysis, Investigation, Methodology, Validation, Visualization, Writing – original draft, Writing – review & editing.
NH	Investigation, Methodology, Writing – review & editing.
RW	Resources, Writing – review & editing.
KN	Writing – review and editing.
KS	Funding acquisition, Writing – review & editing.
RMK	Writing – review & editing.
BRS	Conceptualization, Data curation, Formal Analysis, Funding acquisition, Investigation, Methodology, Project administration, Supervision, Validation, Writing – original draft, Writing review & editing.

3.1 Abstract

Seawater temperature is an essential quantity for paleoclimatological and paleoecological studies. A potential archive that can provide century-long, temporally well-constrained and high-resolution temperature proxy data is available in the form of bivalve shells. However, the number of well-accepted and robust temperature proxies contained in shells is limited to stable oxygen isotopes and carbonate clumped isotopes. Many studies have therefore investigated the possibility to reconstruct temperature from element/Ca properties, specifically Sr/Ca ratios in case of aragonitic shells. As demonstrated here, in agreement with thermodynamic expectations and the lattice strain model, shell Sr/Ca of laboratory-grown *Arctica islandica* specimens is strongly positively coupled to water temperature. If ultrastructure-related bias is mathematically eliminated, up to 75 % of the variability in shell Sr/Ca data can be explained by water temperature. However, in field-grown specimens, this relationship is superimposed by other environmental variables that can hardly be quantified and mathematically eliminated. The explained variability of Sr/Ca is reduced to merely 26 % and the prediction uncertainty too large for reliable temperature estimates. Most likely, the equable, less biased conditions in the laboratory resulted in the production of a more uniform shell ultrastructure (with larger and more elongated biomineral units) which in turn was associated with less variable Sr/Ca values and a stronger link to water temperature. Without a detailed understanding and quantification of the factors controlling ultrastructural variations in field-grown bivalves, it remains impossible to employ shell Sr/Ca of wild *A. islandica* specimens for precise temperature estimates, merely a qualitative temperature reconstruction seems feasible.

3.2 Introduction

Ocean temperature is a crucial quantity in paleoclimatological and paleoecological research. Amongst other aspects, seasonally to annually resolved and temporally well-constrained temperature data are needed to verify and refine numerical climate models (Schmidt et al., 2014; Cauquoin et al., 2019), understand biogeographic distribution patterns (Adey and Steneck, 2001; Zacherl et al., 2003; Belanger et al., 2012) and assess the impact of short-term temperature changes on biota, specifically in coastal nearshore environments (Goberville et al., 2010; Węsławski et al., 2011). Potential archives that provide such data include shells of bivalve mollusks (Wanamaker et al., 2012; Butler et al., 2013; Lohmann and Schöne, 2013; Black et al., 2016). Bivalves are often abundant and sometimes well-preserved in the fossil record, extending their potential use back in time. They are widely distributed globally and some species such as the ocean quahog, *Arctica islandica*, can live for several hundred years (Schöne et al., 2005; Wanamaker et al., 2008a; Butler et al., 2013). More importantly, they record changes of ambient environmental conditions in their shells in precise chronological order (Jones, 1981; Witbaard et al., 1994; Schöne et al., 2005, 2023; Wanamaker et al., 2012, 2019). This environmental record is also spatially well-constrained, because bivalves are sessile organisms, compared to data extracted from mobile or migrating animals, e.g., fish (Schöne and Krause, 2016). However, extracting quantitative temperature data from bivalve shells remains a challenging task for a variety of reasons.

Due to known limitations of $\delta^{18}O$ and Δ_{47}-based temperature estimates (Witbaard et al., 1994; Eiler, 2011; De Winter et al., 2022), repeated attempts have been undertaken to explore the potential use of element/Ca ratios as paleothermometers, especially Sr/Ca values in aragonitic shells (Surge and Walker, 2006; Foster et al., 2009; Schöne et al., 2011, 2013, 2023) and Mg/Ca in calcitic shells (e.g., Wanamaker et al., 2008b; Tynan et al., 2017). Unlike $\delta^{18}O$, these element/Ca values are assumed to be fairly stable in marine waters (above a salinity of approx. 10; Dodd and Crisp, 1982) through time and space and can thus be assumed constant in paleothermometry equations. Furthermore, with *in-situ* analytical techniques (e.g., LA-ICP-MS), element/Ca data can be measured quickly, precisely and at very high spatial resolution. While Sr/Ca and Mg/Ca values are routinely used in many non-molluscan biogenic carbonates to reconstruct temperature histories (Beck et al., 1992; Rosenheim et al., 2004; Corrège, 2006), their use in bivalve shells (Dodd, 1965; Stecher et al., 1996; Zhao et al., 2017) is controversially debated, even in the same species. Reports on *A. islandica* range from positive (Hart and Blusztajn, 1998; Toland et al., 2000; Brosset et al., 2022) to negative (Schöne et al., 2013; Yan et al., 2013) to no correlation (Wanamaker and Gillikin, 2019) between shell Sr/Ca or Mg/Ca and temperature. Partly, these controversial findings are related to the experimental design, e.g., averaging Sr/Ca data from very slow and fast-growing shell portions, growth lines and growth increments, respectively (Schöne

et al., 2013). Even if there was a relationship between shell Sr/Ca and temperature, the correlation remained low (ca. $R^2 < 0.30$). Only a single study explored this relationship in laboratory-grown *A. islandica* specimens, but merely at two different temperature regimes and without studying the underlying shell ultrastructure (Wanamaker and Gillikin, 2019).

As with most other trace and minor elements, the incorporation of Sr and Mg into bivalve shells is reported to be strongly controlled by vital and/or kinetic effects (e.g., Foster et al., 2009), possibly to maintain certain mechanical properties of the shell. As a result, their concentration typically remains well below values observed in abiogenic aragonite and scleractinian corals (Gaetani and Cohen, 2006), and their temperature sensitivity (= the slope of the regression curve between shell Sr/Ca or Mg/Ca and temperature) often deviates from that of abiogenic aragonite (compare, e.g., Gaetani and Cohen, 2006 with Schöne et al., 2013). Furthermore, a strong coupling with growth rate (Stecher et al., 1996; Gillikin et al., 2005), ontogenetic age (Freitas et al., 2005; Schöne et al., 2011, 2023) and shell ultrastructure (Shirai et al., 2008; Foster et al., 2009; Schöne et al., 2013; Füllenbach et al., 2017; Roger et al., 2017) has been reported. For example, in annual growth lines of *Arctica islandica* which consist of irregular simple/spherulitic prismatic (ISP) ultrastructure (Ropes, 1984), the Sr concentration is much higher than in the annual increments, i.e., the fast-growing portions between adjacent growth lines (Schöne et al., 2013). In the outer portion of the outer shell layer (oOSL), annual growth increments consist predominantly of homogeneous (HOM) ultrastructure, whereas in the inner portion of the outer shell layer (iOSL) crossed-acicular (CA) and fine-complex crossed-lamellar ultrastructures prevail (Ropes, 1984). As recently demonstrated (Brosset et al., 2022), the shell Sr/Ca values in annual increments (reflecting the main growing season) of juvenile field-grown *A. islandica* specimens from NE Iceland are weakly positively correlated to water temperature. After mathematical elimination of growth rate and/or ultrastructure-related bias, only a slightly stronger positive correlation was observed implying that other environmental variables exert a strong control on shell Sr/Ca (Brosset et al., 2022). Notably, the positive relationship between Sr/Ca and temperature differs from such found in synthetic aragonite and scleractinian corals (negative correlation) but agrees with thermodynamic expectations and the lattice strain model (Gaetani and Cohen, 2006).

The present study explores whether juvenile *A. islandica* specimens record water temperature in shell Sr/Ca values if grown in laboratory tanks under controlled conditions, largely devoid of environmental disturbances. Furthermore, by comparison to data of conspecific specimens grown in the field, the potential use of shell Sr/Ca as a paleothermometer is evaluated. The following hypotheses were tested. (i) After mathematical correction for shell growth rate and ultrastructural biases, shell Sr/Ca values of specimens raised under controlled conditions in laboratory tanks are more strongly correlated to water temperature and show a stronger

temperature sensitivity than specimens grown in the field. (ii) The uniformity of shell ultrastructure in tank-grown specimens is expected to facilitate the analysis of the Sr/Ca-temperature relationship. Results of this study have implications for future paleotemperature estimates based on molar Sr/Ca ratios of bivalve shells.

3.3 Materials and methods

3.3.1 Sample collection and experimental conditions

For the present work, shells of twenty-one juvenile specimens of *Arctica islandica* of two laboratory growth experiments were used (Witbaard et al., 1997; Beirne et al., 2012; Table 3.1). All bivalves were raised in tanks under controlled temperature regimes. Some of the material of Beirne et al. (2012) was also analyzed by Wanamaker and Gillikin (2019) for element chemical properties and growth rate, whereas specimens of Witbaard et al. (1997) were used by Höche et al. (2021) largely for the ultrastructure analysis in the hinge portion of the shells (which differs from such in the ventral margin).

Table 3.1 Overview of laboratory-grown specimens of *Arctica islandica* used in the present study. For a detailed description of experimental settings, see Witbaard et al. (1997) and Wanamaker and Gillikin (2019). One data point includes element chemical data obtained by LA-ICP-MS and ultrastructure analysis in scanning electron microscope images.

Sampling locality	Duration of experiment	Temperature regime	# Specimens	# Data points	Ontogenetic age (years)	Shell height (mm)	Shell thickness (mm)
Baltic Sea (54°52′59′′N, 010°08′00′′E)	95 days	1.1 °C	2	109	5	16.77 ± 2.29	0.47 ± 0.04
		3.2 °C	2	105			
		6.2 °C	3	272			
		9.2 °C	3	112			
		12 °C	2	78			
		15 °C	3	145			
Gulf of Maine (44°26′10′′ N, 067°26′18′′W)	47 days	10.3 °C	6	315	3	38.25 ± 0.22	1.21 ± 0.33
	69 days	15 °C		273			

Fifteen specimens employed in the studies by Witbaard et al. (1997) and Höche et al. (2021) were collected at 20 m water depth in the western Baltic Sea, Germany (Table 3.1). After a one-month acclimatization to fully marine conditions in laboratory tanks at Texel, The Netherlands, bivalves were allowed to grow for 95 days in a total of six tanks under stable temperatures, with aerated and filtered seawater regularly replaced. The six stable temperature regimes used for culturing were 1.1, 3.2, 6.2, 9.2, 12 °C and 15 °C (for details on the experimental

conditions, see Witbaard et al., 1997; note that the experiment conducted at 15 °C was not reported in their study, but culturing conditions were identical). Two to three bivalves were selected for this study from the nine specimens cultured in each tank with *ad libitum* food composed of a phytoplankton mixture of *Isochrysis galbana* and *Dunaliella marina*.

Six additional specimens came from 82 m water depth in the Gulf of Maine (Beirne et al., 2012). Bivalves were then transported to the Darling Marine Center (University of Maine, Orono) in Walpole, Maine and exposed to ambient temperature, food, and salinity (Beirne et al., 2012). After ca. 1.5 years, the specimens were raised in a muddy estuarine sediment with ambient seawater under stable temperature conditions of 10.3 ± 0.2 °C for 47 days, followed by another 69 days at 15 ± 0.3 °C (for details, see Beirne et al., 2012 and Wanamaker and Gillikin, 2019).

3.3.2 Sample preparation

After the experiments, all specimens were shucked, and their shells rinsed with tap water. The right valves of the Baltic Sea (BS) specimens and the left valves of the Gulf of Maine (GOM) shells were mounted on acrylic glass cubes using a plastic welder (WIKO Multi Power 3). The subsequent preparation was done in accordance with methods described in Höche et al. (2022). Briefly, a protective layer of metal epoxy resin (WIKO 05) was applied to the shell surfaces along the planned cutting axis. From each valve, two approx. 2.5 mm thick sections were cut along the maximum growth using a low-speed saw (Buehler IsoMet 1000) operated at 200 rpm. The saw was equipped with a 0.4 mm diamond-coated blade. As shells from the Baltic Sea specimens were very thin (approx. 0.5 mm), the cross-sectioned slabs were embedded in epoxy resin (Araldite 2020) to avoid damage during the cutting process. Furthermore, the epoxy was mixed with a conductive filler (Buehler 20-8500) for subsequent scanning electron microscopic (SEM) analysis. All sections were then ground with F800 and F1200 SiC suspensions on glass plates, and polished using Al_2O_3 suspension (1 µm grain size) on a Buehler MasterTex cloth. Between each grinding and polishing step specimens were ultrasonically cleaned in tap water. Once dried from air, one slab of each specimen was attached with a carbon sticker to a one-inch sample holder for SEM analysis. The mirroring section was glued to a glass slide used for *in-situ* trace element analysis by laser ablation inductively coupled plasma mass spectrometry (LA-ICP-MS).

3.3.3 *In-situ* chemical analysis

The trace element analysis of the shells of the laboratory-grown specimens was done by LA-ICP-MS at the Institute of Geosciences, University of Mainz, following the same method and settings used in Brosset et al. (2022) for field-grown specimens. Briefly, the system consisted of a 193 nm ArF Eximer laser (ESI NWR 193; repetition rate = 10 Hz; energy density = approx. 3 J/cm^2)

equipped with a TwoVol2 ablation cell, coupled to a quadrupole inductively coupled plasma mass spectrometer (Agilent 7500ce). The laser spots (n = 1,409; 60 µm diameter) were placed 90 µm apart (center to center). In each of the two sublayers (outer, inner) of the outer shell layer (oOSL, iOSL) of the ventral margin, one transect of LA spots was placed parallel to the main growth axis (Fig. 3.1). Strontium concentration in the shells was monitored using the ^{88}Sr intensity. Data were reduced using an in-house software program following the calculations of Longerich et al. (1996) and Jochum et al. (2011). NIST SRM 610 and NIST SRM 612 were used for calibration, and USGS MACS-3, BCR-2G, JCp-1 and JCt-1 as quality control materials, with the preferred values given in the GeoReM database (available at http://georem.mpch-mainz.gwdg.de, ver. 34, last access: 16 Dec. 2022; Jochum et al., 2005, 2012; Table S3.1). The element concentrations determined for the quality control materials were in the range of published values, and average detection limit ($3\sigma_{background}$, Jochum et al., 2012) and element-specific Relative Standard Deviation (RSD%) values are shown in Table S3.1. Data from the reference materials and bivalve shells were normalized using ^{43}Ca as internal standard, and molar Sr/Ca ratios were calculated from Sr concentrations using a shell calcium content of 380,000 µg/g (Marali et al., 2017).

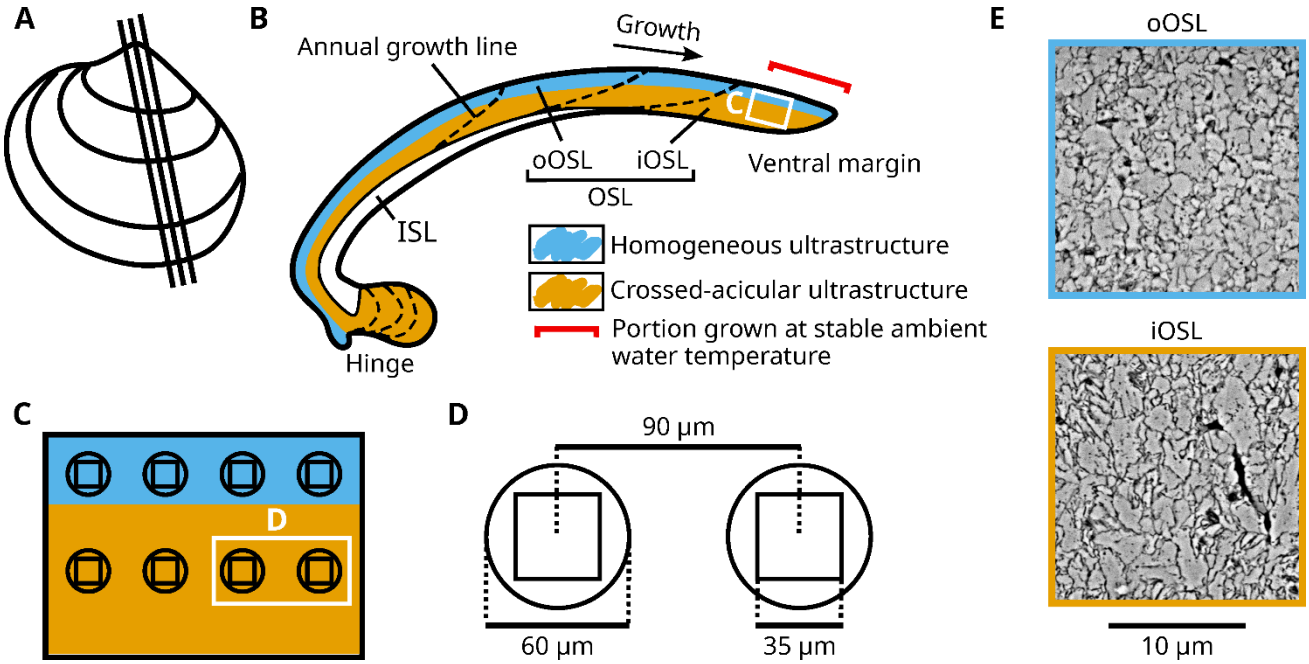

Figure 3.1 Overview of the sampling positions for ultrastructural and *in-situ* element chemical analyses in shells of *Arctica islandica* specimens cultured at 1.1, 3.2, 6.2, 9.2, 10.3, 12 and 15 °C. (A) Depiction of a left valve from a cultured specimen illustrating the cutting axes of the studied shell. (B) Schematic representation of a shell slab. The shell is divided into an inner and outer shell layer (ISL, OSL), separated by the myostracum. The outer portion of the OSL (oOSL) primarily consists of homogeneous ultrastructure (blue), while crossed-acicular ultrastructure (orange) dominates in the inner portion of the OSL (iOSL). The portion of the shell grown during the experimental interval is indicated by the red bracket. (C) Enlargement of panel (B) showing the sampling positions for LA-ICP-MS and SEM for the two shell

sections analyzed for every specimen. (D) Enlarged schematic representation of the SEM images (35 µm^2) compared to the laser spots (60 µm diameter, 90 µm between LA centers) depicted in panel (C). (E) Example of SEM image obtained in the oOSL and the iOSL. The scale applies to both images.

3.3.4 Ultrastructure morphometry

The other polished cross-section of each specimen was used for ultrastructural properties analysis by means of SEM, following the method reported by Höche et al. (2022). An ultrafine chemo-mechanical polishing, i.e., superficial oxidation of the intercrystalline organics and smoothing of the carbonate phase, was performed on the cross-sections to better distinguish individual biomineral units (BMUs). Accordingly, the shell slabs were polished for ca. 10 min with a 60 nm suspension (Buehler MasterMet, pH ca. 10.1) on a Buehler MasterTex polishing cloth mounted on a rotational lap (Buehler MetaServ 2000; 50 rpm).

For direct comparison of the Sr/Ca data with the ultrastructural properties, both sections of each specimen were photographed with a digital camera under a light microscope with reflective illumination (Leica Stemi 508), and images were stitched together using the opensource software Hugin (available at https://sourceforge.net/projects/hugin/, last access: 19 Jul. 2023). In each specimen, the width of the portion grown in the laboratory was measured along the maximum growth axis, and the shell daily growth rates were approximated assuming a constant shell growth during the respective experimental intervals (for details on laboratory-grown sections identification, see Beirne et al., 2012 and Höche et al., 2021). The BigWarp tool (Fiji built-in BigDataViewer plugin available at https://imagej.net/software/fiji/, last access: 16 Dec. 2022) of the software ImageJ (Schindelin et al., 2012; Bogovic et al., 2016) was employed to align both sections of each specimen, and thus to align ultrastructure data to Sr/Ca data (Fig. 3.1). To this avail, one SEM image (35 µm × 35 µm) was taken in corresponding shell portions in which the chemical measurements were completed. A 3rd generation Phenom Pro Desktop SEM equipped with a backscatter electron detector and a CeB_6 electron source was used to take 1,409 SEM images at 7,700× magnification and 10keV.

Prior to morphometric analyses, individual BMUs were detected in the SEM photographs following the segmentation method depicted in Höche et al. (2021). Briefly, the machine learning software Ilastik (Berg et al., 2019) was trained to recognize individual BMUs on a sample set of the studied SEM images. Subsequently, all SEM images were processed semi-automatically. The quality of the segmentations was manually assessed, and the software training refined if necessary. Morphometrical parameters, including BMU area and BMU elongation (= ratio between the minor and major axes of an ellipse fitted to the BMU), were automatically measured using the scikit-image processing library (van der Walt et al., 2014) operated through a python script (Höche et al., 2021). For each experimental temperature regime and OSL sublayers,

examples of BMU segmentations are depicted in Figures S3.1, S3.2. The 15 % largest BMUs of each SEM image were considered for consecutive analysis. According to previous work, this threshold value reveals the highest BMU morphology variation and provides the strongest link between the size of individual BMUs in the shell of *A. islandica* and water temperature (Höche et al., 2021).

3.3.5 Statistical analysis and detrending of shell Sr/Ca and ultrastructure

To assess the mathematical correlation between water temperature and shell properties, shell growth rate, Sr/Ca, BMU area and BMU elongation data were plotted against temperature (section 3.3.1). Kruskal-Wallis (KW) rank tests were used to compare data between all temperature regimes, and Dunn tests (generalized Bonferroni adjustment for multiple comparisons; Table S3.2) were used to compare data between pairs of two temperature regimes. Data from the oOSL and the iOSL were compared using Mann-Whitney *U* (MWU) two-sample rank tests. At each temperature regime and for both shell sublayers (oOSL and iOSL), median values weighted for the number of studied specimens were calculated for Sr/Ca, BMU area and BMU elongation, and were used for the subsequent analyses.

To identify potential links between shell growth rate, ultrastructure and chemical properties that could have biased the temperature sensitivity of these shell properties, crossplots were generated between (i) growth rate and Sr/Ca, (ii) Sr/Ca and ultrastructural properties, and (iii) growth rate and ultrastructural properties (BMU area and elongation). Based on these crossplots, non-linear (natural logarithm) regression models were computed and subsequently used to detrend the chemical and ultrastructural data. For this purpose, predicted values given by these regression models were subtracted from the chemical and ultrastructural data, resulting in growth rate-detrended Sr/Ca data (d_{GR}Sr/Ca), BMU area-detrended Sr/Ca data (d_{AR}Sr/Ca) as well as BMU elongation-detrended Sr/Ca data (d_{EL}Sr/Ca) i.e., residuals for each of these parameters after detrending (section 3.3.2). Furthermore, Sr/Ca data were mathematically corrected for combinations of growth rate and BMU area (d_{GRAR}Sr/Ca), growth rate and BMU elongation (d_{GREL}Sr/Ca), as well as growth rate, BMU area and elongation (d_{GRAREL}Sr/Ca). Also, the correlation with growth rate was eliminated from ultrastructural properties (section 3.3.2) to obtain growth rate-detrended BMU area data (d_{GRAR}) and growth rate-detrended BMU elongation data (d_{GREL}).

All computations were done separately for each OSL sublayer (oOSL and iOSL; Tables 3.2, 3.3). As indicated by previous studies, *A. islandica* shell growth rate differs significantly between populations and sampling localities (e.g., Begum et al., 2010; Höche et al., 2022). Therefore, data

detrending for shell growth-related effects was performed independently between BS and GOM specimens. All other calculations were done with data from BS and GOM combined. In order to achieve the best description of all detrended and undetrended data, linear regressions were computed between Sr/Ca and water temperature, whereas natural logarithms models were used between water temperature and shell ultrastructural properties, i.e., BMU area and elongation. Subsequently, these models were employed to compute temperature prediction intervals (1σ) based on detrended and undetrended shell Sr/Ca. These intervals were then compared with data gathered from field-grown *A. islandica* specimens from NE Iceland (Brosset et al., 2022). Alternatively, for all analyses, models using specimen-specific medians or non-weighted median values, as well as linear and/or natural logarithm detrending and regressions to water temperature for both experiments combined or exclusive to the Baltic Sea experiment, can be found in the online repository of the present study, i.e., in Brosset et al. (2023).

Table 3.2 Overview of the regression parameters (slope; R^2, coefficient of determination; p, probability) between shell Sr/Ca data of cultured *Arctica islandica* specimens and shell growth rate (GR; data from Baltic Sea and Gulf of Maine in regular and italic font, respectively), ultrastructural properties, i.e., area and elongation of the biomineral units (AR and EL, respectively), and temperature of the laboratory tanks (T). The regression curves were examined in the outer and inner portions of the outer shell layer (oOSL and iOSL, respectively) for undetrended Sr/Ca, as well as for Sr/Ca detrended (d) by GR, AR and EL, as well as combinations of GR and AR (GRAR), GR and EL (GREL), and GR, AR and EL (GRAREL). Natural logarithm models were applied for regressions between Sr/Ca and GR, AR and EL, whereas linear models were applied for relationships between Sr/Ca and T. For all regressions, ns, non-significant at $p > 0.05$.

Variables		Sr/Ca		d_{GR}Sr/Ca	d_{AR}Sr/Ca	d_{EL}Sr/Ca	d_{GRAR}Sr/Ca	d_{GREL}Sr/Ca	d_{GRAREL}Sr/Ca
oOSL									
	slope	-0.20 ± 0.07	0.02 ± 0.01						
ln(GR)	R^2	0.40	0.35						
	P	< 0.05	< 0.05						
	slope	-0.38 ± 0.72		0.08 ± 0.58					
ln(AR)	R^2	0		0					
	P	ns		ns					
	slope	-7.96 ± 1.53		-6.08 ± 1.30			-11.61 ± 2.61		
ln(EL)	R^2	0.53		0.48			0.45		
	P	< 0.001		< 0.001			< 0.001		
	slope	0.02 ± 0.01		0.01 ± 0.01	0.02 ± 0.01	0.03 ± 0.004	0.04 ± 0.02	0.04 ± 0.01	0.06 ± 0.01
T	R^2	0.22		0.16	0.19	0.63	0.20	0.37	0.41
	P	< 0.05		< 0.05	< 0.05	< 0.001	< 0.05	< 0.001	< 0.001
iOSL									
	slope	-0.11 ± 0.08	0.10 ± 0.04						
ln(GR)	R^2	0.05	0.35						
	P	ns	< 0.05						
	slope	0.80 ± 0.15		0.88 ± 0.17					
ln(AR)	R^2	0.53		0.53					
	P	< 0.001		< 0.001					
	slope	0.36 ± 1.74		-0.31 ± 1.91			-1.00 ± 2.77		
ln(EL)	R^2	0		0			0		
	P	ns		ns			ns		
	slope	0.03 ± 0.01		0.04 ± 0.01	0.03 ± 0.003	0.03 ± 0.01	0.06 ± 0.01	0.06 ± 0.02	0.09 ± 0.02
T	R^2	0.38		0.41	0.75	0.29	0.56	0.30	0.44
	P	< 0.001		< 0.001	< 0.001	< 0.01	< 0.001	< 0.01	< 0.001

Table 3.3 Overview of the regression parameters (slope; R^2, coefficient of determination; p, probability) between shell ultrastructural properties of cultured *Arctica islandica* specimens, i.e., area and elongation of the biomineral units (AR and EL, respectively), shell growth rate (GR; data from Baltic Sea and Gulf of Maine in regular and italic font, respectively), and temperature of the laboratory tanks (T). The regression curves were examined in the outer and inner portions of the outer shell layer (oOSL and iOSL, respectively) for undetrended AR and EL as well as growth rate (GR)-detrended AR and EL data. Natural logarithm models were applied for regressions between ultrastructural data (AR and EL), GR and T. For all regressions, ns, non-significant at $p > 0.05$.

Variables		**AR**		**d_{GR}AR**	**EL**		**d_{GR}EL**
oOSL							
	slope	0.20 ± 0.07	*-0.05 ± 0.02*		0.04 ± 0.02	*-0.03 ± 0.01*	
ln(GR)	R^2	0.37	*0.35*		0.13	*0.35*	
	p	< 0.05	*< 0.05*		ns	*< 0.05*	
	slope	-0.007 ± 0.03		-0.02 ± 0.03	0.003 ± 0.01		-0.005 ± 0.01
ln(T)	R^2	0		0	0		0
	p	ns		ns	ns		ns
iOSL							
	slope	0.31 ± 0.12	*0.39 ± 0.15*		-0.05 ± 0.05	*-0.001 ± 0.0004*	
ln(GR)	R^2	0.33	*0.35*		0	*0.35*	
	p	< 0.05	*< 0.05*		ns	*< 0.05*	
	slope	0.10 ± 0.11		0.22 ± 0.08	0.05 ± 0.01		0.03 ± 0.01
ln(T)	R^2	0		0.23	0.29		0.19
	p	ns		< 0.05	< 0.01		< 0.05

3.4 Results

A. islandica specimens from the Baltic Sea (BS) and the Gulf of Maine (GOM) differed in shell height, thickness and ontogenetic age (Table 3.1). GOM specimens were younger (3 years-old) than those originating from BS (5 years-old). However, shells from GOM were larger (average height: 38.25 ± 0.22 mm) and thicker (1.21 ± 0.33 mm) than those from BS (height = 16.77 ± 2.29 mm, thickness = 0.27 ± 0.04 mm; Table 3.1). Given these differences, shell growth rates were calculated separately for BS and GOM specimens (Fig. 3.2A), and size differences were also considered when shell chemical and ultrastructural properties were compared with water temperature.

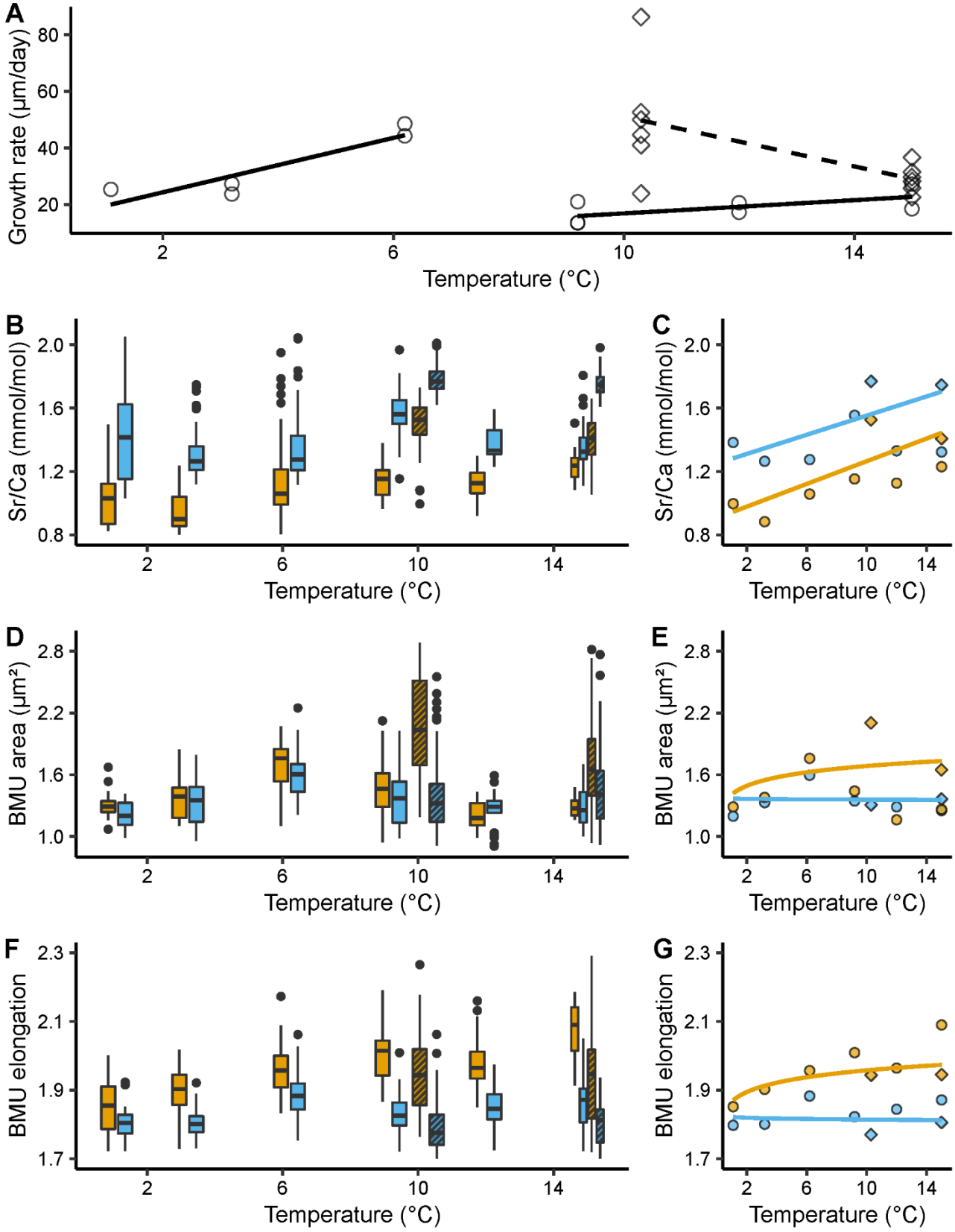

Figure 3.2 Shell growth rate (µm/day), molar Sr/Ca ratios (mmol/mol) and ultrastructural properties, i.e., biomineral unit (BMU) area (µm²) and elongation, from the outer portion of the outer shell layer (oOSL, blue) and the inner portion of the outer shell layer (iOSL, orange) of *Arctica islandica* specimens cultured

at 1.1, 3.2, 6.2, 9.2, 10.3, 12 and 15 °C. (A) Shell growth rate of studied specimens. Black solid line: linear model for Baltic Sea (BS); black dashed line: linear model for Gulf of Maine (GOM). (B) Shell Sr/Ca values and corresponding (C) median values weighted for the number of specimens (linear regression). (D) Area of the BMUs and corresponding (E) median values weighted for the number of specimens (natural logarithm regression). (F) Elongation of the BMUs and corresponding (G) median values weighted for the number of specimens (natural logarithm regression). In (A, C, E, G), circles represent data from the BS experiment, while squares stand for data from the GOM experiment. In (B, D, F), the bold black line represents the median, lower and upper limits of the boxes stand for the first and third quartiles, vertical lines denote the minimum and maximum values, and black dots equal outliers. Solid filled boxes = data from the Baltic Sea experiment; striped boxes = data from the Gulf of Maine experiment.

3.4.1 Relationship between shell properties and water temperature

3.4.1.1 Shell Sr/Ca and water temperature

In both sublayers of the outer shell layer, Sr/Ca was significantly ($p < 0.05$) positively linked to water temperature and differed significantly between the adjacent temperature regimes (KW, $p < 0.001$; Fig. 3.2B, C). When adjusted for multiple comparisons, i.e., Bonferroni correction, this relationship remained significant in more than 60 % of the groups tested (Dunn, $p < 0.025$; Table S3.2). Noteworthy, Sr/Ca ratios of the oOSL were significantly higher than those of the iOSL, on average, by 0.28 ± 0.02 mmol/mol (MWU, $p < 0.001$), with a range of 1.26 to 1.77 and 0.88 to 1.53 mmol/mol in the oOSL and iOSL, respectively (Fig. 3.2B, C). Sr/Ca of the iOSL was more strongly coupled to water temperature, i.e., showed a higher temperature sensitivity (slope = 0.03 ± 0.01 mmol/mol/°C, $R^2 = 0.38$, $p < 0.001$) than that of the oOSL (slope = 0.02 ± 0.01 mmol/ mol/°C, $R^2 = 0.22$, $p < 0.05$; Fig. 3.2C, Table 3.2).

3.4.1.2 Shell ultrastructure and water temperature

At some temperature settings, ultrastructural properties differed significantly between the oOSL and iOSL (MWU, $p < 0.001$; Fig. 3.2D, E). For example, at 1.1, 6.2 and 15 °C, BMUs were significantly larger in the iOSL than in oOSL (MWU, $p < 0.05$), whereas nearly identical sizes were observed at the remaining studied temperature regimes (MWU, $p > 0.05$). In the iOSL, the weak tendency toward larger BMUs forming in warmer water was not significant (slope = 0.10 ± 0.11 μm^2/°C, $p > 0.05$). Nevertheless, in over 66 % of the temperature pairs assessed, a significant difference in the area of the BMUs was obtained (Dunn, $p < 0.025$; Table S3.2). In contrast, irrespective on the prevailing temperature, the BMU area of the oOSL remained largely unchanged (Dunn, $p > 0.025$ for more than 70 % of the tested pairs; Table S3.2).

The two sublayers of the OSL differed more clearly with respect to BMU elongation. BMUs were approx. 0.14 ± 0.002 more elongated in the iOSL than the oOSL (Fig. 3.2F, G). Between adjacent temperature regimes, the BMU elongation statistically differed (KW, $p < 0.001$), but after

Bonferroni adjustment only half of the paired temperature regime comparisons remained significant (Dunn, $p < 0.025$; Table S3.2). In the iOSL, slightly more needle-shaped BMUs were formed in warmer waters (slope = 0.05 ± 0.01, $R^2 = 0.29$, $p < 0.01$), which was not the case in the oOSL ($p > 0.05$; Table 3.3).

Compared with field-grown juveniles from NE Iceland (Brosset et al., 2022), the ultrastructure of the studied lab-grown specimens of *A. islandica* was more uniform. The difference cannot only be visually identified (Fig. S3.3), but also expressed in numbers. For example, the size of BMUs varied less in shells of tank-raised bivalves than specimens grown in the field (relative 1σ variance of the mean in the oOSL: 21 vs 18 %; iOSL: 20 vs 18 %; Table S3.3). Furthermore, in tank-raised specimens, BMUs were generally much larger (oOSL: 1.47 vs 0.85 µm^2; iOSL: 1.54 vs 0.97 µm^2) and more elongated (oOSL: 1.85 vs 1.78; iOSL: 1.96 vs 1.77; Table S3.3) than in field specimens.

3.4.1.3 Shell growth rate and water temperature

At large, the shell growth rate of the specimens selected for this study decreased with temperature (Fig. 3.2A). This trend was steep in GOM shells (slope = -4.39 ± 1.83 µm/day/°C, $R^2 = 0.30$, $p < 0.01$) but non-significant in BS specimens (slope = -0.84 ± 0.71 µm/day/°C, $p > 0.05$). The relationship between BS shell growth rate and temperature could also be described with two linear trends, which would better address the abrupt decline of shell growth rate at around 6 °C (Fig. 3.2A). Between 1.1 and 6.2 °C, shell growth rate of BS specimens increased by 76 % (slope = 4.81 ± 1.27 µm/day/°C, $R^2 = 0.77$, $p < 0.01$), ranging from approx. 24.23 ± 1.07 µm/day at 1.1 °C to 42.71 ± 6.36 µm/day at 6.2 °C. In warmer water, shell growth of BS shells declined and merely 16.60 ± 3.73 µm were added per day at 9.2 ° C. Between 9.2 and 15 °C, daily growth rate increased slightly (slope = 1.17 ± 0.63 µm/day/°C, $R^2 = 0.29$, $p < 0.05$), but only attained 27.53 ± 5.51 µm/day. In contrast, GOM specimens grew, on average, much faster than shells from BS, i.e., 54.79 ± 19.46 µm/day at 10.3 °C and 29.88 ± 4.47 µm/day at 15 °C, which translated into a gradual reduction of shell growth by nearly 10 % for every degree Celsius increase. Growth at 15 °C was still significantly faster (on average, 7.21 ± 1.02 µm/day faster, $p < 0.001$) in GOM specimens than in shells from BS. It should be added that the six GOM specimens showed high variability in daily growth rate at 10.3 °C, ranging from 23.89 to 86.26 µm/day (Fig. 3.2A).

3.4.2 Relationship between shell properties

3.4.2.1 Sr/Ca vs growth rate

In both OSL sublayers, Sr/Ca correlated with the shell growth rate of the specimens considered, but the signs differed between the two experiments (Fig. 3.3A and Table 3.2). In BS specimens, faster shell growth was associated with lower Sr/Ca values (Table 3.2), specifically, in the oOSL (slope = -0.20 ± 0.07 mmol/mol per 1 µm/day, R^2 = 0.40, $p < 0.05$). In contrast, shell growth rate was predominantly positively linked to Sr/Ca in GOM shells, specifically in the iOSL (slope = 0.10 ± 0.04 mmol/mol per 1 µm/day, R^2 = 0.35, $p < 0.05$), while the slope was less steep in the oOSL (slope = 0.02 ± 0.01, R^2 = 0.35, $p < 0.05$; Table 3.2).

3.4.2.2 Sr/Ca vs ultrastructure

Sr/Ca was significantly correlated to the ultrastructural properties of the shells, with a comparable Sr/Ca difference between the OSL sublayers for both experiments (Fig. 3.3C, E and Table 2). In the iOSL, 53 % of the Sr/Ca variance could be explained by the size of the BMUs, with an increase of 0.80 ± 0.15 mmol/mol/µm^2 ($p < 0.001$), whereas only a non-significant positive correlation was found between Sr/Ca and BMU elongation ($p > 0.05$). The link between Sr/Ca and BMU elongation was negative, significant and much stronger in the oOSL (R^2 = 0.53, $p < 0.001$) indicating that the strontium content was higher in rounder BMUs (Table 3.2). In contrast, Sr/Ca was not significantly correlated to the BMU area in the oOSL ($p > 0.05$).

3.4.2.3 Shell growth vs ultrastructure

Ultrastructural properties and shell growth rate were significantly correlated (Table 3.3). For example, in the iOSL, the BMU area variability explained by the shell growth rate varied between 33 and 35 % for BS and GOM shells, respectively ($p < 0.05$; Fig. 3.4A and Table 3.3). The size of the BMUs increased between 0.31 ± 0.12 µm^2 (BS) and 0.39 ± 0.15 µm^2 (GOM) for each µm/day of shell growth (Table 3.3). In the oOSL of BS specimens, larger BMUs were also formed during faster shell growth (slope = 0.20 ± 0.07 µm^2 per µm/day, R^2 = 0.37, $p < 0.05$), whereas the BMU area decreased slightly with growth rate in GOM shells (slope = -0.05 ± 0.02, R^2 = 0.35, $p < 0.05$; Table 3.3).

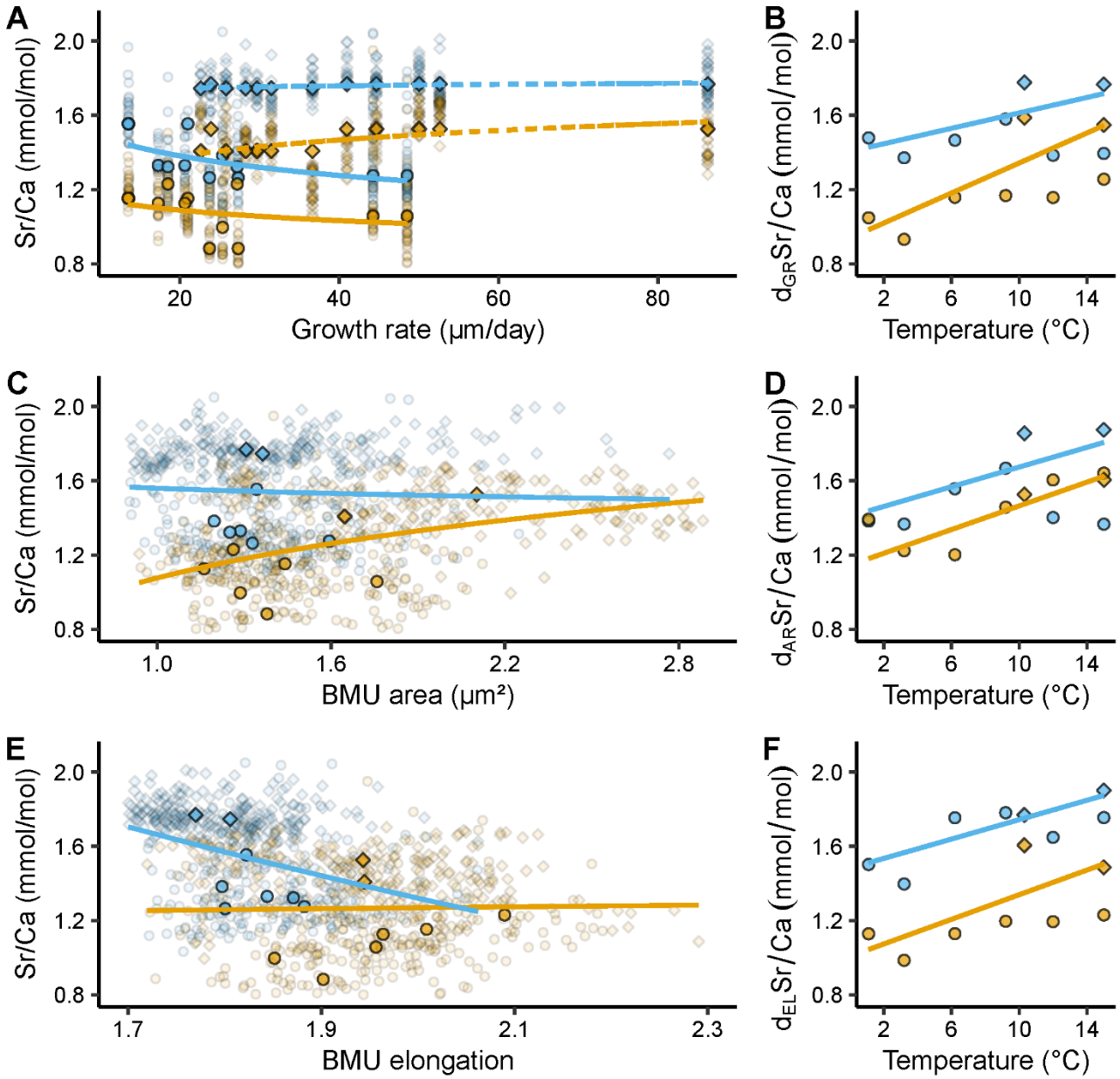

Figure 3.3 Relationships between shell Sr/Ca ratios (mmol/mol) and growth rate (µm/day), ultrastructural properties, i.e., biomineral unit (BMU) area (µm^2) and elongation, and temperature (°C). Blue and orange denote data from the outer and inner portion of the outer shell layer (oOSL, iOSL), respectively, of *Arctica islandica* specimens cultured at 1.1, 3.2, 6.2, 9.2, 10.3, 12 and 15 °C. (A) Relationship between shell Sr/Ca and growth rate (GR) (solid line = Baltic Sea specimens; dashed line = Gulf of Maine specimens). (B) Relationship between detrended (d) Sr/Ca and temperature (T), after removal of GR-related effects. (C) Relationship between Sr/Ca and BMU area (AR). (D) AR-detrended Sr/Ca vs T. (E) Relationship between Sr/Ca and BMU elongation (EL). (F) EL-detrended Sr/Ca vs T. Circles denote data from the Baltic Sea experiment, while squares stand for data from the Gulf of Maine experiment. In (A, C, E) opaque symbols = median weighted for the number of specimens, translucent symbols = raw data from which medians were calculated. All regression models were fitted to the median Sr/Ca values of a given temperature regime, weighted for the number of specimens, with a natural logarithm function for GR, AR and EL, and a linear function for T (regression parameters depicted in Table 3.2).

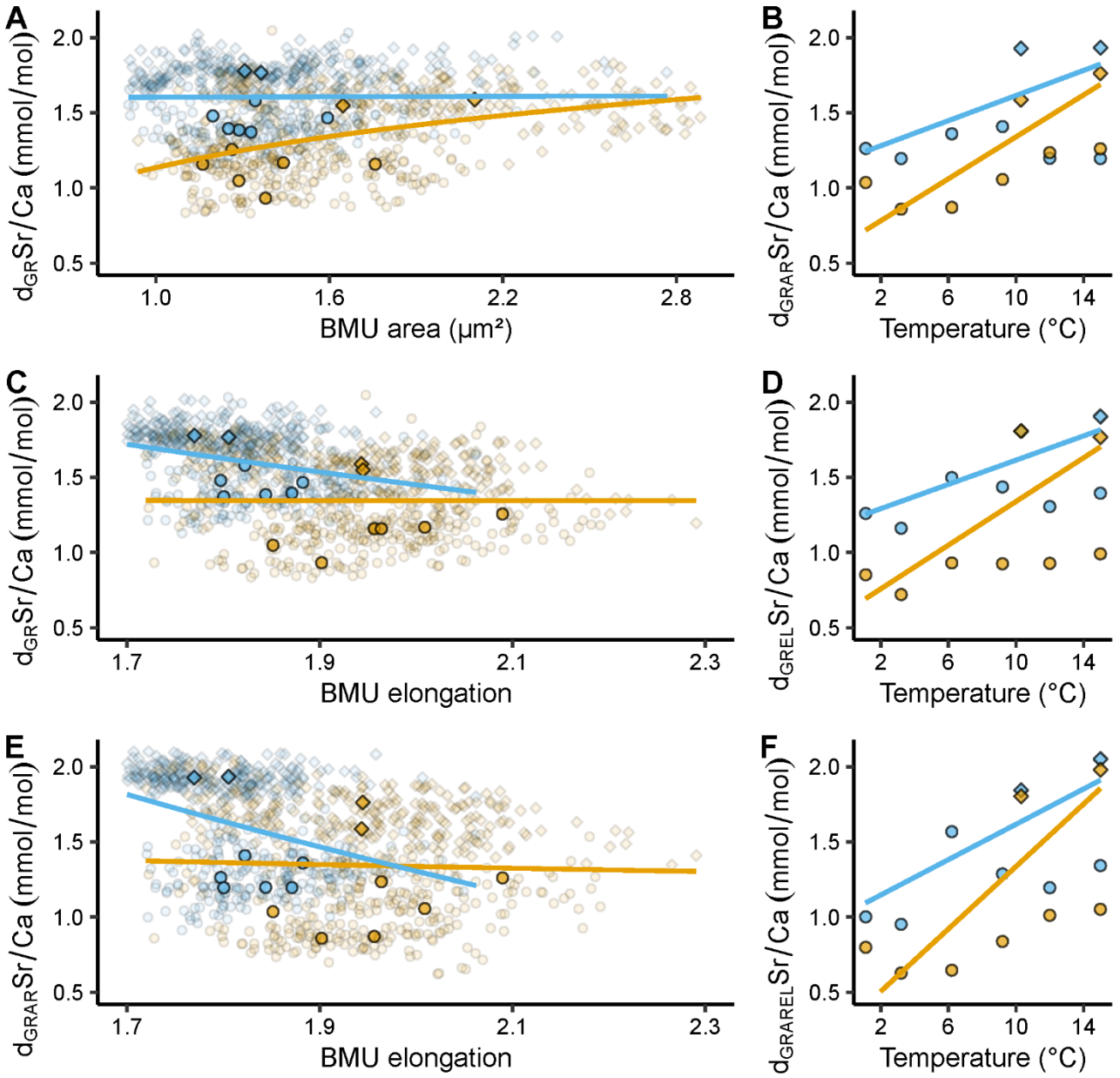

Figure 3.4 Relationships between shell ultrastructural properties, i.e., biomineral unit (BMU) area (µm²) and elongation, growth rate (µm/day), and temperature (°C). Blue and orange denote data from the outer and inner portion of the outer shell layer (oOSL, iOSL), respectively, of *Arctica islandica* specimens cultured at 1.1, 3.2, 6.2, 9.2, 10.3, 12 and 15 °C. (A) Relationship between BMU area and shell growth rate (GR). (B) Relationship between GR-detrended (d) BMU area (AR) and temperature (T). (C) Relationship between BMU elongation (EL) and GR. (D) GR-detrended EL vs T. In (A, C) solid line = Baltic Sea specimens; dashed line = Gulf of Maine specimens. Circles denote data from the Baltic Sea experiment, while squares stand for data from the Gulf of Maine experiment. Opaque symbols = median weighted for the number of specimens; translucent symbols = raw data from which medians were calculated. All regression models were fitted to the median BMU area and elongation values of a given temperature regime, weighted for the number of specimens, with a natural logarithm function for GR and T (regression parameters depicted in Table 3.3).

3.4.3 Relationship between detrended shell properties and water temperature

3.4.3.1 Ultrastructure-detrended Sr/Ca vs temperature

Once the correlation between Sr/Ca and BMU elongation was mathematically eliminated, d_{EL}Sr/Ca values of the oOSL correlated much stronger with water temperature than undetrended Sr/Ca (R^2 = 0.63, $p < 0.001$ vs R^2 = 0.22, $p < 0.05$, respectively; Fig. 3.3E and Table 3.2). Likewise, mathematical elimination of BMU area-related effects from shell Sr/Ca ratios increased the correlation between Sr/Ca and water temperature. For example, 75 % of d_{AR}Sr/Ca variance in the iOSL was explained by the temperature (Fig. 3.3D and Table 3.2).

3.4.3.2 Growth rate-detrended Sr/Ca vs temperature

After elimination of growth rate-related effects, shell Sr/Ca data (d_{GR}Sr/Ca) were still positively correlated to water temperature (Fig. 3.3B), but the temperature sensitivity of Sr/Ca of the oOSL was weaker than before detrending (slope = 0.01 ± 0.01 mmol/mol/°C, R^2 = 0.16, $p < 0.05$; compare Fig. 3.3B and 3.2B). In contrast, 41 % of the iOSL d_{GR}Sr/Ca variance was explained by water temperature, i.e., an increase by more than 7 % compared to undetrended Sr/Ca data (Table 3.2).

3.4.3.3 Combined shell growth and ultrastructure-detrended Sr/Ca vs temperature

Similar to undetrended Sr/Ca, d_{GR}Sr/Ca was positively linked to the BMU area in the iOSL (R^2 = 0.53, $p < 0.001$; Fig. 3.5A, C and Table 3.2). Therefore, the double-detrending of Sr/Ca (i.e., detrending by shell growth rate and BMU area [GRAR]), resulted in comparable results as those obtained by simple detrending (GR, AR), and no significant increase in R^2 was identified for d_{GRAR}Sr/Ca vs temperature (Table 3.2). However, the temperature sensitivity of d_{GRA}RSr/Ca of the iOSL doubled compared to simple detrending (0.06 ± 0.01 vs 0.03 ± 0.01 mmol/mol/°C; Fig. 3.5B, D). In the oOSL, the temperature sensitivity increased up to 0.04 ± 0.01 mmol/mol/°C for d_{GREL}Sr/Ca. Furthermore, a combined detrending of Sr/Ca by growth rate, BMU area and elongation (d_{GRAREL}Sr/Ca; Fig. 3.5E) tripled the temperature sensitivity of Sr/Ca of the oOSL and increased the temperature sensitivity by 0.06 ± 0.002 mmol/mol/°C in the iOSL (Fig. 3.5F), albeit at the expense of explained variability (Table 3.2). However, in both OSL sublayers, the linear models between d_{GRAREL}Sr/Ca and water temperature still showed a better fit than those obtained with undetrended Sr/Ca data (R^2 = 0.41 and 0.44 in the oOSL and iOSL, respectively, $p < 0.001$; Table 3.2).

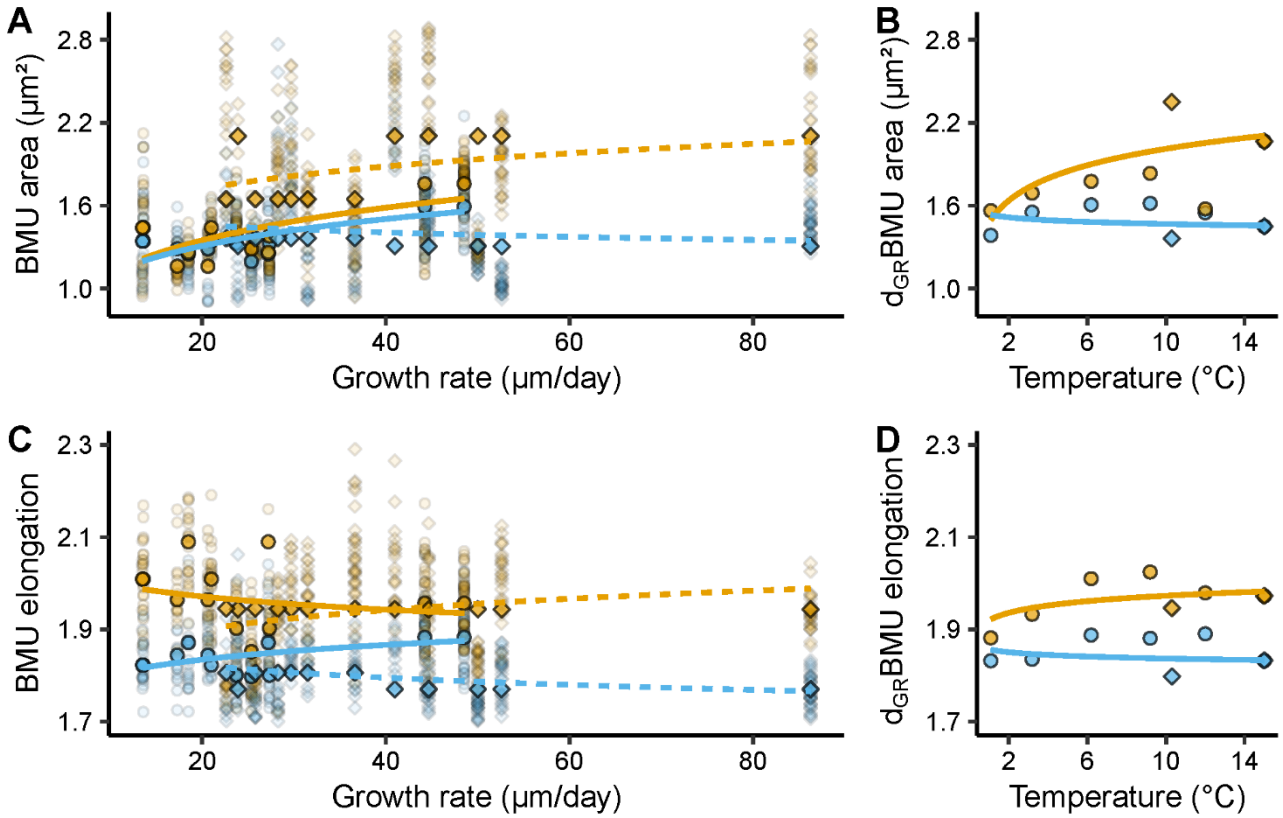

Figure 3.5 Relationships between shell Sr/Ca ratios (mmol/mol), ultrastructural properties, i.e., biomineral unit (BMU) area (µm^2) and elongation, and temperature (°C). Blue and orange denote data from the outer and inner portion of the outer shell layer (oOSL, iOSL), respectively, of *Arctica islandica* specimens cultured at 1.1, 3.2, 6.2, 9.2, 10.3, 12 and 15 °C. (A) Relationship between growth rate (GR)-detrended (d) shell Sr/Ca data and BMU area (AR). (B) Relationship between GR and AR-detrended Sr/Ca data and temperature (T). (C) Relationship between GR-detrended shell Sr/Ca data and BMU elongation (EL). (D) GR and EL-detrended Sr/Ca data vs T. (E) Relationship between GR and AR-detrended shell Sr/Ca data and EL. (F) GRAREL-detrended Sr/Ca data vs T. Circles denote data from the Baltic Sea experiment, while squares stand for data from the Gulf of Maine experiment. In (A, C, E), opaque symbols = median weighted for the number of specimens; translucent symbols = raw data from which medians were calculated. All regression models were fitted to the median Sr/Ca values of a given temperature regime, weighted for the number of specimens, with a natural logarithm function for GR, AR and EL, and a linear function for T (regression parameters depicted in Table 3.2).

3.4.3.4 Growth rate-detrended ultrastructural properties vs temperature

Growth rate-detrended BMU area (d_{GRAR}) data were positively correlated to water temperature in the iOSL (Fig. 3.4B and Table 3.3). 23 % of the d_{GRAR} variance in the iOSL could be significantly ($p < 0.05$) explained by water temperature (natural logarithm model) and sensitivity increased to 0.23 ± 0.08 µm^2/°C, whereas the regression model was not significant for undetrended BMU area data (Fig. 3.4B and Table 3.3). Detrending of the BMU elongation values for growth rate-related effects resulted in lower R^2 data and reduced temperature sensitivity compared to undetrended data of the iOSL (slope = 0.03 ± 0.01 per °C, $R^2 = 0.19$, $p < 0.05$; Fig. 3.4D and Table 3.3).

3.5 Discussion

The present study provided new insights into the complex relationships between shell Sr/Ca of *Arctica islandica* and water temperature and confirmed previous observations and assumptions. For example, a layer-specific chemical analysis is mandatory, because the Sr content is strongly linked to the prevailing ultrastructure and is higher in the oOSL than iOSL (HOM vs CA ultrastructure). Similar findings were reported for the ocean quahog by many previous studies (e.g., Schöne et al., 2011, 2013; Karney et al., 2012; Shirai et al., 2014). In addition, to properly identify relationships between shell Sr/Ca and temperature, a broad range of different experimental temperature conditions needs to be assessed (here: 1 to 15 °C), specifically near the optimal growth temperature of 12 to 18 °C of *A. islandica* (Witbaard et al., 1997).

Most importantly, the present study confirmed the finding by Brosset et al. (2022) according to which shell Sr/Ca of field-grown *A. islandica* contains information on water temperature (positive correlation; Fig. 3.2B, C and Table 3.2), but is also controlled by growth rate, ultrastructure and other environmental variables. However, as shown here, shell Sr/Ca values of laboratory-raised specimens provided much more robust temperature estimates than field-grown bivalves, especially after mathematical elimination of ultrastructure-related effects from Sr/Ca data (Fig. 3.2-3.5 and Table 3.2). In tangible terms, the correlation of (ultrastructure-detrended) shell Sr/Ca with water temperature was much stronger in specimens grown in laboratory tanks (up to R^2 = 0.75; this study) than in nature (R^2 = 0.26; Brosset et al., 2022). Very likely, this can be attributed to more equable growth conditions in the laboratory minimizing environmental biases.

The present work also demonstrated that transfer functions calibrated with tank specimens cannot be used to compute temperature from Sr/Ca data of field-grown *A. islandica* specimens. This is partly due to the fact that the temperature sensitivity of Sr/Ca was stronger in tank shells than in shells of specimens from the field (oOSL: 0.03 vs 0.007 mmol/mol/°C; iOSL: 0.03 vs 0.02 mmol/mol/°C). In addition, BMUs of lab-grown specimens were larger (oOSL) and more elongated (iOSL) than in wild specimens, so that transfer functions based on ultrastructure-detrended Sr/Ca data can likewise not be applied to specimens from the field.

Overall, the findings suggested that the shell Sr/Ca thermometer of ocean quahogs merely works well under artificial laboratory conditions (temperature predicted up to ± 2.6 °C in the oOSL, ± 1.0 °C in the iOSL; Fig. 3.6), but not in nature where the Sr/Ca vs temperature relationship is apparently strongly biased by environmental conditions that can hardly be quantified and corrected for. In field grown specimens, the explained variability of shell Sr/Ca is simply too low (R^2 = 0.04 and 0.30 in the oOSL and the iOSL, respectively; Fig. 3.6) and the prediction uncertainty

too large for a reliable reconstruction of water temperature (prediction interval of ± 2.1 °C and ± 2.4 °C in the iOSL and oOSL, respectively; Fig. 3.6). It is important to note that Sr/Ca values in seawater can vary temporally and regionally, particularly in coastal areas (Lebrato et al., 2020, 2021; Khare et al., 2023). Assuming a constant Sr/Ca composition of the water can introduce bias in temperature estimates from bivalve shell Sr/Ca, especially when the temperature sensitivity of shell Sr/Ca is low. This underlines the need to obtain highly resolved seasonal location-specific Sr/Ca_{water} data in future studies, particularly in regions affected by riverine influx (e.g., Khare et al., 2023).

3.5.1 Predicted and observed relationship of Sr/Ca vs temperature

The observed positive correlation between shell Sr/Ca and temperature is in agreement with both thermodynamic expectations and the lattice strain model (Gaetani and Cohen, 2006). Note that the same trend is obtained if only the data from the Baltic Sea are used (see Brosset et al., 2023). In the crystal lattice of aragonite, Sr^{2+} can substitute for Ca^{2+} due to the same charge and similar ion size (Sr^{2+} measures 1.31 Å in 9-fold coordination, Ca^{2+}1.18 Å; Shannon, 1976). This enables strontium ions to occupy the same sites as calcium ions without significantly disrupting the lattice structure. With rising temperature, the lattice distortions increase and allow for more Sr^{2+} to be incorporated, resulting in higher Sr/Ca ratios (Gaetani and Cohen, 2006). The temperature sensitivity of shell Sr/Ca was nearly identical to such expected for thermodynamic equilibrium, i.e., 0.04 mmol/mol/°C (Table 3.2; Gaetani and Cohen, 2006). This suggests that the increase in strontium partition coefficient during moderate and rapid shell growth (HOM and CA ultrastructure) was primarily governed by thermodynamic factors.

In contrast to the temperature sensitivity, significant differences were found between predicted and observed Sr/Ca levels. For example, the Sr/Ca values of the CA ultrastructure of the iOSL (1.37 ± 0.15 mmol/mol at 15 °C; Fig. 3.2B) were almost three times higher than predicted by thermodynamics and the lattice strain model (0.51 mmol/mol at 15 °C; Gaetani and Cohen, 2006). Even higher values were measured in the homogenous oOSL (1.64 ± 0.19 mmol/mol at 15 °C; Fig. 3.2B) and, in particular, in the ISP ultrastructure of annual growth lines (> 3 mmol/mol; Schöne et al., 2013, 2023), indicating that additional factors controlled the incorporation of strontium into the shell.

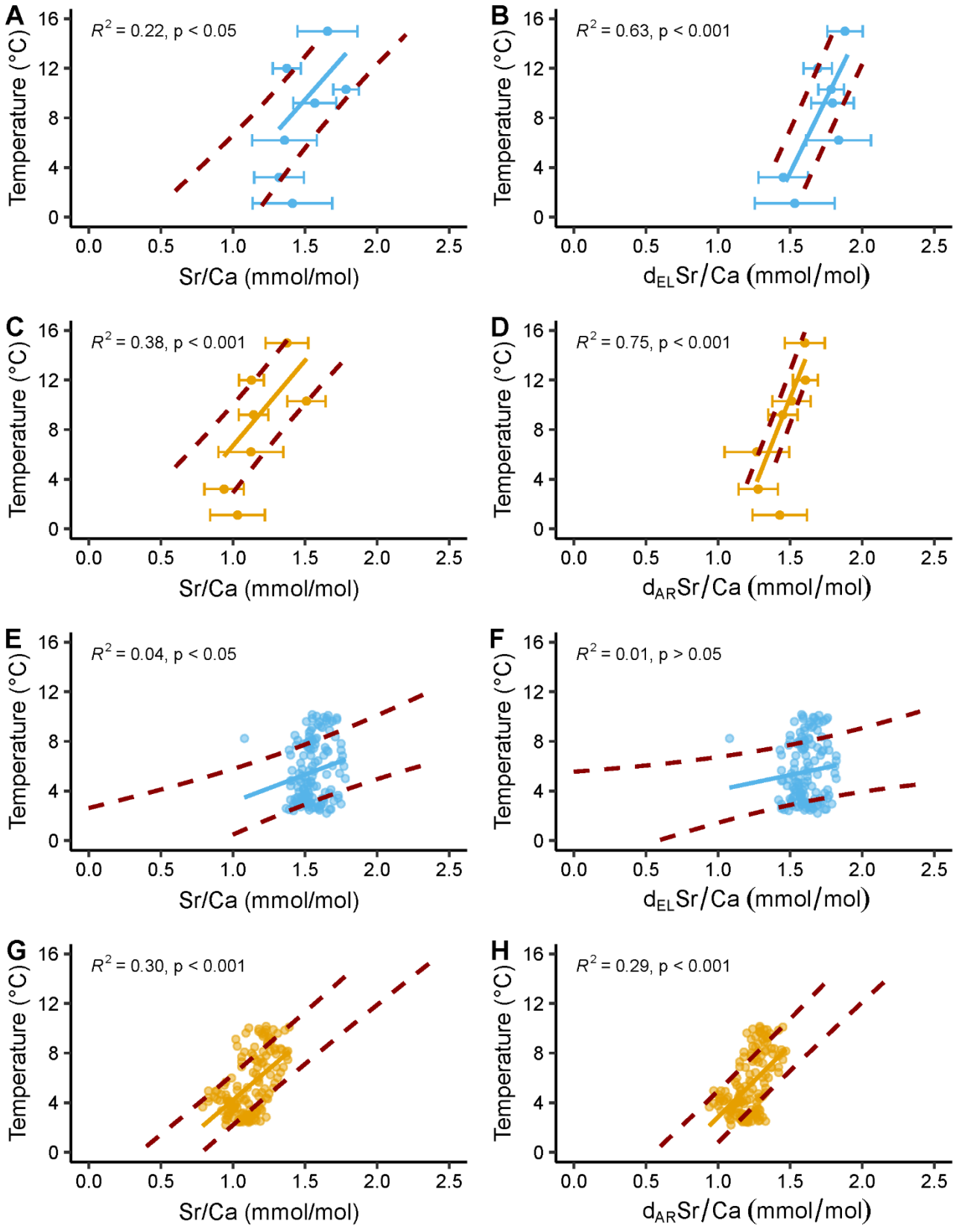

Figure 3.6 Temperature predicted from shell Sr/Ca ratios of laboratory-grown and field-grown *A. islandica* specimens. Blue and orange denote data from the outer and inner portion of the outer shell layer (oOSL, iOSL), respectively. Solid line = linear regression between predicted temperature and measured

Sr/Ca; red dashed lines = upper and lower limits of the 1σ temperature interval predicted from measured Sr/Ca data. (A-D) Data from Baltic Sea and Gulf of Maine specimens cultured at 1.1, 3.2, 6.2, 9.2, 10.3, 12 and 15 °C in laboratory tanks. Error bars = average ± 1σ. (E-H) Data from NE Iceland specimens grown in nature (Brosset et al., 2022). In (B, F) Sr/Ca data are detrended (d) for the elongation (EL) of individual biomineral units (BMUs) of the shell ultrastructure, whereas Sr/Ca data detrended for the area (AR) of the BMUs are depicted in (D, H).

As outlined in more detail in Brosset et al. (2022), the size and shape of BMUs and ultimately, the habit of aragonite crystals could have been responsible for the Sr enrichment in the studied shells. The varying strontium concentrations in the different ultrastructure types (CA < HOM < ISP) may be explained by the amount of specific crystal faces facilitating the incorporation of trace impurities, for example, due to lattice defects (e.g., Plummer and Busenberg, 1987; Paquette and Reeder, 1995; Mavromatis et al., 2022). The substitution of Ca^{2+} by compatible ions is energetically less costly in crystals with a larger number of lattice defects. Furthermore, in aragonite, much less energy is required to substitute Ca^{2+} by Sr^{2+} ions on the surface than deeper inside of the crystal (Menadakis et al., 2008). Large, exposed aragonite crystal faces thus promote the substitution of Ca^{2+} by Sr^{2+} (Menadakis et al., 2008). This may explain why the large, blocky, idiomorphic BMUs occurring at the annual growth lines contain much more strontium than xenomorphic BMUs lacking a distinct habit such as the granular HOM-BMUs of the oOSL (often irregularly shaped twinned crystallites). The highly ramified and convoluted CA-BMUs of the iOSL likely have the least developed primary crystal faces and thus come with the lowest Sr/Ca values.

An alternative or complementary explanation for the strongly varying Sr concentrations (CA < HOM < ISP) and the different relationships between Sr/Ca and temperature in the different ultrastructures (positive in HOM and CA, negative if ISP is included) may include differences in energy allocation or availability. Given that Sr/Ca values in shells of ocean quahogs remain below such observed in synthetic aragonite and above values expected for thermodynamic equilibrium, an active, energy-consumptive process seems to regulate the amount of trace impurities that end up in the shell aragonite. Such a control may be required to maintain specific mechanical properties of the shell and facilitate the formation of specific ultrastructures. It remains unclear how exactly this is achieved, e.g., by pumping undesirable ions out of the extrapallial space or by producing molecules capable to capture undesirable ions to prevent their incorporation into the shell carbonate.

It is further hypothesized that more primitive ultrastructures, i.e., ISP, are formed when less energy is available or less energy is allocated for biomineralization. In *A. islandica*, ISP ultrastructures are formed during times of strongly reduced metabolic rate during formation of annual growth lines (Schöne et al., 2023). In addition, ISP is increasingly formed during later stages of life as a result of gradually declining shell growth rate and energy-rerouting to body

maintenance and gonad production, rather than biomineralization and active control over trace impurity content of the shell. As a consequence, ISP ultrastructures are then not limited to annual growth lines, but are also produced during other times of the growing season and hence, the proportion of ISP relative to CA and HOM increases gradually through lifetime. Increasingly narrower growth bands are deposited as the bivalve ages and the actual annual growth lines may be challenging to identify. Very likely, during later stages of life, shell growth with CA and HOM formation only occurs when sufficient food is available. This would be supported by the high valve gape activity and shell growth observed in *A. islandica* specimens at high [Chl-a], i.e., during phytoplankton blooms (Ballesta-Artero et al., 2017).

It is hypothesized here that during ISP formation, similar mechanisms are at work that control the incorporation of Sr into abiogenic aragonite, i.e., surface entrapment during crystal growth (Watson, 1996, 2004; Gaetani and Cohen, 2006). At lower temperatures, the rate of crystal growth is faster than the transport of Sr^{2+} to the near-surface region of the crystal and solid solution diffusion thus limited. The chemistry of the near-surface region thus becomes 'entrapped' resulting in higher Sr/Ca values in the crystal. With increasing temperature, the solid solution diffusion rate increases and the Sr/Ca values of the forming crystal decrease gradually. This mechanism has been evoked to explain the negative correlation between Sr/Ca and temperature in synthetic aragonite (Gaetani and Cohen, 2006), and may likewise be at work during ISP formation, i.e., during times when vital effects are at minimum. In contrast, when sufficient energy is available, the bivalve exerts strong control over the amount of Sr^{2+} that substitutes for Ca^{2+} in the crystal lattice and perhaps, thermodynamic processes prevail over surface entrapment so that a positive relationship establishes between shell Sr/Ca and temperature.

The positive correlation between Sr/Ca and temperature in laboratory-grown shells further increases (up to $R^2 = 0.75$; Table 3.2), if the Sr/Ca data are mathematically corrected for ultrastructure and growth rate-related effects. According to these findings, the relationship between shell Sr/Ca and temperature in laboratory-grown *A. islandica* specimens is predominantly governed by ultrastructure properties or processes related to ultrastructure formation. However, the temperature sensitivity of Sr/Ca ratios corrected for ultrastructure and growth rate-related effects (d_{GRAR}, d_{GREL} and d_{GRAREL}Sr/Ca) exceeded predictions of the lattice strain model as well as thermodynamics and reached values of up to 0.09 ± 0.02 mmol/mol/°C (d_{GRAREL}Sr/Ca of the iOSL vs T; Table 3.2). We currently do not have a conclusive explanation for this observation.

Noteworthy, the shell growth rate of the specimens selected for this study showed highly inconsistent trends with water temperature, both between the two experiments and across the studied temperature range (Fig. 3.2A). It should be added that the mathematical elimination of

growth rate-related effects from shell Sr/Ca data barely improved the correlation between Sr and temperature (Fig. 3.3B and Table 3.2). Accordingly, for specimens grown under stable laboratory conditions selected for this study, kinetics do not seem to be the main factor regulating the incorporation of strontium into shells of *A. islandica*.

3.5.2 Sr/Ca thermometer only works in laboratory-grown *A. islandica*

As expected, tank-grown specimens formed shells with more uniform ultrastructure than wild specimens, possibly as a result of more equable, undisturbed growth conditions. For example, aside from HOM (oOSL) and CA (iOSL), no other ultrastructure type was formed under laboratory conditions after the acclimatization period. Specifically, fine-complex cross-lamellar ultrastructure was absent, which was often reported in conjunction with stressful environmental conditions (Höche et al., 2022). Likewise, no ISP was produced, which typically occurs during annual growth line formation, i.e., during times of very slow growth (Dunca et al., 2009; Schöne et al., 2011, 2013; Karney et al., 2012). Also, at a given temperature regime and within a given temperature range, BMU sizes exhibited less variability in tank-grown bivalves than specimens grown in the field (Table S3.3). Notably, BMUs in shells of tank specimens were 73 % (oOSL) to 59 % (iOSL) larger and 4 % (oOSL) to 11 % (iOSL) more needle-shaped than in shells of wild specimens (Table S3.3).

Most likely, the more uniform ultrastructure in conjunction with larger/more elongated BMUs of laboratory-grown specimens was the main reason why shell Sr/Ca was more strongly coupled with temperature than Sr/Ca of wild *A. islandica*. As illustrated by many previous studies, some element chemical properties, specifically for Sr and Mg, are strongly tied to the prevailing shell nanoarchitecture (e.g., Schöne et al., 2011, 2013; Karney et al., 2012; Shirai et al., 2014; Höche et al., 2022). Accordingly, if the shell ultrastructure properties change as the result of physiological or environmental variations (other than temperature, compare Höche et al., 2022), the relationship between shell Sr/Ca and temperature will break down. If that assumption holds true, Sr/Ca-based temperature reconstructions are limited to ocean quahogs grown under optimum conditions in laboratory tanks, unless the factors controlling ultrastructural variations in the field are known in detail and can be quantified. It may be worthwhile to study if similar observations can be made in other species.

3.5.3 Considerations on tank experiments

Although the relationship between shell Sr/Ca and temperature observed in *A. islandica* specimens grown in laboratory tanks cannot be used to reconstruct temperature from field grown specimens, such experiments can provide insights into principles behind the Sr incorporation into shells. Specifically, controlled tank experiments can help to quantify the degree to which Sr/Ca values of bivalve shells are controlled by a single environmental variable, here water temperature, while other environmental disturbances are kept at minimum. In comparison with field-grown specimens this can reveal which environmental variables mask the temperature information recorded in shell Sr/Ca. Potentially, this can lead to the development of methods capable of retaining a larger proportion of the temperature signal encoded in this element/Ca ratio of wild *A. islandica* than currently possible.

To reliably identify relationships between shell properties and temperature, tank experiments should be conducted at a broad range of different thermal regimes (not just two as in Wanamaker and Gillikin, 2019) encompassing the species-specific optimum growth temperature. This is particularly relevant if specimens exhibit large individual differences in growth rate and ultrastructure, which was the case in the GOM specimens at 10.3 °C (Fig. 3.2A, D, F). Data from the BS experiment provided a more robust insight into the temperature sensitivity of shell Sr/Ca, because specimens were exposed a broad spectrum of different temperatures ranging from 1 to 15 °C, i.e., close to the lower growth temperature threshold and overlapping with the reported optimum growth temperature range (12-18 °C; Witbaard et al., 1997). It would have been interesting to assess the extent of Sr incorporation into the shell of the GOM specimens grown below 10 °C. Such an experiment would also have revealed whether individual variations in shell properties were attributable to population specific (genotypic or epigenetic) differences or arose from ontogenetic factors such as age or size. For example, the high individual variability in growth rate observed at 10.3 °C could indicate that specimens of the GOM population exhibited a broader thermal tolerance and growth response to temperature variations (Wanamaker et al., 2019) than *A. islandica* from BS (Table 3.2).

Slightly different results on the relationship between shell properties and water temperature may also relate to the experimental designs. In the BS experiment of Witbaard et al. (1997), all bivalves were fed *ad libitum* with a known composition of algae (*Isochrysis galbana* and *Dunaliella marina*) and experienced the exact same environmental conditions, i.e, the same water chemistry and salinity (although these were not quantified), but different water temperatures. This approach (parallel experiments) allowed to study the effect of temperature on shell properties of this species (or population) but could not unravel the response of individual specimens to changes of the thermal regime. The latter was possible with the GOM experiment (serial experiment), where the same bivalves were successively exposed to different thermal

regimes. However, during the GOM experiment, food supply and salinity varied throughout the experiment (30.20 ± 0.70 at 10.3 °C; 30.70 ± 0.70 at 15 °C; Beirne et al., 2012; Wanamaker and Gillikin, 2019; food supply was not monitored), because laboratory aquaria were supplied with ambient seawater.

3.6 Summary and conclusions

As demonstrated here, shell Sr/Ca of laboratory-grown *A. islandica* specimens can be used to reconstruct water temperature with 1σ prediction uncertainty of 1°C. Shell Sr/Cr values increased with water temperature by 0.03 mmol/mol/°C which agrees with thermodynamic expectations. The explained variability was significantly higher than in field-grown specimens (Brosset et al., 2022) and attained 63 % in the oOSL (homogeneous ultrastructure) and 75 % in the iOSL (crossed-acicular ultrastructure). Most likely, the equable, less biased conditions in the laboratory resulted in the production of a more uniform shell ultrastructure (with larger and more elongated biomineral units) which in turn was associated with less variable Sr/Ca values and a stronger link to water temperature.

Transfer functions based on laboratory specimens cannot be used to compute temperature from Sr/Ca data of field-grown *A. islandica*. Firstly, this is impossible because the temperature sensitivity of Sr/Ca was stronger in tank-grown shells than in wild specimens (oOSL: 0.02 vs 0.007 mmol/mol/°C; iOSL: 0.03 vs 0.02 mmol/mol/°C). Secondly, BMUs of lab-grown specimens were larger (oOSL) and more elongated (iOSL) than in field-grown specimens, so that ultrastructure-detrending of Sr/Ca data leads to different results.

While the shell Sr/Ca thermometer of ocean quahogs works well under artificial laboratory conditions, the Sr/Ca vs temperature relationship is strongly biased by environmental conditions that can hardly be quantified and mathematically eliminated. In field-grown specimens, the explained variability of shell Sr/Ca is too low and the prediction uncertainty too large for a reliable reconstruction of water temperature.

3.7 Supplementary material

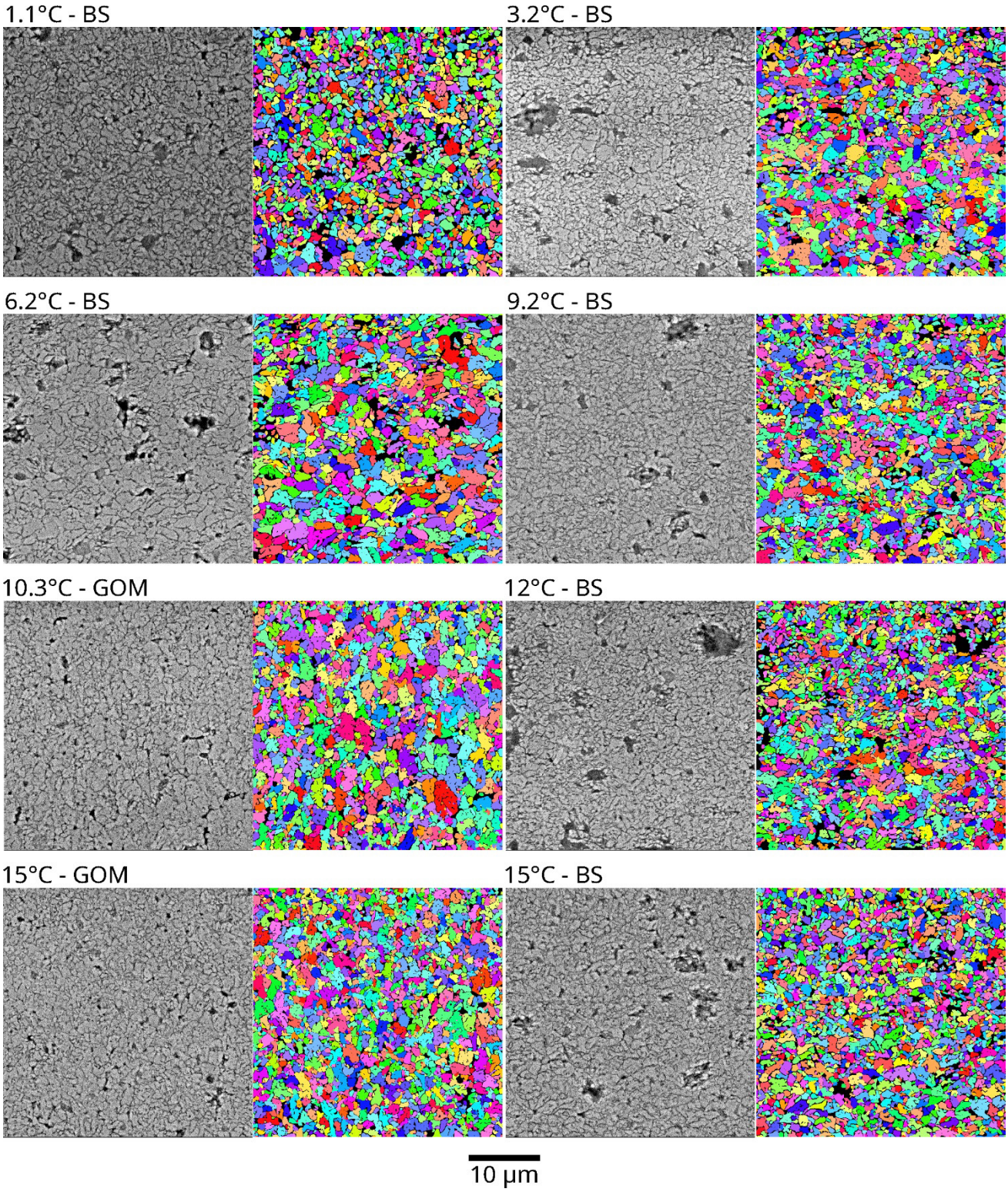

Figure S3.1 Example of SEM images taken at 7700× magnification (grayscale) and their respective segmentation (colored) for discrimination of individual biomineral units (BMUs; various colors) of the homogeneous ultrastructure from the outer portion of the outer shell layer (oOSL) of *Arctica islandica* specimens cultured at 1.1, 3.2, 6.2, 9.2, 10.3, 12 and 15 °C. For each image, the culturing temperature of the laboratory tank is given (top left corner) as well as the origin of the specimen (BS = Baltic Sea experiment; GOM = Gulf of Maine). The scale applies to all images.

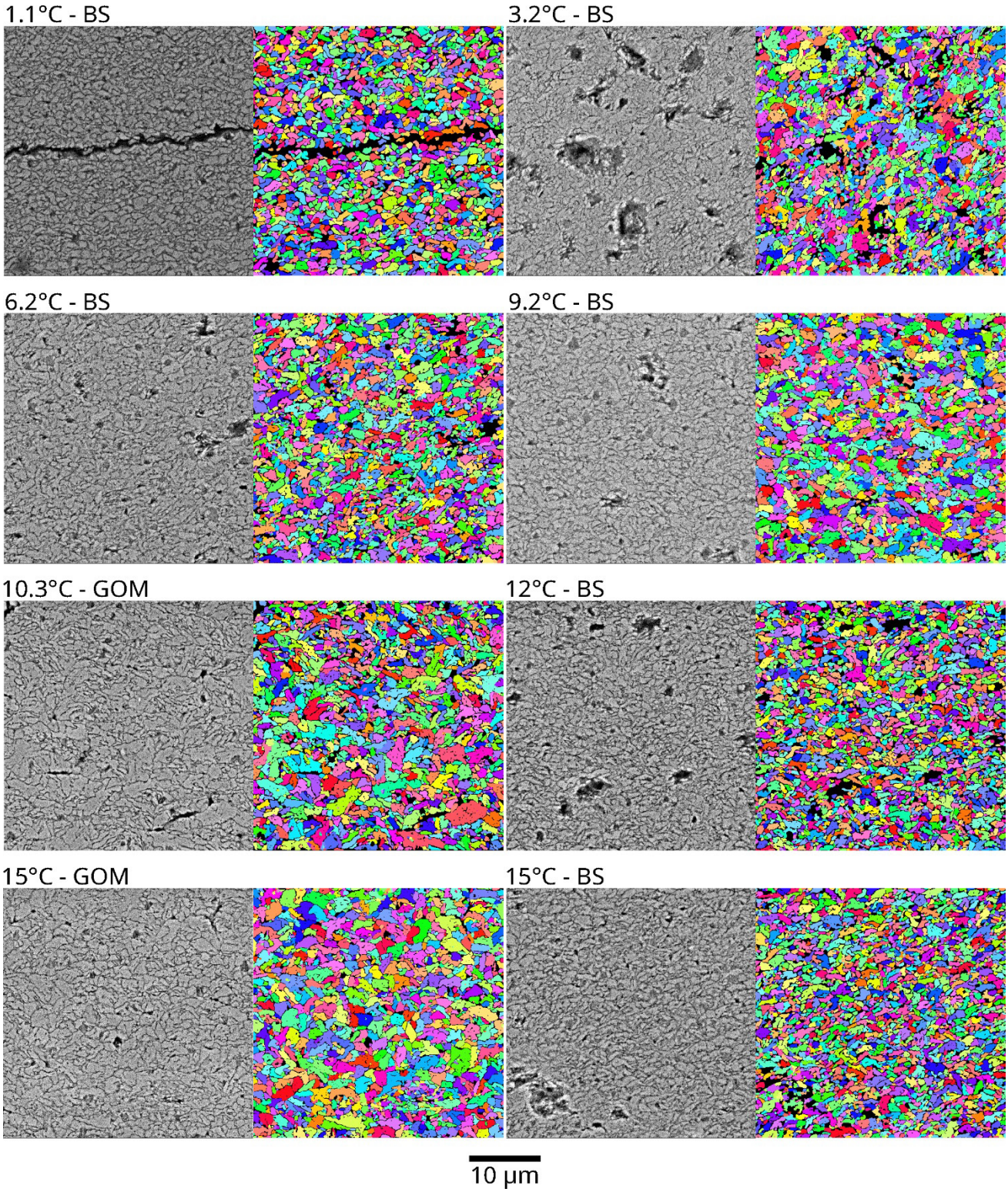

Figure S3.2 Example of SEM images taken at 7700× magnification (grayscale) and their respective segmentation (colored) for discrimination of individual biomineral units (BMUs; various colors) of the crossed-acicular ultrastructure from the outer portion of the outer shell layer (iOSL) of *Arctica islandica* specimens cultured at 1.1, 3.2, 6.2, 9.2, 10.3, 12 and 15 °C. For each image, the culturing temperature of the laboratory tank is given (top left corner) as well as the origin of the specimen (BS = Baltic Sea experiment; GOM = Gulf of Maine). The scale applies to all images.

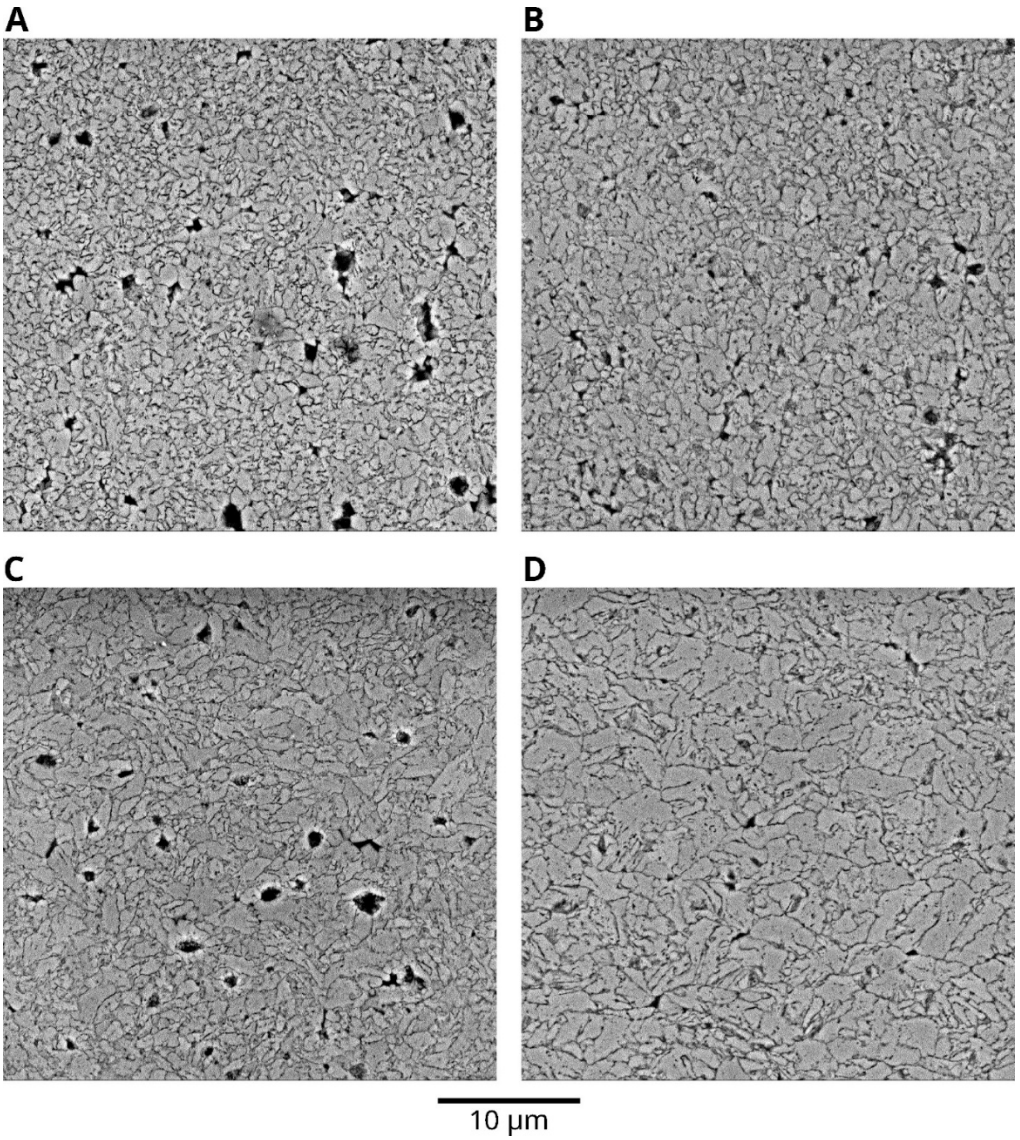

Figure S3.3 Example of SEM images taken at 7700× magnification from the outer shell layer (OSL) of field-grown (NE Iceland) and laboratory-grown specimens of *Arctica islandica*. Laboratory specimens were kept at stable ambient temperature (Baltic Sea and Gulf of Maine experiments). (A-B) SEM images of the homogeneous ultrastructure of the outer portion of the OSL (oOSL). (C-D) SEM images of the crossed-acicular ultrastructure of the inner portion of the OSL (iOSL). SEM images of the shell of field-grown specimens are depicted in A and C, while B and D illustrate the shell of specimens grown in laboratory tanks. The scale applies to all images.

Table S3.1 Quality control data for ^{88}Sr LA-ICP-MS measurements conducted on cultured shells of *Arctica islandica*. NIST SRM 610 and NIST SRM 612 were used for calibration of the ^{88}Sr concentrations of the shells. The strontium-specific relative standard deviation (RSD%) was calculated for each quality control material (QCM) from their respective preferred literature value (Longerich et al., 1996; Jochum et al., 2011, 2015). conc. = concentration.

Average calibrated ^{88}Sr conc. (µg/g)	**Average detection limit ^{88}Sr (µg/g)**	**QCM**	**Average ^{88}Sr conc. (µg/g)**	**Literature ^{88}Sr conc. (µg/g)**	**RSD%**
NIST SRM 610 515.5 ± 1	0.11 ± 0.01	BCR-2G	333.04 ± 4.87	342 ± 4	0.72
		MACS3-3	6703.12 ± 109.27	6640 ± 170	0.76
NIST SRM 612 78.4 ± 0.2		JCp-1	7150.00 ± 109.29	6890 ± 330	0.76
		JCt-1	1387.17 ± 66.39	1410 ± 50	0.76

Table S3.2 Results of Dunn tests using generalized Bonferroni-adjustment for multiple comparisons of shell properties measured in laboratory-grown *Arctica islandica* specimens. Shell Sr/Ca, the area (AR) of the biomineral units (BMUs) and the elongation of the BMUs were compared between pairs of culturing temperatures (1.1, 3.2, 6.2, 9.2, 10.3, 12 and 15 °C) and separately for the outer and inner portions of the outer shell layer (oOSL in blue and iOSL in orange, respectively). For all comparisons: ns = non-significant at $p > 0.025$, * = significant at $p < 0.025$.

Temperature regime	**1.1 °C**	**3.2 °C**	**6.2 °C**	**9.2 °C**	**10.3 °C**	**12 °C**	**15 °C**
Sr/Ca							
1.1 °C		ns	ns	ns	*	ns	*
3.2 °C	ns		ns	*	*	ns	*
6.2 °C	ns	*		*	*	ns	*
9.2 °C	ns	*	ns		*	ns	ns
10.3 °C	*	*	*	*		*	*
12 °C	ns	ns	ns	ns	*		*
15 °C	*	*	*	*	*	*	
AR							
1.1 °C		ns	*	ns	ns	ns	ns
3.2 °C	ns		*	ns	ns	ns	ns
6.2 °C	*	*		*	*	*	*
9.2 °C	ns	ns	*		ns	ns	ns
10.3 °C	*	*	*	*		ns	ns
12 °C	ns	ns	*	*	*		ns
15 °C	*	*	ns	ns	*	*	
EL							
1.1 °C		ns	*	ns	ns	ns	ns
3.2 °C	ns		*	*	ns	ns	ns
6.2 °C	*	*		*	*	ns	*
9.2 °C	*	*	ns		*	ns	ns
10.3 °C	*	ns	ns	*		*	*
12 °C	*	*	ns	ns	ns		ns
15 °C	*	*	ns	ns	ns	ns	

Table S3.3 Ultrastructure of the outer shell layer (OSL) of field-grown (NE Iceland) and laboratory-grown (Baltic Sea and Gulf of Maine experiments) *Arctica islandica* specimens. The average area (AR; μm^2) and elongation (EL) of the biomineral units and the relative variance (%) of these ultrastructural properties are given separately for the outer portion of the OSL (oOSL), dominated by homogeneous ultrastructure, and the inner portion of the OSL (iOSL), primarily composed of crossed-acicular ultrastructure.

Growth environment	Temperature	AR (μm^2)	AR relative variance (%)	EL	EL relative variance (%)
oOSL					
Field	2-10 °C	0.85 ± 0.18	21.09	1.78 ± 0.06	3.09
Laboratory tank	3.2-9.2 °C	1.47 ± 0.26	17.52	1.85 ± 0.07	3.52
iOSL					
Field	2-10°C	0.97 ± 0.19	20.18	1.77 ± 0.05	2.72
Laboratory tank	3.2-9.2°C	1.54 ± 0.27	17.72	1.96 ± 0.08	4.03

References

Adey, W. H., Steneck, R. S., 2001. Thermogeography over time creates biogeographic regions: A temperature/space/time-integrated model and an abundance-weighted test for benthic marine algae. J. Phycol. 37, 677–698.

Ballesta-Artero, I., Witbaard, R., Carroll, M. L., Van Der Meer, J., 2017. Environmental factors regulating gaping activity of the bivalve *Arctica islandica* in Northern Norway. Mar. Biol. 164, 116.

Beck, J. W., Edwards, R. L., Ito, E., Taylor, F. W., Recy, J., Rougerie, F., Joannot, P., Henin, C., 1992. Sea-surface temperature from coral skeletal strontium/calcium ratios. Science 257, 644–647.

Begum, S., Basova, L., Heilmayer, O., Philipp, E. E. R., Abele, D., Brey, T., 2010. Growth and energy budget models of the bivalve *Arctica islandica* at six different sites in the Northeast Atlantic realm. J. Shellfish Res. 29, 107–115.

Beirne, E. C., Wanamaker, A. D., Feindel, S. C., 2012. Experimental validation of environmental controls on the $\delta^{13}C$ of *Arctica islandica* (ocean quahog) shell carbonate. Geochim. Cosmochim. Acta 84, 395–409.

Belanger, C. L., Jablonski, D., Roy, K., Berke, S. K., Krug, A. Z., Valentine, J. W., 2012. Global environmental predictors of benthic marine biogeographic structure. Proc. Natl. Acad. Sci. U.S.A. 109, 14046–14051.

Berg, S., Kutra, D., Kroeger, T., Straehle, C. N., Kausler, B. X., Haubold, C., Schiegg, M., Ales, J., Beier, T., Rudy, M., Eren, K., Cervantes, J. I., Xu, B., Beuttenmueller, F., Wolny, A., Zhang, C., Koethe, U., Hamprecht, F. A., Kreshuk, A., 2019. ilastik: Interactive machine learning for (bio)image analysis. Nat. Methods 16, 1226–1232.

Black, B. A., Griffin, D., van der Sleen, P., Wanamaker, A. D., Speer, J. H., Frank, D. C., Stahle, D. W., Pederson, N., Copenheaver, C. A., Trouet, V., Griffin, S., Gillanders, B. M., 2016. The value of crossdating to retain high-frequency variability, climate signals, and extreme events in environmental proxies. Glob. Change Biol. 22, 2582–2595.

Bogovic, J. A., Hanslovsky, P., Wong, A., Saalfeld, S., 2016. Robust registration of calcium images by learned contrast synthesis. In: 2016 IEEE 13th International Symposium on Biomedical Imaging (ISBI). Prague, Czech Republic: IEEE, 1123–1126.

Brosset, C., Höche, N., Shirai, K., Nishida, K., Mertz-Kraus, R., Schöne, B. R., 2022. Strong coupling between biomineral morphology and Sr/Ca of *Arctica islandica* (Bivalvia) – Implications for shell Sr/Ca-based temperature estimates. Minerals 12, 500.

Brosset, C., Höche, N., Witbaard, R., Nishida, K., Shirai, K., Mertz-Kraus, R., Schöne, B. R., 2023. Data for "Sr/Ca in shells of laboratory-grown bivalves (*Arctica islandica*) serves as a proxy for water temperature – Perspectives for (paleo)environmental research?"

Butler, P. G., Wanamaker, A. D., Scourse, J. D., Richardson, C. A., Reynolds, D. J., 2013. Variability of marine climate on the North Icelandic Shelf in a 1357-year proxy archive based on

growth increments in the bivalve *Arctica islandica*. Palaeogeogr. Palaeoclimatol. Palaeoecol. 373, 141–151.

Cauquoin, A., Werner, M., Lohmann, G., 2019. Water isotopes – climate relationships for the mid-Holocene and preindustrial period simulated with an isotope-enabled version of MPI-ESM. Clim. Past 15, 1913–1937.

Cooper, R. N., Houghton, J. T., McCarthy, J. J., Metz, B., 2002. Climate Change 2001: The Scientific Basis. Foreign Affairs 81, 208.

Corrège, T., 2006. Sea surface temperature and salinity reconstruction from coral geochemical tracers. Palaeogeogr. Palaeoclimatol. Palaeoecol. 232, 408–428.

De Winter, N. J., Witbaard, R., Kocken, I. J., Müller, I. A., Guo, J., Goudsmit, B., Ziegler, M., 2022. Temperature dependence of clumped isotopes (Δ_{47}) in aragonite. Geophys. Res. Lett 49, 1–12.

Dodd, J. R., Crisp, E. L., 1982. Non-linear variation with salinity of Sr/Ca and Mg/Ca ratios in water and aragonitic bivalve shells and implications for paleosalinity studies. Palaeogeogr. Palaeoclimatol. Palaeoecol. 38, 45–56.

Dodd, J. R., 1965. Environmental control of strontium and magnesium in *Mytilus*. Geochim. Cosmochim. Acta 29, 385–398.

Dunca, E., Mutvei, H., Göransson, P., Mörth, C.-M., Schöne, B. R., Whitehouse, M. J., Elfman, M., Baden, S. P., 2009. Using ocean quahog (*Arctica islandica*) shells to reconstruct palaeoenvironment in Öresund, Kattegat and Skagerrak, Sweden. Int. J. Earth Sci. 98, 3–17.

Eiler, J. M., 2011. Paleoclimate reconstruction using carbonate clumped isotope thermometry. Quat. Sci. Rev. 30, 3575–3588.

Foster, L. C., Allison, N., Finch, A. A., Andersson, C., 2009. Strontium distribution in the shell of the aragonite bivalve *Arctica islandica*. Geochem. Geophys. Geosyst. 10, 1–14.

Freitas, P., Clarke, L. J., Kennedy, H., Richardson, C., Abrantes, F., 2005. Mg/Ca, Sr/Ca, and stable-isotope (δ^{18}O and δ^{13}C) ratio profiles from the fan mussel *Pinna nobilis*: Seasonal records and temperature relationships. Geochem. Geophys. Geosyst. 6, 1–16.

Füllenbach, C. S., Schöne, B. R., Shirai, K., Takahata, N., Ishida, A., Sano, Y., 2017. Minute co-variations of Sr/Ca ratios and microstructures in the aragonitic shell of *Cerastoderma edule* (Bivalvia) – Are geochemical variations at the ultra-scale masking potential environmental signals? Geochim. Cosmochim. Acta 205, 256–271.

Gaetani, G. A., Cohen, A. L., 2006. Element partitioning during precipitation of aragonite from seawater: A framework for understanding paleoproxies. Geochim. Cosmochim. Acta 70, 4617–4634.

Gillikin, D. P., De Ridder, F., Ulens, H., Elskens, M., Keppens, E., Baeyens, W., Dehairs, F., 2005. Assessing the reproducibility and reliability of estuarine bivalve shells (*Saxidomus giganteus*) for sea surface temperature reconstruction: Implications for paleoclimate studies. Palaeogeogr. Palaeoclimatol. Palaeoecol. 228, 70–85.

Goberville, E., Beaugrand, G., Sautour, B., Tréguer, P., Somlit, T., 2010. Climate-driven changes in coastal marine systems of western Europe. Mar. Ecol. Prog. Ser. 408, 129–147.

Hart, S. R., Blusztajn, J., 1998. Clams as recorders of ocean ridge volcanism and hydrothermal vent field activity. Science 280, 883–886.

Höche, N., Walliser, E. O., de Winter, N. J., Witbaard, R., Schöne, B. R., 2021. Temperature-induced microstructural changes in shells of laboratory-grown *Arctica islandica* (Bivalvia). PLoS ONE 16, e0247968.

Höche, N., Walliser, E. O., Schöne, B. R., 2022. Microstructural mapping of *Arctica islandica* shells reveals environmental and physiological controls on biomineral size. Front. Earth Sci. 9, 781305.

Jochum, K. P., Nohl, U., Herwig, K., Lammel, E., Stoll, B., Hofmann, A. W., 2005. GeoReM: A new geochemical database for reference materials and isotopic standards. Geostand. Geoanalyt. Res. 29, 333–338.

Jochum, K. P., Weis, U., Stoll, B., Kuzmin, D., Yang, Q., Raczek, I., Jacob, D. E., Stracke, A., Birbaum, K., Frick, D. A., Günther, D., Enzweiler, J., 2011. Determination of Reference Values for NIST SRM 610-617 Glasses Following ISO Guidelines. Geostand. Geoanal. Res. 35, 397–429.

Jochum, K. P., Scholz, D., Stoll, B., Weis, U., Wilson, S. A., Yang, Q., Schwalb, A., Börner, N., Jacob, D. E., Andreae, M. O., 2012. Accurate trace element analysis of speleothems and biogenic calcium carbonates by LA-ICP-MS. Chem. Geol. 318–319, 31–44.

Jones, D. S., 1981. Annual growth increments in shells of *Spisula solidissima* record marine temperature variability. Science 211, 165–167.

Karney, G. B., Butler, P. G., Speller, S., Scourse, J. D., Richardson, C. A., Schröder, M., Hughes, G. M., Czernuszka, J. T., Grovenor, C. R. M., 2012. Characterizing the microstructure of *Arctica islandica* shells using NanoSIMS and EBSD. Geochem. Geophys. Geosyst. 13, Q04002.

Khare, A., Hughes, H. P., Schijf, J., Kilbourne, K. H., 2023. Apparently seasonal variations of the seawater Sr/Ca ratio across the Florida Keys Reef Tract. Geochem. Geophys. Geosyst. 24, e2022GC010728.

Lebrato, M., Garbe-Schönberg, D., Müller, M. N., Blanco-Ameijeiras, S., Feely, R. A., Lorenzoni, L., Molinero, J.-C., Bremer, K., Jones, D. O. B., Iglesias-Rodriguez, D., Greeley, D., Lamare, M. D., Paulmier, A., Graco, M., Cartes, J., Barcelos E Ramos, J., De Lara, A., Sanchez-Leal, R., Jimenez, P., Paparazzo, F. E., Hartman, S. E., Westernströer, U., Küter, M., Benavides, R., Da Silva, A. F., Bell, S., Payne, C., Olafsdottir, S., Robinson, K., Jantunen, L. M., Korablev, A., Webster, R. J., Jones, E. M., Gilg, O., Bailly Du Bois, P., Beldowski, J., Ashjian, C., Yahia, N. D., Twining, B., Chen, X.-G., Tseng, L.-C., Hwang, J.-S., Dahms, H.-U., Oschlies, A., 2020. Global variability in seawater Mg:Ca and Sr:Ca ratios in the modern ocean. Proc. Natl. Acad. Sci. U.S.A. 117, 22281–22292.

Lebrato, M., Garbe-Schönberg, D., Müller, M. N., Blanco-Ameijeiras, S., Feely, R. A., Lorenzoni, L., Molinero, J.-C., Bremer, K., Jones, D. O. B., Iglesias-Rodriguez, D., Greeley, D., Lamare, M. D., Paulmier, A., Graco, M., Cartes, J., Barcelos E Ramos, J., De Lara, A., Sanchez-Leal, R., Jimenez, P., Paparazzo, F. E., Hartman, S. E., Westernströer, U., Küter, M., Benavides,

R., Da Silva, A. F., Bell, S., Payne, C., Olafsdottir, S., Robinson, K., Jantunen, L. M., Korablev, A., Webster, R. J., Jones, E. M., Gilg, O., Bailly Du Bois, P., Beldowski, J., Ashjian, C., Yahia, N. D., Twining, B., Chen, X.-G., Tseng, L.-C., Hwang, J.-S., Dahms, H.-U., Oschlies, A., 2021. Correction for Lebrato et al., Global variability in seawater Mg:Ca and Sr:Ca ratios in the modern ocean. Proc. Natl. Acad. Sci. U.S.A. 118, e2119099118.

Lohmann, G., Schöne, B. R., 2013. Climate signatures on decadal to interdecadal time scales as obtained from mollusk shells (*Arctica islandica*) from Iceland. Palaeogeogr. Palaeoclimatol. Palaeoecol. 373, 152–162.

Longerich, H. P., Jackson, S. E., Günther, D., 1996. Laser ablation inductively coupled plasma mass spectrometric transient signal data acquisition and analyte concentration calculation. J. Anal. At. Spectrom. 11, 899–904.

Marali, S., Schöne, B. R., Mertz-Kraus, R., Griffin, S. M., Wanamaker, A. D., Butler, P. G., Holland, H. A., Jochum, K. P., 2017. Reproducibility of trace element time-series (Na/Ca, Mg/Ca, Mn/Ca, Sr/Ca, and Ba/Ca) within and between specimens of the bivalve *Arctica islandica* – A LA-ICP-MS line scan study. Palaeogeogr. Palaeoclimatol. Palaeoecol. 484, 109–128.

Mavromatis, V., Brazier, J.-M., Goetschl, K. E., 2022. Controls of temperature and mineral growth rate on Mg incorporation in aragonite. Geochim. Cosmochim. Acta 317, 53–64.

Menadakis, M., Maroulis, G., Koutsoukos, P. G., 2008. Incorporation of Mg^{2+}, Sr^{2+}, Ba^{2+} and Zn^{2+} into aragonite and comparison with calcite. J. Math. Chem. 46, 484–491.

Paquette, J., Reeder, R. J., 1995. Relationship between surface structure, growth mechanism, and trace element incorporation in calcite. Geochim. Cosmochim. Acta 59, 735–749.

Plummer, L. N., Busenberg, E., 1987. Thermodynamics of aragonite-strontianite solid solutions: Results from stoichiometric solubility at 25 and 76°C. Geochim. Cosmochim. Acta 51, 1393–1411.

Roger, L. M., George, A. D., Shaw, J., Hart, R. D., Roberts, M., Becker, T., McDonald, B. J., Evans, N. J., 2017. Geochemical and microstructural characterisation of two species of cool-water bivalves (*Fulvia tenuicostata* and *Soletellina biradiata*) from Western Australia. Biogeosciences 14, 1721–1737.

Ropes, J. H., 1984. Procedures for preparing acetate peels and evidence validating the annual periodicity of growth lines formed in the shells of ocean quahogs, *Arctica islandica*. Mar. Fish. Rev. 46, 27–35.

Rosenheim, B. E., Swart, P. K., Thorrold, S. R., Willenz, P., Berry, L., Latkoczy, C., 2004. High-resolution Sr/Ca records in sclerosponges calibrated to temperature in situ. Geology 32, 145.

Schindelin, J., Arganda-Carreras, I., Frise, E., Kaynig, V., Longair, M., Pietzsch, T., Preibisch, S., Rueden, C., Saalfeld, S., Schmid, B., Tinevez, J.-Y., White, D. J., Hartenstein, V., Eliceiri, K., Tomancak, P., Cardona, A., 2012. Fiji: An open-source platform for biological-image analysis. Nat. Methods 9, 676–682.

Schmidt, G. A., Annan, J. D., Bartlein, P. J., Cook, B. I., Guilyardi, E., Hargreaves, J. C., Harrison, S. P., Kageyama, M., LeGrande, A. N., Konecky, B., Lovejoy, S., Mann, M. E., Masson-

Delmotte, V., Risi, C., Thompson, D., Timmermann, A., Tremblay, L.-B., Yiou, P., 2014. Using palaeo-climate comparisons to constrain future projections in CMIP5. Clim. Past 10, 221–250.

Schöne, B. R., Fiebig, J., Pfeiffer, M., Gleβ, R., Hickson, J., Johnson, A. L. A., Dreyer, W., Oschmann, W., 2005. Climate records from a bivalved Methuselah (*Arctica islandica*, Mollusca; Iceland). Palaeogeogr. Palaeoclimatol. Palaeoecol. 228, 130–148.

Schöne, B. R., Zhang, Z., Radermacher, P., Thébault, J., Jacob, D. E., Nunn, E. V., Maurer, A.-F., 2011. Sr/Ca and Mg/Ca ratios of ontogenetically old, long-lived bivalve shells (*Arctica islandica*) and their function as paleotemperature proxies. Palaeogeogr. Palaeoclimatol. Palaeoecol. 302, 52–64.

Schöne, B. R., Radermacher, P., Zhang, Z., Jacob, D. E., 2013. Crystal fabrics and element impurities (Sr/Ca, Mg/Ca, and Ba/Ca) in shells of *Arctica islandica* – Implications for paleoclimate reconstructions. Palaeogeogr. Palaeoclimatol. Palaeoecol. 373, 50–59.

Schöne, B. R., Krause, R. A., 2016. Retrospective environmental biomonitoring – Mussel Watch expanded. Glob. Planet. Change 144, 228–251.

Schöne, B. R., Marali, S., Jantschke, A., Mertz-Kraus, R., Butler, P. G., Fröhlich, L., 2023. Can element chemical impurities in aragonitic shells of marine bivalves serve as proxies for environmental variability? Chem. Geol. 616, 121215.

Shannon, R. D., 1976. Revised effective ionic radii and systematic studies of interatomic distances in halides and chalcogenides. Acta Crystallogr. A 32, 751–767.

Shirai, K., Takahata, N., Yamamoto, H., Omata, T., Sasaki, T., Sano, Y., 2008. Novel analytical approach to bivalve shell biogeochemistry: A case study of hydrothermal mussel shell. Geochem. J. 42, 413–420.

Shirai, K., Schöne, B. R., Miyaji, T., Radarmacher, P., Krause, R. A., Tanabe, K., 2014. Assessment of the mechanism of elemental incorporation into bivalve shells (*Arctica islandica*) based on elemental distribution at the microstructural scale. Geochim. Cosmochim. Acta 126, 307–320.

Stecher, H. A., Krantz, D. E., Lord, C. J., Luther, G. W., Bock, K. W., 1996. Profiles of strontium and barium in *Mercenaria mercenaria* and *Spisula solidissima* shells. Geochim. Cosmochim. Acta 60, 3445–3456.

Surge, D., Walker, K. J., 2006. Geochemical variation in microstructural shell layers of the southern quahog (*Mercenaria campechiensis*): Implications for reconstructing seasonality. Palaeogeogr. Palaeoclimatol. Palaeoecol. 237, 182–190.

Toland, H., Perkins, B., Pearce, N., Keenan, F., Leng, M. J., 2000. A study of sclerochronology by laser ablation ICP-MS. J. Anal. At. Spectrom. 15, 1143–1148.

Tynan, S., Opdyke, B. N., Walczak, M., Eggins, S., Dutton, A., 2017. Assessment of Mg/Ca in *Saccostrea glomerata* (the Sydney rock oyster) shell as a potential temperature record. Palaeogeogr. Palaeoclimatol. Palaeoecol. 484, 79–88.

van der Walt, S., Schönberger, J. L., Nunez-Iglesias, J., Boulogne, F., Warner, J. D., Yager, N., Gouillart, E., Yu, T., 2014. scikit-image: Image processing in Python. PeerJ 2, e453.

Wanamaker, A. D., Kreutz, K. J., Wilson, T., Borns Jr, H. W., Introne, D. S., Feindel, S., 2008a. Experimentally determined Mg/Ca and Sr/Ca ratios in juvenile bivalve calcite for *Mytilus edulis*: Implications for paleotemperature reconstructions. Geo-Mar. Lett. 28, 359–368.

Wanamaker, A. D., Heinemeier, J., Scourse, J. D., Richardson, C. A., Butler, P. G., Eiríksson, J., Knudsen, K. L., 2008b. Very long-lived mollusks confirm 17th century AD tephra-based radiocarbon reservoir ages for north Icelandic shelf waters. Radiocarbon 50, 399–412.

Wanamaker, A. D., Butler, P. G., Scourse, J. D., Heinemeier, J., Eiríksson, J., Knudsen, K. L., Richardson, C. A., 2012. Surface changes in the North Atlantic meridional overturning circulation during the last millennium. Nat. Commun. 3, 1–7.

Wanamaker, A. D., Griffin, S. M., Ummenhofer, C. C., Whitney, N. M., Black, B., Parfitt, R., Lower-Spies, E. E., Introne, D., Kreutz, K. J., 2019. Pacific climate influences on ocean conditions and extreme shell growth events in the Northwestern Atlantic (Gulf of Maine). Clim. Dyn. 52, 6339–6356.

Wanamaker, A. D., Gillikin, D. P., 2019. Strontium, magnesium, and barium incorporation in aragonitic shells of juvenile *Arctica islandica*: Insights from temperature controlled experiments. Chem. Geol. 526, 117–129.

Watson, E. B., 1996. Surface enrichment and trace-element uptake during crystal growth. Geochim. Cosmochim. Acta 60, 5013–5020.

Watson, E. B., 2004. A conceptual model for near-surface kinetic controls on the trace-element and stable isotope composition of abiogenic calcite crystals. Geochim. Cosmochim. Acta 68, 1473–1488.

Węsławski, J. M., Kendall, M. A., Włodarska-Kowalczuk, M., Iken, K., Kędra, M., Legezynska, J., Sejr, M. K., 2011. Climate change effects on Arctic fjord and coastal macrobenthic diversity – Observations and predictions. Mar. Biodivers. 41, 71–85.

Witbaard, R., Jenness, M. I., Van Der Borg, K., Ganssen, G., 1994. Verification of annual growth increments in *Arctica islandica* L. from the North Sea by means of oxygen and carbon isotopes. J. Sea Res. 33, 91–101.

Witbaard, R., Franken, R., Visser, B., 1997. Growth of juvenile *Arctica islandica* under experimental conditions. Helgoländer Meeresunters. 51, 417–431.

Yan, H., Shao, D., Wang, Y., Sun, L., 2013. Sr/Ca profile of long-lived *Tridacna gigas* bivalves from South China Sea: A new high-resolution SST proxy. Geochim. Cosmochim. Acta 112, 52–65.

Zacherl, D., Gaines, S. D., Lonhart, S. I., 2003. The limits to biogeographical distributions: insights from the northward range extension of the marine snail, *Kelletia kelletii* (Forbes, 1852): Northward range extension of *Kelletia kelletii*. J. Biogeogr. 30, 913–924.

Zhao, L., Schöne, B. R., Mertz-Kraus, R., 2017. Controls on strontium and barium incorporation into freshwater bivalve shells (*Corbicula fluminea*). Palaeogeogr. Palaeoclimatol. Palaeoecol. 465, 386–394.

4 Integrating high-resolution Sr/Ca and ultrastructural analyses of the *Tridacna squamosa* shell to reconstruct sub-daily seawater temperature variation

Cornélia BROSSET[1], Chengcheng LIU[2], Haotian YANG[2], Hong YAN[2], Bernd R. SCHÖNE[1]

[1]*Institute of Geosciences, University of Mainz, Mainz, Germany*

[2]*State Key Laboratory of Loess and Quaternary Geology, Institute of Earth Environment, Chinese Academy of Sciences, Xi'an, China*

Brosset, C., Liu, C., Yang, H., Yan, H., Schöne, B. R., 2025. Integrating high-resolution Sr/Ca and ultrastructural analyses of the *Tridacna squamosa* shell to reconstruct sub-daily seawater temperature variation. *Palaeogeogr. Palaeoclimatol. Palaeoecol.* 659, 112663.

In this chapter, the potential use of shell Sr/Ca for sub-daily temperature reconstruction was examined in *Tridacna squamosa* through high-resolution analyses of distinct growth features. Sr/Ca values in daily growth increments increased with temperature, although the resulting Sr/Ca-thermometer lacked robustness. Shell Sr/Ca also exhibited consistent daily patterns independent of ultrastructural variation, suggesting common underlying drivers rather than direct coupling. This manuscript was published in the journal "*Palaeogeography, Palaeoclimatology, Palaeoecology*". I contributed to the conceptualization, data curation, formal analysis, investigation, methodology, validation, visualization, writing – original draft and writing – review and editing of the manuscript. This work was supported by the Sino-German Center for Research Promotion grant [M-0163] to BRS and HYan, the German Research Foundation (DFG) grant [SCHO793/23] to BRS and the National Natural Science Foundation of China (NSFC) grant [42103084] to CL and HYan.

Author contributions:

CB	Conceptualization, Data curation, Formal analysis, Investigation, Methodology, Validation, Visualization, Writing - original draft, Writing - review & editing.
CL	Funding acquisition, Resources, Writing - review & editing.
HYang	Resources, Writing - review & editing.
HYan	Funding acquisition, Project administration, Resources, Writing - review & editing.
BRS	Conceptualization, Funding acquisition, Investigation, Project administration, Resources, Supervision, Validation, Writing - original draft, Writing - review & editing.

4.1 Abstract

Modern and fossil bivalves record environmental variability in their shells in the form of chemical and ultrastructural properties as well as changes in growth rate. These proxy data can be placed in precise temporal context based on growth pattern analysis. Some species such as tridacnids grow particularly fast providing unique insights into environmental changes on the time scale of weather which opens new opportunities for paleoclimate research. Here, we assessed the potential use of the fluted giant clam (*Tridacna squamosa*) to reconstruct sub-daily sea surface temperature (SST) fluctuations from shell Sr/Ca ratios. Through a combined µm-scale analysis of shell Sr/Ca (NanoSIMS) and ultrastructure (SEM) it was possible to study shell material produced during daytime (growth increments) and nighttime (growth lines) separately. Unlike coarser resolution chemical analysis (LA-ICP-MS and ICP-OES), this approach revealed a significant positive correlation between SST and Sr/Ca during daytime ($R^2 = 0.36$, $p < 0.001$). The correlation further increased when the NanoSIMS data of several consecutive daily increments were combined to match the sampling resolution of LA-ICP-MS and ICP-OES data, i.e., four days to two weeks (R^2 of up to 0.86, $p < 0.001$). With an uncertainty of at least ± 1.5 °C, the applicability of the Sr/Ca thermometer remains limited considering that *T. squamosa* only occurs in ecosystems with minimal seasonal temperature amplitudes. Consistent daily Sr/Ca cycles were observed with local maxima at growth lines. This cyclic pattern was found even when the ultrastructure morphology varied or when the complex crossed-lamellar ultrastructure of the shell deviated from its typical configuration during extreme weather events. Therefore, Sr/Ca is likely not directly linked to the shell ultrastructure, but instead both properties are driven by underlying physiological factors.

4.2 Introduction

Bivalves record environmental variability in their shells in the form of chemical and structural properties (Peharda et al., 2021). These data can be accurately aligned in time by means of growth pattern analysis, specifically if the date of death is known (Jones, 1981; Fritz and Haven, 1983; Chauvaud et al., 1998; Clark, 2005). Shells of long-lived, slow-growing species can provide unique insights into the climatic history of aquatic ecosystems and inform about environmental changes on time-scales of decades to centuries and possibly beyond (Jones, 1980, 1981; Weidman et al., 1994; Marchitto et al., 2000; Schöne et al., 2005, 2020; Butler et al., 2013; Reynolds et al., 2016; Tanabe et al., 2017). Environmental data on the time-scale of seasons and weather, on the other hand, can be obtained from either shorter-lived species (Carré et al., 2013; Jolivet et al., 2015; Füllenbach et al., 2015) or juvenile shell portions of long-lived bivalves (Yan et al., 2013; 2015; 2020), because both grow rapidly enough to enable the reconstruction of changes on time-scales of days or even hours.

Tridacnids, also known as giant clams, belong to the latter category. They inhabit shallow waters in the sub/tropical Indo-Pacific since ca. 55 million years (Rosewater, 1965). These bivalves are renowned for their long lifespan (up to 100 years) (Rosewater, 1965), large size (of up to 1 m in length) (Rosewater, 1965) and rapid biomineralization during youth with growth rates of several cm per year (Lucas et al., 1989; Van Wynsberge et al., 2017). During the first years of life, they lay down distinct daily growth bands (Aharon and Chappell, 1986; Pätzold et al., 1991; Watanabe and Oba, 1999; Hori et al., 2015; Yan, 2020; Arndt et al., 2023) consisting of couplets of a growth line (formed during the night) and a growth increment (formed during the day). Due to their autofluorescence, the daily growth lines can be studied most effectively by means of Laser Scanning Confocal Microscopy (LSCM) (Liu et al., 2022) and provide a means to date each shell portion to the nearest day. As in other bivalve species, the most critical and hotly debated aspect is how specific environmental variables can be quantitatively reconstructed from the shells (Peharda et al., 2021), in particular the most relevant climate parameter, water temperature. While this is traditionally accomplished with shell oxygen isotope ($\delta^{18}O$) values (Epstein et al., 1953; Mook and Vogel, 1968; Aharon, 1983; Watanabe and Oba, 1999), in settings with seasonally fluctuating $\delta^{18}O_{water}$ values (and salinity to which $\delta^{18}O_{water}$ is linearly correlated), it would be advantageous to verify temperature estimates with another proxy or use both in combination to infer past temperature and salinity data. Shell Sr/Ca has made it on the shortlist, because this ratio works well in many scleractinian corals (Beck et al., 1992; Corrège, 2006) and abiogenic aragonite (Gaetani and Cohen, 2006). In addition, Sr/Ca_{water} (other than $\delta^{18}O_{water}$) is considered relatively stable above a salinity of 10 (Dodd and Crisp, 1982) and can thus be neglected in respective paleothermometry equations. However, in bivalves including tridacnids the use of Sr/Ca as a temperature indicator is controversially debated. While in some studies a negative

correlation between shell Sr/Ca of giant clams and the seasonal temperature variation was reported (Sano et al., 2012; Yan et al., 2013; Liu et al., 2021), other authors found the opposite (Arias-Ruiz et al., 2017; Liu et al., 2021). As tridacnids host photosymbionts in their tissue which supply the bivalve with energy to regulate physiological processes (Bonham, 1965; Rosewater, 1965; Klumpp and Lucas, 1994; Griffiths and Klumpp, 1996), shell Sr/Ca fluctuations on both daily and seasonal time-scales have been linked to photosynthetic efficiency and insolation (Sano et al., 2012). Still others explained the diurnal Sr/Ca changes by physiological processes related to circadian biological rhythms (Warter et al., 2018).

Physiological processes not only influence the shell element chemical content (Lorens and Bender, 1977; Ballesta-Artero et al., 2017; Barrat et al., 2023), but also ultrastructural patterns (Ballesta-Artero et al., 2017; Höche et al., 2022). As a result, a mathematical correlation may be found between these two properties (Lazareth et al., 2013; DeWinter et al., 2021; Brosset et al., 2022, 2023). For example, higher Sr concentrations are typically measured in growth lines (reflecting times of reduced shell growth) rather than growth increments (reflecting periods of fast growth and thus the main growing portion of each day) (Foster et al., 2009; Schöne et al., 2011, 2013; Shirai et al., 2014; Füllenbach et al., 2017). The former often consists of irregular simple/spherulitic prismatic ultrastructure, whereas the latter is ultrastructurally more complex (Schöne et al., 2013). In tridacnids, shell Sr/Ca profiles also exhibit local peaks at daily growth lines (Sano et al., 2012; Warter and Müller, 2017; Warter et al., 2018; Yan et al., 2020), which likewise consist of irregular prisms. Lower Sr/Ca values, however, are observed in the daily growth increments, which are primarily composed of a complex crossed-lamellar (CCL) ultrastructure (Agbaje et al., 2017; Mills et al., 2024a). Such ultrastructural variability supposedly biases temperature reconstructions based on shell Sr/Ca. As demonstrated recently by Brosset et al. (2023), Sr/Ca values of laboratory-grown bivalve shells revealed stronger positive correlations with temperature than such formed in the field. Furthermore, in tridacnid shells, ultrastructural changes correlate with Sr/Ca (Mills et al., 2024b), likely due to environmental stress. Following these authors, shells of *Tridacna squamosa* grown in turbid waters contained CCL ultrastructure covered by prisms (CCL-P configuration). Sr/Ca ratios in CCL-P were lower than in the typical shell ultrastructure (CCL-I configuration, without prisms) formed in clearer waters. Therefore, a detailed understanding of the link between shell strontium content and ultrastructure may be crucial to accurately interpret Sr/Ca data from tridacnid shells.

The goal of the present study was to investigate the variability of shell Sr/Ca ratios in *T. squamosa* in relation to SST fluctuations. High-resolution in-situ analytical techniques (NanoSIMS, LA-ICP-MS) were used to assess links between Sr/Ca and ultrastructure properties, understand the environmental information preserved in shell Sr/Ca ratios and determine the precision of shell Sr/Ca-based seawater temperature estimates. Results of this study can

potentially contribute to a more efficient use of shell Sr/Ca to reconstruct past water temperatures in sub/tropical settings.

4.3 Materials and methods

4.3.1 Sample collection and preparation

To reconstruct sub-daily SST variations using Sr/Ca ratios from the shell of the fluted giant clam, *T. squamosa*, while accounting for shell architecture variability, high-resolution Sr/Ca and ultrastructural analyses were performed on specimen XB10. It is to be noted that XB10 was misidentified as *Tridacna derasa* in earlier studies (e.g., Yan et al., 2020) and was recently confirmed as *T. squamosa* (Liu et al., 2024). This specimen was collected from the North Reef (17°05′N, 111°30′E) in the northern South China Sea on 9 December 2013. After removal of the soft tissues, one valve was sectioned (Fig. 4.1A) using a diamond-coated saw blade attached to a cutting machine (for details see Yan et al., 2020). The radial growth portion of the shell slab (Fig. 4.1B) was embedded in epoxy resin and polished using a fine diamond grain sheet followed by a 0.5 µm diamond suspension. Images of the polished shell section were obtained using a Nikon A1 LSCM (State Key Laboratory for Manufacturing Systems Engineering, Xi'an Jiatong University; Fig. 4.1D). Triggering the auto-fluorescence of the shell material revealed daily growth lines in the shell (Fig. 4.1D; Yan et al., 2020).

4.3.2 Element chemistry and ultrastructure analyses

Shell Sr/Ca data were obtained from specimen XB10 using a CAMECA NanoSIMS 50L (CAMECA, Paris, France), as detailed in Yan et al. (2020). Briefly, the shell was sampled using a Cs^+ beam of approx. 150 pA, 16 kV and approx. 300 nm of diameter after carbon coating of the surface. 25 blocks of 10 cycles were measured by scanning the primary beam across areas of 2 μm^2 for a total of approx. 200 seconds of integration time and 2 µm spot-by-spot interval. The multi-collector system (mass resolving power of approx. 6000; 10 % definition) enabled the simultaneous measurements of $^{40}Ca^{16}O$ and $^{88}Sr^{16}O$, which were used to obtain semi-quantitative Sr/Ca values in counts/counts. For this study, the data from 15 July 2012 to 3 March 2013 were selected (approx. 4.5 mm representing 7 months of shell growth) as the shell growth lines from this portion were particularly distinctly developed, sharper and clearly separated by growth increments in LSCM images (Fig. 4.1D).

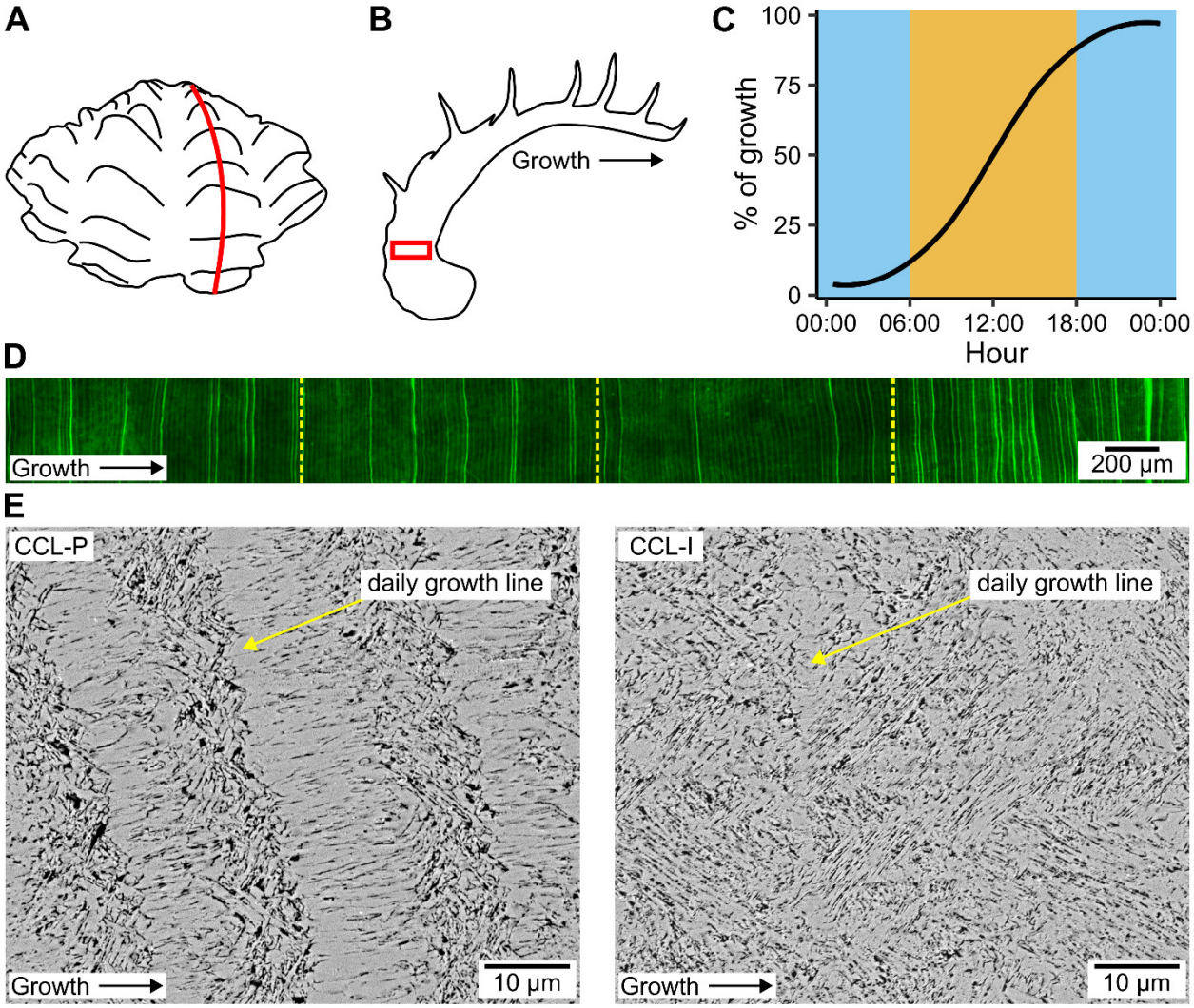

Figure 4.1 Overview of sampling and analysis of the studied *Tridacna squamosa* shell. (A) Sketch of the shell. Red line = cutting axis. (B) Schematic cross-section highlighting the area selected for element chemical and ultrastructural analyses (red rectangle). (C) Daily non-linear growth model used for automated temporal alignment of the Sr/Ca and ultrastructural data (size, shape and fractal dimension of the individual biomineral units). Blue and yellow represent data assigned to daily growth lines (formed during night) and increments (formed during day), respectively. (D) Autofluorescence image from Laser Scanning Confocal Microscopy (LSCM) showing the 7-month growth period analyzed in this study, with yellow dashed lines marking the virtual division of the sample into four smaller areas of interest. Daily growth bands are discernable, with growth lines showing higher fluorescence intensity than increments (details in Yan et al., 2020). Note variable LSCM intensity of daily growth lines. (E) Scanning Electron Microscope (SEM) images of the complex crossed-lamellar (CCL) ultrastructure of the shell. The CCL ultrastructure occurs in two configurations, namely complexly intertwined with prisms to the left (CCL-P), and without such prisms to the right (CCL-I). An exemplary daily growth line is indicated by a yellow arrow in each CCL ultrastructure configuration. In panels (B, D, E), the growth direction of the shell is indicated by an arrow.

Lower resolution quantitative shell Sr/Ca data (mmol/mol) were used for comparison with sub-daily Sr/Ca data obtained by NanoSIMS. Yan et al. (2020) reported Sr/Ca data obtained

via inductively coupled plasma – optical emission spectroscopy (ICP-OES). Low-resolution Sr/Ca data, reported by Liu et al. (2024), were also measured by laser ablation – ICP – mass spectrometry (LA-ICP-MS).

After element chemical analysis, the shell portion was ground using F800 and F1200 SiC suspensions on glass plates and polished using a 1 µm Al_2O_3 suspension on a Buehler MasterTex cloth. Following each grinding and polishing step, the sample was ultrasonically rinsed in water. The polished shell portion was immersed for 30 min in a 3 vol% H_2O_2 solution to remove organic material from the surface layer (i.e., surface oxidation) of the individual biomineral units (BMUs) of the shell complex crossed-lamellar ultrastructure, facilitating their visualization. The section was then mounted on a one-inch sample holder using a carbon sticker and placed in a Leica EM ACE200 Vacuum Coater for directional sputtering using a 5 nm platinum layer.

To manage the computational load of the SEM analysis and facilitate further image processing, the 4.5 mm long sample was divided into four smaller areas of interest (Fig. 4.1D). Results from these regions were later recombined to generate a comprehensive dataset. Using a preliminary low-resolution SEM scan, a shell portion for which the visualization of the BMUs was optimal and representative of the ultrastructural diversity of the sample – including daily growth lines and increments as well as CCL-I and CCL-P configurations – was selected for each area of interest. Each portion had a standard height of approx. 500 µm, ensuring replicability between areas of interest, and was analyzed using automated high-resolution mapping at 5245× magnification performed with a 3rd generation Phenom Pro Desktop SEM, equipped with a backscatter electron detector and a CeB_6 electron source at 10 keV. Individual SEM images were stitched together using the software Fiji/ImageJ (available at https://imagej.net/software/fiji/, last access: 15 April 2024; Schindelin et al., 2012).

4.3.3 Ultrastructure morphometry

The morphological characteristics of the BMUs (size [area], shape [elongation], complexity [fractal dimension]) were quantified with the Fiji/ImageJ MorphoLibJ plugin (Bogovic et al., 2016; Legland et al., 2016), adapting the methods developed by Höche et al. (2020). To visualize BMU boundaries and remove noise, the contrast of each stitched SEM image was increased and the median grey value subtracted. Images were then converted to binary format, with white representing the BMUs and black the boundaries between them. A watershed transformation algorithm (part of the MorphoLibJ plugin) was used to reconstruct fragmented boundaries. For details see Höche et al. (2020). Once all individual BMUs were labeled with unique identification numbers, the MorphoLibJ plugin was used to determine their size and shape, i.e., the area and elongation.

Each BMU was saved as a region of interest (ROI) using the LabelsToRois plugin (Waisman et al., 2021), allowing for the determination of their fractal dimension using the FracLac plugin (Karperien, 2013) and the box-counting method. For the latter, the number of grid boxes needed to fully cover BMUs is determined. This process is repeated with different grid sizes, and the fractal dimension is determined by analyzing the logarithmic relationship between the number of boxes and the inverse of the box size. For a BMU shape observed in SEM images (2D), the slope of this relationship represents the fractal dimension, which ranges from 1 to 2. A more complex BMU will have a fractal dimension closer to 2, while simpler shapes will have values closer to 1. Thus, the fractal dimension of each BMU in the XB10 shell ultrastructure was calculated as an additional morphometrical parameter indicating complexity and self-similarity.

4.3.4 Sub-daily temporal alignment of the data

In previous research, the sub-daily temporal alignment of the shell element-to-calcium profiles was accomplished by linear interpolation, assigning a set number of data points to each day, as described by Yan et al. (2020, 2021) and Liu et al. (2022). Here, we applied a revised alignment technique which takes into account that the energy available for shell growth in *T. squamosa* is influenced by the photosynthetic efficiency of its zooxanthellae symbionts (Bonham, 1965; Rosewater, 1965; Griffiths and Klumpp, 1996). Thus, shell growth does not occur at a constant rate throughout the day but follows a non-linear model (Fig. 4.1C) which was empirically developed considering the activity patterns of photosymbiotic giant clams (Killam et al., 2023b) and the local solar cycle (average sunrise and sunset timing at the collection site). Following this model, 75 % of daily shell growth occurs between 6 am and 6 pm (daylight), with growth rate peaking at noon, while the remaining 25 % of growth occurs between 6 pm and 6 am during nighttime when the daily growth lines are formed. The highest Sr/Ca value of each day occurred in the daily growth lines and was manually assigned to midnight. The remaining data points were temporally aligned according to the non-linear growth model.

Temporal alignment of the BMU morphology data with the shell Sr/Ca profile was achieved through several steps of image processing using ImageJ. For each day, two ROIs were identified and delineated on the SEM mappings: One ROI representing the daily growth line and the other the daily growth increment (= main daily growth period), both identified by their corresponding date. An ImageJ macro (see Brosset et al., 2024) was used to save the coordinates of all pixels within each ROI, and the pixel coordinates of every BMU in the stitched SEM images were also obtained. An R script developed for this study (see Brosset et al., 2024) enabled an automatic timestamp assignment. Briefly, to integrate the non-linear growth model with the temporal alignment of BMU morphology data (Fig. 4.1C), the width of each ROI assigned to a

daily growth increment was segmented into sub-sections. This segmentation divided the X coordinates (width) of each ROI into sub-sections corresponding to the number of Sr/Ca data points available for that increment, with widths adjusted according to the non-linear growth model (Fig. 4.1C). This process was repeated for each Y coordinate (height) of the SEM mapping and for each daily increment, effectively generating sub-ROIs that matched the timestamps of the Sr/Ca data. Consequently, sub-ROIs representing periods of rapid growth (e.g., 12 h) became broader than such of slower growth phases.

Subsequently, the SEM mappings were converted into matrices, with each matrix address corresponding to a pixel in the original image. In each matrix, daily sub-ROIs were indexed with unique identification numbers, and all matrix addresses for each sub-ROI were assigned to that identification number. Each pixel of a BMU was then allocated to the appropriate sub-ROI identification number based on its coordinates in the matrix. Once every pixel was assigned correctly, each BMU was assigned to the sub-ROI containing the majority of its pixels, providing a precise date and timestamp for each BMU in the SEM image. The 15 % largest BMUs within each sub-ROI were selected to facilitate further analysis, as previous studies have shown that most BMU morphological variation and its relationship with water temperature are predominantly observed in this size group (Höche et al., 2020, 2021). For each timestamp, median values of all morphometric parameters were calculated. This process yielded an Sr/Ca value and an average BMU shape (area, elongation, fractal dimension) for each timestamp, resulting in a sub-daily resolved 7-month time-series for the XB10 specimen. The number of data points collected per daily growth band (= couplet of one increment and one line) ranged from 5 to 15, leading to variability in the time represented by each data point due to the non-linear nature of shell growth. To standardize the effects of time-averaging, the dataset was resampled using linear interpolation to five data points per day at fixed timestamps (00:00, 04:48, 09:36, 14:24 and 19:02). For coherent analysis with environmental variables, SST data measured at the bivalve collection site with a 3-hour resolution (see Yan et al., 2020) was similarly resampled to match these sub-daily timestamps of the XB10 data. Alternatively, a high-pass filter was applied to the shell Sr/Ca data from the daily growth increments in order to generate a dataset (see Brosset et al., 2024) without the low-frequency component.

4.3.5 Statistical analysis and temperature reconstruction

Non-parametric tests were used for statistical analysis as the data from XB10 were not normally distributed (Shapiro tests, $p < 0.05$). Element chemical differences in shell properties associated with extreme events at the timescale of weather (WEEs; see Yan et al., 2020) and such unaffected by WEEs were evaluated using Mann-Whitney *U* (MWU) rank tests. MWU tests also assessed the

impact of shell architecture by comparing Sr/Ca and BMU morphology data from different shell portions (daily growth lines and increments) and ultrastructure configurations (CCL-P and CCL-I; Fig. 4.1E), identified through SEM image visual examination. Daily variations and potential cycles of all shell properties were examined using autocorrelation analysis and MWU tests.

Linear regression was employed to explore the relationship between shell properties and SST. To compare the Sr/Ca values obtained by quantitative analyses (ICP-OES and LA-ICP-MS) and the semi-quantitative method (NanoSIMS), paired Fligner-Killeen tests were conducted to assess the equality of variances in the data. A Kruskal-Wallis test was also used to compare the results of the quantitative methods.

The NanoSIMS Sr/Ca data assigned to the daily growth increments were combined across consecutive days to match the resolutions of each quantitative method, with 4 days for LA-ICP-MS line scan, 1 week for ICP-OES and LA-ICP-MS with a 90 µm laser spot diameter, and 2 weeks for LA-ICP-MS with a 110 µm laser spot diameter. Linear regressions were then performed between the resulting Sr/Ca values and SST to compute temperature transfer functions. The precision of Sr/Ca-based temperature predictions was assessed for each sampling method and resolution, including sub-daily and daily averaged NanoSIMS Sr/Ca data, by calculating temperature prediction intervals (1σ). The accuracy of these temperature estimates was evaluated by calculating the mean absolute difference between the SST computed for each analytical method and the instrumental SST data from the XB10 collection site.

4.4 Results

4.4.1 Temporal variation of shell Sr/Ca and ultrastructure morphometry

The element chemistry and ultrastructure morphology of the studied shell varied independently over time (Fig. 4.2). Shell Sr/Ca ratios obtained by NanoSIMS increased by approx. 7 % during WEEs in comparison to periods of limited environmental stress (Fig. 4.2A). This difference in average shell Sr/Ca was statistically significant (MWU, $p < 0.001$), whereas none of the ultrastructure morphology parameters showed a significant difference between WEEs and non-WEE periods (Fig. 4.2C, E, G). On average, the BMUs measured 5.65 ± 0.90 µm^2 and their elongation and fractal dimension were approx. 1.83 ± 0.22 and 1.52 ± 0.02, respectively (Fig. 4.2C, E, G).

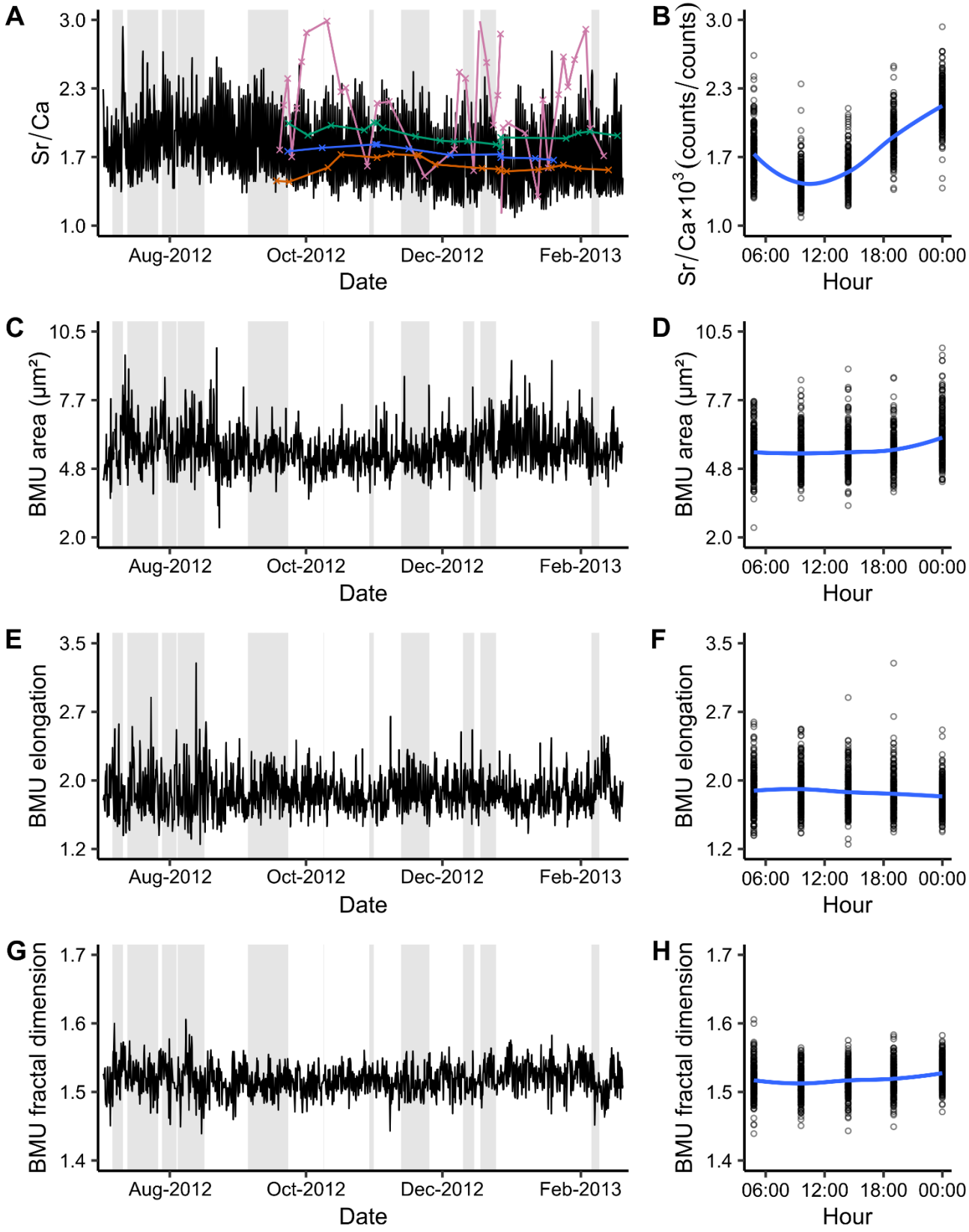

Figure 4.2 Temporal variation of Sr/Ca ratios and ultrastructural properties, i.e., biomineral unit (BMU) area, elongation and fractal dimension, in the shell of the *Tridacna squamosa*. (A, C, E, G) Daily variation during a seven-month interval, with weather-scale extreme events (WEEs; details in Yan et al., 2020)

indicated by grey areas. (B, D, F, H) illustrate the variation of each parameter on a sub-daily basis, with a blue line representing the average values. In (A), the black line represents Sr/ Ca data measured by NanoSIMS, while the colored lines show molar Sr/Ca data based on LA-ICP-MS operated in line scan mode (pink), LA-ICP-MS operated in spot mode (90 µm spot diameter: green; 110 µm spots: blue) and ICP-OES (orange). Sr/Ca data depicted in (B) are exclusively from NanoSIMS.

On a daily scale, consistent Sr/Ca cycles were observed (autocorrelation factor = 0.8, $p < 0.05$; Fig. 4.2B). Diurnal maxima occurred at the growth lines, with shell Sr/Ca values being approx. 54 % higher than diurnal minima (Fig. 4.2B). This difference was significant (MWU, $p < 0.001$) and consistent during both WEEs and more stable conditions. The ultrastructure morphology, i.e., the size, elongation and complexity of the BMUs, varied during the day (Fig. 4.2D, F, H). On average, BMUs observed at the daily Sr/Ca peaks were 0.59 µm^2 larger (MWU, $p < 0.001$) than those formed during the rest of the daily growth band (Fig. 4.2D). The corresponding difference in BMU elongation and fractal dimension was significant (MWU, $p < 0.001$) but represented less than 3 % of the variation (Fig. 4.2F, H). Despite these slight differences in the BMU morphology of the daily growth lines and increments, none of the studied ultrastructure properties showed a clear daily cycle (autocorrelation factor < 0.2, $p < 0.05$; Fig. 4.2D, F, H).

In contrast to high-resolution NanoSIMS data, the sampling resolution of LA-ICP-MS and ICP-OES was too coarse to distinguish between Sr/Ca ratios in daily growth lines and increments. Data representing several days and nights of growth masked the diurnal Sr/Ca maxima. Molar Sr/Ca data varied slightly between the different quantitative methods. The highest mean and variance was obtained by LA-ICP-MS operated in line scan mode (2.17 ± 0.47 mmol/mol; Fig. 4.2A). Sr/Ca data measured by ICP-OES equaled 1.57 ± 0.08 mmol/mol (Fig. 4.2A). When measured by LA-ICP-MS in spot mode, Sr/Ca values were 1.88 ± 0.08 and 1.71 ± 0.05 mmol/mol for spot diameters of 90 and 110 µm, respectively (Fig. 4.2A). Furthermore, compared to the semi-quantitative shell Sr/Ca analysis (NanoSIMS), the variance of the molar Sr/Ca ratios differed significantly (Fligner-Killeen, $p < 0.001$) and also showed statistical differences between each quantitative analytical method (Kruskal-Wallis, $p < 0.001$; Fig. 4.2A). It should be added that the much larger variance of line scan LA-ICP-MS data compared to such obtained in spot mode results from much shorter acquisition times.

4.4.2 Relationship between shell properties, temperature and ultrastructure configuration

The strontium content of the *T. squamosa* shell showed a significant positive correlation with water temperature (Fig. 4.3A). The strongest correlation with SST was found for Sr/Ca ratios measured within the main growing portions of the shell, i.e., daily growth increments, with R^2 =

0.36 ($p < 0.001$; Fig. 4.3A). It needs to be pointed out that such correlation remained unchanged when a high-pass filter was applied to the Sr/Ca data from the daily growth increments (see also Brosset et al., 2024). Shell Sr/Ca increased by 5 % / °C during daytime (Fig. 4.3A). In contrast, less than 10 % of the Sr/Ca variations could be explained by temperature if only data from the growth lines were considered or when Sr/Ca ratios from the day and night (= one daily growth band) were combined ($R^2 = 0.06$ and 0.08, respectively, $p < 0.001$; Fig. 4.3A). Additionally, no significant relationship ($p > 0.05$) was found between SST and the morphology of the shell ultrastructure, whether the BMU area (Fig. 4.3B), elongation (Fig. 4.3C) and fractal dimension (Fig. 4.3D) were considered separately or combined between shell daily growth lines and increments.

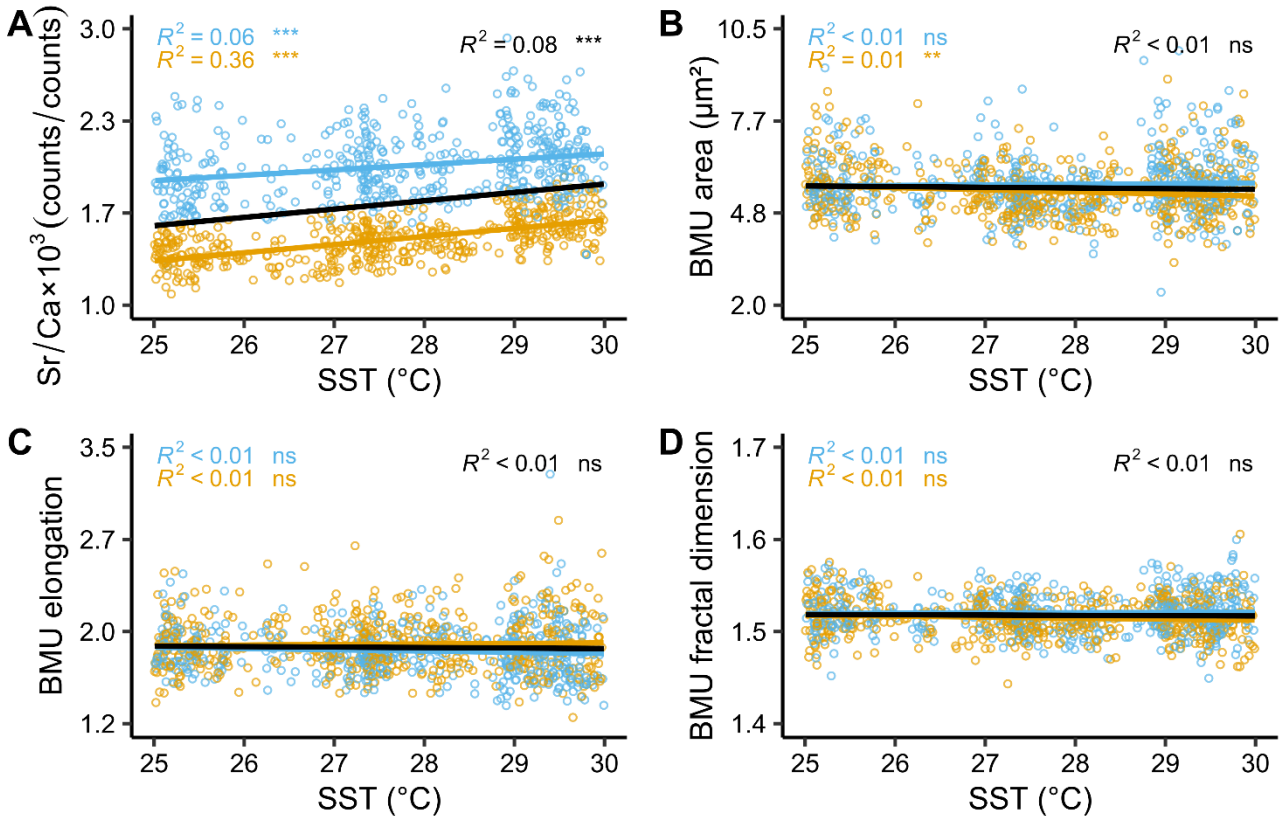

Figure 4.3 Relationship between shell Sr/Ca ratios and ultrastructural properties, i.e., biomineral unit (BMU) area, elongation and fractal dimension, and sea surface temperature (SST). Blue and orange denote data from the daily growth lines and the daily increments, respectively, of studied specimen of *Tridacna squamosa*. Blue, orange and black lines stand for linear regressions computed with data from the growth lines, the increments and both growth lines and increments combined, respectively. Coefficients of determination (R^2) and significance levels are depicted for each of the linear regressions (*** $p < 0.001$, ** $p < 0.01$, * $p < 0.05$, and ns indicates $p > 0.05$). (A) Relationship between shell Sr/Ca and SST. (B) Relationship between BMU area and SST. (C) Relationship between BMU elongation and SST. (D) Relationship between BMU fractal dimension and SST.

Shell portions formed during WEEs showed prismatic features within the ultrastructure, i.e., CCL-P configuration (Fig. 4.1E), nearly 30 % more frequently than shell portions deposited during more stable growth conditions. During non-WEE periods, more than 60 % of the complex-crossed lamellar pattern of the shell was devoid of intricated prisms, i.e., the CCL-I configuration (Fig. 4.1E). On average, shell growth increments with a CCL-P configuration had significantly higher Sr/Ca ratios compared to those found in CCL-I increments (MWU, $p < 0.01$), although they only differed morphometrically by 2 % (Fig. 4.4A). The size of the BMUs was indistinguishable between CCL-I and CCL-P ultrastructural configurations ($p > 0.05$; Fig. 4.4B). However, BMUs from CCL-I increments were significantly (MWU, $p < 0.01$) less round (average elongation = 1.85 ± 0.22) and complex (average fractal dimension = 1.51 ± 0.02) than those found in areas with intricated prisms (average elongation = 1.80 ± 0.22 and average fractal dimension = 1.52 ± 0.02; Fig. 4.4C, D).

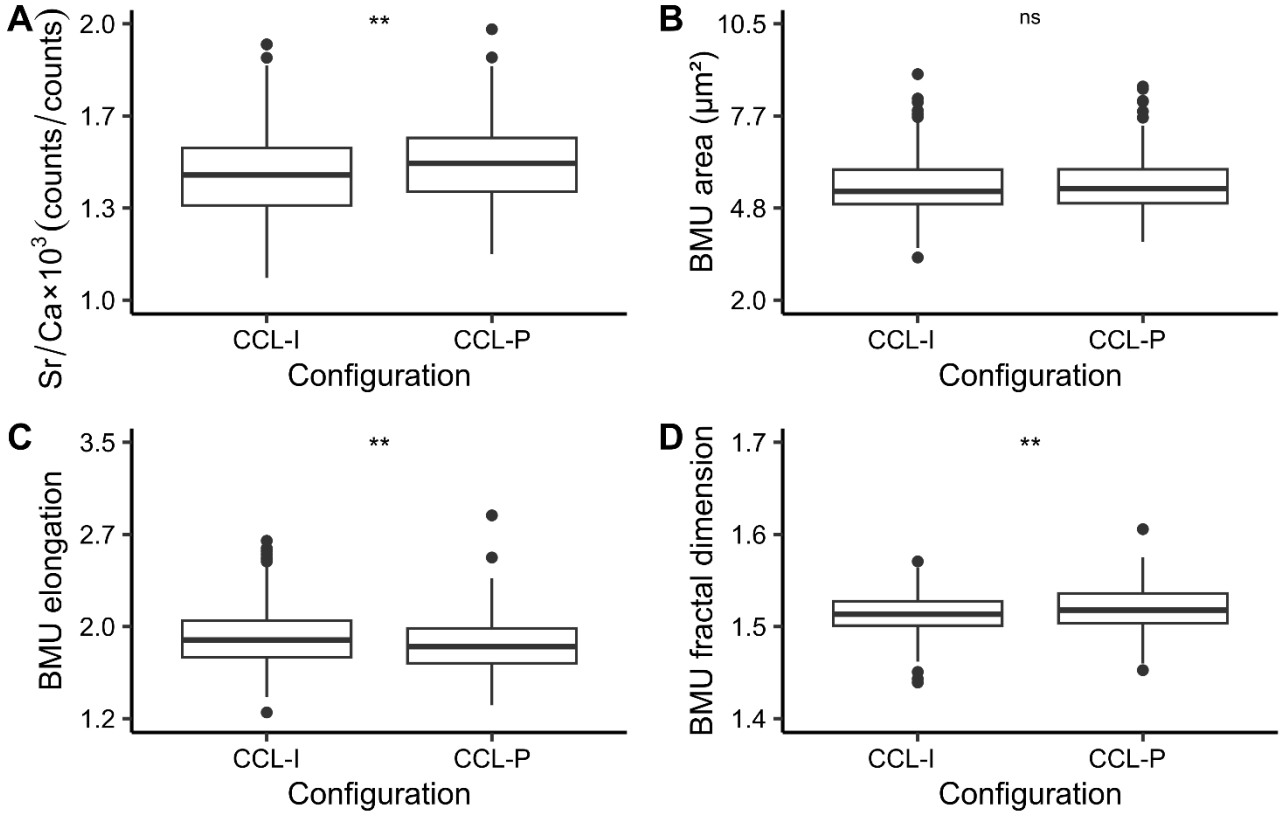

Figure 4.4 Shell Sr/Ca and ultrastructural properties, i.e., biomineral unit (BMU) area, elongation and fractal dimension, from the complex crossed-lamellar (CCL) ultrastructure of the *Tridacna squamosa*. CCL-P = CCL ultrastructure with intricated prisms; CCL-I = prism-free configuration of CCL ultrastructure. (A) Shell Sr/Ca. (B) BMU area, (C) elongation and (D) fractal dimension. The bold black line represents the median, the lower and upper limits of the boxes indicate the first and third quartiles, vertical lines denote the minimum and maximum values, and black dots represent outliers. Significance of the Mann-Whitney *U* test between CCL-P and CCL-I data is depicted in each panel (*** $p < 0.001$, ** $p < 0.01$, * $p < 0.05$, and ns indicates $p > 0.05$).

4.4.3 Significance of Sr/Ca-based temperature reconstructions

The correlation between shell Sr/Ca and SST was significantly stronger when NanoSIMS data were aggregated over several consecutive daily increments, compared to similar temporal resolutions obtained from LA-ICP-MS and ICP-OES analyses (Fig. 4.5). At a 4-day resolution, no relationship was found between molar Sr/Ca ratios and SST ($p > 0.05$; Fig. 4.5A), while 78 % of the Sr/Ca variance was explained by SST variation using NanoSIMS data from 4 consecutive daily increments ($p < 0.001$; Fig. 4.5B). Similarly, 83 % of the variance in weekly averaged increment Sr/Ca data (NanoSIMS) was explained by temperature variation ($p < 0.001$; Fig. 4.5D, F), with no significant relationship identified in weekly molar Sr/Ca ratios obtained via ICP-OES ($p > 0.05$; Fig. 4.5C). Shell Sr/Ca data from LA-ICP-MS spot analyses (90 µm and 110 µm diameters) were significantly correlated with weekly ($R^2 = 0.30$, $p < 0.02$; Fig. 4.5E) and bi-weekly ($R^2 = 0.50$, $p < 0.01$; Fig. 4.5G) SST variations, although the Sr/Ca ratios increased only by 4 and 3 % per °C, respectively. In contrast, NanoSIMS data from daily increments exhibited a temperature sensitivity of 6 % / °C across all considered temporal resolutions (Fig. 4.5B, D, F, H), explaining up to 86 % of the shell Sr/Ca variance by SST (Fig. 4.5H).

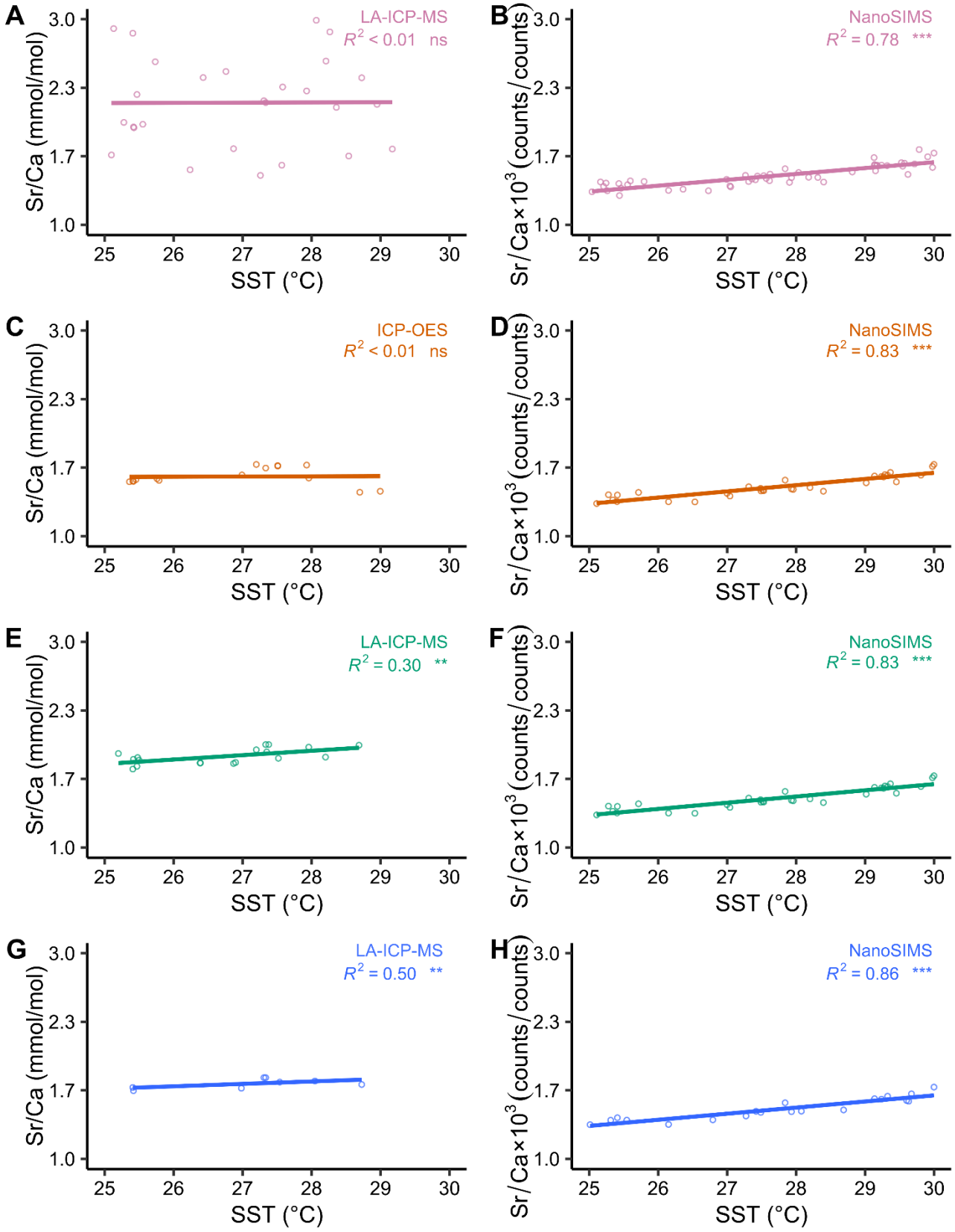

Figure 4.5 Relationship between shell Sr/Ca (*Tridacna squamosa*) and sea surface temperature (SST). (A) Molar Sr/Ca data obtained by LA-ICP-MS operated in line scan mode (4-day resolution) and (B) corresponding (down-sampled) NanoSIMS data from the daily growth increments. (C) Weekly resolved

molar Sr/Ca data obtained by ICP-OES and (D) corresponding (down-sampled) NanoSIMS data from the daily growth increments. (E) Weekly resolved molar Sr/Ca data obtained by LA-ICP-MS operated in spot mode (spot diameter: 90 µm) and (F) corresponding (down-sampled) NanoSIMS data from the daily growth increments. (G) Bi-weekly resolved molar Sr/Ca data obtained by LA-ICP-MS operated in spot mode (spot diameter: 110 µm) and (H) corresponding (down-sampled) NanoSIMS data from the daily growth increments. Coefficients of determination (R^2) and significance levels are depicted for each of the linear regressions (*** $p < 0.001$, ** $p < 0.01$, * $p < 0.05$, and ns indicating $p > 0.05$).

Sub-daily water temperature variation could be predicted to the nearest ± 2.8 °C using shell NanoSIMS Sr/Ca data from daily growth increments (Fig. 4.6A). Daily averaging narrowed the prediction interval to ± 2.2 °C (Fig. 4.6B). Combining data from 4, 7, and 14 consecutive daily increments further reduced the prediction intervals to ± 1.7 °C, ± 1.6 °C, and ± 1.5 °C, respectively (Fig. 4.6D, F, H, J). In comparison, molar Sr/Ca ratios that included multiple daily growth bands resulted in prediction intervals of, at best, ± 2.2 °C for a weekly resolution (LA-ICP-MS 90 µm spots; Fig. 4.6G) and ± 2.5 °C for a bi-weekly resolution (LA-ICP-MS 110 µm spots; Fig. 4.6I). The prediction models were not significant for the data obtained from a LA-ICP-MS line scan (4-day resolution; Fig. 4.6C) and ICP-OES (1-week resolution; Fig. 4.6E).

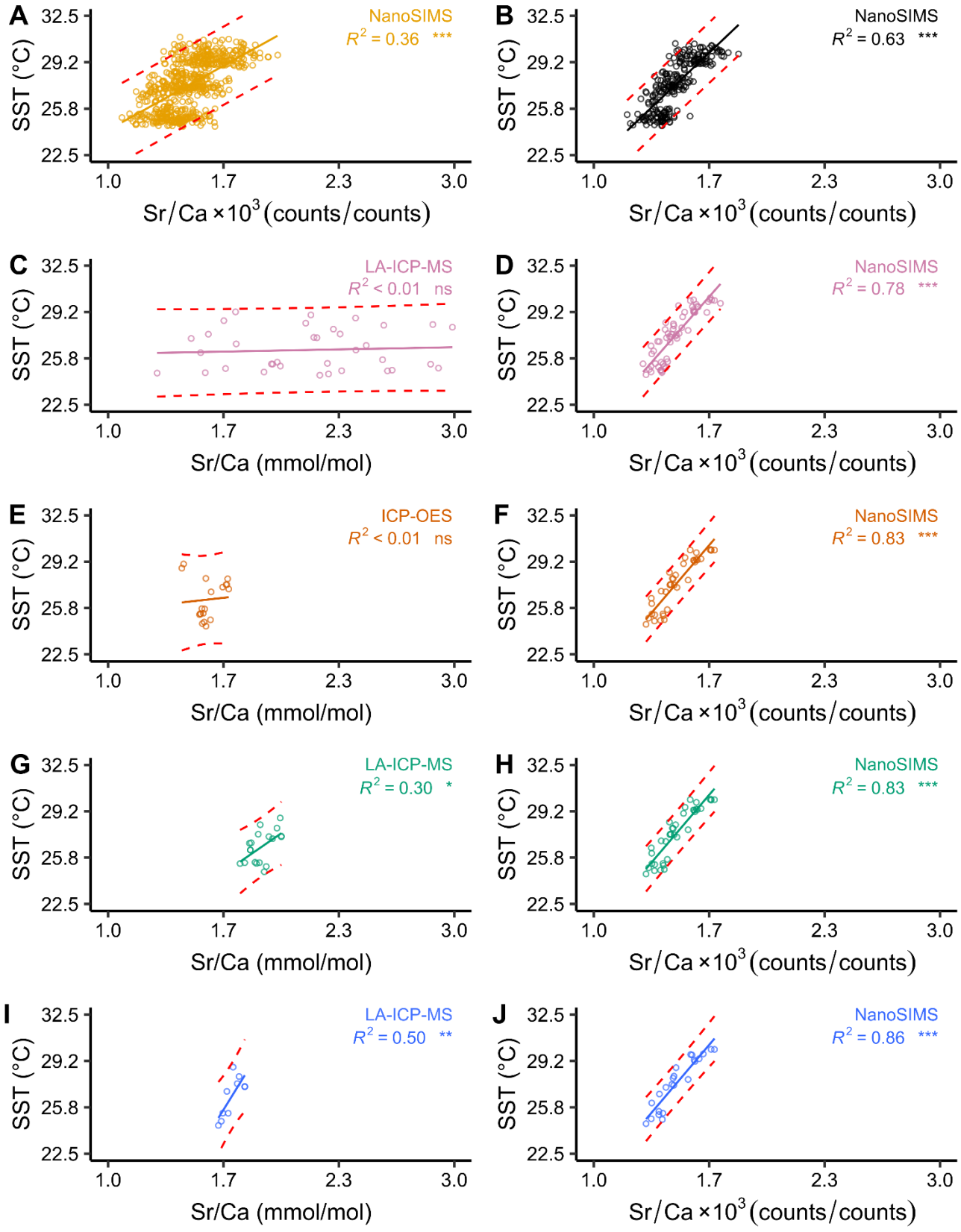

Figure 4.6 Sea surface temperature (SST) reconstructed from shell Sr/Ca ratios of studied *Tridacna squamosa* specimen. Linear regression (solid lines) with 95 % prediction intervals (dashed red lines). (A + B) SST computed from NanoSIMS Sr/Ca data determined in daily growth increments (A = raw, B = daily

averages). (C) SST predicted from Sr/Ca data (mmol/mol) measured by LA-ICP-MS in line scan mode (4-day resolution) and (D) corresponding SST computed from down-sampled NanoSIMS data of the daily growth increments. (E) Weekly SST predicted from ICP-OES Sr/Ca data and (F) corresponding SST computed from down-sampled NanoSIMS data of the daily growth increments. (G) Weekly SST calculated from Sr/Ca measured by LA-ICP-MS in spot mode (90 µm laser spots) and (H) corresponding SST derived from down-sampled NanoSIMS data of the daily growth increments. (I) Biweekly SST predicted from Sr/Ca data measured by LA-ICP-MS in spot mode (110 µm laser spots) and (J) corresponding SST inferred from down-sampled NanoSIMS of the daily growth increments.

The most accurate temperature estimates from shell Sr/Ca ratios were obtained from NanoSIMS data averaged over multiple consecutive daily growth increments (Fig. 4.7). Bi-weekly resolved reconstructed SST differed, on average, by approx. 0.58 °C from instrumental SST, and both datasets were strongly correlated (Pearson $r = 0.93$, $p < 0.001$), showing no significant difference (MWU, $p > 0.05$). SST estimates were more accurate during WEEs or for shell portions with prismatic features (CCL-P), with an average difference of 0.48 °C and a Pearson correlation of up to 0.95 between reconstructed and instrumental SST profiles ($p < 0.001$), compared to more stable conditions or CCL-I increments, which differed by up to 0.63 °C.

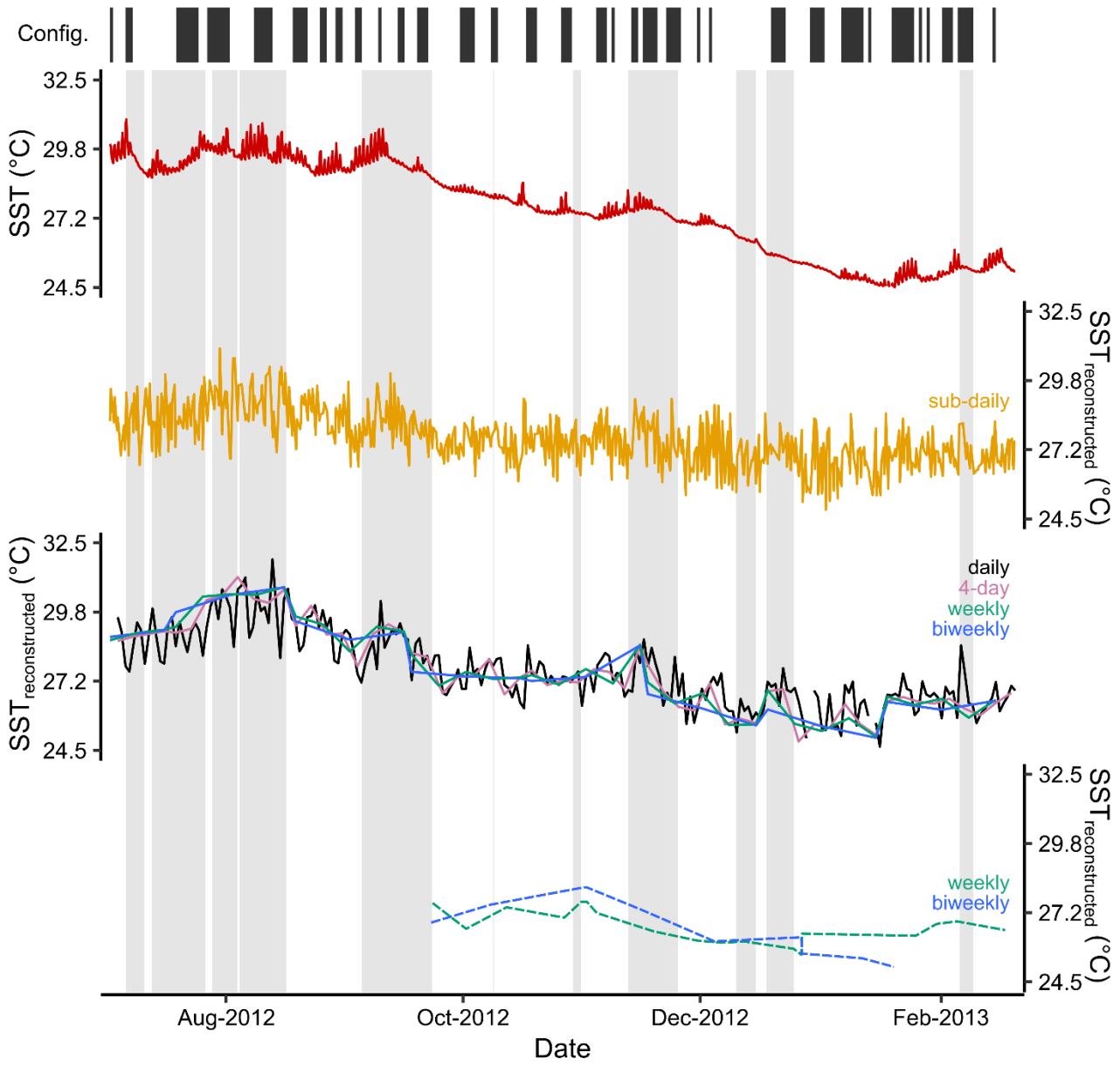

Figure 4.7 Temporal variation of sea surface temperature (SST) measured at the site where the studied *Tridacna squamosa* specimen lived in comparison to average SST reconstructed from shell Sr/Ca ratios. Weather-scale extreme events (WEEs; for details see Yan et al., 2020) are indicated by grey areas. The solid red line represents instrumental SST data, while the other solid lines show SST reconstructed from NanoSIMS Sr/Ca data of the daily growth increments. SST reconstructions based on LA-ICP-MS Sr/Ca data are depicted as dashed lines. Sub-daily SST estimates are shown in orange, daily in black, 4-day resolution in pink, weekly resolved data in green and biweekly data in blue. The top portion illustrates the configuration (Config.) of the complex crossed-lamellar (CCL) ultrastructure (CCL-P = CCL with intricated prisms = black, CCL without prisms = white).

4.5 Discussion

The meaning of Sr/Ca variations in tridacnids (and other bivalve taxa) is still a matter of debate (Yan et al., 2011; Sano et al., 2012; Warter et al., 2018; Peharda et al., 2021; DeWinter et al., 2023). Whereas on the seasonal scale, temperature seems to be negatively correlated to shell Sr/Ca of several different giant clam species (e.g., Yan et al., 2011, 2013, 2014) and positively in others including *T. squamosa* and *T. derasa* (Liu et al., 2021), such link could not be verified on shorter time-scales (e.g., in *Tridacna gigas*: Elliot et al., 2009), specifically on the diurnal time-scale (Sano et al., 2012). While Sano et al. (2012) likewise observed a negative coupling with temperature on the seasonal scale, shell Sr/Ca of *T. derasa* was also negatively correlated to seasonal changes in insolation. Furthermore, the seasonal Sr/Ca changes were as large as such between day and night despite nearly unchanged diurnal water temperature. As in the present study, Sano et al. (2012) found diurnal Sr/Ca cycles, with higher Sr/Ca values in daily growth lines (= shell portions produced during nighttime when growth rate was retarded) than in daily growth increments (= shell portions produced during the day when the photosymbionts were active and the shell was growing fast). Based on these observations, Sano et al. (2012) concluded that changes in shell Sr/Ca of giant clams are inversely correlated with light availability, both on daily and seasonal time-scales, but not temperature. However, Warter et al. (2018) found the same diurnal Sr/Ca cycles in shells of *Tridacna crocea* grown in laboratory tanks under constant illumination. These authors therefore suggested that circadian biological rhythms control the Sr incorporation into the shells rather than temperature or the light cycle. Our findings partly support this view.

4.5.1 Shell Sr/Ca as a temperature proxy

As indicated by the results herein, shell Sr/Ca values of *T. squamosa* are positively correlated to water temperature and can be used to reconstruct SST with an uncertainty of ± 1.5 to 2.8 °C, provided that only shell portions formed during daytime (daily growth increments) are considered (section 4.3.3). This finding was possible through an ultra-high-resolution chemical analysis of the shell via NanoSIMS combined with growth pattern and ultrastructure investigations. The isolated analysis of chemical properties in daily growth lines and increments seemed advised and necessary, because in many other bivalve species, Sr levels differ markedly between ultrastructurally different shell portions: Higher Sr/Ca values were observed in growth lines, typically composed of irregular simple prisms (as in *T. squamosa*), and lower values in growth increments (made of other ultrastructures, here CCL ultrastructure). This likewise applies to daily (Füllenbach et al., 2017; Sano et al., 2012) as well as annual growth patterns (Foster et al., 2009; Schöne et al., 2011, 2013; Shirai et al., 2014).

Whereas 36 % of the Sr/Ca variation of daily growth increments could be explained by temperature, the explained variability remained below 10 % if only data from the daily growth lines were considered or data from both daily increments and lines were combined (section 4.3.2). Noteworthy, all correlations were statistically highly significant ($p < 0.001$), despite a large proportion of the variance being unrelated to SST fluctuations but rather linked to the bivalve physiology and/or variations in its ecosystem. Therefore, the transfer functions for Sr/Ca data on the sub-daily time-scale come with a relatively large uncertainty of ± 2.8 °C (section 4.3.3) that may limit applications in tropical regions where the seasonal temperature amplitude is barely larger than that. This uncertainty can be cut in half (± 1.5 °C) if biweekly SST averages are computed from Sr/Ca data of daily increments (section 4.3.3). Through this averaging, Sr/Ca variations between days were smoothed and short-term environmental fluctuations eliminated. Consequently, the range of Sr/Ca data was smaller, leading to a stronger correlation of shell Sr/Ca with SST (Fig. 4.5B, D, F, H) and narrower prediction intervals of the water temperature (Fig. 4.6D, F, H, J). The broader prediction intervals and weaker correlation obtained at higher resolution, i.e., on sub-daily and daily time-scales (Fig. 4.6A, B), were likely caused by short-term environmental and/or physiological fluctuations affecting shell Sr/Ca ratios.

In *Arctica islandica* and *Mytilus edulis*, shell Sr/Ca and temperature were likewise weakly correlated, but the sign, slope and intercept varied significantly between localities (and environmental conditions) and ultrastructurally different shell portions (Wanamaker et al., 2008; Schöne et al., 2013; Brosset et al., 2023). This variability was associated with strong biological control over the biomineralization process and trace element incorporation as well as other factors such as salinity (Dodd and Crisp, 1982; Yan et al., 2013), growth rate (Carré et al., 2006) and food intake (Goodwin et al., 2013; Piwoni-Piórewicz et al., 2021). All such influences can result in a lower correlation between Sr/Ca and water temperature regardless of the sampling resolution. The differences observed across the range of resolutions (section 4.3.3) suggest that while shell Sr/Ca of *Tridacna* spp. captures temperature trends, especially when accounting for shell architectural heterogeneity, they are also influenced by other environmental factors operating on the sub-daily scale (Sano et al., 2012; Warter et al., 2018; Yan et al., 2020; Liu et al., 2021).

Sr/Ca increased by ca. 5 % per °C (Fig. 4.2A). The rate of change is similar to that reported from other tridacnids (Yan et al., 2014, 2015) as well as other biogenic archives (Beck et al., 1992; Sun et al., 2004; Corrège, 2006; Schöne et al., 2013), but comes with the opposite sign. The positive correlation between temperature and shell Sr/Ca ratios as well as the temperature sensitivity of shell Sr/Ca of *T. squamosa* reported herein is consistent with thermodynamic principles (temperature sensitivity: 4 % / °C; Gaetani and Cohen, 2006). Strontium ions (Sr^{2+}) can substitute for calcium ions (Ca^{2+}) with minimal distortions in the crystal lattice of aragonite (Gaetani and

Cohen, 2006) because their ionic radii are similar (Ca^{2+} = 1.18 Å, Sr^{2+} = 1.31 Å in a 9-fold coordination; Shannon, 1976). Higher temperatures not only favor larger distortions of the crystal lattice but also increase the kinetic energy of ions in the biomineralizing environment and thus facilitate the diffusion of Sr^{2+} into the aragonite at the calcifying front (Gaetani and Cohen, 2006; Menadakis et al., 2008).

However, the absolute Sr/Ca values of *T. squamosa* are higher (between approx. 1.57 and 2.17 mmol/mol; Fig. 4.2A) than thermodynamically expected (approx. 1.3 mmol/mol at 25 °C; Gaetani and Cohen, 2006). Possibly, this difference can be explained with the surface entrapment model discussed by Gaetani and Cohen (2006). Following this model, aragonite crystal growth can outpace the ion diffusion rate required for equilibrium partitioning with the calcifying fluid (Watson, 1996, 2004). This mechanism leads to the entrapment of additional Sr^{2+} at the near-surface of the aragonite crystals (Watson, 1996, 2004; Gaetani and Cohen, 2006).

4.5.2 Shell element chemistry and ultrastructural dynamics

In *T. squamosa*, the shell element chemistry and ultrastructure morphology varied independently over time (section 3.3.1). For instance, shell Sr/Ca increased significantly when the complex crossed-lamellar ultrastructure contained prisms (CCL-P; Fig. 4.4A). Notably, this ultrastructural modification only resulted in a 2 % change of the BMU shape and complexity (Fig. 4.4C, D) and no change in BMU size (Fig. 4.4B). Similarly, the consistent diurnal cycles of shell Sr/Ca (Fig. 4.2B) contrasted with the lack of corresponding fluctuations in BMU morphology (Fig. 4.2D, F, H). Instead, the shape of BMUs differed significantly between portions grown during daytime and nighttime ($p < 0.001$; Fig. 4.2D, F, H). The asynchrony between element chemical and ultrastructural dynamics suggests that both shell Sr/Ca ratios and BMU morphology are influenced by common physiological factors rather than being directly linked. While the Sr/Ca variability was partly attributable to temperature fluctuations (sections 4.3.2, 4.3.3, and 4.4.1), none of the BMU morphology parameters correlated with SST (Fig. 4.2B, C, D), contrary to the results of ultrastructural analyses performed in some other bivalve species (*A. islandica* and *Glycymeris bimaculata*; Höche et al., 2020, 2021). This suggests that these shell properties are driven by different factors in *T. squamosa*, and while SST is a key determinant of the shell ultrastructure in non-photosymbiotic bivalves (Höche et al., 2020, 2021, 2022), light conditions likely prevail over water temperature as the primary control in photosymbiotic species like tridacnids.

In adult tridacnid specimens, most of the energy used to regulate physiological processes derives from their symbiotic relationship with photosynthetic organisms (Bonham, 1965; Rosewater, 1965; Klumpp and Lucas, 1994; Griffiths and Klumpp, 1996), i.e., zooxanthellae

symbionts hosted in the mantle of the bivalve (Ip et al., 2017). During daytime, when light is available, the bivalve is active and valves are gaping (Killam et al., 2023b), maximizing symbiont exposure to sunlight and enhancing photosynthetic efficiency (Ip and Chew, 2021). As a consequence, more nutrients are available for the animal (Killam et al., 2023a) which propel its metabolic rates (Ip and Chew, 2021). Under such favorable growth conditions, the shell grows fast in association to the formation of small and elongated BMUs (Fig. 4.2D, F), typically found in the CCL ultrastructure of *Tridacna* spp. (Agbaje et al., 2017; Mills et al., 2024a). During daytime, the bivalve also has more energy available to actively preclude trace impurities from ending up in the shell, such as unwanted Sr^{2+} ions. Since protein and gene expression levels related to calcification processes in *Tridacna* spp. are enhanced by insolation (Ip et al., 2015, 2017), light exposure likely facilitates biomineralization through increased activity of the Ca^{2+}-ATPase transport. These processes result in lower shell Sr/Ca ratios during daytime than during night (Fig. 4.2B). At night, the cessation of photosynthesis leads to decreased metabolic rates and energy levels (Klumpp and Lucas 1994), also favored by the predator avoidance strategy of the bivalve (partial mantle retraction; Johnson et al., 2017) and manifested by a reduced nocturnal activity (Killam et al., 2023b). Slower shell growth occurring during nighttime resulted in larger BMUs (Fig. 4.2D). The combination of slow growth and low energy availability resulted in diurnal Sr/Ca maxima at the daily growth lines (Fig. 4.2B). On the daily time-scale, the offset between chemical and ultrastructural dynamics – with Sr/Ca showing a clear cyclic pattern and BMU morphology simply varying with the prevailing shell architecture – suggests that while Sr/Ca is influenced to some degree by SST and insolation, BMU morphology seems to be ultimately (and primarily) driven by the availability of light (Gannon et al., 2017) and the energy provided by the photosymbionts.

Temperature and solar irradiance are coupled variables, and while they seem to independently affect the shell properties of *T. squamosa*, changes in insolation lead to fluctuations of the water temperature. During daytime, favorable weather causes a gradual increase in SST, but due to the thermal inertia of water, SST decreases more slowly than insolation at the end of the day (Gentemann et al., 2003; Sano et al., 2012). The gradual temperature decline likely explains the continuous variation of shell Sr/Ca during the day, while the more abrupt ultrastructural difference between daytime and nighttime would primarily reflect distinct differences of light availability.

Diurnal Sr/Ca cycles were also observed in shells of tridacnids cultured under constant illumination (Warter et al., 2018) and constant water temperature (Sano et al., 2012). Although these studies did not explicitly consider changes of the shell architecture, they confirm that variations in SST and light availability do not fully explain the Sr/Ca variability in giant clam shells. In the specimen investigated here, for which the potential impact of shell ultrastructure

was considered, diurnal Sr/Ca cycles persisted during WEEs and at times during which the typical ultrastructural pattern (prisms at the daily growth lines and CCL-I in daily growth increments) was replaced by CCL-P. Thus, diurnal shell Sr/Ca cycles are not only influenced by SST and insolation but most likely also by a biological clock, as suggested by Warter et al. (2018) and DeWinter et al. (2023), and other physiological changes. For instance, when illuminated, the photosymbionts of *T. squamosa* regulate and absorb the host metabolic waste, as indicated by higher levels of proteins involved in ammonia transport (Pang et al., 2022). This process may signal favorable growth conditions to the host and likely promotes the formation of daily increments during daytime through the conversion of ammonia into amino acids, ultimately providing organic components essential for $CaCO_3$ deposition (Teh et al., 2021).

4.5.3 Implications of shell element chemical and ultrastructural dynamics for proxy studies

As demonstrated here, to properly interpret the meaning of shell Sr/Ca variations, it is crucial to consider the shell architecture of *Tridacna* spp., or more specifically, the time during which they grow, day or night. Sr is heterogeneously distributed across the daily growth bands of the fluted giant clam, i.e., enriched in the daily growth lines and depleted in the increments (Fig. 4.2B). NanoSIMS analysis (spot size = 2 μm^2) was essential to isolate data from shell portions grown during daytime. In the studied specimen, the average daily growth band measured 18.5 µm in width (Yan et al., 2020), with most shell material deposited during daytime (= daily growth increment) and only a small fraction at night (= daily growth line). The automated temporal alignment method developed in this study, enabled by high-resolution chemical and ultrastructural analyses (sections 4.2.2, 4.2.3, 4.2.4 and 4.2.5), addressed the limitations of coarser-resolution sampling methods such as LA-ICP-MS and ICP-OES. These methods provided a time-averaging of 4 to 14 days per data point (45 to 150 µm), which is much broader than the daily growth band width of the studied species (approx. 18.5 µm). This sampling resolution is evidently too coarse to isolate data from daily growth increments. It should be noted that coarser-resolution sampling methods may bias quantitative Sr/Ca data towards lower molar ratios, because shell portions formed during daytime are over-represented in each data point in comparison to shell material deposited at night due to the architectural heterogeneity of the shell daily growth bands. Therefore, the ultra-high-resolution approach used in this study can refine the interpretation of shell Sr/Ca profiles in *T. squamosa* and would be applicable to other bivalve species that grow sufficiently fast.

A detailed analysis of the studied specimen revealed distinct ultrastructural configurations, likely resulting from environmental stress. Specifically, prismatic features within

the CCL ultrastructure (CCL-P) were more frequent during weather extremes and had significantly higher Sr/Ca values (Fig. 4.4A). Complex ultrastructural patterns in *Tridacna* spp. shells are known to enhance the mechanical resistance of the shell material (Agbaje et al., 2017), suggesting that the formation of the complex BMUs found in CCL-P (Fig. 4.4D) was triggered by unfavorable growth conditions. This could indicate a biologically mediated adaptation of the bivalve to withstand variable environmental conditions (Agbaje et al., 2017; Gannon et al., 2017; Mills et al., 2024b). Furthermore, temperature reconstructions using Sr/Ca data from CCL-P shell portions or those grown during WEEs were in better agreement with instrumental SST than those of CCL-I shell portions and times without extreme weather events (Fig. 4.7). This suggests that the biological control over strontium incorporation into the shell decreases under less favorable growth conditions, leading to more accurate SST reconstructions. In tropical environments, such as reefs where *T. squamosa* lives, temperature variations seem to lack sufficient magnitude to cause significant changes in shell Sr/Ca compared to times of increased physiological stress. Furthermore, since CCL-P appears to be associated with WEEs, the occurrence of such ultrastructure could serve as a useful tool in paleo-weather research to identify episodes of environmental stress.

While the methods developed in this study offer potential for future research, it is important to note that the observed variations in element chemistry and ultrastructural configurations may be species-specific responses to environmental stress. *T. squamosa* is one of the most widely distributed giant clam species (bin Othman et al., 2010). It can inhabit a range of water depths (Jantzen et al., 2008) and rely on various levels of autotrophic and heterotrophic energy sources (Klumpp and Griffiths, 1994; Jantzen et al., 2008), displaying great flexibility to fluctuations in its environment. For example, the presence of CCL-P in the shell of *T. squamosa* is correlated to increased water turbidity and results in lower Sr/Ca levels compared to CCL-I (Mills et al., 2024b), contrasting with our findings and likely reflecting the remarkable plasticity of this species. Future research aimed at reconstructing seawater temperature using Sr/Ca ratios from tridacnid shells should prioritize species-specific studies of shell properties (element chemistry and ultrastructure) using ultra-high-resolution methods. Culture experiments would also allow to generate precise sub-daily species-specific shell growth models, which could be used to refine the Sr/Ca thermometer. Furthermore, such experiments could shed light on the actual influence of environmental variables such as water temperature, turbidity and insolation on the element chemical and ultrastructural properties of the shells. All this could improve the understanding of the adaptive responses of tridacnids to changing environments and open new perspectives for paleoclimate research.

4.6 Summary and conclusions

This study explored the complex relationships between environmental conditions and both shell Sr/Ca and ultrastructure properties of *Tridacna squamosa*. The results highlighted the potential of shell Sr/Ca as a proxy for sea surface temperature. Significant correlations were only observed between water temperature and Sr/Ca ratios of the daily growth increments. Ultra-high-resolution analytical techniques (NanoSIMS and SEM) were essential to isolate such data, thereby improving temperature reconstructions. The observed positive relationship between shell Sr/Ca and SST aligns with thermodynamic predictions and confirms the potential of the Sr/Ca thermometer in shells of *T. squamosa*. Upcoming studies should check if the same applies to other tridacnid species. The results of this study also suggest that shell Sr/Ca and ultrastructural properties are not directly linked but are instead both driven by underlying physiological processes. While Sr/Ca values were influenced by both light availability and SST, BMU morphology seemed to be primarily driven by insolation due to the photosynthetic activity of the symbionts. Ultrastructural changes probably reflect diurnal variations in metabolic rate. Furthermore, distinct ultrastructural patterns, namely the CCL ultrastructure with intricated prisms (CCL-P) were formed during massive environmental stress and may provide valuable insights into the frequency of paleo-weather extremes.

References

Agbaje, O. B. A., Wirth, R., Morales, L. F. G., Shirai, K., Kosnik, M., Watanabe, T., Jacob, D. E., 2017. Architecture of crossed-lamellar bivalve shells: The southern giant clam (*Tridacna derasa*, Röding, 1798). R. Soc. Open Sci. 4, 170622.

Aharon, P., 1983. 140,000-yr isotope climatic record from raised coral reefs in New Guinea. Nature 304, 720–723.

Aharon, P., Chappell, J., 1986. Oxygen isotopes, sea level changes and the temperature history of a coral reef environment in New Guinea over the last 105 years. Palaeogeogr. Palaeoclimatol. Palaeoecol. 56, 337–379.

Arias-Ruiz, C., Elliot, M., Bézos, A., Pedoja, K., Husson, L., Cahyarini, S. Y., Cariou, E., Michel, E., La, C., Manssouri, F., 2017. Geochemical fingerprints of climate variation and the extreme La Niña 2010–11 as recorded in a *Tridacna squamosa* shell from Sulawesi, Indonesia. Palaeogeogr. Palaeoclimatol. Palaeoecol. 487, 216–228.

Arndt, I., Coenen, D., Evans, D., Renema, W., Müller, W., 2023. Quantifying sub-seasonal growth rate changes in fossil giant clams using wavelet transformation of daily Mg/Ca cycles. Geochem. Geophys. Geosyst. 24, e2023GC010992.

Ballesta-Artero, I., Witbaard, R., Carroll, M. L., Van Der Meer, J., 2017. Environmental factors regulating gaping activity of the bivalve *Arctica islandica* in Northern Norway. Mar. Biol. 164, 116.

Barrat, J.-A., Chauvaud, L., Olivier, F., Poitevin, P., Rouget, M.-L., 2023. Trace elements in bivalve shells: How “vital effects” can bias environmental studies. Chem. Geol., 121695.

Beck, J. W., Edwards, R. L., Ito, E., Taylor, F. W., Recy, J., Rougerie, F., Joannot, P., Henin, C., 1992. Sea-surface temperature from coral skeletal strontium/calcium ratios. Science 257, 644–647.

Bin Othman, A. S., Goh, G. H., Todd, P. A., 2010. The distribution and status of giant clams (family Tridacnidae) – A short review. Raffles Bull. Zool. 58, 103–111.

Bogovic, J. A., Hanslovsky, P., Wong, A., Saalfeld, S., 2016. Robust registration of calcium images by learned contrast synthesis. In: 2016 IEEE 13th International Symposium on Biomedical Imaging (ISBI). Prague, Czech Republic: IEEE, 1123–1126.

Bonham, K., 1965. Growth rate of giant clam *Tridacna gigas* at Bikini Atoll as revealed by radioautography. Science 149, 300–302.

Brosset, C., Höche, N., Shirai, K., Nishida, K., Mertz-Kraus, R., Schöne, B. R., 2022. Strong coupling between biomineral morphology and Sr/Ca of *Arctica islandica* (Bivalvia) – Implications for shell Sr/Ca-based temperature estimates. Minerals 12, 500.

Brosset, C., Höche, N., Witbaard, R., Nishida, K., Shirai, K., Mertz-Kraus, R., Schöne, B. R., 2023. Sr/Ca in shells of laboratory-grown bivalves (*Arctica islandica*) serves as a proxy for water temperature – Implications for (paleo)environmental research? Front. Mar. Sci. 10, 1279164.

Brosset, C., Liu, C., Yang, H., Yan, H., Schöne, B. R., 2024. Data for "Integrating high-resolution Sr/Ca and ultrastructural analyses of the *Tridacna squamosa* shell to reconstruct sub-daily seawater temperature variation."

Butler, P. G., Wanamaker, A. D., Scourse, J. D., Richardson, C. A., Reynolds, D. J., 2013. Variability of marine climate on the North Icelandic Shelf in a 1357-year proxy archive based on growth increments in the bivalve *Arctica islandica*. Palaeogeogr. Palaeoclimatol. Palaeoecol. 373, 141–151.

Carré, M., Bentaleb, I., Bruguier, O., Ordinola, E., Barrett, N. T., Fontugne, M., 2006. Calcification rate influence on trace element concentrations in aragonitic bivalve shells: Evidences and mechanisms. Geochim. Cosmochim. Acta 70, 4906–4920.

Carré, M., Sachs, J. P., Schauer, A. J., Rodrguez, W. E., Ramos, F. C., 2013. Reconstructing El Niño-Southern Oscillation activity and ocean temperature seasonality from short-lived marine mollusk shells from Peru. Palaeogeogr. Palaeoclimatol. Palaeoecol. 371, 45–53.

Chauvaud, L., Thouzeau, G., Paulet, Y.-M., 1998. Effects of environmental factors on the daily growth rate of *Pecten maximus* juveniles in the Bay of Brest (France). J. Exp. Mar. Biol. Ecol. 227, 83–111.

Clark, G. R., 2005. Daily growth lines in some living Pectens (Mollusca: Bivalvia), and some applications in a fossil relative: Time and tide will tell. Palaeogeogr. Palaeoclimatol. Palaeoecol. 228, 26–42.

Corrège, T., 2006. Sea surface temperature and salinity reconstruction from coral geochemical tracers. Palaeogeogr. Palaeoclimatol. Palaeoecol. 232, 408–428.

De Winter, N. J., Dämmer, L. K., Falkenroth, M., Reichart, G.-J., Moretti, S., Martínez-García, A., Höche, N., Schöne, B. R., Rodiouchkina, K., Goderis, S., Vanhaecke, F., Van Leeuwen, S. M., Ziegler, M., 2021. Multi-isotopic and trace element evidence against different formation pathways for oyster microstructures. Geochim. Cosmochim. Acta 308, 326–352.

De Winter, N. J., Killam, D., Fröhlich, L., De Nooijer, L., Boer, W., Schöne, B. R., Thébault, J., Reichart, G.-J., 2023. Ultradian rhythms in shell composition of photosymbiotic and non-photosymbiotic mollusks. Biogeosciences 20, 3027–3052.

Dodd, J. R., Crisp, E. L., 1982. Non-linear variation with salinity of Sr/Ca and Mg/Ca ratios in water and aragonitic bivalve shells and implications for paleosalinity studies. Palaeogeogr. Palaeoclimatol. Palaeoecol. 38, 45–56.

Elliot, M., Welsh, K., Chilcott, C., McCulloch, M., Chappell, J., Ayling, B., 2009. Profiles of trace elements and stable isotopes derived from giant long-lived *Tridacna gigas* bivalves: Potential applications in paleoclimate studies. Palaeogeogr. Palaeoclimatol. Palaeoecol. 280, 132–142.

Epstein, S., Buchsbaum, R., Lowenstam, H. A., Urey, H. C., 1953. Revised carbonate-water isotopic temperature scale. Geol. Soc. America Bull. 64, 1315.

Foster, L. C., Allison, N., Finch, A. A., Andersson, C., 2009. Strontium distribution in the shell of the aragonite bivalve *Arctica islandica*. Geochem. Geophys. Geosyst. 10, 1–14.

Fritz, L. W., Haven, D. S., 1983. Hard clam, *Mercenaria mercenaria*: Shell growth patterns in Chesapeake Bay. Fish. Bull. 81, 697–708.

Füllenbach, C. S., Schöne, B. R., Mertz-Kraus, R., 2015. Strontium/lithium ratio in aragonitic shells of *Cerastoderma edule* (Bivalvia) – A new potential temperature proxy for brackish environments. Chem. Geol. 417, 341–355.

Füllenbach, C. S., Schöne, B. R., Shirai, K., Takahata, N., Ishida, A., Sano, Y., 2017. Minute co-variations of Sr/Ca ratios and microstructures in the aragonitic shell of *Cerastoderma edule* (Bivalvia) – Are geochemical variations at the ultra-scale masking potential environmental signals? Geochim. Cosmochim. Acta 205, 256–271.

Gaetani, G. A., Cohen, A. L., 2006. Element partitioning during precipitation of aragonite from seawater: A framework for understanding paleoproxies. Geochim. Cosmochim. Acta 70, 4617–4634.

Gannon, M. E., Pérez-Huerta, A., Aharon, P., Street, S. C., 2017. A biomineralization study of the Indo-Pacific giant clam *Tridacna gigas*. Coral Reefs 36, 503–517.

Gentemann, C. L., Donlon, C. J., Stuart-Menteth, A., Wentz, F. J., 2003. Diurnal signals in satellite sea surface temperature measurements. Geophys. Res. Lett. 30, 2002GL016291.

Goodwin, D. H., Gillikin, D. P., Roopnarine, P. D., 2013. Preliminary evaluation of potential stable isotope and trace element productivity proxies in the oyster *Crassostrea gigas*. Palaeogeogr. Palaeoclimatol. Palaeoecol. 373, 88–97.

Griffiths, C., Klumpp, D., 1996. Relationships between size, mantle area and zooxanthellae numbers in five species of giant clam (Tridacnidae). Mar. Ecol. Prog. Ser. 137, 139–147.

Höche, N., Peharda, M., Walliser, E. O., Schöne, B. R., 2020. Morphological variations of crossed-lamellar ultrastructures of *Glycymeris bimaculata* (Bivalvia) serve as a marine temperature proxy. Estuar. Coast. Shelf Sci. 237, 106658.

Höche, N., Walliser, E. O., de Winter, N. J., Witbaard, R., Schöne, B. R., 2021. Temperature-induced microstructural changes in shells of laboratory-grown *Arctica islandica* (Bivalvia). PLoS ONE 16, e0247968.

Höche, N., Walliser, E. O., Schöne, B. R., 2022. Microstructural mapping of *Arctica islandica* shells reveals environmental and physiological controls on biomineral size. Front. Earth Sci. 9, 781305.

Hori, M., Sano, Y., Ishida, A., Takahata, N., Shirai, K., Watanabe, T., 2015. Middle Holocene daily light cycle reconstructed from the strontium/calcium ratios of a fossil giant clam shell. Sci. Rep. 5, 8734.

Ip, Y. K., Ching, B., Hiong, K. C., Choo, C. Y. L., Boo, M. V., Wong, W. P., Chew, S. F., 2015. Light induces changes in activities of Na^+/K^+-ATPase, H^+/K^+-ATPase and glutamine synthetase in tissues involved directly or indirectly in light-enhanced calcification in the giant clam, *Tridacna squamosa*. Front. Physiol. 6.

Ip, Y. K., Hiong, K. C., Goh, E. J. K., Boo, M. V., Choo, C. Y. L., Ching, B., Wong, W. P., Chew, S. F., 2017. The whitish inner mantle of the giant clam, *Tridacna squamosa*, expresses an Apical

Plasma Membrane Ca^{2+}-ATPase (PMCA) which displays light-dependent gene and protein expressions. Front. Physiol. 8, 781.

Ip, Y. K., Chew, S. F., 2021. Light-dependent phenomena and related molecular mechanisms in giant clam-dinoflagellate associations: A review. Front. Mar. Sci. 8, 627722.

Jantzen, C., Wild, C., El-Zibdah, M., Roa-Quiaoit, H. A., Haacke, C., Richter, C., 2008. Photosynthetic performance of giant clams, *Tridacna maxima* and *T. squamosa*, Red Sea. Mar. Biol. 155, 211–221.

Johnson, G. C., Karajah, M. T., Mayo, K., Armenta, T. C., Blumstein, D. T., 2017. The bigger they are the better they taste: Size predicts predation risk and anti-predator behavior in giant clams. J. Zool. 301, 102–107.

Jolivet, A., Asplin, L., Strand, Ø., Thébault, J., Chauvaud, L., 2015. Coastal upwelling in Norway recorded in Great Scallop shells. Limnol. Oceanogr 60, 1265–1275.

Jones, D. S., 1981. Annual growth increments in shells of *Spisula solidissima* record marine temperature variability. Science 211, 165–167.

Jones, D. S., 1980. Annual cycle of shell growth increment formation in two continental shelf bivalves and its paleoecologic significance. Paleobiology 6, 331–340.

Karperien, A., 2013. FracLac for ImageJ. NIH.

Killam, D., Thompson, D., Morgan, K., Russell, M., 2023a. Giant clams as open-source, scalable reef environmental biomonitors. PLoS ONE 18, e0278752.

Killam, D., Das, S., Martindale, R. C., Gray, K. E., Paytan, A., Junium, C. K., 2023b. Photosymbiosis and nutrient utilization in giant clams revealed by nitrogen isotope sclerochronology. Geochim. Cosmochim. Acta. 359, 165–175.

Klumpp, D. W., Lucas, J. S., 1994. Nutritional ecology of the giant clams *Tridacna tevoroa* and *T. derasa* from Tonga: Influence of light on filter-feeding and photosynthesis. Mar. Ecol. Prog. Ser. 107, 147–156.

Klumpp, D., Griffiths, C., 1994. Contributions of phototrophic and heterotrophic nutrition to the metabolic and growth requirements of four species of giant clam (Tridacnidae). Mar. Ecol. Prog. Ser. 115, 103–115.

Lazareth, C. E., Le Cornec, F., Candaudap, F., Freydier, R., 2013. Trace element heterogeneity along isochronous growth layers in bivalve shell: Consequences for environmental reconstruction. Palaeogeogr. Palaeoclimatol. Palaeoecol. 373, 39–49.

Legland, D., Arganda-Carreras, I., Andrey, P., 2016. MorphoLibJ: Integrated library and plugins for mathematical morphology with ImageJ. Bioinformatics 32, 3532–3534.

Liu, C., Yan, H., Wang, G., Zhao, L., Hu, Y., Zhou, P., Luo, F., Yang, H., Dodson, J., 2021. Species specific Sr/Ca-$\delta^{18}O$ relationships for three Tridacnidae species from the northern South China Sea. Chem. Geol. 584, 120519.

Liu, C., Zhao, L., Zhao, N., Yang, W., Hao, J., Qu, X., Liu, S., Dodson, J., Yan, H., 2022. Novel methods of resolving daily growth patterns in giant clam (*Tridacna* spp.) shells. Ecol. Indic. 134, 108480.

Liu, C., Yan, H., Zhao, L., Zhao, N., Luo, F., Wen, H., Yang, H., Yang, W., Hao, J., Liang, C., Tanaka, K., Murakami-Sugihara, N., Shirai, K., Takahata, N., Dodson, J., Schöne, B. R., 2024. Potential environment effect on ultrahigh resolution Sr/Ca of giant clam shells from South China Sea. Coral Reefs 43, 1511–1521.

Lorens, R. B., Bender, M. L., 1977. Physiological exclusion of magnesium from *Mytilus edulis* calcite. Nature 269, 793–794.

Lucas, J. S., Nash, W. J., Crawford, C. M., Braley, R. D., 1989. Environmental influences on growth and survival during the ocean-nursery rearing of giant clams, *Tridacna gigas* (L.). Aquaculture 80, 45–61.

Marchitto, T. M., Jones, G. A., Goodfriend, G. A., Weidman, C. R., 2000. Precise temporal correlation of Holocene mollusk shells using sclerochronology. Quat. res. 53, 236–246.

Menadakis, M., Maroulis, G., Koutsoukos, P. G., 2008. Incorporation of Mg^{2+}, Sr^{2+}, Ba^{2+} and Zn^{2+} into aragonite and comparison with calcite. J. Math. Chem. 46, 484–491.

Mills, K., Sosdian, S., Muir, D., John, E., Nadia, S., Johnson, K., Buse, B., Waheed, Z., 2024a. Giant clams modify crystallographic and geochemical pathways of shell formation in response to turbidity. In Review.

Mills, K., Muir, D. D., Oldroyd, A., John, E. H., Santodomingo, N., Johnson, K. G., Hussein, M. A. S., Sosdian, S., 2024b. Microstructure and crystallographic texture data in modern giant clam shells (*Tridacna squamosa* and *Hippopus hippopus*). Data Brief 52, 109947.

Mook, W. G., Vogel, J. C., 1968. Isotopic equilibrium between shells and their environment. Science 159, 874–875.

Pang, C. Z., Boo, M. V., Ip, Y. K., Chew, S. F., 2022. Symbiotic dinoflagellates of the giant clam, *Tridacna squamosa*, express Ammonium Transporter 2 at the plasma membrane and increase its expression levels during illumination. Front. Mar. Sci. 9, 835574.

Pätzold, J., Heinrichs, J. P., Wolschendorf, K., Wefer, G., 1991. Correlation of stable oxygen isotope temperature record with light attenuation profiles in reef-dwelling *Tridacna* shells. Coral Reefs 10, 65–69.

Peharda, M., Schöne, B. R., Black, B. A., Corrège, T., 2021. Advances of sclerochronology research in the last decade. Palaeogeogr. Palaeoclimatol. Palaeoecol. 570, 110371.

Piwoni-Piórewicz, A., Strekopytov, S., Humphreys-Williams, E., Kukliński, P., 2021. The patterns of elemental concentration (Ca, Na, Sr, Mg, Mn, Ba, Cu, Pb, V, Y, U and Cd) in shells of invertebrates representing different $CaCO_3$ polymorphs: A case study from the brackish Gulf of Gdańsk (the Baltic Sea). Biogeosciences 18, 707–728.

Reynolds, D. J., Scourse, J. D., Halloran, P. R., Nederbragt, A. J., Wanamaker, A. D., Butler, P. G., Richardson, C. A., Heinemeier, J., Eiríksson, J., Knudsen, K. L., Hall, I. R., 2016. Annually resolved North Atlantic marine climate over the last millennium. Nat. Commun. 7, 13502.

Rosewater, J., 1965. The family Tridacnidae in the Indo-Pacific. In: Department of Mollusks, Academy of Natural Sciences of Philadelphia.

Sano, Y., Kobayashi, S., Shirai, K., Takahata, N., Matsumoto, K., Watanabe, T., Sowa, K., Iwai, K., 2012. Past daily light cycle recorded in the strontium/calcium ratios of giant clam shells. Nat. Commun. 3, 761.

Schindelin, J., Arganda-Carreras, I., Frise, E., Kaynig, V., Longair, M., Pietzsch, T., Preibisch, S., Rueden, C., Saalfeld, S., Schmid, B., Tinevez, J.-Y., White, D. J., Hartenstein, V., Eliceiri, K., Tomancak, P., Cardona, A., 2012. Fiji: An open-source platform for biological-image analysis. Nat. Methods 9, 676–682.

Schöne, B. R., Fiebig, J., Pfeiffer, M., Gleβ, R., Hickson, J., Johnson, A. L. A., Dreyer, W., Oschmann, W., 2005. Climate records from a bivalved Methuselah (*Arctica islandica*, Mollusca; Iceland). Palaeogeogr. Palaeoclimatol. Palaeoecol. 228, 130–148.

Schöne, B. R., Zhang, Z., Radermacher, P., Thébault, J., Jacob, D. E., Nunn, E. V., Maurer, A.-F., 2011. Sr/Ca and Mg/Ca ratios of ontogenetically old, long-lived bivalve shells (*Arctica islandica*) and their function as paleotemperature proxies. Palaeogeogr. Palaeoclimatol. Palaeoecol. 302, 52–64.

Schöne, B. R., Radermacher, P., Zhang, Z., Jacob, D. E., 2013. Crystal fabrics and element impurities (Sr/Ca, Mg/Ca, and Ba/Ca) in shells of *Arctica islandica* – Implications for paleoclimate reconstructions. Palaeogeogr. Palaeoclimatol. Palaeoecol. 373, 50–59.

Schöne, B. R., Meret, A. E., Baier, S. M., Fiebig, J., Esper, J., McDonnell, J., Pfister, L., 2020. Freshwater pearl mussels from northern Sweden serve as long-term, high-resolution stream water isotope recorders. Hydrol. Earth Syst. Sci. 24, 673–696.

Shannon, R. D., 1976. Revised effective ionic radii and systematic studies of interatomic distances in halides and chalcogenides. Acta Crystallogr. A 32, 751–767.

Shirai, K., Schöne, B. R., Miyaji, T., Radarmacher, P., Krause, R. A., Tanabe, K., 2014. Assessment of the mechanism of elemental incorporation into bivalve shells (*Arctica islandica*) based on elemental distribution at the microstructural scale. Geochim. Cosmochim. Acta 126, 307–320.

Sun, Y., Sun, M., Wei, G., Lee, T., Nie, B., Yu, Z., 2004. Strontium contents of a Porites coral from Xisha Island, South China Sea: A proxy for sea-surface temperature of the 20th century. Paleoceanography 19.

Tanabe, K., Mimura, T., Miyaji, T., Shirai, K., Kubota, K., Murakami-Sugihara, N., Schöne, B. R., 2017. Interannual to decadal variability of summer sea surface temperature in the Sea of Okhotsk recorded in the shell growth history of Stimpson's hard clams (*Mercenaria stimpsoni*). Glob. Planet. Change. 157, 35–47.

Teh, L. S. X., Poo, J. S. T., Boo, M. V., Chew, S. F., Ip, Y. K., 2021. Using glutamine synthetase 1 to evaluate the symbionts' potential of ammonia assimilation and their responses to illumination in five organs of the giant clam, *Tridacna squamosa*. Comp. Biochem. Physiol. A Mol. Integr. Physiol. 255, 110914.

Van Wynsberge, S., Andréfouët, S., Gaertner-Mazouni, N., Wabnitz, C. C. C., Menoud, M., Le Moullac, G., Levy, P., Gilbert, A., Remoissenet, G., 2017. Growth, survival and reproduction of the giant clam *Tridacna maxima* (Röding 1798, Bivalvia) in two contrasting lagoons in French Polynesia. PLoS ONE 12, e0170565.

Waisman, A., Norris, A. M., Elías Costa, M., Kopinke, D., 2021. Automatic and unbiased segmentation and quantification of myofibers in skeletal muscle. Sci. Rep. 11, 11793.

Wanamaker, A. D., Kreutz, K. J., Wilson, T., Borns Jr, H. W., Introne, D. S., Feindel, S., 2008. Experimentally determined Mg/Ca and Sr/Ca ratios in juvenile bivalve calcite for *Mytilus edulis*: Implications for paleotemperature reconstructions. Geo-Mar. Lett. 28, 359–368.

Warter, V., Müller, W., 2017. Daily growth and tidal rhythms in Miocene and modern giant clams revealed via ultra-high resolution LA-ICPMS analysis – A novel methodological approach towards improved sclerochemistry. Palaeogeogr. Palaeoclimatol. Palaeoecol. 465, 362–375.

Warter, V., Erez, J., Müller, W., 2018. Environmental and physiological controls on daily trace element incorporation in *Tridacna crocea* from combined laboratory culturing and ultra-high resolution LA-ICP-MS analysis. Palaeogeogr. Palaeoclimatol. Palaeoecol. 496, 32–47.

Watanabe, T., Oba, T., 1999. Daily reconstruction of water temperature from oxygen isotopic ratios of a modern *Tridacna* shell using a freezing microtome sampling technique. J. Geophys. Res. 104, 20667–20674.

Watson, E. B., 1996. Surface enrichment and trace-element uptake during crystal growth. Geochim. Cosmochim. Acta 60, 5013–5020.

Watson, E. B., 2004. A conceptual model for near-surface kinetic controls on the trace-element and stable isotope composition of abiogenic calcite crystals. Geochim. Cosmochim. Acta 68, 1473–1488.

Weidman, C. R., Jones, G. A., Kyger, 1994. The long-lived mollusc *Arctica islandica*: A new paleoceanographic tool for the reconstruction of bottom temperatures for the continental shelves of the northern North Atlantic Ocean. J. Geophys. Res. 99, 18305–18314.

Yan, H., Shao, D., Wang, Y., Sun, L., 2011. High resolution Sr/Ca profile of *Tridacna gigas* from Xisha Islands of South China Sea and its potential application on sea surface temperature reconstruction. J. Earth Environ., 381-386 (In Chinese with English abstract).

Yan, H., Shao, D., Wang, Y., Sun, L., 2013. Sr/Ca profile of long-lived *Tridacna gigas* bivalves from South China Sea: A new high-resolution SST proxy. Geochim. Cosmochim. Acta 112, 52–65.

Yan, H., Shao, D., Wang, Y., Sun, L., 2014. Sr/Ca differences within and among three Tridacnidae species from the South China Sea: Implication for paleoclimate reconstruction. Chem. Geol. 390, 22–31.

Yan, H., Sun, L., Shao, D., Wang, Y., 2015. Seawater temperature seasonality in the South China Sea during the Late Holocene derived from high-resolution Sr/Ca ratios of *Tridacna gigas*. Quat. Res. 83, 298–306.

Yan, H., 2020. Daily growth bands of giant clam shell: A potential paleoweather recorder. Solid Earth Sci 5, 249–253.

Yan, H., Liu, C., An, Z., Yang, W., Yang, Y., Huang, P., Qiu, S., Zhou, P., Zhao, N., Fei, H., Ma, X., Shi, G., Dodson, J., Hao, J., Yu, K., Wei, G., Yang, Y., Jin, Z., Zhou, W., 2020. Extreme weather

events recorded by daily to hourly resolution biogeochemical proxies of marine giant clam shells. Proc. Natl. Acad. Sci. U.S.A. 117, 7038–7043.

Yan, H., Zhao, N., Zhou, P., Liu, C., Fei, H., Li, M., Liu, F., Yang, Y., Yang, W., Dodson, J., 2021. The first detection of the Madden-Julian Oscillation signal in daily to hourly resolution proxy records derived from a natural archive of giant clam shell (*Tridacna* spp.). Earth Planet. Sci. Lett. 555, 116703.

5 Summary and outlook

The purpose of this thesis was to address key limitations of the Sr/Ca-thermometer in marine bivalve shells, whose application in sclerochronological research remains constrained by the complex interplay of environmental variability, individual physiological processes and biomineralization dynamics. Specifically, Sr/Ca profiles measured in bivalve shells might reflect variability in their architectural and ultrastructural composition (e.g., Shirai et al., 2008; Foster et al., 2009; Lazareth et al., 2013; Füllenbach et al., 2017; Marali et al., 2017; Roger et al., 2017), which remains a critical knowledge gap in the calibration of the Sr/Ca proxy and in the reliability of Sr/Ca-based temperature reconstructions. This work addressed this limitation through a detailed analysis of shell properties (architecture, ultrastructure and growth patterns) aimed at quantifying, for the first time, the relationship between shell ultrastructural composition (BMU morphology across distinct shell layers, ultrastructure types and growth features) and Sr/Ca profiles across several timescales (from sub-daily to seasonal resolution) and growth conditions (field and laboratory-grown specimens). The reliability of Sr/Ca-based temperature estimates is then assessed when structural and growth rate-related biases are identified and adjusted for. For this purpose, two long-lived aragonitic bivalve species widely used in sclerochronology and climate research were selected, i.e., *Arctica islandica* and *Tridacna squamosa*. Both species were chosen for their complementary characteristics (boreal vs tropical, annual vs daily growth patterns, heterotrophic vs photosymbiotic metabolism), enabling comparisons across environments, temporal resolutions and ecological strategies. The main findings of this project are outlined hereafter through the results presented in each chapter.

Manuscript 1 studied the relationship between shell Sr/Ca and seasonal temperature variation in juvenile wild specimens of *A. islandica*. The shell of this long-lived marine bivalve species exhibits ultrastructurally distinct OSL sublayers (HOM in the oOSL and CA in the iOSL), making it suitable for evaluating structural and growth-related influences on the Sr/Ca-temperature relationship. Shell Sr/Ca was measured in annual growth increments using LA-ICP-MS and interpreted alongside SEM-based ultrastructure morphometry and growth rate estimates. Shell Sr/Ca profiles along the direction of growth were largely consistent between coeval specimens, suggesting an environmental control on strontium incorporation. Shell Sr/Ca

showed a positive correlation with seasonal temperature (Pearson r = 0.15), consistent with thermodynamic predictions (Gaetani and Cohen, 2006), but the relationship remained weak even after mathematical correction for individual ultrastructure- and growth-related influences (maximum Pearson r = 0.51). The temperature signal appeared to be superimposed by external environmental drivers (e.g., food availability, salinity), which likely influence Sr^{2+} incorporation both directly and through the shell ultrastructural variability. The findings of this study show that shell Sr/Ca from wild *A. islandica* specimens cannot be used for seasonal temperature reconstruction until the environmental variables influencing the signal are more clearly understood.

Manuscript 2 investigated the relationship between shell Sr/Ca and temperature in *A. islandica* grown under stable laboratory conditions, assessing whether structural and growth-related biases affecting the Sr/Ca-thermometer could be minimized by isolating temperature as the dominant environmental driver. Juvenile specimens were cultured at stable temperatures (1, 3, 6, 9, 10.3, 12, and 15 °C) and data were acquired using protocols consistent with the previous study. As observed in nature, and following thermodynamic principles (Gaetani and Cohen, 2006), shell Sr/Ca increased with warmer conditions. However, compared to results obtained in field-grown specimens (R^2 = 0.26, at best), Sr/Ca correlated more strongly with temperature in laboratory-grown shells, especially in the iOSL (R^2 = 0.38) and after adjustment for growth rate and BMU morphology influences (R^2 up to 0.75). These findings confirmed that additional environmental forcings in the natural habitat of *A. islandica* (e.g., food availability, salinity) mask part of the temperature signal contained in shell Sr/Ca profiles. In conclusion, while shell Sr/Ca can reflect ambient water temperature under equable conditions, transfer functions calibrated from laboratory experiments (uncertainty of ± 1.0 °C, at best) cannot be directly applied to wild specimens (uncertainty of ± 2.1 °C, at best).

Manuscript 3 evaluated the reliability of sub-daily resolved temperature data inferred from Sr/Ca profiles measured in the shell of *T. squamosa*. Tridacnids are tropical bivalves particularly valuable for proxy-based climate research as they grow rapidly in early ontogeny, can reach large size and form internal daily growth bands that support high-resolution analyses. Previous studies investigating tridacnid shells at high-resolution reported inconsistent relationships between temperature and Sr/Ca, likely due to oversimplified assumptions on growth rates (i.e., linear models) and lack of consideration for internal structural heterogeneity. Therefore, dedicated protocols for SEM-based BMU morphometry were developed to analyze ultrastructures separately (i.e., within daily growth lines and increments each composed of ISP and CCL, respectively), while accounting for the non-linear growth of this photosymbiotic bivalve and temporally aligning both chemical and ultrastructural data at sub-daily resolution. This approach revealed that, consistent with thermodynamic predictions (Gaetani and Cohen, 2006),

Sr/Ca in daily increments increased with warmer conditions (R^2 = 0.36 in increments only, R^2 < 0.10 if growth lines are also included). Accordingly, shell Sr/Ca profiles captured short-term temperature variations. However, the uncertainty of the estimates (± 1.5 to 2.8 °C) remained close to the natural temperature amplitude of tropical reefs where tridacnids are found. Additionally, consistent daily Sr/Ca cycles with local maxima at growth lines were observed regardless of ultrastructural variability (i.e., BMU morphology and deviations from the typical CCL configuration during extreme weather events), suggesting that shell Sr/Ca and ultrastructural properties are driven by common underlying processes rather than directly coupled. This study demonstrated that high-resolution quantitative and ultrastructure specific analyses of shell properties can provide new insights for environmental proxy development (e.g., Sr/Ca-thermometer) and further highlight the exceptional value of climate archives that support fine-scale analytical precision and resolution, such as tridacnid shells.

In conclusion, this work demonstrated that structural variability in marine bivalve shells significantly influences the geochemical proxies used for environmental reconstruction. The Sr/Ca-thermometer appears more reliable when shell ultrastructural variability is minimized, as reflected by stronger correlations between shell Sr/Ca and temperature under equable conditions. The accuracy of shell Sr/Ca-based temperature estimates can be improved by correcting for BMU morphology and growth-related biases through quantitative ultrastructure-specific analyses aligned with the species-specific architecture of bivalve shells. In natural settings, however, obtaining precise temperature information from Sr/Ca remains challenging, because the seasonal signal is strongly influenced by additional environmental and physiological drivers. High-resolution analyses revealed synchronous, fine-scale variations in both shell Sr/Ca and ultrastructure that suggested common underlying drivers rather than direct causal relationships. Therefore, this work provides new insight into the coupling between bivalve shell biomineralization processes and environmental variability. The methodological approaches developed and applied here not only enabled precise analysis of shell Sr/Ca and ultrastructure across multiple temporal scales but also offer a practical framework for future studies to implement similar analyses across taxa and ecological settings. By reducing preparation time and improving analytical consistency, this thesis directly supports the refinement of proxy calibration strategies in sclerochronological research.

Future research targeting calibration of trace and minor element-based environmental proxies in bivalve shells is expected to benefit from systematically integrating ultrastructure-specific analyses. As demonstrated in this thesis, Sr/Ca-temperature correlations that appeared ambiguous or absent in earlier work became evident only when data were isolated by ultrastructure types, an approach that is only possible through high-resolution analyses. Applying this process to other trace and minor elements (e.g., Ba, Mn and Mg/Ca) may resolve

similar uncertainties in their relationships with environmental parameters and improve the reliability of proxy-based reconstructions. Comparable analyses should be extended to shells that exhibit structural patterns beyond those investigated here in order to assess the broader applicability of this technique to shell ultrastructures in other modern and fossil specimens of the same species as studied here, other bivalve taxa and geographic regions. Such work will likely reveal cases in which specific environmental parameters can be reconstructed with higher reliability when structural variability is considered. The techniques for semi-automated temporal alignment and ultrastructural morphometry presented in this thesis (applied to ISP, CCL, CA and HOM) provide a methodological foundation that can, with minimal effort, be refined and adapted for biogenic archives with different internal architectures as long as the timing of material deposition is well constrained, further facilitating proxy-based climate research.

References

Foster, L. C., Allison, N., Finch, A. A., Andersson, C., 2009. Strontium distribution in the shell of the aragonite bivalve *Arctica islandica*. Geochem. Geophys. Geosyst. 10, 1–14.

Füllenbach, C. S., Schöne, B. R., Shirai, K., Takahata, N., Ishida, A., Sano, Y., 2017. Minute co-variations of Sr/Ca ratios and microstructures in the aragonitic shell of *Cerastoderma edule* (Bivalvia) – Are geochemical variations at the ultra-scale masking potential environmental signals? Geochim. Cosmochim. Acta 205, 256–271.

Gaetani, G. A., Cohen, A. L., 2006. Element partitioning during precipitation of aragonite from seawater: A framework for understanding paleoproxies. Geochim. Cosmochim. Acta 70, 4617–4634.

Lazareth, C. E., Cornec, F. L., Candaudap, F., Freydier, R., 2013. Trace element heterogeneity along isochronous growth layers in bivalve shell: Consequences for environmental reconstruction. Palaeogeogr. Palaeoclimatol. Palaeoecol. 373, 39–49.

Marali, S., Schöne, B. R., Mertz-Kraus, R., Griffin, S. M., Wanamaker, A. D., Butler, P. G., Holland, H. A., Jochum, K. P., 2017. Reproducibility of trace element time-series (Na/Ca, Mg/Ca, Mn/Ca, Sr/Ca, and Ba/Ca) within and between specimens of the bivalve *Arctica islandica* – A LA-ICP-MS line scan study. Palaeogeogr. Palaeoclimatol. Palaeoecol. 484, 109–128.

Roger, L. M., George, A. D., Shaw, J., Hart, R. D., Roberts, M., Becker, T., McDonald, B. J., Evans, N. J., 2017. Geochemical and microstructural characterisation of two species of cool-water bivalves (*Fulvia tenuicostata* and *Soletellina biradiata*) from Western Australia. Biogeosciences 14, 1721–1737.

Shirai, K., Takahata, N., Yamamoto, H., Omata, T., Sasaki, T., Sano, Y., 2008. Novel analytical approach to bivalve shell biogeochemistry: A case study of hydrothermal mussel shell. Geochem. J. 42, 413–420.